

QATAR UNIVERSITY

COLLEGE OF ENGINEERING

PROSPECTS OF AMINO ACIDS AND IONIC LIQUIDS AS NATURAL GAS

HYDRATE INHIBITORS FOR OFFSHORE FLOW ASSURANCE

BY

M FAHED AZIZ QURESHI

A Dissertation Submitted to  
the Faculty of the College of

Engineering

in Partial Fulfillment

of the Requirements

for the Degree of

Doctorate of Philosophy in Chemical Engineering

June 2018

© 2018. M. Fahed Aziz Qureshi. All Rights Reserved.

## COMMITTEE PAGE

The members of the Committee approve the Dissertation of M Fahed Aziz  
Qureshi defended on 08/05/2018.

---

Prof Majeda Khraisheh  
Thesis/Dissertation Supervisor

---

Dr. M A Saleh  
Committee Member

---

Dr. Mustafa Saleh Nasser  
Committee Member

---

Prof. Hazim Ali Mohd Qiblawey  
Committee Member

---

Prof. Ibelwaleed Ali Hussein  
Committee Member

Approved:08 May 2018

---

Khalifa Al-Khalifa, Dean, College of Engineering

## ABSTRACT

QURESHI, M. FAHED, AZIZ, Doctorate : June : [2018]

Doctorate of Philosophy in Chemical Engineering

Title: Prospects of Amino Acids and Ionic Liquids as Natural Gas Hydrate Inhibitors for Offshore Flow Assurance

Supervisor of Dissertation: Majeda, Khraisheh.

Gas hydrates are ice-like compounds that are formed when small gas molecules get trapped within the water molecules at high pressure and low-temperature conditions. The formation of gas hydrates in the offshore subsea lines can lead to unwanted blockages and cause operations shut down. To prevent hydrate formation the chemical inhibitors like methanol and mono-ethylene glycol (MEG) are injected at the wellhead. But, the major drawbacks of using these inhibitors is that they are toxic, flammable, have environmental constraints and are required in bulk quantities (> 30 wt%).

In this work, for the first time, a comprehensive experimental study on the use of amino acids and ionic liquids as the natural gas hydrate inhibitors in the presence of synergent (PEO) have been conducted at wide process conditions (38-120 bars). The results show that the selected amino acids and ionic liquids exhibit dual functional behaviour by providing the temperature shift of around 1.5-2.3 °C and delaying the hydrate formation time from 0.5-1.5 hr. By the addition of synergent (PEO) with amino acids and ionic liquids, the hydrate formation time was delayed by 6 - 24 hr.

The ionic liquids with shorter cationic alkyl chain and amino acids with higher solubility were observed to provide better hydrate inhibition effect. The inhibitors tend to show better hydrate inhibition effect at low pressures (40 bars) and their inhibition effect decreases as the pressure rises. At the same concentration (10 wt%), the ammonium-based ionic liquid [EA][Of] provided the inhibition effect similar to MEG and at the higher concentration (20 wt%) the amino acid glycine provided better hydrate inhibition effect than the MEG. This indicates that both amino acids and ionic liquids are potential gas hydrate inhibitors, but amino acids and their synergent mixtures are more suited for the large-scale usage due to their biological nature and widescale production.

The effect of stirring on the hydrate crystal formation at different stirring rates (100-1400 RPM) was also investigated. It was found that a threshold limit exists for the stirring rate, above and below which no hydrate formation is likely to occur within the selected system. The maximum hydrate crystal formation occurs at moderate stirring rates and very high or low stirring rates are not suited for the stable hydrate crystal growth and formation.

This work intends to provide industry with new generation of inhibitors that are cost effective, environmentally benign and offer strong hydrate inhibition strength. This work is beneficial for the industry and academic researchers as the required dosage of hydrate inhibitors has been reduced from 40 wt% to 5 wt%, which helps to reduce the

overall CAPEX cost and reduce environmental concerns related to the disposal of the hydrate inhibitors. This work offers new arena of research in the area of hydrate inhibitors + synergents mixtures. These mixtures are effective and have potential to replace conventional hydrate inhibitors like methanol and MEG

## DEDICATION

*"I would like to dedicate this thesis to people suffering from Cancer"*

## ACKNOWLEDGMENTS

I would like to acknowledge Qatar National Research funds (QNRF), member of Qatar Foundation, for sponsoring this Ph.D. work and awarding me with Graduate Studies Research Award (GSRA). This work was made possible by grant GSRA # 2-1-0603-14012 from the QNRF (a member of Qatar Foundation).

Firstly, I would like to gladly express my gratitude to Prof. Majeda Khraisheh for supervising my Ph.D. study and providing me with her valuable feedback and directions. I am also grateful to Dr. Mohd Ali H. Saleh, Dr. Mert Atilhan, Dr. Tausif Altamash, Dr. Muhammad Tariq, Dr. Ahmed El Khatat and Prof. Hazim Qiblawey for their support during the Ph.D. period. I would also like to extend my thanks to Mr. Said Gad for providing technical assistance and helping in the setting up of the laboratory equipment.

This Ph.D. has been a challenging and life-changing journey, in which I had to overcome many setbacks and struggles to accomplish this goal. During this period I was well supported and applauded by my parents (Mr & Mrs Aziz Qureshi) and spouse (Beenish). Accordingly, I would like to express sincere gratitude to all of them and to my friends Dr. Oussama Gharbi, Eng. Samahat Samim and Eng. Shekaib Afzal for keeping me motivated and cheering me up throughout this journey.

At last, I would also like to acknowledge all my colleagues in Department of Chemical Engineering, Qatar University. The people in the department are approachable,

cooperative and it has been a privilege for me to work with them. I would also like to thank QNRF GSRA program for all the financial help they provided me and the college of engineering research office for all their support.



## TABLE OF CONTENTS

DEDICATION.....	vi
ACKNOWLEDGMENTS.....	vii
LIST OF TABLES.....	xii
LIST OF FIGURES.....	xiv
LIST OF ABBREVIATION.....	xx
CHAPTER 1: INTRODUCTION.....	1
1.1 Hydrate Structures & Properties.....	5
1.2 Hydrate Plugging and Offshore Flow assurance.....	9
1.3 Hydrate Inhibitors.....	15
1.3.1 Thermodynamic Hydrate Inhibitors.....	15
1.3.2 Kinetic Hydrate Inhibitors.....	19
1.4 Research Objectives.....	23
1.5 Thesis Structure.....	25
CHAPTER 2: BACKGROUND.....	27
2.1 Hydrate Inhibition using Ionic Liquids (ILs).....	28
2.1.1 Ionic liquids: Synthesis & Application.....	30
2.1.2 Ionic liquids: Thermo-physical Properties.....	35
2.1.3 Ionic liquids: Recycle & Recovery.....	40
2.1.4 Ionic liquids: Hydrate inhibition studies.....	48
2.2 Hydrate Inhibition using Amino Acids.....	62
2.2.1 Amino acids: Synthesis & Application.....	65
2.2.2 Amino acids: Physio-Chemical Properties.....	74
2.2.3 Amino acids: Recycle & Recovery.....	80
2.2.4 Amino acids: Hydrate Inhibition Studies.....	84
2.3 Enhancing Hydrate Inhibition using Synergents.....	90
2.3.1 Sodium Chloride (NaCl).....	91
2.3.2 Poly-vinyl caprolactam (PVCap).....	92
2.3.3 Poly-ethylene Oxide.....	94
2.4 Factors affecting the rate of hydrate formation.....	98

2.4.1	Mechanical agitation.....	100
CHAPTER 3:	EXPERIMENTAL METHODOLOGY .....	106
3.1	Materials .....	106
3.1.1	Gas mixture .....	110
3.1.2	GC-Analysis for Quaternary Gas Mixture (QM) .....	111
3.2	Equipment .....	112
3.2.1	High-Pressure Cell (HPC).....	112
3.2.2	Rocking Cell Assembly (RC-5).....	119
3.2.3	Equipment Calibration & Un-certainty .....	123
3.3	Experimental Procedures .....	127
3.3.1	High-Pressure Cell (HPC).....	127
3.3.2	Rocking Cell Assembly (RC-5).....	129
3.3.3	Extracting hydrate dissociation and formation point .....	131
CHAPTER 4:	EXPERIMENTAL RESULTS & DISCUSSION .....	133
4.1	Hydrate Formation and Inhibition in the Quaternary gas mixture (QM) .....	133
4.1.1	Effect of Magnetic Stirring on QM hydrate formation .....	134
4.1.2	Effect of Pyrrolidinium Ionic Liquids on QM hydrate inhibition .....	147
4.1.3	Co-effect of Pyrrolidinium Ionic Liquids and synergents on QM hydrate inhibition .....	169
4.2	Hydrate Formation and Inhibition in pure methane (CH <sub>4</sub> ) gas.....	181
4.2.1	Effect of Ammonium Ionic liquids on CH <sub>4</sub> hydrate inhibition.....	181
4.2.2	Co-effect of Ammonium-based Ionic liquids and Synergent on CH <sub>4</sub> hydrate formation .....	199
4.2.3	Effect of Amino Acids on CH <sub>4</sub> hydrate inhibition .....	203
4.2.4	Co effect of Amino Acids and synergent on CH <sub>4</sub> hydrate inhibition .....	223
4.3	Inhibitors Effectiveness Comparison.....	228
4.3.1	Comparison with Choline based Ionic Liquids .....	228
4.3.2	Comparison with Imidazolium-based Ionic Liquids .....	232
4.3.3	Comparison with Methanol and Ethylene Glycol .....	237
4.3.4	Comparison between Amino Acids & Ionic Liquids Synergent Mixtures .	242
4.3.5	Economic Evaluation.....	246
CHAPTER 5:	CONCLUSIONS.....	248

5.1	Future Work .....	258
	References.....	264

## LIST OF TABLES

Table 1-1: Showing Hydrate crystal structure properties (data taken from Sloan <sup>1</sup> ) .....	7
Table 1-2: Comparison of the properties of ice, hydrate structure I, structure II (data taken from <sup>19-20</sup> ) .....	9
Table 2-1: Production process and application of the key amino acids <sup>195</sup> .....	69
Table 2-2: Advantages and disadvantages of different methods used for the production of amino acids on the large-scale <sup>195</sup> .....	73
Table 3-1: List of Ionic Liquids (ILs) and synergents studied in this dissertation.....	107
Table 3-2: List of Ionic Liquids (ILs) studied in this dissertation .....	108
Table 3-3: List of amino acids used in this work .....	109
Table 3-4: Mol Composition of the QM mixture as per GC analysis .....	110
Table 3-5: GC Analysis Report for the QM gas mixture .....	111
Table 3-6: High-Pressure Cell (HPC) specifications by the manufacturer .....	115
Table 3-7: System specification for the Rocking Cell Assembly (RC-5) provided by the manufacturer .....	121
Table 4-1: Hydrates dissociation points for the QM gas mixture .....	148
Table 4-2: QM gas mixture hydrate dissociation points obtained in the presence of the ionic liquids (ILs).....	160
Table 4-3: The hydrate dissociation points experimentally obtained for the IL-synergent mixtures. ....	174
Table 4-4: CH <sub>4</sub> Hydrate dissociation points in the presence of 5wt% and 10 wt%	

ammonium based ionic liquids .....	192
Table 4-5: CH <sub>4</sub> Hydrates dissociation points (P-T) obtained in the presence of the amino acids at different concentrations .....	213

## LIST OF FIGURES

Figure 1-1: A typical offshore oil and gas production facility.....	2
Figure 1-2: Gas Hydrate crystal structures .....	6
Figure 1-3: Gas Hydrate plug formation inside pipeline. ....	11
Figure 1-4: Mechanism of the hydrate formation .....	12
Figure 1-5: The major flow assurance issues in the subsea tie back system .....	14
Figure 1-6: The pure methane Hydrate Vapor-Liquid Equilibrium (HVLE) points at different pressure conditions.....	17
Figure 1-7: Kinetic hydrate inhibition mechanisms reported in the literature .....	21
Figure 2-1: Application of Ionic liquids (ILs) in different disciplines. ....	33
Figure 2-2: (a) Physical Structure of amino acid (b) Dipolar form of the amino acid with R the side chain group.....	74
Figure 2-3: Classification of 20 key amino acids into different groups based on their respective side chains.....	76
Figure 2-4: Shows the optical configuration of L-Glyceraldehyde, L-Amino Acid, and D- Amino Acid.....	79
Figure 2-5: The amount of pure methane gas and water present in the one volume of the gas at Standard Temperature and Pressure (STP). ....	99
Figure 3-1: A schematic diagram of the High-pressure cell (HPC) used for studying the effect of stirring on the QM mixture hydrate formation. ....	113
Figure 3-2: The CAD drawing showing the dimensions of the High-Pressure Cell (HPC) .....	114

Figure 3-3: A) A high-pressure cell assembly with the valves and pressure transducer, B) The top view of the high pressure cell .....	116
Figure 3-4: The liquid sample cylinder where the magnetic stirrer is located .....	117
Figure 3-5: Magnetic stirrer inside the high-pressure cell that is agitated using the lab mixture placed below the high-pressure cell .....	118
Figure 3-6: A schematic diagram of Rocking Cell assembly (RC-5) used for the inhibitors test. ....	120
Figure 3-7: a) Shows cells submerged in cooling bath, b) Shows the stainless steel balls that provide agitation inside the cells, c) Shows the stainless steel rocking cell with a temperature sensor and the cap (lab pictures). ....	122
Figure 3-8: The comparison between the methane Hydrate liquid vapour equilibrium (HLVE) data points obtained experimentally from RC-5 and the methane HLVE data points reported in the literature previously. ....	125
Figure 3-9: Comparison of the Quaternary Gas Mixture (QM) HLVE data points obtained experimentally using RC-5 and the QM HLVE data points obtained using commercial simulation software WatGas V2011. ....	126
Figure 3-10: Experimental kinetic loop showing cooling, heating and isothermal steps in the stirring effect study on QM mixture inside the High-Pressure Cell (HPC). ....	128
Figure 3-11: The experimental loop showing the hydrate formation and dissociation in the Rocking Cell Assembly (RC-5). ....	131
Figure 3-12: Shows the hydrate formation/ induction point that is considered to occur right before the steep pressure drop within the system. ....	132

Figure 4-1: Pressure drops observed at different stirring rates (RPM) inside the high-pressure cell (HPC). .....	135
Figure 4-2: The total average pressure drops observed within the HPC at different stirring speed evaluated by conducting a minimum of three experimental trials. ....	139
Figure 4-3: Shows the visual scenes of mixing taking place within the High-pressure cell (HPC) at different stirring rates. ....	141
Figure 4-4: Hydrate crystal formation rate (HCFR) during the 1st, 2nd and 3rd hour after the hydrate induction time within the High-pressure cell (HPC). ....	145
Figure 4-5: The shift in the HLVE curve of the quaternary gas mixture (QM) in the presence of 1 wt% of pyrrolidinium-based ionic liquids. ....	150
Figure 4-6: The shift in the HLVE curve of the quaternary gas mixture (QM) in the presence of 5 wt% of pyrrolidinium-based ionic liquids. ....	152
Figure 4-7: The hydrate suppression temperature obtained at different pressure conditions in the presence of 5 wt% [PMPy][Triflate] and 5 wt% [PMPy][Cl]. ....	155
Figure 4-8: The shift in the HLVE curve of the quaternary gas mixture (QM) in the presence of 10 wt % methanol and the mixture 5wt% [PMPy][Triflate] + 5wt% [PMPy][Cl]. ....	158
Figure 4-9: The time delay in the quaternary gas mixture (QM) hydrate formation in the presence of 5 wt% ILs [PMPy]Triflate] and IL [PMPy][Chloride]. ....	163
Figure 4-10: The time delay in the quaternary gas mixture (QM) hydrate formation in the presence of 5 wt% IL [PMPy][Cl] and 5 wt% IL [PMPy][Triflate] at 40 bars. ....	164
Figure 4-11: The time delay in the quaternary gas mixture (QM) hydrate formation in the	



presence of 5wt% IL [PMPy][Cl] and 5wt% IL [PMPy][Triflate] at 100 bars. ....	166
Figure 4-12: The time delay in the quaternary gas mixture (QM) hydrate formation in the presence of a mixture of 5wt% IL [PMPy][Cl] and 5wt% IL [PMPy][Triflate] at different pressure conditions.....	167
Figure 4-13: The shift in the HLVE curve of the quaternary gas mixture (QM) in the presence of equal ratio IL-synergent mixtures [PMPy][Cl] + PEO and [PMPy][Cl] + VCAP at wide process conditions.....	171
Figure 4-14: The shift in the HLVE curve of the quaternary gas mixture (QM) in the presence of equal ratio IL-synergent mixtures [PMPy][Triflate] + PEO and [PMPy][Triflate] + VCAP.. .....	172
Figure 4-15: The delay in the QM gas mixture hydrate formation time in the presence of equal ratio IL-synergent mixtures [PMPy][Cl] + PEO and [PMPy][Cl] + VCAP.. .....	177
Figure 4-16: The delay in the QM gas mixture hydrate formation time in the presence of equal ratio IL-synergent mixtures [PMPy][Triflate] + PEO and [PMPy][Triflate] +VCAP.....	178
Figure 4-17: The shift in HLVE curve of methane (CH <sub>4</sub> ) hydrate in the presence of 5wt% ammonium based ionic liquids. ....	184
Figure 4-18: The CH <sub>4</sub> hydrate suppression temperatures at 100 bars observed using 5wt% ammonium-based ILs.....	186
Figure 4-19: The shift in HLVE curve of methane (CH <sub>4</sub> ) hydrate in the presence of 10 wt% ammonium based ionic liquids at wide process conditions.....	187
Figure 4-20: The CH <sub>4</sub> hydrate suppression temperatures at 65 bars observed using 10	

wt% ammonium-based ILs.. .....	188
Figure 4-21: The CH <sub>4</sub> hydrate suppression temperatures at 100 bars observed using 10 wt% ammonium-based ILs.. .....	189
Figure 4-22: The time delay in the CH <sub>4</sub> hydrate formation in the presence of 5wt% ammonium based ILs [TBA][Of], [EA][Of], [DMA][Of] and [DMEA][Of].. .....	195
Figure 4-23: The time delay in the CH <sub>4</sub> hydrate formation in the presence of 10 wt% ammonium based ILs [TBA][Of], [EA][Of], [DMA][Of] and [DMEA][Of].. .....	196
Figure 4-24: The kinetic delay in the CH <sub>4</sub> hydrate formation in the presence of 5wt% ammonium ILs + 1 wt% PEO mixtures at wide process conditions.....	201
Figure 4-25: The HLVE curve of CH <sub>4</sub> is the presence of 1 wt% Amino Acids. ....	205
Figure 4-26: The shift in HLVE curve of CH <sub>4</sub> in the presence of 4-5 wt% amino acids (AA).. .....	206
Figure 4-27: The shift in the HLVE curve of CH <sub>4</sub> at different concentrations of L-Alanine.....	209
Figure 4-28: The shift in HLVE curve of CH <sub>4</sub> at different concentrations of Glycine..	211
Figure 4-29: The time delay in the CH <sub>4</sub> hydrate formation in the presence of 1 wt% amino acids.. .....	216
Figure 4-30: The time delay in the CH <sub>4</sub> hydrate formation in the presence of 5 wt% amino acids. ....	219
Figure 4-31: The time delay in the CH <sub>4</sub> hydrate formation in the presence of amino acids 5wt% L-Alanine, 5wt% Glycine and 4wt% Histidine at the low pressure of 40 bars.. ..	221
Figure 4-32: The time delay in the CH <sub>4</sub> hydrate formation in the presence of amino acids	

1 wt% PEO mixtures at wide process conditions..	225
Figure 4-33: The shift in the CH <sub>4</sub> HLVE curve in the presence of 5wt% choline ILs <sup>305</sup> , 5wt% amino acids, 5wt% ammonium ILs and 5wt% pyrrolidinium ILs. C.....	230
Figure 4-34: Comparison in the shift obtained for CH <sub>4</sub> HLVE curve in the presence of 10 wt% ammonium-based ILs [(DMEA)(Of), (DMA)(Of), (TBA)(Of) and (EA)(Of)]This work, 10 wt% amino acids [L-alanine, glycine], and 10 wt% imidazolium ILs [BMIM & EMIM].	234
Figure 4-35: Comparison in the shift obtained for CH <sub>4</sub> HLVE curve in the presence of 10 wt% Ammonium-based ILs [(DMEA)(Of), (TBA)(Of) and (EA)(Of)]This work, 10 wt% Amino Acids [L-alanine, glycine], and 10 wt% ethylene glycol [EG].....	237
Figure 4-36: Comparison in the shift obtained in CH <sub>4</sub> HLVE curve in the presence of different concentrations of amino acid glycine <sup>336</sup> and 10 wt % methanol.....	240
Figure 4-37: The comparison in the delay in CH <sub>4</sub> hydrate formation obtained for different amino acids + PEO and ionic liquids + PEO mixtures at 60 bars.....	243
Figure 4-38: Shows the comparison in the delay in CH <sub>4</sub> hydrate formation obtained for different amino acids + PEO and ionic liquids + PEO mixtures at 78 bars.....	244

## LIST OF ABBREVIATION

<b>Ionic Liquid</b>	<b>Abbreviation</b>	<b>Ionic Liquid</b>	<b>Abbreviation</b>
[Amim][Cl]	1-Alkyl-3-methylimidazolium chloride	[EMIM][EtSO <sub>4</sub> ]	1-ethyl-3-methylimidazolium ethyl sulfate
[BMIM][Ac]	1-butyl-3-methylimidazolium acetate	[EMIM][HSO <sub>4</sub> ]	1-ethyl-3-methylimidazolium hydrogen sulfate
[BMIM][BF <sub>4</sub> ]	1-butyl-3-methylimidazolium tetra-fluoroborate	[Emim][SCN],	1-ethyl-3-methylimidazolium thiocyanate
[BMIM][Br]	1-butyl-3-methylimidazolium bromide	[EMIM-BF <sub>4</sub> ]	N-ethyl-N-methylimidazolium tetrafluoroborate
[BMIM][CF <sub>3</sub> SO <sub>3</sub> ]	1-butyl-3-methylimidazolium sulfonate	[EMIM-BF <sub>4</sub> ],	1-ethyl-3-methylimidazolium tetrafluoroborate
[BMIM][CH <sub>3</sub> SO <sub>4</sub> ]	1-butyl-3-methylimidazolium methyl sulfate	[EMIM-Br]	1-ethyl-3-methylimidazolium bromide
[BMIM][Cl]	1-butyl-3-methylimidazolium chloride	[EMIM-CF <sub>3</sub> SO <sub>3</sub> ]	1-ethyl-3-methylimidazolium trifluoro-methane-sulfonate
[BMIM][ClO <sub>4</sub> ],	1-butyl-3-methylimidazolium perchlorate	[EMIM-Cl]	1-ethyl-3-methylimidazolium chloride
[BMIM][MeSO <sub>4</sub> ]	1-butyl-3-imidazolium methyl sulfate	[EMIM-EtSO <sub>4</sub> ]	1-ethyl-3-methylimidazolium ethyl sulfate
[BMIM][N(CN) <sub>2</sub> ]	1-butyl-3-methylimidazolium dicynamide	[EMIM-N(CN) <sub>2</sub> ]	1-ethyl-3-methylimidazolium dicynamide

[BMIM-BF <sub>4</sub> ]	1-butyl-3-methylimidazolium tetrafluoroborate	[EMMor][BF <sub>4</sub> ]	N-ethyl-N-methylmorpholinium tetrafluoroborate
[BMIM-Br]	1-butyl-3-methylimidazolium bromide	[EMMor][Br]	N-ethyl-N-methylmorpholinium bromide
[BMIM-Cl]	1-butyl-3-methylimidazolium chloride	[EMP-BF <sub>4</sub> ]	1-Ethyl-1-methylpyrrolidine tetrafluoroborate
[BMIM-DCA]	1-butyl-3-methylimidazolium dicyanamide	[EMP-Br]	1-Ethyl-1-methylpyrrolidine bromide
[BMIM-I]	1-butyl-3-methylimidazolium iodide	[EMP-Cl]	1-ethyl-1-methylpyrrolidine chloride
[BMIM-N(CN) <sub>2</sub> ]	1-butyl-3-methylimidazolium dicynamide	[EMPip][BF <sub>4</sub> ]	N-ethyl-N-methylpiperidinium tetrafluoroborate
[BMP][BF <sub>4</sub> ]	N-butyl-N-methylpyrrolidinium tetrafluoroborate	[EMPip][Br]	N-ethyl-N-methylpiperidinium bromide
[BMP-BF <sub>4</sub> ]	1-butyl-1-methylpyrrolidinium tetrafluoroborate	[HEMM-BF <sub>4</sub> ]	1-hydroxyethyl-1-methylmorpholinium tetrafluoroborate
[BMP-Br]	1-butyl-1-methylpyrrolidinium bromide	[HEMM-Cl]	1-hydroxyethyl-1-methylmorpholinium chloride
[BMP-Cl]	1-Butyl-1-methylpyrrolidine chloride	[HEMP][BF <sub>4</sub> ]	N-(2-hydroxyethyl)-N-methyl-pyrrolidinium tetra fluoroborate
[C <sub>10</sub> MIM][BF <sub>4</sub> ]	1-Decyl-3-Methylimidazolium Tetra fluoro borate	[HEMP-BF <sub>4</sub> ]	1-hydroxyethyl-1-methyl-pyrrolidinium-tetra-fluoroborate
[C2mim][OAc]	1-ethyl-3-methylimidazolium chloride	[HEMP-Cl]	1-hydroxyethyl-1-methylpyrrolidinium-chloride

[C <sub>4</sub> mim][PF <sub>6</sub> ]	1-Butyl-3-methylimidazolium hexafluorophosphate	[HMIM-Cl]	1-hexyl-3-methylimidazolium chloride
[Ch-But]	Choline butyrate	[N(CN) <sub>2</sub> ]	Dicynamide
[Ch-Hex]	Choline Hexanoate	[N <sub>2,2,2,2</sub> -Cl]	Tetra-ethyl-ammonium chloride
[Ch-iB]	Choline iso-butyrate	[OH-C <sub>2</sub> MIM-Cl]	1-hydroxyethyl-3-methylimidazolium chloride
[Ch-Oct]	Choline Octanoate	[OH-EMIM][BF <sub>4</sub> ]	1-(2-hydroxyethyl)-3-methylimidazolium tetrafluoroborate
[DMA][Of]	Dimethylammonium formate	[OH-EMIM][Br]	1-(2-hydroxyethyl) 3-methylimidazolium bromide
[DMEA][Of]	Dimethyl-ethylammonium formate	[OH-EMIM][Cl]	1-(2-hydroxyethyl) 3-methylimidazolium chloride
[DMIM-Cl]	1-decyl-3-methylimidazolium chloride	[OH-Emim][ClO <sub>4</sub> ]	1-hydroxyethyl-3-methylimidazolium perchlorate
[EA][Of]	Ethylammonium formate	[OH-Emmim][Cl]	1-hydroxyethyl-2,3-dimethylimidazolium chloride
[Emim][Ac]	1-ethyl-3-methylimidazolium acetate	[PMIM-I]	1-propyl-3-methylimidazolium iodide
[Emim][Cl]	1-ethyl-3-methylimidazolium chloride	[PMPy][Cl]	1-methyl-1-Propylpyrrolidinium Chloride
[Emim][Cl]	1-ethyl-3-methylimidazolium chloride	[PMPy][Triflate]	1-methyl-1-Propylpyrrolidinium Triflate

[Emim][ClO <sub>4</sub> ]	1-ethyl-3-methyl imidazolium per chlorate	[TBMA][O <sub>f</sub> ]	Tri-butylmethyl ammonium formate
---------------------------	---	-------------------------	-------------------------------------

TMAOH	Tetra-methyl ammonium hydroxide
-------	------------------------------------

<b>Compound</b>	<b>Abbreviation</b>	<b>Compound</b>	<b>Abbreviation</b>
AG	Anti-Agglomerates	MEG	Mono-ethylene glycol
Al <sub>2</sub> O <sub>3</sub>	Alumina	N <sub>2</sub>	Nitrogen
AlCl <sub>3</sub>	Aluminium (III) Chloride	Na <sub>2</sub> CO <sub>3</sub>	Sodium Carbonate
AlEtCl <sub>2</sub>	Ethyl aluminium Dichloride	Na <sub>2</sub> SO <sub>4</sub>	Sodium Sulfate
Ar	Argon	NH <sub>2</sub>	Amine
BCl <sub>3</sub>	Boron Trichloride	NO <sub>2</sub>	Nitrogen Dioxide
BF <sub>4</sub>	Tetra-Fluoroborate	NO <sub>3</sub>	Tritrate
Br <sup>-</sup>	Bromide	O <sub>2</sub>	Oxygen
C <sub>1</sub>	Methane	PEO	Polyethylene Oxide
C <sub>2</sub>	Ethane	PF <sub>6</sub>	Hexa-Fluoro-phosphate
CH <sub>3</sub> CO <sub>2</sub> <sup>-</sup>	Acetate	PIL	Protic Ionic liquids
CH <sub>4</sub>	Methane	PPM	Parts per million
Cl <sup>-</sup>	Chloride	PVCap	Poly-vinyl caprolactam

CO <sub>2</sub>	Carbon Dioxide	PVP	Poly-vinyl pyrrolidone
COOH	Carboxylic Acid	QM	Quaternary Gas Mixture
CuCl	Copper (I) Chloride	QSPRC	Quantitative structure property relationships
DSC	Differential scanning calorimeter	RC-5	Rocking Cell Assembly
EGME	ethylene glycol methyl ether	RPM	Rotations per minute
FCM	Functional Carbonaceous Material	Sc-CO <sub>2</sub>	Supercritical carbon dioxide
HLVE	Hydrate-Liquid Vapor Equilibrium	SiO <sub>2</sub>	Silica
HPC	High-Pressure Cell	SO <sub>4</sub>	Sulfate
ILs	Ionic Liquids	TEACL	Tetraethyl ammonium chloride
K <sub>2</sub> CO <sub>3</sub>	Potassium Carbonate	TGA	Thermogravimetric analysis
K <sub>3</sub> PO <sub>4</sub>	Potassium Phosphate	THF	Tetrahydrofuran
K <sub>3</sub> PO <sub>4</sub>	Potassium Phosphate	THI	Thermodynamic Hydrate Inhibitor
KHI	Kinetic Hydrate Inhibitor	TI	Thermodynamic inhibition
Kr	Krypton	VCAP	Caprolactum
LNG	Liquefied Natural Gas	Wt	Weight percent
NaCl	Sodium Chloride		



## CHAPTER 1: INTRODUCTION

Over the past decades, the offshore exploration and production of natural gas has increased all over the globe due to rising demand in the supply of natural gas and presence of rich oil and gas reserves in the oceans. Natural gas is widely used in many industrial processes as it causes fewer pollution problems and also produces less CO<sub>2</sub> emission in comparison to oil and coal. <sup>1</sup> This is the main reason that many power plants have been converted from coal to natural gas and many vehicles across the globe have been converted from petrol to natural gas fuel.

It is estimated that one-third of total oil and gas global demand is met from offshore sources and the demand for the natural gas fuel will increase significantly over the next decade.<sup>2</sup> Therefore, the natural gas exploration needs to be carried out in deep oceans and permafrost region, where high pressures and lower temperature conditions are common, leading to the major flow assurance issues [Figure 1-1].

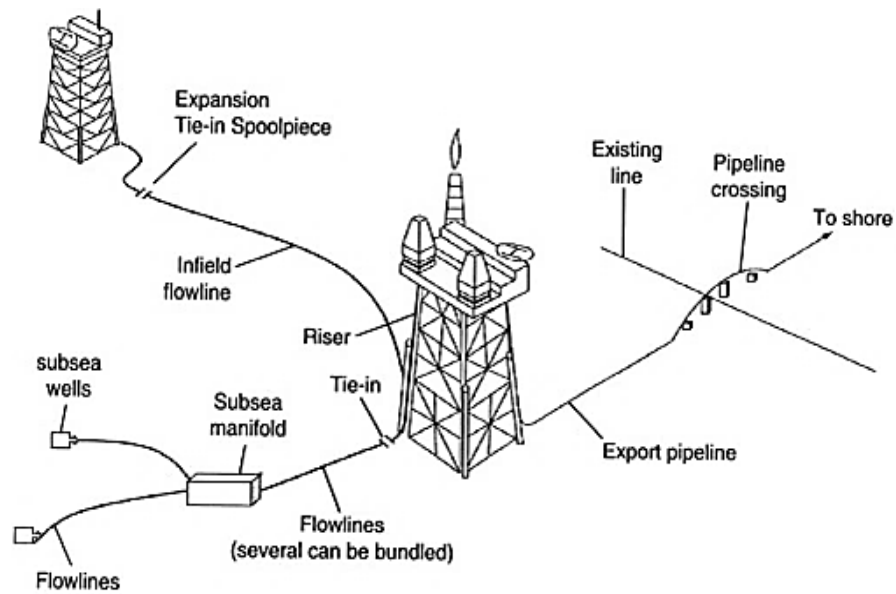


Figure 1-1: A typical offshore oil and gas production facility ( taken from Barrette <sup>3</sup>)

The flow assurance is considered to be a major challenge in the offshore exploration and production. In a simple terminology, the flow assurance focuses on the entire production life cycle from the reservoir to the refining unit to ensure the smooth transfer of hydrocarbons from the reservoir to the refinery without any interruption.<sup>4</sup> According to Hill, et al. <sup>5</sup>, the term flow assurance actually refers to the practice of ensuring that the production fluids are transported from the wellhead to the production facility without any hindrance or obstacle.

Hill, et al. <sup>5</sup>, stated that the major flow assurance issues involve plugging and blockages in the pipelines as result of the formation of hydrates, waxes, and asphaltenes in them. In a study involving 50 senior flow assurance experts from different industries, the formation of hydrates was identified as the major threat to the flow assurance.<sup>6</sup> These crystalline compounds tend to easily form in the subsea lines and can lead to the blockages in the subsea lines.<sup>7</sup>

*Figure 1-1*, shows a typical offshore facility where hydrate formation is likely to take place. According to Sloan, et al. <sup>8</sup>, the hydrate formation is likely to occur in the free water, just downstream of water accumulation, where the change in the flow geometry takes place ( such as a bend in the pipeline or restriction across the valve) or at other free sites where hydrates can get the place for nucleation. Sloan, et al. <sup>8</sup>, stated that the formation of hydrate plugs take place during momentary operations such as operational start-up, operational shut-in, restart of the system after an emergency or when the free water is present in the pipeline due to the failure of the dehydrator or inhibitor injection pump.

Kinnari, et al. <sup>9</sup>, also stated that the hydrate formation is most likely to occur during operations shut in, when inhibitor delivery pumps are not functioning well or when the water content in the subsea lines is high.<sup>9</sup> Aminnaji, et al. <sup>10</sup>, stated that the blockage in pipelines due to hydrate formation can also occur in some cases due to

underestimation of water cut production, unplanned shut-in or inappropriate inhibitor injection method.<sup>10</sup>

Sloan, et al. <sup>8</sup>, also highlighted that the oil-dominated systems due to higher heat capacity are less likely to suffer from hydrate plugs in comparison to the gas-dominated system. The oil production flow lines are well insulated, which allows maintaining flow line temperature as high as possible. In comparison, the gas dominated system tends to cool more rapidly and requires the injection of hydrate inhibitors for the prevention of hydrate plugs.

The major cause of concern for the hydrate formation occurs during the plant shutdown. During the shutdown period, the pipeline fluid tends to cool down to the seabed temperature, which can lead to hydrate formation unless the pipeline is depressurized. According to Kanu, et al. <sup>11</sup>, the hydrate formation can also occur also in the multiphase flow of oil and gas systems. <sup>11</sup> According to Teixeira, et al. <sup>12</sup>, the other major concern of hydrate formation occurs at the point of depressurization. As the gas extracted from the offshore reservoir carries extremely high pressure that pipeline may not be able to support. Therefore, the gas must be depressurized prior it is diverted towards the pipeline and the depressurization can lead to the reduction of temperature facilitating the formation of hydrates.

## 1.1 Hydrate Structures & Properties

Natural gas hydrates are solid, non-stoichiometric compounds that are composed of small gas molecules and water.<sup>13</sup> The formation of hydrates occurs when smaller gas molecules like methane or ethane get trapped within the micro-cavities of water molecules at low temperature and high-pressure conditions. Physically, these compounds are non-flowing crystalline solids that are heavier than typical fluid hydrocarbons.<sup>14</sup> The gas hydrates were discovered in 1810 by Sir Humphry Davy when during experiments he observed that solution of chlorine in gas froze more rapidly compared to pure water.<sup>15</sup>

Figure 1-2, the X-ray analysis<sup>15-16</sup> show that gas hydrate exists in three typical structures such as cubic structure I (sI), cubic structure II (sII) and hexagonal structure H (sH).<sup>17</sup> The small gas molecules such as CH<sub>4</sub>, and CO<sub>2</sub> form sI cubic structure, the C<sub>3</sub>H<sub>8</sub> and iso-C<sub>4</sub>H<sub>10</sub> form sII cubic structure and larger molecules form hexagonal structure (sH)<sup>1</sup>. The structures SI and SII are most likely to occur in the industry.

The hydrate cluster formation occurs when small (< 0.9 nm) guest molecules like CH<sub>4</sub> or CO<sub>2</sub> get in contact with water molecules at ambient temperature (less than 300 K) and moderate pressure (more than 6 bars). These small guest molecules are en-caged in the hydrate clusters via hydrogen-bonded water cavities in these non-stoichiometric structures. The repulsion caused by these guest molecules opens different sizes of water cages, which come together to form a cubic crystal structure.

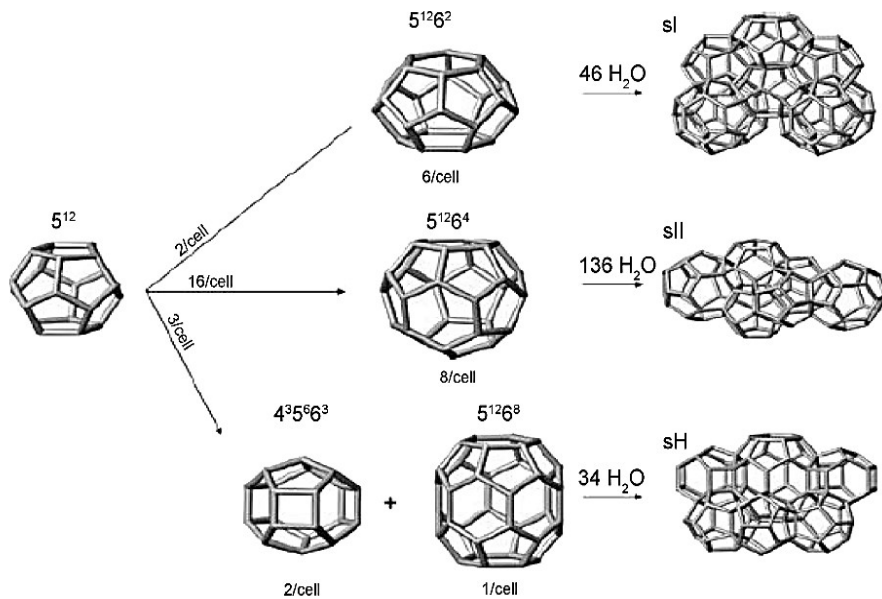


Figure 1-2: Gas Hydrate crystal structures (taken from Sulaimon and Tajuddin<sup>18</sup>)

Table 1-1, shows the hydrate crystal structure properties. The cubic structure SI dominates the earth's atmosphere and contains small guest molecules (0.4-0.55 nm). The structure SII contain larger guest molecules (0.6-0.7 nm) and the structure H contains mixtures of both small and large guest molecules (0.8-0.9 nm). The guest molecules smaller than 0.4 nm (Ar, Kr, O<sub>2</sub>, and N<sub>2</sub>) are likely to form structure SII. The comparison between the properties of ice and hydrate structure I & II is shown in Table 1-2.

In all three structures of gas hydrates, there is only one guest molecule that lies within each cage [Table 1-1]. However, at very high pressure it's likely to have multiple

cage occupancy with small guest molecules like hydrogen or noble gases. The three crystal structures have similar components concentrations: 85 mol % water and 15 mol % gas molecules. It is known that the hydrate formation occurs at the interface between the bulk guest and aqueous phases.

Table 1-1: *Showing Hydrate crystal structure properties (data taken from Sloan <sup>1</sup>)*

Hydrate Crystal	I		II		H		
Structure							
Cavity	Small	Large	Small	Large	Small	Medium	Large
Dimension	5 <sup>12</sup>	5 <sup>12</sup> 6 <sup>2</sup>	5 <sup>12</sup>	5 <sup>12</sup> 6 <sup>4</sup>	5 <sup>12</sup>	4 <sup>3</sup> 5 <sup>6</sup> 6 <sup>3</sup>	5 <sup>12</sup> 6 <sup>8</sup>
Number of cavities per unit cell	2	6	16	8	3	2	1
Average cavity radius (Å)	3.95	4.33	3.91	4.73	3.91 <sup>∞</sup>	4.06 <sup>∞</sup>	5.71 <sup>∞</sup>
Coordination number*	20	24	20	28	20	20	36
Number of waters per unit cell	46		136		34		
Guest Molecule	Methane, Ethane, Carbon dioxide etc		Propane, Iso-butane etc		Methane + Neo-hexane, Methane + Cyclo-pentane		

\* Number of oxygen at the periphery of each activity  
<sup>∞</sup>Estimate of structure H cavities from geometric models

The flow assurance issue caused by natural gas hydrates takes place as a result of slow cooling of oil and gas in the pipeline or due to rapid cooling as the result of

depressurization in the valves installed on the pipeline or other offshore units.<sup>19</sup> The key conditions which lead to the formation of the gas hydrates in the oil and gas pipelines include the presence of water and components, the low temperature, the high pressures and other prompting factors like high fluid velocities, agitation, pulsations or any other source of fluid turbulence.<sup>20</sup>

The comparison of the properties of ice, hydrate structure I and hydrate structure II is shown in Table 1-2. The section 2.4 will discuss the effect of agitation on the rate of hydrate formation, from the perspective of natural storage and transportation



Table 1-2: Comparison of the properties of ice, hydrate structure I, structure II (data taken from <sup>19-20</sup>)

Property	Ice	Hydrate Structure I	Hydrate Structure II
Water Molecule Number	4	46	136
Lattice parameters at 273 K, nm	A=0.452, c= 0.736	1.20	1.73
Dielectric constant at 273 K	94	~58	58
Water diffusion correlation time, $\mu$ s	220	240	25
Water diffusion activation energy, bindkJ/m	58.1	50	50
Isothermal Young's modulus at 268 K, $10^9$ Pa	9.5	~8.4	~8.2
Poisson's ratio	0.33	~0.33	~0.33
Bulk modulus (272 K)	8.8	5.6	N/A
Shear modulus (272 K)	3.9	2.4	N/A
Compressional velocity ( $V_p$ ), m/s	3870.1	3778.0	3821.0
Shear velocity ( $V_p$ ), m/s	1949	1963.6	2001.1
Heat Capacity, $J kg^{-1} K^{-1}$	3800	3300	3600
Thermal conductivity (263K), $W m^{-1} K^{-1}$	2.23	$0.49 \pm 0.02$	$0.51 \pm 0.02$
Density, $Kg m^{-3}$	916	912	940

## 1.2 Hydrate Plugging and Offshore Flow assurance

In deep sea water the temperature is much cooler than the surface air temperature, if there is no thermal insulation layer surrounding the pipe wall, the hydrocarbon fluid heat can be easily lost to the sea water. This is the most likely case when the water current surrounding the submerged sea water pipeline is strong. <sup>21</sup>

When the subsea pipeline is not well insulated the heat transfer coefficient is

high due to forced convection by the sea water movement. This lowers the fluid temperature inside the pipeline causing the formation of hydrate and blockage of the flow. If the fluid temperature in the pipeline drops low enough the formation of wax occurs and it starts depositing on the pipe wall.<sup>21</sup>

Generally, in the deep sea water, the pipeline is followed up by a riser, which tends to go from the bottom of the sea to the surface processing facilities [Figure 1-1]. The deeper the water, the longer is the production riser. The longer the production riser, the higher the pipeline operating pressure should be due to hydrostatic head in the riser. Therefore, for the same fluid temperature, the higher operating pressure may lead to the formation of the hydrate slug, which may be proportional to the length of the riser.<sup>21</sup>

Figure 1-3, shows the formation of the hydrate plug in the pipeline. According to Makogon<sup>22</sup>, the hydrate plugging in the pipeline can cause operation shut down and it can take weeks for the plug removal in the offshore gas pipeline.<sup>22</sup> This is likely to cause financial losses and maintenance issues. In the worse cases, the formation of hydrates can cause a rupture in the pipeline and post a safety threat to nearby operators.

As shown in Figure 1-3, the formation of hydrates reduces the internal diameter of tubular piping and restricts the flow of hydrocarbons across the pipelines. The

formation of hydrates also increases the surface roughness of the pipe wall, increases the pumping pressure, reduces the flow throughput, causes accumulations in the process vessels and storage tanks and cause interference with the valve operation and instrumentation.<sup>23</sup> Generally, the hydrate formation is likely to occur due to the presence of free water in the pipeline, drop of pipeline temperature to 4°C or lower and higher operating pressure of up to 12 bars.<sup>23</sup>



*Figure 1-3: Gas Hydrate plug formation inside pipeline (Excerpted from Makogon <sup>22</sup>, Boschee <sup>24</sup> and Bratland <sup>25</sup>) courtesy BP, Petro-bas, SPE and Offshore Engineering.*

Figure 1-4, shows the hydrate formation mechanism proposed by Lederhos, et al. <sup>26</sup> According to Lederhos, et al. <sup>26</sup>, the hydrate formation process consists of four key stages. Initially, the temperature and pressure parameters exist within the hydrate formation zone, however, no gas molecules dissolve within the water may be due to lack of driving force. But as the temperature goes further down or pressure increases, the water and gas molecules interact and form small clusters [B]. At the interval [B], the newly formed hydrate clusters are unstable. These small clusters can either further grow into metastable hydrate cells or may dissociate back into gas and water [Figure 1-4]

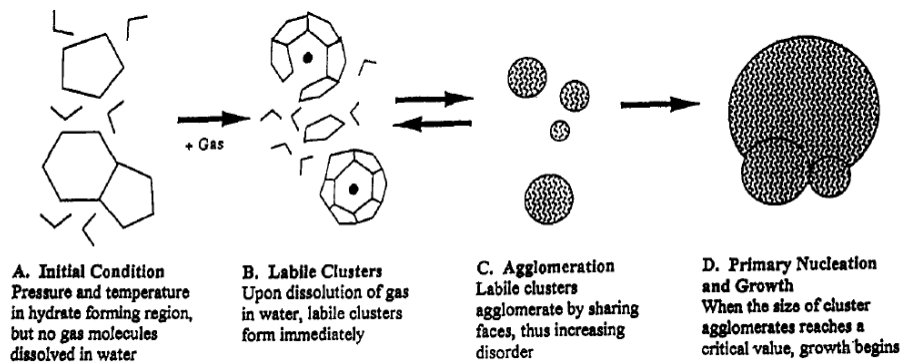


Figure 1-4: Mechanism of the hydrate formation ( taken from Lederhos, et al. <sup>26</sup>)

However, if the conditions permit, these clusters tend to agglomerate and form metastable hydrate unit cells [C]. Then may be due to stochastic process (via Brownian motion) these metastable hydrate unit cells may grow larger in size at a slower pace until they reach a critical size. Once these metastable hydrate unit cells reach a critical radius, they tend to grow spontaneously at much faster rate [D]. This period of faster hydrate growth is known as the interval of catastrophic hydrate growth. It is the period of catastrophic hydrate growth which considered as the main cause of plugging in the pipelines [Figure 1-4]

Sun and Firoozabadi <sup>27</sup>, proposed that the surface of the hydrate is intrinsically hydrophilic and a tinny layer of liquid water film lie on the hydrate surface which causes the occurrence of a capillary bridge between hydrate particles.<sup>27</sup> It is the capillary force that is liable for holding the hydrate particles together and causes agglomeration which causes plugging in offshore subsea pipelines.<sup>28 29</sup>

The gas hydrate plugging issues have been reported in many fields and most incidents reported in the literature correspond to gas-dominated fields. The hydrate formation is frequently reported in the Caspian Sea, the North Sea and permafrost regions like Alaska, where crude oil is transferred under high pressures and low temperatures conditions, causing the formation of hydrates and subsea line blockages.<sup>30</sup> In the Gulf of Mexico, where the drilling operations are conducted at the water depth of 3 Km, the pressure tends to go as high as 300 bar, and the temperature can go down

to 2–4 °C, leading to the formation of in pipelines.<sup>31</sup> In the middle-east region, the risk of hydrates formation is a threat during the winter months.<sup>32</sup>

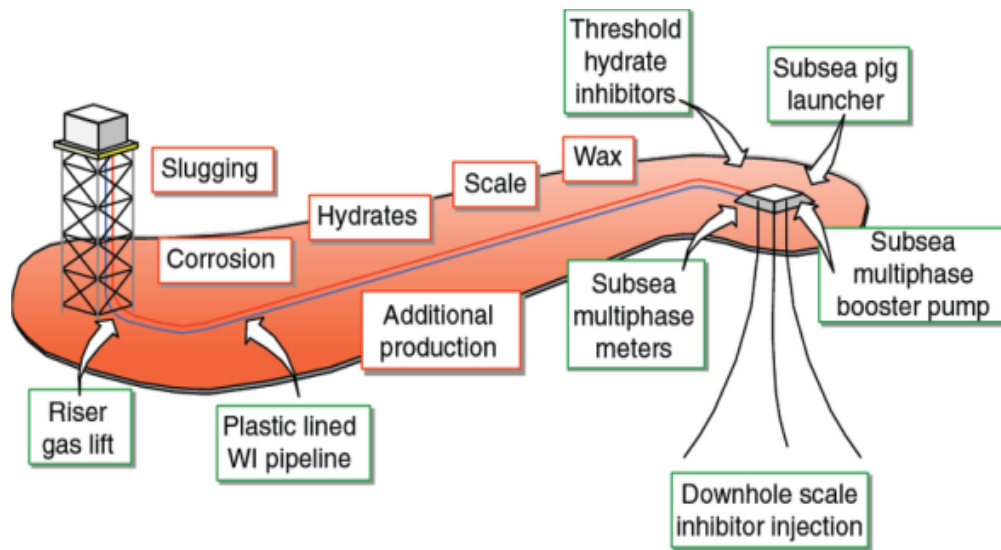


Figure 1-5: The major flow assurance issues in the subsea tie back system [Courtesy BP].

(taken from Arnold<sup>4</sup>)

Severe hydrate plugging issues have also been reported in the >20 miles subsea tieback [Figure 1-5] in the Gulf of Mexico<sup>33</sup>, in gas injection line in Gulf of Guinea<sup>34</sup>, an export gas pipeline in the Gulf of Mexico<sup>35</sup>, and main gas export pipeline from Pompano platform<sup>36</sup>. BP (British Petroleum) also reported hydrate blockage in a 16-in jumper connecting the Atlantis gas export line to the Mardi Gras gas transport system in the

Gulf of Mexico. Chevron also reported the hydrate blockage issue in the gas condensate well in offshore South America.<sup>37</sup> The hydrate plugging issue was also reported in the Statoil offshore gas field in the Barents Sea as well.<sup>38</sup> In addition to that, the formation of gas hydrate is also considered the cause of Deep Water Horizon rig explosion in the Gulf of Mexico in 2010.<sup>39</sup> Therefore, annually the oil and gas industry spends over a billion US \$ on the hydrate prevention procedures that include the use of large dosages of chemical thermodynamic hydrate inhibitors.<sup>40</sup>

### **1.3 Hydrate Inhibitors**

The hydrate inhibitors can be classified into three categories which include thermodynamic hydrate inhibitors (THIs), kinetic hydrate inhibitors (KHIs) and anti-agglomerants (AAs). The THI function by shifting the hydrate liquid-vapour equilibrium (HLVE) curve to lower temperature or unfavourable conditions. The KHIs function by slowing down the hydrate formation or kinetics of hydrate nucleation. The AAs do not interfere with thermodynamics or kinetics of hydrate formation, they are just dispersing agent and they prevent the growth of the hydrate plugs. These anti-agglomerates (AG) prevent hydrate crystals from growing larger in sizes, but do not inhibit the hydrate formation.<sup>41</sup>

#### ***1.3.1 Thermodynamic Hydrate Inhibitors***

The common industrial practice for preventing the risk of hydrate formation involves the use of thermodynamic hydrate inhibitors (THIs) like methanol or monoethylene glycol (MEG). These THI prevent the risk of hydrate formation by shifting the

hydrate liquid vapour-liquid equilibrium (HLVE) curve to lower temperatures.<sup>42</sup> These THIs tend to be hydrophilic compounds that are required in high concentration (> 30 wt%) in the liquid phase in order to bind strongly with the water molecules and reduce water molecules fugacity and potential activity.<sup>12</sup>

As THIs are required in high concentration, they can also be classified as high dosage inhibitor. Some other examples of THI include di-ethylene glycol (DEG), tri-ethylene glycol (TEG), small chain alcohols like ethanol and hydrophilic inorganic salts like NaCl and KCl. The effectiveness of most THI does not rely on the temperature and they can be used over a wide range of temperatures, with exception of TEG and DEG which can cause problems at lower temperatures.<sup>12</sup>

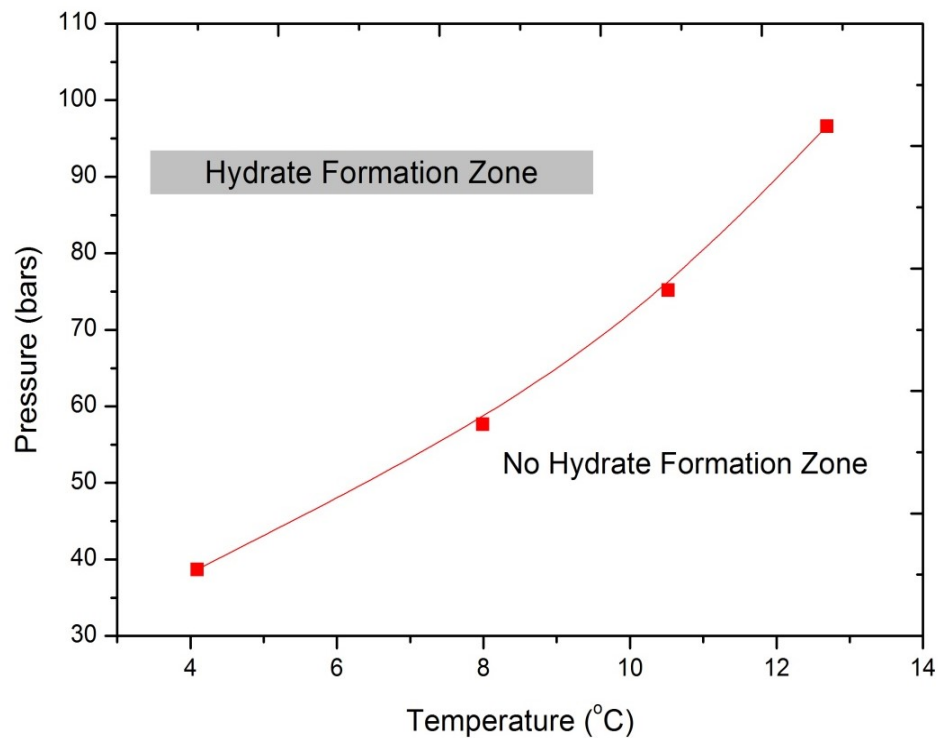
Normally, the oil, and gas industry injects THIs like mono-ethylene glycol into the flowing stream at the wellhead to reduce the water available for the solid hydrates.<sup>1</sup> For example, mono-ethylene glycol is added to the wellhead in proportional to the water flow rate to prevent the hydrate formation in subsea lines. The MEG is widely used as the THI due to its favourable features like low losses to vapour phase, low solubility in condensate phase, high depression of water freezing point, high depression for gas hydrate formation temperature and ability to weaken the corrosion potential of water.

43

As shown in Figure 1-6, the thermodynamic inhibitor MEG function by shifting the hydrate HLVE curve to lower temperature conditions and prevent the hydrate



formation by adhering with free water molecules in the subsea line. The MEG tends to get contaminated with water molecules and impurities present in the subsea line (aqueous MEG contains at least 25 wt% of water and salts) and it comes out the onshore facility as the Rich-MEG. Due to the high cost of replacing a large amount of THI, the Rich-MEG needs to be recycled in the special MEG recovery units.<sup>43</sup>



*Figure 1-6:* The pure methane Hydrate Vapor-Liquid Equilibrium (HVLE) points at different pressure conditions.

On the onshore MEG recovery units, the MEG is de-contaminated and recycled back towards the wellhead as the Lean-MEG to be injected again in the subsea lines. However, the recycled Lean-MEG (80 wt% of MEG) loses its potential to adhere with free water molecules over the period of time and it needs to be replaced with the new MEG.<sup>43</sup>

The THIs like MEG work well, but as mentioned above they are required in bulk quantity ( $\geq 30$  wt%), making them environmentally prohibitive.<sup>44</sup> Also, many storage and disposal issues are associated with them. Therefore, by reducing the required dosage of hydrate inhibitors and reducing their negative environmental impact, a potential environmental and economic advantage can be achieved.

It was reported by Sloan<sup>1</sup>, that annually the industry spends over 200 million US\$ on the purchase of THI like methanol to prevent hydrate formation. Also, a large sum of money is required to develop and maintain methanol storage facility on offshore plate forms and financial penalties need to be paid for the methanol contaminations ( $> 50$  ppm) in refinery feedstocks.<sup>1</sup> This is the main reason that industry interest has shifted towards the use of kinetic hydrate inhibitors (KHI).<sup>41</sup> The appealing factor for the industrial usage of KHIs is that there is no need for recovery of KHIs if they meet environmental constraints and are cost effective. This can help to save the cost of building and maintaining inhibitor recovery and separation units.

### ***1.3.2 Kinetic Hydrate Inhibitors***

The low-dosage hydrate inhibitors (LDHI) in the form of kinetic hydrate inhibitors are gaining wide attention due to their ability to provide hydrate inhibition at very low dosages ( $\leq 1$  wt%) and the appealing factor that there is no need to recover these inhibitors after usage provided they meet environmental constraints and are cost effective.<sup>45</sup> The KHIs is also being used together with THI to reduce the large quantity of THI required to provide the necessary hydrate inhibition and also it is reported that these KHI does not need to be recycled, which helps to reduce the CAPEX cost.<sup>46</sup>

The KHIs tend to adhere to the initial hydrate nucleating particle and retard the further nucleation and growth of hydrate particles. The temperature does have an effect on the inhibition performance of the KHI, as low temperatures can affect the anti-nucleating action of these KHIs. However, these KHIs don't require the presence of liquid hydrocarbons with water in order to be effective.<sup>43</sup>

The first commercial kinetic hydrate inhibitors (KHI) used for hydrate inhibition were the homo and copolymers of N-vinyl lactams such as N-vinylpyrrolidone (VP) and N-vinyl caprolactam (VCap).<sup>47</sup> It was also observed that these polymers function well and provide good kinetic inhibition performance when used in combination with solvents like glycol ether and mono-ethylene glycol.<sup>48</sup> It has been observed that by increasing the lactam ring size the kinetic inhibition performance of these KHI increases.<sup>49</sup> The actual mechanism of hydrate inhibition by kinetic hydrate inhibitor is still not

clear. However, there are some hypotheses reported regarding the inhibition mechanisms of the kinetic hydrate inhibitors reported in the literature previously.

King Jr, et al.<sup>50</sup>, proposed that KHI tend to function by adhering on the surfaces of growing hydrate crystals (sub-critical or super-critical size), which inhibits and prevents the further growth of hydrate crystals.<sup>50</sup> Lederhos, et al.<sup>26</sup>, also proposed that the KHI like polymers tend to adsorb on the hydrate surface and block the further growth of the hydrate crystals. According to Lederhos, et al.<sup>26</sup>, suggested that the KHI extends its network between the small and stable hydrate particles and block the most active growth sites of the hydrate crystals. This prevents the further growth of the hydrate crystals. However, this proposed mechanism is different from the mechanism proposed by Storr, et al.<sup>51</sup>.

According to Storr, et al.<sup>51</sup>, instead adhering on hydrate crystal surface, the KHI inhibitors adhere on the surface of the “foreign” particles that would otherwise act as a site for heterogeneous hydrate nucleation.<sup>51</sup> However, based on the molecular simulation observations a different mechanism was proposed by the Long, et al.<sup>52</sup>

Long, et al.<sup>52</sup>, based on the simulation observation, proposed that perturbation of liquid water structure by the KHI prevents the growth of hydrate crystals to the critical cluster size or destabilizes the partially formed hydrate clusters completely.<sup>52</sup> Figure 1-7, shows the illustration of both perturbation inhibition and the adsorption

inhibition mechanisms of the KHI.

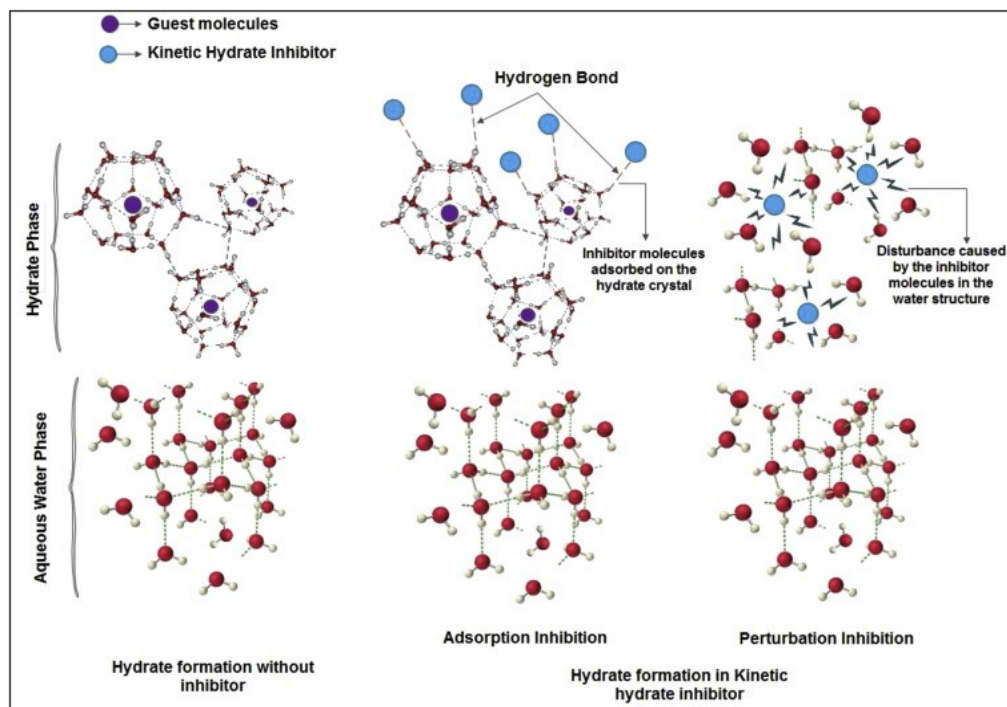


Figure 1-7: Kinetic hydrate inhibition mechanisms reported in the literature (taken from Kakati, et al. <sup>53</sup>)

### 1.3.2.1 A new class of kinetic hydrate inhibitors (KHIs)

The ionic liquids (ILs) are considered as the new class of kinetic hydrate inhibitors that are well known as dual-functional inhibitors. <sup>54</sup> They are classified as organic salts that can exist in a liquid phase at the ambient temperature. The tunable nature of ionic liquids allows designing them as environmentally friendly compounds by carefully selecting the right combination of cation and anion. The ILs have negligible vapour pressure and higher decomposition temperature. <sup>27, 28</sup>

Many studies have deemed them as “environmentally friendly inhibitors”<sup>55</sup> The ILs can be categorized as aprotic and protic ILs.<sup>56</sup> The aprotic ILs are considered to be classic or traditional ILs and the protic ionic liquids (PILs) are relatively new class of ionic liquids that are gaining wide attention due to their excellent electrolytic properties and low-cost compared to classic ILs.

Amino acids are biological compounds containing amine (-NH<sub>2</sub>) and carboxylic acid functional groups (-COOH) that naturally exist in nature and are manufactured on large scale. They can also be considered as a new class of KHIs, which have been previously used as environmentally friendly corrosion inhibitors<sup>57</sup>. In comparison to ILs, the amino acids are manufactured on a larger scale and their usage as hydrate inhibitors can be more economical and environmentally suited.

In this dissertation, both amino acids and ionic liquids have been tested as the THI and KHI on the pure methane gas and its mixture with and without the presence of synergents at wide process conditions. The synergents were added with amino acids and ionic liquids, to reduce their required dosage and test if these synergents can help to improve the overall hydrate inhibition effect of both amino acids and ionic liquids. The hydrate inhibition results obtained for both amino acids and ionic liquids were then compared with the hydrate inhibitors reported in the literature.

## 1.4 Research Objectives

Qatar has the world's third-largest reserves of natural gas which is estimated at 885 trillion cubic feet and LNG exports of around 77 Million metric tones (MMT) annually.<sup>58</sup> Normally, due to its warm climate the gas hydrate formation was considered an unlikely event in Qatar. However, hydrate formation can also occur at the warm temperature of around 35 °C, if the high pressure and high water contents are present within the pipeline<sup>43</sup>

It is also important to mention that Qatar natural gas reserves are located 80 km offshore North Field and the reliable supply of Qatar Liquefied natural gas (LNG) relies on the continuous flow from offshore wellheads to onshore processing facilities. According to Mohamed<sup>59</sup>, the Qatar Oil and Gas industry also faced hydrate formation threats between the period 2011 and 2013 which lead to un-expected production shut down. Therefore, this theses work intents to develop knowledge and facilitate the on-going research work in the area of hydrate prevention and mitigation. This dissertation provides a new insight into the chemical compounds that have a potential to act as a hydrate inhibitor. All the dissertation findings are backed by the strong experimental evidence and a good comparison with the literature results has also been provided. Following are the key research objectives of this Ph.D. dissertation:

- i. Analyze the potential of using pyrrolidinium based ionic liquids as hydrate inhibitors and study the effect of different anions, different ionic liquid dosages and different experimental pressures (40-120 bar) on the QM mixture hydrate

inhibition. Correspondingly, examine the role of synergents in enhancing the hydrate inhibition effect of pyrrolidinium at different pressure conditions.

- ii. Analyze the potential of using ammonium-based protic ionic liquids as hydrate inhibitors and study the effect of different cations, different ionic liquid concentrations and various experimental pressures (40-120 bar) on the pure methane hydrate inhibition. Comparably, inspect the role of synergent PEO in stimulating the kinetic inhibition effect of ammonium ionic liquids at diverse pressure conditions.
- iii. Inspect the prospect of using amino acids as hydrate inhibitors and explore the effect of solubility factor and different pressure conditions on the hydrate inhibition strength of amino acids. Additionally, probe the role of synergent PEO in prompting the kinetic inhibition performance of the amino acids.
- iv. Analyze the effect of mechanical factors like stirring or agitation on the rate of hydrate formation at variable speeds (100-1400 RPM) and identify the interval of catastrophic hydrate crystal formation inside the stirred cell.



## 1.5 Thesis Structure

An overview of the hydrates, hydrate inhibitors, and flow assurance issues related to hydrates have been provided in this chapter. This dissertation work is mainly experimental and the commercial simulation software like WatGas has been only used to validate our experimental results. A brief description of the dissertation chapters is provided below:

Chapter 1: Is an introductory chapter that provides an insight to the problem of hydrate formation in the oil and gas industry. It describes hydrate formation mechanism and also highlights different types of chemical inhibitors used in the industry for hydrate prevention. The chapter also lists key research objectives and briefly describes different hydrate structures and their relevant properties.

Chapter 2: Provides a literature review/ background on the relevant research work conducted using ionic liquids, amino acids, and synergents as methane gas hydrate inhibitors over the period of last 5-10 years. Also, a section on the effect of stirring on hydrate formation has been provided. In addition to that, a brief review of ionic liquids, ionic liquids industrial applications, ionic liquids thermo-physical properties, and ionic liquids synthesis has also been provided. The section also provides fundamental details and mechanisms behind hydrate inhibition carried out using amino acids and ionic liquids.

Chapter 3: Presents experimental details about the methods and procedure used for testing the ionic liquids and amino acids as methane hydrate inhibitors. The experimental work has been conducted using pure methane gas and quaternary gas mixture (QM). The chapter also provides the list of ionic liquids and amino acids tested in this work along with their purity index and relevant solubility in aqueous solution.

Chapter 4: Offers an insight into the experimental results obtained for the tests conducted using ionic liquids, amino acids, and synergents. The results obtained for effect of stirring on hydrate formation is also discussed in detail. Moreover, the results obtained for the amino acids and ionic liquids as methane inhibitors have been compared with the 21 imidazolium ionic liquids, 5 choline ionic liquids, 2 ammonium ionic liquids and 2 industrial hydrate inhibitors methanol and mono-ethylene glycol reported in the literature.

Chapter 5: Provides the conclusion and overall discussion of the experimental findings and draws a comparison between the effectiveness of ionic liquids and amino acids as the hydrate inhibitors for the industrial usage. It also highlights the new areas of research that emerge out of the work conducted in this dissertation. This work was mainly based on the gas dominated system, in future the same work needs to be conducted on the oil dominated system with some actual field tests in collaboration with industry.

## CHAPTER 2: BACKGROUND

In this chapter, an overview of ionic liquids and amino acids characteristics has been provided. The details about their synthesis procedures, industrial applications and thermo-physical properties have been provided in sections 2.1 and 2.2. Accordingly, a comprehensive literature review of the research work conducted using ionic liquids and amino acid in the field of gas hydrates is also provided. The reported inhibition mechanisms using amino acids and the factors that affect the performance of ionic liquids and amino acids as the hydrate inhibitors have also been discussed in detail.

Correspondingly, there is a section 2.3 in a chapter that provides a background on the role of synergents in accelerating the inhibition performance of the hydrate inhibitors. The relevant studies conducted using synergents in the field of gas hydrate have also been reported in section 2.3.

The section 2.4 of the chapter, discusses the factors, other than the chemical promoter, that can accelerate the rate of hydrate formation from the perspective of gas hydrate storage and transportation. The background details on the effect of mechanical factors like agitation or stirring on the rate of hydrate formation have been discussed along with the literature reference.

## 2.1 Hydrate Inhibition using Ionic Liquids (ILs)

Ionic liquids (ILs) also known as liquid salts or ionic fluids are organic salts that have a low melting point and exists in a liquid state at ambient temperature.<sup>60</sup> The ILs are widely used in green chemical processes as they have low vapour pressure.<sup>61</sup> They have a tendency to offer high electrical conductivity; high selectivity and many classes of ILs tend to be non-flammable.<sup>62</sup> Therefore, it's beneficial to use ILs as organic solvents from both environmental and technological perspectives.<sup>63</sup>

Generally, ILs tend to be stable in the water and air medium. Their physical properties rely on the alkyl chain length of the cation or the type of the anion used.<sup>64</sup> ILs are also known as tailor-made solvents as they can be designed for specific processes. The structure of ILs normally consists of cations that are bulky organic molecules containing positively charged nitrogen, sulfur or phosphorus atom.

The most commonly studied ILs in the literature include N, N-dialkyl imidazolium<sup>65</sup>, N-alkyl pyridinium<sup>66</sup>, alky-ammonium<sup>67</sup>, alkyl-phosphonium<sup>68</sup> and alkyl-sulphonium<sup>69</sup> cations. The most common anions used for ILs are inorganic and organic species which includes halides [Br<sup>-</sup>, Cl<sup>-</sup>], tetra-fluoroborate [BF<sub>4</sub><sup>-</sup>], hexa-fluoro-phosphate [PF<sub>6</sub><sup>-</sup>], acetate [CH<sub>3</sub>CO<sub>2</sub><sup>-</sup>] and dicyanamide [N(CN)<sub>2</sub><sup>-</sup>].<sup>70</sup>

The ILs can be classified as aprotic and protic ILs.<sup>56</sup> The aprotic ILs are considered

to be classic or traditional ILs and their structures consist of bulky organic cations such as imidazolium or pyridinium and anions such as  $\text{Cl}^-$ ,  $\text{Br}^-$ ,  $\text{BF}_4^-$  and  $\text{PF}_6^-$ .<sup>71</sup> The protic ILs, on the other hand, are made via proton transfer from Bronsted acid to Bronsted base.<sup>72</sup> The protic ionic liquids (PILs) are known to be an excellent electrolytic material offering good ionic conductivity, long-term durability and are being used in lithium batteries as an electrolyte.

The protic ionic liquid also offers good optical transparency and high photo-stability of the electrolyte<sup>73</sup>. They are also favourable as they offer high thermal and chemical stability, good electrochemical properties, low vapour pressure and have the ability to intercalate into polymers and electrolytic solutions. They are also used in multiple applications such as organic synthesis<sup>74</sup>, fuel cells and chemical sensors<sup>75</sup>, biosensors, electrodeposition, electrochemical Exfoliation etc. Additionally, PILs are also actively used in different biological applications (Biomass Conversion, Extraction of Bioactives, Biocatalysis and Protein Crystallization).<sup>76</sup>

Most literature works, advertise ILs as non-flammable compounds with negligible vapour pressure and strong thermal stability (250 °C - 450 °C). However, not all ILs can be considered safe and environmentally friendly. According to Smiglak, et al.<sup>77</sup>, special precaution are required when working with imidazolium, pyridinium and phosphonium ILs near an ignition source. Similarly, Meine, et al.<sup>78</sup> found that 10 percent of imidazolium-based IL with bromide halide degraded when the temperature was raised

to 200 °C and maintained for 24 hrs.

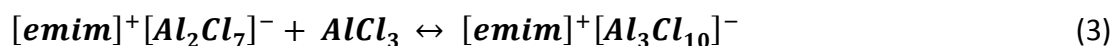
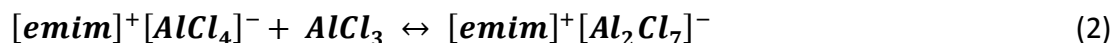
### ***2.1.1 Ionic liquids: Synthesis & Application***

The synthesis of ILs relies on the factor that they must be either hydrophilic or hygroscopic.<sup>79</sup> If the components used in the synthesis of ILs are hydrophobic they will exist in a separate phase from water and won't be able to access water molecules.<sup>80</sup> The second functional groups like oxygen or hydroxyl group are added into the IL structure in order to make intermolecular hydrogen bonding with the hydroxyl groups of water molecules.<sup>81</sup>

The process of ILs synthesis mainly consists of two steps. The first step is the formation of the required cation. The cation required can be synthesized either by protonation of the amine by an acid or via quaternization reactions of the amine with a haloalkane and heating of the mixture. The second step involves an anion exchange.<sup>82</sup> The anion exchange reactions can be conducted via the treatment of halide salts with Lewis acids to form Lewis acid based ILs or via anion metathesis.<sup>82</sup> The most widely used Lewis acid based ILs are AlCl<sub>3</sub> based salts.<sup>83</sup>

According to Lewis theory of acid-base reactions, the bases give the pairs of electrons and the acids accept a pair of electrons. Therefore, Lewis acid is a substance, such as H<sup>+</sup> ion, that can accept a pair of non-bonding electron. These salts are composed by simply mixing of the Lewis acid and the halide salt that results in the

formation of more than one anionic species depending on the ratio of quaternary halide salt Q<sup>+</sup>X and Lewis acid MX<sub>n</sub> as shown by the reaction between [emim][Cl] and AlCl<sub>3</sub> (Scheme 1).<sup>84</sup>

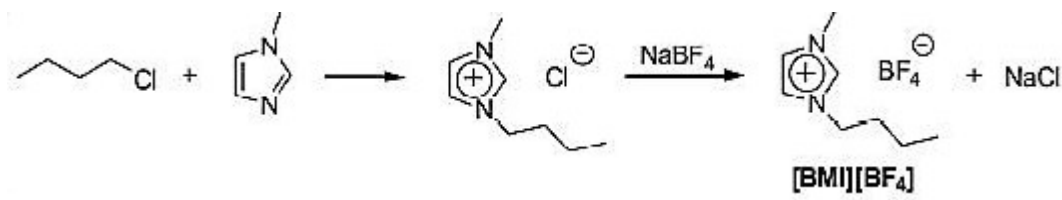


Scheme 1: Reaction between [emim][Cl] and AlCl<sub>3</sub> adapted from Ratti<sup>84</sup>

The formation of basic IL occurs when the [emim][Cl] is present in excess molality over AlCl<sub>3</sub> (Scheme 1-1). The molar excess of AlCl<sub>3</sub> results in the formation of an acidic IL (Scheme 1-3) and when both [emim][Cl] and AlCl<sub>3</sub> are present in the equal ratio the formation of a neutral IL takes place (Scheme 1-2). In addition to AlCl<sub>3</sub>, the other Lewis acid used in the preparation of ILs includes AlEtCl<sub>2</sub><sup>85</sup>, CuCl<sup>86</sup> and BCl<sub>3</sub><sup>87</sup>.

Another procedure used to prepare ILs that are stable in air and water such as 1,3-dialkyl imidazolium cations is known as anion metathesis. The metathesis reaction is simply an exchange between cations and anions of the compounds involved. Metathesis procedure involves the treatment of halide salt with silver, sodium and potassium salts of NO<sub>2</sub><sup>-</sup>, NO<sub>3</sub><sup>-</sup>, BF<sub>4</sub><sup>-</sup>, SO<sub>4</sub><sup>-2</sup> or with the free acid of a suitable anion. Scheme 2, shows a

reaction of 1-*n*-butyl-3-methylimidazolium chloride with sodium tetrafluoroborate in acetone at room temperature, which provides a quantitative yield of [BMI][BF<sub>4</sub>] after 24 hours of reaction.<sup>88</sup>

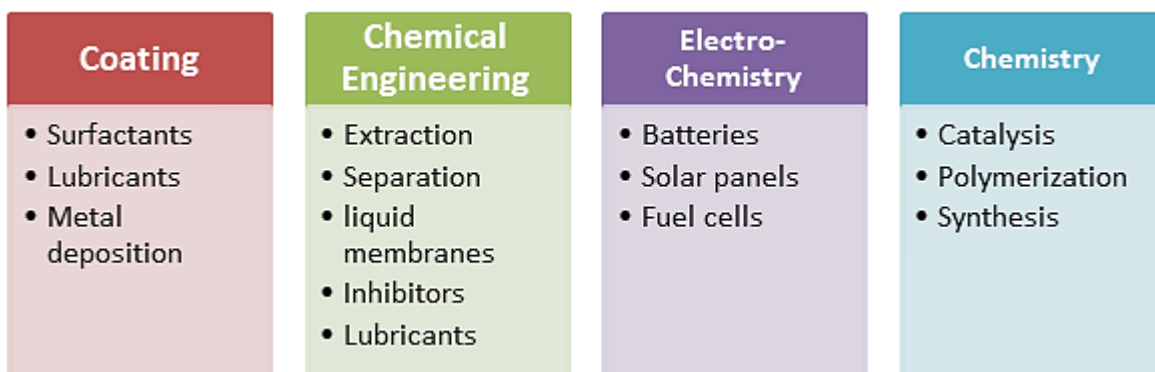


*Scheme 2:* Synthesis of 1-*n*-butyl-3-methylimidazolium tetrafluoroborate via 1-methylimidazolium and butyl chloride adapted from Andreani and Rocha<sup>89</sup>

As shown in Scheme 2, the above procedure allows the preparation of large number of ILs by simply combining different cations and anions together. Other procedures such as use microwaves irradiation (MW) and power ultrasound (US) can also be used with above procedures to improve the synthesis of ILs, reduce the reaction times and enhance the yields.<sup>90</sup> In addition to that, in future the use of efficient, solventless and one pot synthetic protocols is likely to make the process of ILs synthesis cheaper and facilitate the synthesis of a large number of ILs.<sup>91</sup>



Currently, ILs are used in a variety of areas which include electrochemistry, bio-catalysis, renewable resource utilization, CO<sub>2</sub> sequestration, corrosion inhibitors, hydrate inhibitors, lubricants and as a heat transfer fluids [Figure 2-1]. According to an estimate, there are about  $1 \cdot 10^{18}$  ILs<sup>92</sup> that can be synthesized using a different combination of cations and anions. Therefore, the term designer solvent is used for ILs as its easier to vary their physical and chemical properties as per the process requirement.



*Figure 2-1:* Application of Ionic liquids (ILs) in different disciplines.

Although the ILs are not widely used in industry, some companies have already started their industrial usage. The French Petroleum Institute has approved the commercial use of ILs in the manufacturing of polybutene using a Difasol process.<sup>93</sup> Polybutene is used for the manufacture of plastics, rubber, and related materials.<sup>93</sup>

The first wide-scale industrial usage of ILs was made in BASF's BASIL process (Biphasic Acid Scavenging Utilizing Ionic Liquids).<sup>94</sup> The BASIL process is used for the manufacturing of precursor alkoxy-phenyl-phosphines. Previously, tri-ethylamine was utilized to scavenge the acid formed during the reaction, but it resulted in the formation of tri-ethyl-ammonium chloride, a thick insoluble paste that was difficult to remove and handle as a waste. Therefore, the tri-ethylamine was replaced by IL 1-methylimidazole which resulted in the formation of 1-methylimidazolium chloride, which easily separates out of the reaction mixture as a distinct phase.

According to BASF, by using 1-methylimidazole the reactor size for the process decreased in size and the yield enhanced from 50 to 98 %. The IL 1-Methylimidazole is recycled through base decomposition of 1-H-3-methylimidazolium chloride in a separate patented process.<sup>95</sup> The process is now carried out in large multi-ton scale.<sup>96</sup>

The institute Francais du Petrole (IFP) was the first to develop an IL plant.<sup>97</sup> The long chain olefins formed in the dimerization process are converted to alcohols, which are then converted to dialkyl- phthalates used for plastic manufacturing. They used IL for the dimersol process that involves dimerization of alkenes such as propene and butane to more valuable branched hexenes and octenes.

The IFP use IL chloro-aluminate (III) as solvents for the nickel-catalyzed dimerization reactions.<sup>98</sup> It is an essential industrial process and there are 35 plants in operation worldwide with each producing 20,000-90,000 tons of dimer annually.<sup>98</sup> The ILs are also used as separation enhancers<sup>99</sup> to break azeotropes of water-ethanol and water tetrahydrofuran.<sup>100</sup> By the use of ILs as separation enhancers, the cost of separation and recycling of entrainer is significantly reduced.

### ***2.1.2 Ionic liquids: Thermo-physical Properties***

In order to incorporate ILs in chemical processes, it's essential to know IL thermophysical properties such as density, viscosity and heat capacity. The presence of IUPAC IL database<sup>101</sup> provides an overview of thermophysical data available for pure and mixed ILs. Many review papers<sup>55b, 64, 102</sup> have been published highlighting the main thermophysical properties of different types of ILs.

There are about  $10^{18}$  possible combinations of ILs according to Rogers and Seddon<sup>103</sup>. However, one of the major obstacles in the use of ILs for industrial processes is the limited knowledge of their thermophysical properties over the wide operating range. A detailed review of ILs thermophysical properties is beyond the scope of this chapter, but a brief summary to IL thermophysical properties will be provided that can help in further development of knowledge in the relevant IL field.

### 2.1.2.1 *Melting Point*

The melting point of IL may vary due to the presence of impurities or as they go through the process of supercooling. Most ILs have high decomposition temperatures that varies between 200- 300°C and this allows the use of ILs as a solvent over the wide temperature range. The high decomposition temperature of many ILs allows their usage as thermal storage fluids facilitating their use in solar thermal power systems.<sup>102b, 104</sup>

The melting point of ILs relies on the balance of cation and anion symmetry, flexibility of chains in the ions and charge accessibility. As the length of alkyl chains of cations increases, the melting point of ILs tends to decrease.<sup>105</sup> The type of anion attached with IL also affects the melting point of IL. As the size of the anion with the same charge increases, a decrease in the melting point occurs for the fixed cation.<sup>106</sup>

A significant effect of dissolved gases on the melting points of different types of ILs has been reported in the literature.<sup>107</sup> The addition of small quantity of CO<sub>2</sub> with ILs can significantly depress the melting point of ILs and this depression is large for ILs with fluorinated anions. The effect of pressure on the melting of ILs has also been studied by Domanska and Moravski<sup>108</sup> and it was found that the melting temperature of the IL increases with respect to increase in the pressure.<sup>109</sup>

Currently, the differential scanning calorimetry (DSC) is the most commonly used method for measuring melting point of IL. As melting temperature of an only small number of ILs is available, different methods have been developed to guess the melting points from the molecular structure of ILs. This includes the use of Quantitative structure-property relationships (QSPRs)<sup>110</sup>, neural networks approach<sup>111</sup> and computational molecular dynamic simulations<sup>55b</sup> to predict the melting points of ILs. However, these methods predict the melting points of ILs with slight errors and the use of simulations to predict ILs melting points is considered to be very expensive.

#### 2.1.2.2 *Volatility*

ILs are widely proclaimed to be non-volatile fluids and it is stated that they have negligible vapor pressure and cannot be distilled. Rebelo, et al.<sup>112</sup> and Paulechka, et al.<sup>113</sup> showed that the ILs can be distilled under low pressure for high temperatures. But, it was found that the ILs vapor pressure remains negligible at the ambient conditions.

The key aspects of volatility in ILs was investigated by MSS Esperança, et al.<sup>114</sup> and it was found that it's complex to measure vapor pressures and enthalpies of vaporization of ILs. Therefore, all the related studies on ILs vapor pressures should provide systematic errors. It's also essential to validate such measurements from both theoretical and practical aspects.

Experimentally, it is difficult to determine the boiling points of ILs at 1 atmosphere because they tend to decompose at a lower temperature. It has been reported that ILs can be distilled at very low pressure and at very low distillation rate.<sup>115</sup> The ionic nature of ILs can be attributed to their negligible vapor pressure in the liquid state and this differentiates them from molecular solvents.<sup>116</sup>

### 2.1.2.3 *Thermal and chemical stability*

The thermal decomposition rate evaluated via fast thermogravimetric analysis (TGA) shows that most ILs have high thermal stability ( $> 380^{\circ}\text{C}$ ). But lower values also exist for long-term stability which is essential to take into account when ILs are utilized in catalytic processes. The Phosphonium ILs tends to decompose completely to volatile products in a single step. But, the ILs that consists of nitrogen cations does not tend to decompose fully and normally produce char residue.<sup>4</sup>

To assess the long-term thermal stability of ILs a methodology was proposed by Seeberger, et al.<sup>117</sup>, that involves the evaluation of the kinetics of mass loss from isothermal and non-isothermal TGA experiments. Kroon, et al.<sup>118</sup>, used quantum chemical calculations to analyze the effect of cation and anion on the IL decomposition and found a good correlation between the calculated and the experimental results.

The thermal stability of the ILs strongly relies on the type of anion used in the synthesis of IL according to Huddleston, et al.<sup>119</sup>. The type of cation has the small effect on the thermal stability of IL. Hence, the increase in the size of the cation does not affect the decomposition temperature of the IL.

#### *2.1.2.4 Conductivity and electrochemical properties*

The ILs have the tendency to act as both solvents and electrolytes in electrochemical reactions. Thus, the conductivity of IL is considered to be their essential property. The ILs have a wide range of conductivities varying from 0.1 to 20 mS cm<sup>-1</sup>. The imidazolium-based ILs tend to have higher conductivities compared to ammonium based ILs. Also, there are variety of factors that can affect the conductivity of ILs and this includes the IL viscosity, density, ion size, aggregations and ionic motions.<sup>21</sup>

The electrochemical window of ILs lies within the range of 4.5-5 V, which is higher compared to other organic solvents and aqueous electrolytes. Ammonium-based ILs tend to be more stable during a reduction in comparison to imidazolium-based ILs. The imidazolium-based ILs tend to form N-heterocyclic carbenes. Currently, the researchers are trying to synthesize ILs that have a wide range of electrochemical window and also offer good electrical conductivity.

#### 2.1.2.5 Density

The density of most ILs is available in the literature.<sup>120</sup> Most ILs are denser than organic solvents or water and their density varies from 1.0 to 1.6 g cm<sup>3</sup>. The model for the density of ILs with respect to pressure and temperature is also available.<sup>121</sup> The most widely used method for measuring the density of ILs is the vibrating tube method<sup>122</sup> and other methods reported in the literature includes the use of bellows<sup>123</sup>, piezometric<sup>124</sup>, and HP denistom<sup>125</sup> to measure the density of ILs.

The majority of IL density data reported in the literature uses vibrating tube density meters (VTD). This technique offers many advantages such as the feasibility to obtain a good number of density measurements over a wide pressure and temperature range. The method is also economical and high accuracy of density measurements can be obtained using VSD technique.

#### 2.1.3 Ionic liquids: Recycle & Recovery

As the ILs are considered to be designer solvents they can be used to develop new chemical processes that can offer environmental and economic benefits.<sup>126</sup> However, as mentioned above there is only a few number of industrial processes that are using ILs as solvent or scavenger due to their high cost.<sup>127</sup>

In order to resolve the issue of high cost of ILs, it's essential to design efficient recycling processes to recover ILs and prevent the mixing of ILs with other products to avoid separation and contamination issues. The recovery of ILs is also essential to



prevent environmental issues related to their disposal and toxicity.<sup>115, 128</sup>

As ILs have a low vapor pressure, the use of distillation process to recover and recycle ILs has always been the most prominent choice. There are other methods such as extraction with organic solvents, extraction with supercritical carbon dioxide (ScCO<sub>2</sub>) and membrane separation process that can be used to recycle ILs. In order to select a right method to recover ILs, it's essential to consider the size of ILs, the hydrophobicity of ILs and the hydrogen bonding ability of both cations and anions in ILs. The chemical nature of anions attached with ILs largely affects the behaviour of IL + water mixture.<sup>129</sup>

The ILs that are hydrophobic and immiscible in water can be easily separated from water phase by the process of decantation. The decantation is processed for separation of mixtures, by removing a layer of the liquid from which the precipitate has settled down. For example, the mixture of kerosene and water can be easily separated using decantation process.<sup>63</sup>

The ILs that are both hydrophobic and hydrophilic have a tendency to form a micelle in water.<sup>130</sup> The extent of micellization of ILs relies on the size of hydrophobic or hydrophilic domains of the ILs. For example, the larger the size of the hydrophobic domain the greater is the tendency of the IL to cause aggregation and form a micelle in water.<sup>40</sup> Such ILs can be separated using membrane-based methods such as filtration or forced separation such as centrifugation.

The recovery of the hydrophilic ILs is considered to be more difficult compared to hydrophobic ILs. For example, the distillation of ILs from aqueous solutions requires a large amount of energy and this makes the recovery process economically unfeasible. Therefore, other methods such as induced phase separation<sup>131</sup> (salting-out process), adsorption and membrane-based methods are being investigated. The selection of the method relies on the characteristics of the system. The brief description of methods that can be used for separation of ILs from the aqueous solution is provided below.

#### *2.1.3.1 Distillation*

This is considered to be the simplest method for the removal of compounds having low boiling points and high thermal stability from the ILs, as a result of ILs negligible vapor pressure. The volatile compounds can be separated from ILs by vacuum evaporation, column distillation, and molecular distillation.

As distillation process requires a large amount of energy, it is usually used as a final step in most of ILs recovery processes. Firstly, the catalysts and reaction products are separated from ILs by decantation, filtration or extraction processes. Then these separated compounds are washed with water and other organic solvents. Then the remaining contaminated solvents and un-separated compounds from ILs are separated from ILs by using the distillation process.<sup>120, 132</sup>

Recovery of the IL [Amim][Cl] from aqueous solution in homogenous cellulose acetylation reaction by molecular distillation was reported by HUANG, et al.<sup>133</sup>. The volatile impurities were removed as a distillate and the residue of IL [Amim][Cl] was recycled and reused five times in the same reaction without any change in its structure.

Similarly, the IL [C<sub>2</sub>mim][OAc] was recovered from its solution with purity >95 % and yield of 90 % in cellulose dissolution reaction using molecular distillation at 0.05 bar and temperature of 170 ° C in a period of 4 hr.<sup>134</sup> Kreher, et al.<sup>135</sup>, stated that the dialkylammonium carbonate ILs formed as a result of condensation of CO<sub>2</sub> with dialkylamine can be easily separated by evaporating at low temperature (60-105 ° C) and high vacuum conditions. The use of microwave heating can also help to improve the recovery time of IL from aqueous solution and also make the process more energy efficient according to Abu-Eishah<sup>136</sup>. Hence, distillation is considered to be the most simple, rapid and robust method for recycling ILs. However, it consumes a large amount of energy making it an expensive method to recover ILs.

### 2.1.3.2 *Extraction*

The separation of non-volatile products from ILs via liquid-liquid extraction is most commonly used the method.<sup>137</sup> The solvents like water are sometimes immiscible with ILs. They get separated into different phases with ILs and this allows separating of materials from the IL solution. Most hydrophilic products can be easily extracted from

hydrophobic ILs with water.<sup>138</sup>

The hydrophobic products that are non-volatile are extracted from ILs via organic solvents such as diethyl ether and hexane.<sup>139</sup> Dibble, et al.<sup>140</sup>, proposed a method to recover [C3mim][OAc] and alginic acid from IL-biomass using a solvent mixture containing water, acetone, and 2-propanol via liquid-liquid extraction technique. Using this technique, short-chain carbohydrates can be separated from ILs via two-stage extraction method and about 89% of ILs can be recovered via this method.

ILs are also used for liquid-liquid extraction of heavy metal ions and they allow to separate heavy metal ions from the aqueous phase.<sup>141</sup> However, in this case, the ILs phase gets contaminated with acidic compounds and stripping with organic solvents is required to clean and reuse the ILs.<sup>142</sup> Solvent extraction method is relatively simple and flexible method to recover solutes from ILs and also allow recycle and reuse of ILs. But, precautions are required as there is the chance of cross-contamination.

The supercritical fluids like supercritical CO<sub>2</sub> (Sc-CO<sub>2</sub>) can be used as an alternative solvent for IL extraction. Sc-CO<sub>2</sub> is widely used as an industrial chemical extraction solvent due to its low toxicity and low cost. CO<sub>2</sub> is considered to be green solvents as it is non-flammable, non-toxic and inexpensive. Generally, the ILs are not soluble in Sc-CO<sub>2</sub> and so the non-polar Sc-CO<sub>2</sub> forms two-phase system with polar and non-volatile ILs.<sup>143</sup>

As most organic compounds are soluble in Sc-CO<sub>2</sub>, these products can be easily transferred from the ILs to the Sc-CO<sub>2</sub> phase. The unique properties of Sc-CO<sub>2</sub> allow the isolation of solutes from ILs without the cross-contamination of the gas phase. Once the solutes are separated from ILs, the pure ILs can be recovered by further extraction and de-pressurization.

Different types of solutes can be extracted from ILs by using ScCO<sub>2</sub> and the recovery rates are reported to be greater than 95%.<sup>144</sup> Blanchard, et al.<sup>145</sup>, stated that 94-96% of naphthalene can be recovered from IL [C<sub>4</sub>mim][PF<sub>6</sub>] using CO<sub>2</sub> at 13.8 MPa and 40 °C. The recovery was reported to depend on the dipole moments of solutes and the concentration of CO<sub>2</sub> used for the extraction.

### 2.1.3.3 Adsorption

The ILs can be recovered from aqueous solution by the process of adsorption via absorbents. Previously, many studies have studied the absorption of ILs on absorbents such as activated carbon<sup>146</sup>, silica (SiO<sub>2</sub>)<sup>147</sup>, alumina (Al<sub>2</sub>O<sub>3</sub>) and different types of clays<sup>148</sup>. Anthony, et al.<sup>149</sup>, suggested the use of activated carbon for the adsorption recovery of IL [C<sub>4</sub>mim][PF<sub>6</sub>] from the wastewater. It was found that the activated carbon was suitable for the purification of the wastewater stream, but it cannot be used for the recovery of ILs due to its less efficiency. Activated carbon is more suited for removing small non-polar compounds like toluene but not polar or ionic species like ILs.

The adsorption of imidazolium-based ILs from aqueous solutions using commercial activated carbon and modified activated carbon adsorbents have been studied in different kinds of literature.<sup>128, 150</sup> These studies deduce that the size and hydrophobic nature of both anion and cation of ILs strongly affect the adsorption efficiency of activated carbon towards IL. The recovery of hydrophobic ILs from aqueous solution using activated carbon was found to be cost-effective.

On the other hand, the adsorption efficiency of hydrophilic ILs via activated carbon could be enhanced by varying the concentration and nature of oxygen groups on the surface of activated carbon. The introduction of the hydroxyl group on the activated carbon surface can promote the hydrogen bonding interactions with basic groups of hydrophilic ILs which helps to improve the overall adsorption efficiency.

Qi, et al.<sup>151</sup>, used a functional carbonaceous material (FCM) containing carboxylic groups in the presence of acrylic acid to recover [C<sub>4</sub>mim][Cl] from aqueous solution. The FCM has a low surface area but its adsorption capacity was found not more than commercial activated carbon. Thus, with certain modifications activated carbon can become a useful IL absorbent.

#### 2.1.3.4 *Induced phase separation*

The ILs solutions tend to form aqueous biphasic systems (ABS) when salts are added in them. This method is known as a salting-out phenomenon that offers another route to recover ILs from aqueous effluents. Initially, Gutowski, et al.<sup>152</sup> showed that when “kosmotropic” salt (like  $K_3PO_4$ ) is added to an aqueous solution of selected IL it tends to promote the phase separation by providing IL-rich phase at the top and salt-rich phase at the bottom.

The recovery of IL [Amim][Cl] via three inorganic salts such as  $K_3PO_4$ ,  $K_2HPO_4$ , and  $K_2CO_3$  was demonstrated by Deng, et al.<sup>153</sup>. Their results show that the efficiency of IL recovery using the selected inorganic salts increases in the following order at the same concentration,  $K_3PO_4 > K_2HPO_4 > K_2CO_3$ . Deng, et al.<sup>153</sup>, also found that efficiency of IL recovery increases with the concentration of the added inorganic salt. The maximum IL recovery efficiency of 96.8 % was reported via the use of 46.48 wt %  $K_2HPO_4$ . Similarly, Li, et al.<sup>154</sup> investigated the effectiveness of sodium based salts in the recovery of IL [C<sub>4</sub>mim][BF<sub>4</sub>] from aqueous solution. These sodium based salts included:  $Na_3PO_4$ ,  $Na_2CO_3$ ,  $Na_2SO_4$ , and NaCl. Their results show that the maximum IL recovery efficiency of 98.77 % is obtainable using 16.94 wt% of  $Na_2CO_3$ .

The recovery of ILs via salting out process is simple, effective, and economical as it requires less expensive salts. In comparison to other recovery processes, it's also simpler to scale up and can be used to recover IL from various chemical processes that

use ILs. However, there are environmental concerns related to using of high inorganic salts for ILs recovery that are not easier to dispose of. Therefore, the use of CO<sub>2</sub> gas instead of inorganic salts to promote phase separation in IL solutions is being investigated and studied in different kinds of literature.<sup>155</sup> Scurto, et al.<sup>144b</sup>, added CO<sub>2</sub> in [C<sub>4</sub>mim][PF<sub>6</sub>] + Methanol mixture and found that CO<sub>2</sub> has a tendency to cause the phase separation by the formation of IL-rich phase and an organic-rich phase.

Generally, the CO<sub>2</sub> tends to be non-polar in nature and does not solvate ions. Hence, as it dissolves in the IL + methanol mixture, the solvent strength of CO<sub>2</sub> expanded liquid is reduced and this causes the formation of another liquid phase that is rich in ILs. Also by raising the process temperature above the CO<sub>2</sub> critical temperature, the methanol-rich phase gets miscible with CO<sub>2</sub>-rich phase, resulting in the formation of the IL-free phase. Thus, this methodology provides a novel way of recovering and recycling IL from chemical processes utilizing IL solvents.

#### ***2.1.4 Ionic liquids: Hydrate inhibition studies***

This section provides a comprehensive background of the thermodynamic and kinetic inhibition studies reported in the literature using different types of ILs at different concentrations and pressure conditions. This helps to figure out the knowledge gap and find the areas that need to be addressed in the respective field.



#### 2.1.4.1 *Imidazolium ILs*

The majority of studies conducted on hydrate inhibition, using ILs are based on imidazolium ILs. Xiao and Adidharma<sup>41</sup>, were the first to figure out ILs as a new methane hydrate inhibitor based on their thermodynamic and kinetic inhibition characteristics. Since then, researchers have been trying to develop an effective class of ILs that can help to replace conventional thermodynamic inhibitors like methanol and mono-ethylene glycol (MEG).

The thermodynamic effect of six dialkyl imidazolium halide ILs on methane hydrate formation at the low concentration of 1wt% and at the pressure range of 105-205 bars using high-pressure differential scanning calorimeter was investigated by Xiao, et al.<sup>156</sup>. The ILs studied included [EMIM-Cl], [EMIM-Br], [PMIM-I], [BMIM-Cl], [BMIM-Br] and [BMIM-I].

The selected ILs acted as thermodynamic and kinetic hydrate inhibitor both at the same time according to Xiao, et al.<sup>156</sup>. The selected ILs as a thermodynamic hydrate inhibitor provided the hydrate suppression temperature within the range of 0.27-1.22 K. The IL EMIM-Cl was found to be the most effective THI with hydrate suppression temperature of 1.22 K and the IL BMIM-BF<sub>4</sub> was found to be the least effective with the hydrate suppression temperature of 0.27 K. It was also observed that the IL containing similar cation, example EMIM or BMIM, the thermal efficiency increases in the order Cl > Br > I > BF<sub>4</sub>. However, the selected ILs were not found to be as effective as the

conventional thermodynamic hydrate inhibitors like mono-ethylene glycol and methanol.

The methane hydrate dissociation conditions in the presence of [EMIM-Cl] and [OH-C<sub>2</sub>MIM-Cl] IL solutions was experimentally studied by Parton, et al.<sup>157</sup>. The effectiveness of these ILs was tested at the low dosage (0.1-0.5 wt%) at the pressure range of 4-12 MPa. The hydrate suppression temperature in the presence of these ILs was observed to be within the range of 0.1-1.5 K. The IL [OH-C<sub>2</sub>MIM-Cl] was found to be more effective thermodynamic hydrate inhibitor compared to [EMIM-Cl]. This thermal effect was attributed to the presence of hydroxyl group in the IL [OH-C<sub>2</sub>MIM-Cl] which allows it to form hydrogen bonding with the water molecules easily and offer better thermal effect<sup>158</sup>.

Likewise, the methane hydrate dissociation conditions in the presence of the IL [EMIM-Cl] at different concentration (10-40 wt%) and pressure range (5-35 MPa) using high-pressure calorimeter was studied by the Chu, et al.<sup>159</sup>. The best hydrate suppression temperature of 12.83 K was obtained at 20 MPa at the concentration of 40 wt%. The suppression temperature of 12.83 is very significant compared to other literary works. However, it requires a high concentration of IL (40 wt%) to obtain suppression temperature of 12.83 K, which is not economically feasible at large industrial scale.

Later, the high-pressure differential scanning calorimeter was used to test the effectiveness of IL imidazolium chloride in mitigating the methane hydrate formation at a concentration of 20 wt% using three different alkyl chains of imidazolium chloride by Chu, et al.<sup>160</sup>. These alkyl chains included: [EMIM-Cl], [HMIM-Cl] and [DMIM-Cl]. The experiments were conducted within the pressure range of 5 to 35 MPa. The IL EMIM-Cl was found to be the most effective and the IL DMIM-Cl was found to be the least effective thermodynamic hydrate inhibitor. The hydrate suppression temperature for IL EMIM-Cl was found to be 3.79 K at 20 wt% at 35 MPa, followed by HMIM-Cl with hydrate suppression temperature of 1.66 K and DMIM-Cl with hydrate suppression temperature of 0.31 K.

Furthermore, the thermodynamic inhibition effect of IL [Emim][NO<sub>3</sub>] on methane hydrate phase equilibrium conditions at a low mass fraction of 0.01, 0.025 and 0.05 within the pressure range of 3.5-15.0 MPa was investigated by Long, et al.<sup>161</sup>. They also investigated the synergistic effect of using a combination of IL [Emim][NO<sub>3</sub>] and IL [Emim][Cl] at both low and high concentrations. It was observed that in the inhibitor systems containing [Emim][NO<sub>3</sub>] or [Emim][Cl] the inhibition efficiency increases with the concentration and pressure. The mixture of [Emim][NO<sub>3</sub>] and [Emim][Cl] does not exhibit synergistic effect at a higher concentration of 0.2 mass fraction. The synergistic effect of mixed ILs systems was only observed at a mass fraction of 0.05 and 0.1.

The experimental results of Long, et al. <sup>161</sup>, furthermore reveal that overall inhibition performance of ILs depends on both cations and anions. The thermodynamic inhibition effectiveness of selected ILs enhanced with the increase in pressure and concentration. At the pressure of 6.40 MPa, the hydrate suppression temperature for [Emim][NO<sub>3</sub>] was about 0.3 K (0.01-0.025 mass fraction), about 0.4 K (0.025-0.05 mass fraction) and 1.2 K (0.1-0.2 mass fraction).

Accordingly, the thermodynamic inhibition performance of IL [EMIM-Cl] on methane hydrate formation at different concentrations and within the pressure range of 10-20 MPa was investigated by Richard and Adidharma <sup>162</sup>. In order to test the synergistic properties of EMIM-Cl, the IL was mixed with conventional thermodynamic hydrate inhibitors such as sodium chloride (NaCl) and mono-ethylene glycol (MEG). In addition to that, the IL EMIM-Cl was also mixed with IL [EMIM-Br] to test its synergistic effect.

It was observed that the higher concentration (60 wt%) of the IL EMIM-Cl can provide better thermodynamic effect than the MEG by Richard and Adidharma <sup>162</sup>. It was also observed that the IL EMIM-Cl can act as synergent when mixed with MEG, NaCl, and EMIM-Br at high pressures. The average hydrate suppression temperature for EMIM-Cl was found to be within the range of 1.0-1.5 K at 10wt% and pressure range of 10-40 MPa.

The average hydrate suppression temperature for MEG + EMIM-Cl mixture with equal ratio (1:1) at 10wt% was found to be 1.5-2.0 K. The average hydrate suppression temperature for EMIM-Cl + NaCl mixture with equal ratio (1:1) at 10wt% was found to be 2.5 K.<sup>162</sup> Similarly, the average hydrate suppression temperature of EMIM-Br + EMIM-Cl mixture with equal ratio (1:1) at 20wt% was found to be within the range 1.2-2.7 K at pressure range of 10-20 MPa.

Previously, the researchers were only looking into the thermodynamic inhibition effect of imidazolium-based ILs. Xiao and Adidharma<sup>41</sup> were the first to test the kinetic effect of imidazolium-based ILs on methane hydrate formation. They tested the effectiveness of five imidazolium-based IL as a kinetic hydrate inhibitor within the pressure range of 30-110 bars using high-pressure differential scanning calorimeter. They found that the ILs can provide the kinetic and thermo effect both simultaneously as they have strong electrostatic charges and ability to form hydrogen bonding with water.

The term dual functional hydrate inhibitors for the imidazolium ILs was first used by Xiao and Adidharma<sup>41</sup>. They tested the ILs: [EMIM-BF<sub>4</sub>], [BMIM-BF<sub>4</sub>], [EMIM-N(CN)<sub>2</sub>], [EMIM-CF<sub>3</sub>SO<sub>3</sub>] and [EMIM-EtSO<sub>4</sub>] as hydrate inhibitors for the pure methane gas. At the concentration of 10wt%, the selected ILs provided the hydrate suppression temperature within the range of 0.7-1.5 °C. However, the selected ILs were not found as effective as the conventional thermodynamic hydrate inhibitors, but they provided the kinetic effect

by delaying the hydrate induction time. This was the major findings that brought the ILs into the spotlight to be used as kinetic hydrate inhibitor.

The methane hydrate induction time in the pure water sample was observed as 0.36 hrs by Xiao and Adidharma <sup>41</sup>. They observed that the addition of 10wt% of the selected imidazolium ILs enhanced this mean induction time to about 0.40-6.48 hrs at 114 bars. The IL EMIM-BF<sub>4</sub> was found to be the most effective kinetic hydrate inhibitor with a mean induction time of 6.48 hrs and the IL EMIM-CF<sub>3</sub>SO<sub>3</sub> was found to be the least effective kinetic hydrate inhibitor with a mean induction time of 0.40 hrs.

In terms of the effectiveness as the kinetic hydrate inhibitor at 10wt% and pressure of 114 bars the selected ILs were listed as EMIM-BF<sub>4</sub> > BMIM-BF<sub>4</sub> > EMIM-N(CN)<sub>2</sub> > EMIM-EtSO<sub>4</sub> > EMIM-CF<sub>3</sub>SO<sub>3</sub>. According to Xiao and Adidharma <sup>41</sup>, the kinetic hydrate inhibition performance of the selected ILs was found to be better than the commercial kinetic hydrate inhibitor Luvicap and PVP. The 10wt% PVP at 114 bars provided the hydrate induction time of 0.95 hrs.

The thermodynamic and kinetic inhibition effect of six dialkyl imidazolium halide ILs on methane hydrate formation at the low concentration of 1wt% and at the pressure range of 105-205 bars using high-pressure differential scanning calorimeter as mentioned earlier was further investigated by Xiao, et al. <sup>156</sup>. The ILs studied included: [EMIM-Cl], [EMIM-Br], [PMIM-I], [BMIM-Cl], [BMIM-Br] and [BMIM-I].

As a kinetic hydrate inhibitor, the selected ILs shifted the hydrate induction time within the range of 1.29 to 5.71 hrs at 1wt%. The IL BMIM-I was found to be the most effective kinetic hydrate inhibitor with hydrate induction time of 5.21 hr and the IL PMIM-I was found to be the least effective with hydrate induction time of 1.29 hrs. However, the IL EMIM-BF<sub>4</sub> was found to be slightly more effective than the BMIM-I. In terms of effectiveness as kinetic hydrate inhibitor the ILs were listed as: EMIM-BF<sub>4</sub> > BMIM-I > BMIM-Br > EMIM-Br > BMIM-Cl > EMIM-Cl > PMIM-I

The effectiveness of IL [C<sub>10</sub>MIM][BF<sub>4</sub>] as a Tetra hydro furan (THF) kinetic hydrate inhibitor was examined by Saikia and Mahto <sup>163</sup> at different concentrations (0.1-1 wt%). The effect of the selected IL on the rheology of the drilling fluid was also studied at the temperature of 2 °C and its kinetic effect was compared with the commercial kinetic inhibitor polyvinylpyrrolidone (PVP). The superheated hydrate test method was used for experiments and it was found that this IL exhibited the properties of anti-agglomerate (AA).

According to the experimental results of Saikia and Mahto <sup>163</sup>, the IL [C<sub>10</sub>MIM][BF<sub>4</sub>] provides kinetic effect even at lower concentration (0.1 wt%) and its performance is similar to PVP. Saikia and Mahto <sup>163</sup> also found that IL [C<sub>10</sub>MIM][BF<sub>4</sub>] is more effective in counteracting memory effect than the PVP. The IL [C<sub>10</sub>MIM][BF<sub>4</sub>] delayed the hydrate induction time by 55 min at the concentration 0.1 wt% and delayed

the hydrate formation by more than 1440 min at a higher concentration of 0.5 wt% and 1.0 wt%.

The kinetic inhibition effect of three imidazolium ILs at different concentration (1-20 wt%) on methane hydrate formation using a stainless steel vessel was tested by Rasoolzadeh, et al. <sup>164</sup>. The ILs tested included: [BMIM-BF<sub>4</sub>], [BMIM-DCA] and [TEACL]. Their experimental results show that the selected imidazolium ILs do have a tendency to delay hydrate formation and increase hydrate induction time. It was observed that the pressure has the reverse effect on the hydrate induction time.

The hydrate induction time of methane hydrate formation at 7 MPa in pure water was found to be 79.80 min. At the same pressure (7MPa) this induction time was delayed to 88.20 min by addition of 1wt% BMIM-BF<sub>4</sub>, delayed to 131.40 min by addition of 10wt% BMIM-BF<sub>4</sub>, delayed to 130.20 min by addition of 10 wt% BMIM-DCA and delayed to 117.60 min by addition of 10 wt% TEACL in aqueous pure water solution. According to Rasoolzadeh, et al. <sup>164</sup> in terms of KI effectiveness, the selected ILs at 10wt% were listed as BMIM-BF<sub>4</sub> > BMIM-DCA > TEACL. It was also found that imidazolium-based ILs are more effective as kinetic hydrate inhibitor than the TEACL.

It has been reported, that by using 0.75 wt% ethylene glycol methyl ether (EGME) with the ILs [BMIM][MeSO<sub>4</sub>] and [OH-EMIM][BF<sub>4</sub>] the promotion of methane hydrate formation occurs according to Zare, et al. <sup>165</sup>. On the contrary, if only 10wt%



EGME is used as the inhibitor, the hydrate inhibition occurs. The IL [BMIM][MeSO<sub>4</sub>] was found to be the most effective kinetic hydrate inhibitor with a mean induction time of 716 min at 12.1 MPa, followed by IL [EMIM][EtSO<sub>4</sub>] with the mean induction time of 408 mins at 12.1 MPa. The other ILs such as [BMIM][BF<sub>4</sub>], [OH-EMIM][BF<sub>4</sub>] and [EMIM][HSO<sub>4</sub>] acted as the hydrate promoters at 12.1 MPa. Hence, in terms of KI effectiveness, the ILs can be listed as [BMIM][MeSO<sub>4</sub>] > [EMIM][EtSO<sub>4</sub>]. According to Ficke and Brennecke<sup>166</sup>, the oxygen atom attached to methyl group of [MeSO<sub>4</sub>]<sup>-</sup> is more electronegative than the ethyl group of [EtSO<sub>4</sub>]. This is the reason that [BMIM][MeSO<sub>4</sub>] acts better as a kinetic hydrate inhibitor compared to [EMIM][EtSO<sub>4</sub>]. In addition to that, the hydrophobicity expands with the increase of alkyl chain length in an IL.

The kinetic inhibition effect of ILs [EMIM-BF<sub>4</sub>] and tetrafluoroborate [BMIM-BF<sub>4</sub>] on sII hydrate crystal formation in a natural gas mixture (methane, ethane, propane, iso-Butane, n-butane, nitrogen and carbon dioxide gas) was studied by Del Villano and Kelland<sup>167</sup>. It was found that the selected imidazolium ILs showed insignificant or poor kinetic effect on hydrate crystal formation (sI & sII) in natural gas mixture compared to commercial kinetic hydrate inhibitor at a pressure range of 85-90 bars. However, both ILs did acts as a synergent for the commercial kinetic hydrate inhibitor RE5131 HIO. The IL EMIM-BF<sub>4</sub> performed better as a synergent compared to IL BMIM-BF<sub>4</sub>.

#### 2.1.4.2 Morpholinium and Piperidinium ILs

The effect of morpholinium and piperidinium based ILs as thermodynamic hydrate inhibitors for the methane hydrates at a mass fraction of 0.1 was examined by Cha, et al. <sup>168</sup>. The ILs used included: [EMMor][Br], [EMMor][BF<sub>4</sub>], [EMPip][Br] and [EMPip][BF<sub>4</sub>]. It was found that the addition of ILs moves the hydrate equilibrium conditions towards higher pressure and lower temperature.

It was also observed that both anion and cation species present in the IL effects the inhibition performance of the particular IL. The piperidinium based ILs showed better thermo effect than the morpholinium based ILs may be due to hydrophobic nature of piperidinium ILs. It was also observed that the TI effect of BF<sub>4</sub><sup>-</sup> ions were better than Br<sup>-</sup> ions for both morpholinium and piperidinium based ILs. The ILs based on their thermodynamic inhibition effectiveness were listed as: [EMPip][BF<sub>4</sub>] > [EMPip][Br] > [EMMor][BF<sub>4</sub>] > [EMMor][Br]

Two morpholinium based ILs [HEMM-Cl] and [HEMM-BF<sub>4</sub>] were synthesized by Lee, et al. <sup>169</sup>. They studied the inhibition effect of these ILs anions on methane hydrate formation kinetics at different concentrations. The IL HEMM-Cl acted as hydrate promoter and the IL HEMM-BF<sub>4</sub> acted as a kinetic hydrate inhibitor. Lee, et al. <sup>169</sup>, found that the hydrate induction time for HEMM-BF<sub>4</sub> increases with its concentration and it also act as a THI by providing the hydrate suppression temperature of 1.6 K at 10 wt% of HEMM-BF<sub>4</sub>. At the same concentration, the HEMM-BF<sub>4</sub> provided the induction time of

135 min. This shows that different types of ILs can act as both hydrate promoter and hydrate inhibitors. The X-ray diffraction pattern of these ILs also shows that there was no amalgamation of IL in the hydrate crystal structure. Therefore, in terms of effectiveness as thermodynamic and kinetic hydrate inhibitors, the ILs were listed as HEMM-BF<sub>4</sub> > HEMM-Cl.

### ***2.1.4.3 Ammonium Hydroxide ILs***

The thermodynamic inhibition effect of IL TMAOH on CH<sub>4</sub> and CO<sub>2</sub> hydrate formation at different concentrations (1-10 wt%) was examined by Khan, et al.<sup>170</sup>. The experiments were conducted within the range of 3.5-8 MPa and 1.8-4.2 MPa respectively. The experimental results show that TMAOH can act like a thermodynamic hydrate inhibitor for both CO<sub>2</sub> and CH<sub>4</sub> hydrates. At the concentration of 10wt%, the thermo effect of TMAOH was significant for CO<sub>2</sub> hydrates with average suppression temperature of 2.24 K. The average suppression temperature for CH<sub>4</sub> hydrates was found to be 1.52 K.

The thermodynamic inhibition effect of IL TMAOH increases with its respective concentration according to Khan, et al.<sup>170</sup>. They also conducted COSMO-RS analysis which showed that the thermo effect of TMAOH was due to its hydrogen bonding affinity for water molecules. In addition to that, the hydrate dissociation enthalpies calculated in both systems show that TMAOH does not participate in the hydrate crystalline structure.

#### 2.1.4.4 *Pyrrolidinium ILs*

The effect of pyrrolidinium ILs on methane hydrate formation as a kinetic and thermodynamic hydrate inhibitors was tested by Kim, et al. <sup>171</sup>. The ILs used for the tests included: [HEMP][BF<sub>4</sub>] and [BMP][BF<sub>4</sub>]. As a thermodynamic hydrate inhibitor at 10wt%, the selected ILs provided the hydrate suppression temperature of 1.3-1.6 K. In comparison, the methanol a well-known industrial thermodynamic hydrate inhibitor provided the hydrate suppression temperature of 2.5-5.0 K.

At 1wt% (70 bars) the IL [EMIM][BF<sub>4</sub>] provided the induction time of 88.4 mins, followed by IL [HEMP][BF<sub>4</sub>] with an induction time of 101.5 min and IL [BMP][BF<sub>4</sub>] with induction time 58.2 min. As the concentration of ILs was increased to 10wt%, the induction time for IL [HEMP][BF<sub>4</sub>] increased to 342.8 min and the induction time for IL [BMP][BF<sub>4</sub>] increased to 233.5 min respectively. Therefore, in terms of effectiveness as a KHI at 1wt% (70 bars) the selected kinetic hydrate inhibitors can be listed as: [HEMP][BF<sub>4</sub>] > [EMIM][BF<sub>4</sub>] > [BMP][BF<sub>4</sub>]

#### 2.1.4.5 *Choline ILs*

Mohamed, et al. <sup>58</sup>, tested three choline based ILs: [ChOAc], [ChNtf2] and [ChCl] for their inhibition effectiveness in mitigating hydrate formation in pure methane gas system and multicomponent Qatari natural gas mixture (QNG-S1). The experiments were conducted using two different concentration of ILs (1wt % & 5 wt%).

The selected ILs behaved differently in each system according to Mohamed, et al. <sup>58</sup>. At 1wt% in pure methane, ChOAc showed slight inhibition effect whereas other choline ILs showed no inhibition effect at a concentration of 1wt%. But, as the concentration of ILs was increased to 5wt% all ILs showed observable TI effect. ChoAc was found to be the most effective thermodynamic hydrate inhibitor and ChNtf2 showed the least thermo effect. At both 1wt% and 5wt%, ChoAc was found to provide a significant shift in HLVE curve at low pressure (< 60 bars) conditions.

### ***Summary***

It is clear from the above literature review, that majority of hydrate inhibition studies has been reported using imidazolium ILs. Only limited studies have been reported using pyrrolidinium and as per the author knowledge no prominent hydrate inhibition studies have been conducted using ammonium-based protic ionic liquids. Also, it's essential to investigate the effect of anions and cations on the inhibition effect of ionic liquids. Hence, the effect of different cations and anions on the inhibition performance of the ionic liquids is discussed in the Section 4.1 and Section 4.2.

The Section 4.1 and Section 4.2, also highlight the thermodynamic and kinetic inhibition effect of pyrrolidinium and ammonium-based ionic liquids at different concentration (1-10 wt%) and different pressure conditions (38-120 bars) using a quaternary gas mixture (QM) and pure methane gas in a rocking cell assembly (RC-5)

## 2.2 Hydrate Inhibition using Amino Acids

Amino acids are biological organic compounds that consist of an amine (-NH<sub>2</sub>) and carboxylic acid (-COOH) functional groups<sup>172</sup>. Naturally, there are 20 amino acids that are found in a living organism and they are considered to be the building blocks of proteins. The physical and chemical properties of the amino acids depend on their side chains and these side chains vary from a polar alkyl chain to a positively or negatively charged moiety<sup>173</sup>. Amino acids play an important role in human and animal nutrition<sup>174</sup> and are used as the animal feed additives (lysine, methionine, threonine), as flavor enhancers (aspartic acid, serine) and as ingredients in cosmetic and medicinal products.<sup>175</sup>

The amino acids can be divided into subgroups as per their similarity in carbon skeleton and substituent groups. The presence of heteroatoms (S, N, and O) and conjugated  $\pi$ -electrons system on their molecular structures is attracting researchers to explore amino acids ability to act as potential chemical inhibitors.<sup>176</sup>

Generally, amino acids are considered to be primary metabolites, which are found in cellular proteins. Earlier, it was thought that amino acids cannot be produced by microbial cells. But, in 1956 two Japanese researchers Shukuo Kinoshita and Shigezo Udaka were successfully able to isolate a bacterium, known as *Corynebacterium glutamicum*(*c-glutamicum*), that has a tendency to produce a significant amount of

glutamic acid.<sup>177</sup> The glutamic acid production by *C. glutamicum* is prompted by biotin limitation<sup>178</sup>, the addition of Tween 40<sup>179</sup> and addition of penicillin<sup>180</sup>.

The large numbers of amino acids have been produced by using microbial cells and market size of amino acids is increasing continuously. Currently, the market for glutamic acid is more than 2.5 million tons per annum and the market size for lysine is around 1 million ton per year.<sup>181</sup>

Amino acids are also widely used in the manufacturing of food products, pharmaceutical drugs, and cosmetic products. Healthy human nutrition requires essential amino acids for effective protein synthesis in the human body.<sup>182</sup> Therefore, the amino acids are widely used in sports supplements and other nutritional products for improving muscle recovery after strenuous workouts.<sup>183</sup> In addition to that, the use of amino acids as a food supplement is considered vital to maintaining a healthy lifestyle.<sup>184</sup> Therefore, the production of amino acids occurs at the scale of million tons and their demand is reported to increase at the rate of 5-7 % per year.<sup>185</sup>

Amino acids as inhibitors are considered to be non-toxic, biodegradable and easier to produce in higher purity.<sup>186</sup> They can be obtained at low cost in large quantities and this makes them an attractive option to be used as a gas inhibitor<sup>187</sup>. Previously many studies have reported the use of amino acids as corrosion inhibitors<sup>57a, 188</sup>.

The amino acids Aspartic acid (Asp), Glutamic acid (Glu), asparagine (Asn) and glutamine (Gln) as the copper corrosion inhibitors in 0.5 M HCl solution were studied by Zhang, et al.<sup>189</sup>. Their experimental results, based on potentiodynamic polarization and electrochemical impedance spectroscopy (EIS) analysis show that all four amino acids offer protection against copper corrosion. Zhang, et al.<sup>189</sup> suggested that these amino acids act by getting adsorb on the copper surface which plays a key role in corrosion prevention. The inhibition effect of these amino acids was found to increase at higher concentration and the effectiveness increases in the following order: Gln > Asn > Glu > Asp.

The inhibition effect of amino acids Alanine (Ala), Glycine (Gly) and Leucine (Leu) against steel corrosion in HCl solution was examined by Ashassi-Sorkhabi, et al.<sup>188a</sup>. Their experimental results show that inhibition efficiency of the selected amino acids depends on their concentration and physiochemical properties.<sup>188a</sup> They also emphasized on the fact that amino acids prevent corrosion by adsorbing on the steel surface and this adsorption follows Langmuir isotherm theorem.<sup>190</sup>

Amino acids are also found to be effective against aluminum corrosion and it's reported that the presence of aromatic ring and heteroatoms (like sulfur and nitrogen) in amino acids structure significantly improve the corrosion inhibition capacity of amino acids<sup>188a</sup>. Thus, the amino acids have been reported to act as a potent inhibitor against copper, steel and aluminum corrosion.



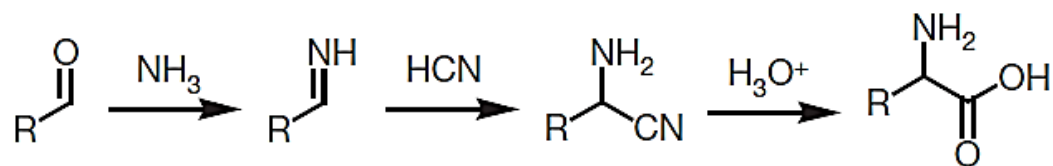
The amino acids are non-volatile in nature which offers them an advantage over other inhibitors<sup>191</sup>. Due to better stability and compatibility, the amino acids can also be easily recovered from the pipelines. The structure and chemical properties of amino acids are also well understood which makes it easier to understand their inhibition mechanism.<sup>176</sup> Thus, the inhibition of gas hydrates by amino acids offer many positive applications in the area of flow assurance.

### ***2.2.1 Amino acids: Synthesis & Application***

The use of chemical synthesis and biotechnology are the two main methods used for the large scale manufacture of amino acids. Both of these methods are described briefly below:

#### ***2.2.1.1 Chemical Synthesis***

Glycine and L-alanine are manufactured using the method of chemical synthesis. Normally, an amino acid is synthesized from an aldehyde or ketone is a series of chemical reactions known as Strecker amino acid synthesis. Zuend, et al.<sup>192</sup>, provided a simplified reaction scheme of strecker amino acid synthesis as shown in the **Scheme 3** below. The synthesis requires the condensation of the aldehyde with ammonium chloride in the presence of potassium cyanide, forming a  $\alpha$ -aminonitrile. This  $\alpha$ -aminonitrile is then hydrolyzed to get the required amino acid.<sup>193</sup>



*Scheme 3:* Shows the simplified reaction Scheme of Strecker amino acid synthesis illustrating the formation of the  $\alpha$ -amino acid.<sup>192</sup>

It is reported that chemical synthesis more likely forms racemic forms of amino acids and an additional step is involved, that requires the utilization of an enzyme known as aminoacylase. The amino acylase is formed by *Aspergillus niger* and this enzyme is required to get the biologically active L-form of amino acids.<sup>174,194</sup> However, this step has a high production cost and the only couple of amino acids such as glycine and methionine are manufactured cost-effectively using chemical synthesis.

The major advantage of using chemical synthesis method is that it provides direct formation of L-isomers of amino acids using a chiral catalyst. But, the major disadvantage is that this method is not considered commercially viable.<sup>195</sup> Therefore, the use of chemical synthesis method is limited and it is only used for the production of alanine, glycine, methionine, phenylalanine, threonine, tryptophan, and valine.<sup>196</sup>

### 2.2.1.2 Use of Biotechnology

The use of biotechnology for the production of amino acids over the wide scale is in practice for over five decades.<sup>197</sup> Generally, the biotechnological methods for the wide-scale production of amino acids can be classified into two main types. This includes the use of microbial enzymes or use of semi or direct fermentation process.

#### ***Microbial Enzymes***

The use of enzyme catalysis for the production of amino acids is the widely used method in the chemical industry.<sup>195</sup> Using this method the amino acid precursor is converted to the desired amino acid using one or two enzymes. The method involves the use of pure enzymes and facilitates the conversion of the amino precursor to desired amino acids without the hassle of microbial growth.<sup>195</sup> For example, L-Cysteine is widely manufactured on a large scale via an enzymatic process in which the thiazoline derivative DL-2-amino-2-thiazoline-4-carboxylic acid is converted to Cysteine by the aid of three enzymes (L-ATC hydrolase, S-carbamoyl-L-cysteine-Hydrolase and ATC racemase) derived from *Pseudomonas thiazolinophilum* using enzyme membrane reactor.<sup>198</sup> The amino acids such as alanine, aspartic acid, cysteine, phenylalanine, serine, and valine are largely produced using this method. The method involves the use of enzyme membrane reactor and several tons of amino acids such as L-methionine and L-Valine are produced annually using this method.<sup>185</sup>

According to Leuchtenberger, et al.<sup>185</sup>, the enzyme catalysis is a popular method of producing D-amino acids and non-protein L-amino acids. The enzymatic manufacturing of L-tryptophan from precursors requires a single reaction step, which is conducted using isolated enzymes such as tryptophan synthase or different types of micro-organisms like E.Coli.<sup>199</sup>

### ***Fermentation Method***

The fermentation method is widely used for the production of L-amino acids. The use of this method requires the conversion of nutrients to several vital components via micro-organisms.<sup>195</sup> During the process, the raw materials like syrups are added to micro-organism culture media and the flourishing micro-organisms end up producing amino acids.<sup>195</sup>

In the fermentation process, the enzymes also play an important in the production of amino acids. The process involves consecutive reactions by 10 to 30 types of enzymes and large numbers of amino acids are produced as the result of these reactions. The fermentation process is carried on a culture medium that constitutes of grains, sugar, yeast or other biological materials.<sup>200</sup> The extraction process is carried out via physical and mechanical methods such as heating or chemical method that involves the use of petroleum solvents, strong acids, strong bases or ion exchange. The final product is extracted as a crystalline powder.<sup>201</sup>

Normally, micro-organisms produce 20 different kinds of amino acids in the amount they require. Table 2-1, shows the list of amino acids with their relevant production processes and application. They have a technique for regulating the quantities and qualities of the enzymes to produce amino acids in the quantity only necessary for them.<sup>197b</sup> Therefore, once a suitable micro-organism for the amino acids production is selected, its potential is enhanced in order to take full benefit of the potential of the organism. This allows large-scale production of desired amino acids.<sup>195</sup> The amount of amino acids produced via micro-organisms depends on the quantities and qualities of the enzymes. The yield of amino acids is enhanced if the related enzymes of the desired amino acids are present in the large quantities under feasible conditions. However, if the enzymes are present in the small quantities the yield of the desired amino acid decreases.<sup>195</sup>

Table 2-1: *Production process and application of the key amino acids*<sup>195</sup>

Amino Acids	Production Process	Organisms	Application
<b>Glycine</b>	Chemical synthesis	--	Buffering agent in antacids, antiperspirants, and cosmetics
<b>L-Alanine</b>	Chemical Synthesis, Enzymatic method	Pseudomonas dacunhae	Ingredient in food supplement for sports athletes helps in muscle recovery and growth
<b>L-Arginine</b>	Fermentation	C.glutamicum, Brevibacterium, and E.Coli	Ingredient in the dental products (tooth paste) and food supplements

Table 2 1: *Production process and application of the key amino acids*<sup>195</sup>

Amino Acids	Production Process	Organisms	Application
<b>L-Aspartic Acid</b>	Enzymatic	E. Coli	Sweetener and food supplement.
<b>L-Cysteine</b>	Enzymatic, Extraction	E. Coli and Pseudomonas thiazolinophilum	Ingredient in the food supplements and as the precursor in the pharmaceutical industry
<b>L-Glutamine</b>	Fermentation	C. glutamicum	Ingredient in the fitness sports supplement and used for treating neuropathic diseases.
<b>L-Histidine</b>	Fermentation	Brevibacterium flavum	Ingredient for food supplement used for treating premenstrual pain and also used in the manufacturing of anti-inflammatory drugs.
<b>L-Isoleucine</b>	Fermentation	C. glutamicum, E.Coli	Ingredient for the fitness sports supplements
<b>L-Leucine</b>	Fermentation and Extraction	Brevibacterium Flavum and E.Coli	Ingredient for the fitness sports supplements. Considered an essential amino acid for muscle growth.
<b>L-Lysine</b>	Fermentation	C. glutamicum	Food supplement for adequate absorption of calcium and formation of collagen for bone, cartilage and body tissues.
<b>L-Proline</b>	Protein hydrolysis, Fermentation	Brevibacterium flavum and E. Coli	Used in the pharmaceutical industry as the stabilizer and osmoprotectant.
<b>L-Serine</b>	Protein hydrolysis, Fermentation	Methylobacterium sp.	Used in drugs or supplements required for treating chronic fatigue syndrome and mental wellness.
<b>L-Tryptophan</b>	Fermentation and Enzymatic method	E. Coli, C. glutamicum, Bacillus sp.	Used in food supplements required for treating sleep disorders, depression, and premenstrual disorder.

Historically, the use of fermentation for the production of amino acids was carried out by KINOSHITA, et al.<sup>202</sup>. They found the soil bacteria named as *Corynebacterium glutamicum* which has a distinctive property of producing large amounts of L-glutamine from sugar and ammonia.<sup>203</sup> Some years later, a mutant of *C. glutamicum* named as homo-serine-Auxo-trophic was found to have an ability to produce large quantities of L-lysine by the process of fermentation.<sup>204</sup>.

The same soil bacteria *Corynebacterium* was found to have an ability to produce amino acids L-Valine, L-isoleucine, L-threonine, L-aspartic acid and L-alanine.<sup>205</sup> The amino acids L-phenyl alanine, L-threonine and L-cysteine can also be derived via fermentation with *E. Coli* strain<sup>206</sup>. Commercially, most amino acids can be manufactured using mutants of *C. glutamicum*<sup>197b</sup> or *E.Coli*<sup>177a, 204b, 207</sup>

The biotechnological methods such as fermentation and use of enzymes for mass amino acids production carry many economic and ecological benefits.<sup>241</sup> The use of enzymatic method allows the production of optically pure amino acids in higher quantities with less number of byproducts.<sup>185</sup> However, this method requires the use of specific substrates that can be converted into amino acids. These specific substrates can be expensive, which limits the commercial scope of this methodology. Therefore, the fermentation method is widely used in the industry for the manufacturing of L-amino

acids.<sup>195</sup>

*The fermentation* and enzyme-based production processes both play an essential role in the manufacturing of L-amino acids that are used as ingredients in the pharmaceutical industry. Both these processes are helping in the expansion of the amino acids market and also helping to reduce the commercial cost of amino acids.<sup>185</sup> However, more research is required to improve these biotechnological methods by varying culture conditions, mutation and combining technologies like genetic engineering and metabolic engineering.<sup>195</sup>

Table 2-2, shows the advantages and disadvantages of different methods used for the amino acids production on the large scale. According to Ikeda<sup>175a</sup>, the economy of fermentation method rely on the factors like the cost of the carbon source, the amount of yield obtained, the purification steps required and the overall productivity of the process. There are certain issues that need to be taken care of during the fermentation process which includes the contamination of the culture with other microorganisms, reproducibility of the yields obtained, loss of genetic material in the production strain and infection of the microorganism culture.<sup>202</sup>

The fermentation and enzyme-based production processes both play an essential role in the manufacturing of L-amino acids that are used as ingredients in the



pharmaceutical industry. Both these processes are helping in the expansion of the amino acids market and also helping to reduce the commercial cost of amino acids.<sup>185</sup> However, more research is required to improve these biotechnological methods by varying culture conditions, mutation and combining technologies like genetic engineering and metabolic engineering.<sup>195</sup>

Table 2-2: *Advantages and disadvantages of different methods used for the production of amino acids on the large-scale*<sup>195</sup>

Production Method	Advantages	Disadvantages
<b>Chemical Synthesis</b>	It's a continuous process so large-scale production of amino acids can be obtained.	It requires an additional optical resolution step to obtain the bio-active L-isomers. This additional step makes the process expensive.
<b>Fermentation</b>	<ol style="list-style-type: none"> <li>1. Simple process</li> <li>2. Holds economic and ecological benefits</li> <li>3. Holds high production capacity</li> <li>4. Can utilize cheap and renewable carbon sources as the raw material.</li> </ol>	Not all types of amino acids (like L-methionine) can be manufactured cost-effectively using this method.
<b>Use of enzymes (Enzymatic Method)</b>	<ol style="list-style-type: none"> <li>1. Can be used to produce optically pure amino acids</li> <li>2. Hold economic and ecological benefits</li> </ol>	Only specific types of substrates can be used as the raw material for the production process. These substrates can be very expensive sometimes.

### 2.2.2 Amino acids: Physio-Chemical Properties

In an aqueous solution with neutral pH, the carboxylic side chain of amino acids gets dissociated into carboxylate and a free proton is liberated ( $-COOH \rightarrow COO^- + H^+$ ) and the amino side which acts as a base is protonated ( $-NH_2 + H^+ \rightarrow -NH_3^+$ ). Due to this reason in an aqueous environment, the predominant form of amino acid exists as a dipolar ion or zwitter ion [Figure 2-2], which consists of a carboxylate anion ( $-COO^-$ ) and an ammonium cation ( $-NH_3^+$ ).<sup>208</sup> Katchalski-Katzir, et al.<sup>208</sup>, illustrated a dipolar form of amino acid with the R- side chain group as shown in Figure 2-2.

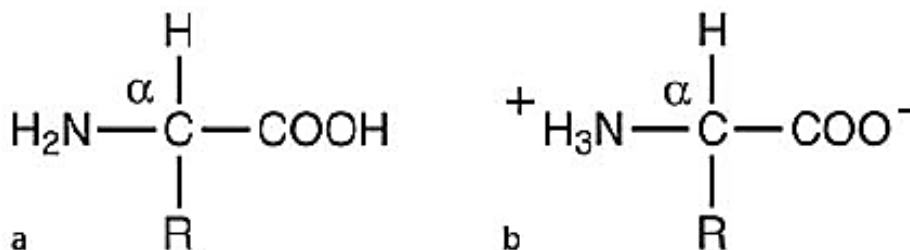


Figure 2-2: (a) Physical Structure of amino acid (b) Dipolar form of the amino acid with R the side chain group<sup>208</sup>

The physical properties of amino acids rely on their dipolar ionic structure. Generally, amino acids can be classified as non-volatile crystalline solid that has a

tendency to melt or decompose at high temperatures in comparison to amines and carboxylic acids.

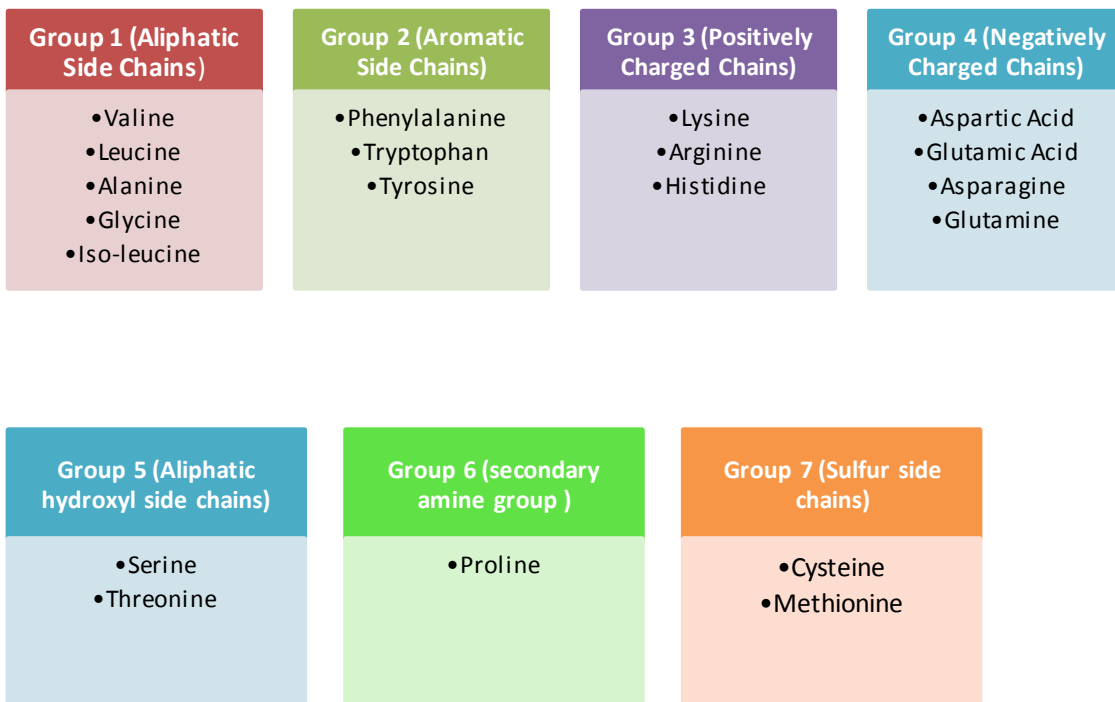
Amino acids tend to have high dielectric constants and high dipole moment.<sup>209</sup> This facilitates the separation of positive and negative charges in their dipolar ionic forms. The high dipole moment also shows that amino acids are insoluble in non-polar solvents such as benzene and ether, but are fairly soluble in water.<sup>208</sup>

#### *2.2.2.1 Classification of Amino Acids*

The physical and chemical features of the amino acids rely on the side chain (R-group) attached to the amino acid structure [Figure 2-2]. Generally, there are two broad classes of amino acids that are categorized as per the hydrophilic or hydrophobic nature of the amino acid side chain.

According to Katchalski-Katzir, et al.<sup>208</sup>, the hydrophobic chemical groups are more suited to dissolve in the non-polar organic solvents, while the hydrophilic groups tend to dissolve more easily in water. The information regarding the hydrophobic or hydrophilic character of the amino acid side chain helps to identify the chemical type of a given protein or a specific region of a protein. The hydrophobic or hydrophilic character of the solute is denoted as hydrophathy.<sup>208</sup> The chemical nature of their side chains the amino acids can be classified into seven different groups [Figure 2-3]. The group 1 includes the amino acids with aliphatic side chains such as Valine, Leucine,

Alanine, Glycine, and Iso-leucine. The group 2 includes the amino acids that consist of aromatic side chains like Phenylalanine, Tryptophan, and Tyrosine. The group 3 includes the amino acids that consist of basic positively charged side chains like Lysine, Arginine, and Histidine. The group 4 contains amino acids with acidic negatively charged side chains like Aspartic Acid, Glutamic Acid, Asparagine, and Glutamine.



*Figure 2-3: Classification of 20 key amino acids into different groups based on their respective side chains* <sup>208</sup>

The group 5 includes the amino acids with aliphatic hydroxyl side chains like Serine and Threonine. The group 6 only consists of amino acid Proline, as it has a secondary amine group that affects the protein backbone conformation and the group 7

consists of amino acids with sulfur-containing side chains like Cysteine and Methionine. The disulfide bond that cross-links between two Cysteine residues exists in many proteins, especially the extracellular proteins such as insulin, immunoglobulins, and antibodies. The Disulfide bonds have an essential role in protein structure stabilization.  
208, 210

### *2.2.2.2 Absorption Spectrum of Amino Acids*

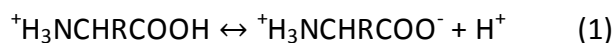
None of the naturally occurring amino acids found in proteins absorbs light in the visible range.<sup>208</sup> But, the amino acids with aromatic side chain (Group 2), such as the one shown in Figure 7, tend to absorb light in the ultraviolet range.

The amino acids mainly tend to absorb light in the far UV range (<220nm) due to the presence of amide bond, peptide bond, and carboxylic groups. The fluorescence of amino acid Tryptophan is very easy to detect and this allows its use as a built-in probe for investigating polypeptide structure and interactions.<sup>208</sup>

### *2.2.2.3 Electrostatic Properties of Amino Acids*

The electrostatic properties of the amino acids rely on the charge present on the  $\alpha$ -amino, the  $\alpha$ -carboxy or the ionizable side chain of the amino acid according to Chipot, et al.<sup>211</sup>. The overall charge is determined by the ionization constant of these ionizable groups and the pH of the aqueous medium in which the amino acids function.<sup>211</sup> Katchalski-Katzir, et al.<sup>208</sup>, provided equations that depict the dissociation

of  $\alpha$ -ammonium and  $\alpha$ -carboxylic groups of amino acids as shown below<sup>208</sup>:



The variations in the pH of the solution in which amino acid function causes a change in the electric charge pattern of the amino acid, due to different ionization states. When the pH of a solution is equal to the isoelectric point (pI) of amino acids, the net charge of the amino acid is equal to zero. According to Katchalski-Katzir, et al.<sup>208</sup>, The acidity constant of an acid ( $K_a$ ) is equal to the apparent equilibrium constant of the dissociation reaction of the acid ( $K'_{eq}$ ). Thus, the  $K_a$  value for the dissociation reaction (1) above can be given by:

$$K'_{eq} = K_a(\alpha\text{COOH}) = [\text{H}^+][{}^+\text{H}_3\text{NCHR}\text{COO}^-] / [{}^+\text{H}_3\text{NCHR}\text{COOH}]^{208}$$

The large the  $K_a$ , the stronger is the acid. The  $\text{p}K_a$  equals  $-\log(K_a)$ , so the smaller the  $\text{p}K_a$  the stronger is the acid. Experimentally, the  $\text{p}K_a$  values of different ionizable groups of amino acids are easily obtainable via potentiometric titration of these groups with strong base or acid. The  $\text{p}K_a$  value of the  $\alpha$ -carboxyl group of amino acids lies within the range of 1.8-2.4 and the  $\text{p}K_a$  value of the  $\alpha$ -ammonium group lies within the range of 9.0-11.0.<sup>208</sup>

#### 2.2.2.4 Optical features and Stereochemistry of Amino Acids

All amino acids that are produced as the result of acid or enzymatic hydrolysis of proteins tend to display optical activity, except the amino acid glycine. The amino acids display the optical activity by rotating the plane of polarized light. The stereochemical analysis of these naturally existing amino acids reveals that they all have the same configuration about the  $\alpha$ -carbon, which is similar to that of the L-glyceraldehyde.<sup>208</sup>

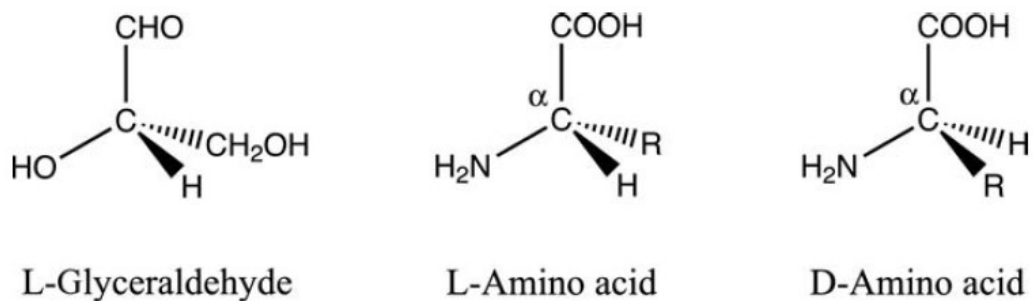


Figure 2-4: Shows the optical configuration of L-Glyceraldehyde, L-Amino Acid, and D-Amino Acid.<sup>208</sup>

As shown in Figure 2-4, there are two stereoisomers of glyceraldehyde which are categorized as L and D. All stereoisomers of amino acids that are related to L-glyceraldehyde are categorized as L, while the stereoisomers of amino acids that are

related to D-glyceraldehyde are categorized as D, irrespective of the direction of rotation of plane-polarized light produced by the isomers [Figure 2-4].<sup>208</sup>

### **2.2.3 Amino acids: Recycle & Recovery**

In 1957, a method to recover the amino acids from the solutions was patented by Blish and Schlaeger<sup>212</sup>. The process involves series of steps to recover glutamic acid and pyrrolidone carboxylic acid from the solutions. The process consists of the columns packed with the activated alumina to adsorb amino acids from the solutions containing them.<sup>212</sup>

When the acid protein hydrolysate solution is passed through a column containing alumina, treated with hydrochloric acid, it was observed that glutamic, aspartic and pyrrolidone carboxylic acids are quantitatively adsorbed from the solution onto the activated alumina.<sup>212</sup> Later these amino acids can be eluted or desorbed by passing an acid or an alkaline solution through the column of alumina. This allows the recovery of the amino acids from the alumina column. Blish and Schlaeger<sup>212</sup>, stated that this method allows the recovery of glutamic acid from amino acid solutions and it also allows recovery of glutamic acid and pyrrolidone carboxylic acid from liquors.<sup>212</sup>

The traditional separation of amino acids from the aqueous solution involves the methods such as ion exchange, a liquid membrane with extractants<sup>213</sup> and the reversed micelle.<sup>214</sup> However, it is reported that most of this method utilizes organic solvents that are flammable and hazardous to humans and other living organisms. Therefore, now the



research is being focused on the use of low environmental impact solvents such as ionic liquids for the recovery of amino acids from the aqueous solutions.<sup>215</sup> In addition to that, the ionic liquids have also found applications in liquid-liquid extractions of metal ions<sup>216</sup> and organic compounds.<sup>217</sup>

The hydrophilic nature of amino acids makes it difficult to extract them using a solvent in the liquid-liquid extraction process according to Leodidis and Hatton<sup>218</sup>. In order to extract amino acids, it's essential to add lipophilic cationic or anionic extractants with the solvent.<sup>218-219</sup> However, this extraction method is not considered very efficient. Therefore, in order to extract amino acids, the researchers have tried the use of macrocyclic compounds that have the tendency to form stable hydrophobic 'host-guest' complexes with amino acids.<sup>220</sup>

The most popular macrocyclic compounds used for the extraction of the amino acids from the aqueous solution is crown ethers according to Noguchi, et al.<sup>220</sup>. These compounds have the tendency to form complexes by hydrogen bonding of protonated amino groups.<sup>221</sup> Therefore, different types of carrier molecules have been designed and studied.<sup>222</sup> Normally, the optimum condition for efficient recovery of amino acids is obtained using hydrophobic counterions.

The amino acids Tryptophan, Glycine, Alanine, Lysine, Arginine and Leucine were

extracted from the aqueous solution by Smirnova, et al.<sup>223</sup>, using the room temperature IL 1-butyl-3-methylimidazolium hexafluorophosphate ( $B_{mim}PF_6$ ) and cyclohexane-18-crown-6 (CE) solvents in the ratio 1:1 and 1:2. These amino acids were extracted at the pH range of 1.5-5.5 and it was found that the most hydrophilic amino acids like glycine are extracted more efficiently than the other amino acids. According to Smirnova, et al.<sup>223</sup>, the system can be used to recover amino acids from the pharmaceutical samples and fermentation media. The major advantage of using ionic liquid for the extraction process is that it helps to eliminate the emulsion formation. The emulsion formation usually takes place when the cationic or anionic extractants are used. This helps to reduce the overall separation and recovery time.

The feasibility of using imidazolium-based ILs  $[C_4mim][PF_6]$ ,  $[C_6mim][PF_6]$ ,  $[C_6mim][BF_4]$  and  $[C_8mim][BF_4]$  as an alternative solvent for the recovery of amino acids from the aqueous medium via extraction equilibrium experiments was investigated by Wang, et al.<sup>215</sup>. By using these IL solvents the feasibility of recovery amino acids such as L-tryptophan, L-tyrosine, L-phenylalanine, L-leucine and D-Valine from the aqueous medium was tested.

The experimental procedure used by Wang, et al.<sup>215</sup>, involves the liquid-liquid contact of an equal molar mixture of aqueous solution of amino acids with the pure ionic liquid inside the glass test tubes (16 \* 75 mm) with stoppers.<sup>215</sup> The system is then vigorously stirred by the help of the magnetic stirrer and then after the stirring of half an

hour, the two phases are carefully separated by the help of the centrifuge. The pH of the aqueous phase is measured by the help of the pH meter and the concentrations of the amino acids in the aqueous solution before and after extraction are measured by the help of the spectrophotometer. For the amino acids mixtures, the concentrations are evaluated by the help of liquid chromatography. Finally, the partition coefficients of amino acids between the IL and aqueous solution are calculated by the following equation<sup>215</sup>:

$$P_{IL/W} = \frac{C_i - C_f}{C_f}$$

In the above expression the  $C_i$  is the initial concentration of the amino acids and the  $C_f$  is the final concentration of the amino acids in the aqueous solution.

The extraction degree of amino acids tends to increase with the increase in the hydrophobicity factor of the amino acids according to Wang, et al.<sup>215</sup>. The partition coefficients of the amino acids rely on the hydrophobicity factor of the amino acids.<sup>215</sup> This indicates that the hydrophobicity factor is the driving force for the partition of the amino acids into the particular ionic liquids. These partition coefficients were found to be strongly affected by the pH of the aqueous phases and the water solubility in the ionic liquids.

It was reported that the partition coefficients increase in value with the rising

solubility of water in ionic liquid phase by Wang, et al.<sup>215</sup>. On contrary, the partition coefficients values decrease drastically by increasing the pH of aqueous phases. It was also found that the ILs containing  $\text{BF}_4^-$  anion tend to provide much higher extraction efficiency for the amino acids compared to the ILs containing  $\text{PF}_6^-$  anion due to stronger effective charge in  $\text{BF}_4^-$ .<sup>215</sup> The ILs  $[\text{C}_6\text{mim}][\text{BF}_4]$  and  $[\text{C}_8\text{mim}][\text{BF}_4]$  were found to be potential IL solvents for the separation of amino acids from the aqueous medium.

The use of ionic liquids and macrocyclic compounds like crown ethers for extraction of amino acids from the aqueous solution holds a good potential. The use of these compounds can be a step forward in the development of the process on the industrial scale for the extraction and recovery of amino acids from the process lines.

#### ***2.2.4 Amino acids: Hydrate Inhibition Studies***

The first hydrate inhibition study using natural amino acids was conducted by Sa, et al.<sup>191</sup> using Glycine, L-Alanine, and L-Valine as thermodynamic hydrate inhibitors for  $\text{CO}_2$  hydrates. According to Sa, et al.<sup>191</sup>, at the concentration 0.5 mol% and pressures of 20 bars and 30 bars the  $\text{CO}_2$  HVLE curve was shifted by  $0.4 \pm 0.1$  K by L-Valine,  $0.35 \pm 0.1$  K by L-Alanine and  $0.30 \pm 0.1$  K by Glycine. Thus, the increasing order of thermodynamic inhibition was found to be in the following order: L-Valine > L-Alanine > Glycine. In the same study, Sa, et al.<sup>191</sup> stated that amino acids do have a tendency to inhibit  $\text{CO}_2$  hydrates and the thermodynamic inhibition strength of amino acids increases with increase in their hydrophobicity. The side alkyl chains of amino acids are hydrophobic

and as the size of an alkyl chain increases the hydrophobicity is enhanced and the disruption of hydrogen bonds between water molecules also increases.

The kinetic inhibition effect of L-Alanine, Aspartic Acid, Asparagine, Phenylalanine, and Histidine on CO<sub>2</sub> hydrates at a low concentration ( < 0.1 wt%) was further investigated by Sa, et al. <sup>224</sup>. It was found that aspartic acid and asparagine exhibit higher kinetic inhibition than alanine. Histidine was also found to be a better CO<sub>2</sub> hydrate Kinetic hydrate inhibitor than alanine and phenylalanine.

It was predicted that the hydrophilic and electrically charged chain of amino acids tends to disrupt the water structure and the hydrophobic part of the amino acid side chain strengthens it when they are in touch with hydrate crystals by Sa, et al. <sup>224</sup>. Hence, the amino acids with stronger hydrophilic side chain are expected to be more effective in delaying hydrate nucleation as they are more likely to cause disruptions in water structure.

Then later Sa, et al. <sup>225</sup>, extended their study by using amino acids Glycine, L-Alanine, L-Valine, Leucine, and Isoleucine as kinetic hydrate inhibitor (KHI) for CO<sub>2</sub> hydrate inhibition. According to Sa, et al. <sup>225</sup>, the amino acids with lower hydrophobicity act better as a KHI and tend to delay the hydrate nucleation and growth by disrupting the water hydrogen bond network. They also stated that the amino acids with higher hydrophobicity tend to strengthen the local water structure and have no or little effect

on hydrate kinetics. This is mainly due to the dual complexity of strengthening of water structure around side chains and disruption of water structure around ionic moieties. The extent of perturbation caused by a particular amino acid is likely to depend on the hydrophobicity of that particular amino acid.<sup>226</sup> Therefore, the perturbation of the water structure around the plays a key role in the kinetic hydrate inhibition.

The glycine to be the most effective CO<sub>2</sub> kinetic hydrate inhibitor, as the small chain amino acids like glycine form strong hydrogen bonds with water molecules according to Sa, et al.<sup>225</sup>. It has also been reported that glycine has the ability to eliminate the memory effect and same is the case found with previously reported antifreeze proteins.<sup>227</sup> The L-Alanine was found to be slightly less efficient than glycine because amino acids with longer alkyl chains tend to less effective as kinetic hydrate inhibitor and some of them can even accelerate the hydrate formation. Therefore, the one with the shorter alkyl chains is better suited as kinetic hydrate inhibitor. The amino acids that are highly hydrophilic tend to disrupt the crystal lattice of water and prevent the hydrate formation. The increasing order of kinetic hydrate inhibition for CO<sub>2</sub> was found to be in the following order: Glycine > L-Alanine > L-Valine > Leucine > Isoleucine.

The inhibition of gas hydrates via amino acids could also occur due to the presence of oxygen atoms of the carbonyl group in amino acids as stated by Roosta, et al.<sup>228</sup>. The oxygen atoms allow the formation of hydrogen bonds with the water molecules causing disruption of hydrate cages.<sup>229</sup>

The hydrophobic side chain of amino acids tends to produce electrostatic interactions with the hydrate crystal structure, which interrupts hydrate nucleation and disrupts the further growth of hydrate crystals. Normally, the amino acids tend to reduce the rate of hydrate formation and delay the hydrate crystal growth during intermediate formation stages.<sup>230</sup>

It was further proposed by Geiger, et al.<sup>231</sup> and Pertsemlidis, et al.<sup>232</sup> that amino acids tend to cause a reduction in water orientation structure dynamics which is favourable for the hydrate inhibition. When the hydrate formation takes place the water molecules reorient themselves in a manner to form cages that can capture small guest molecules like methane and ethane.

The amino acids affect the re-orientation behaviour of the water molecules through hydrogen bonding and this causes hydrate thermodynamic inhibition effect as shown in their hydrate multi dynamics simulation study conducted by Carver, et al.<sup>233</sup>. They observed that as the hydrogen bonding energy of amino acids increases, the water reorientation, and disruption increases. This improves the overall thermodynamic inhibition impact.

The methane hydrate dissociation in the presence of 0.01wt %, 0.03 wt%, and

0.3 wt% tryptophan was studied by Veluswamy, et al. <sup>234</sup> and it was found that with the increase in the concentration of amino acid there is a slight incremental increase in the rate of the hydrate dissociation.

The kinetic inhibition effect of amino acids glycine and leucine on Tetra hydro furan (THF) and Ethane hydrates was studied by Naeiji, et al. <sup>235</sup> and Rad, et al. <sup>236</sup>. In both studies, glycine was found to be a better kinetic hydrate inhibitor than leucine. Liu, et al. <sup>237</sup> and Veluswamy, et al. <sup>238</sup> showed in their studies that leucine kinetically promotes CH<sub>4</sub> hydrates.

The use of amino acid tyrosine as kinetic hydrate inhibitor for the natural gas was suggested by Talaghat <sup>239</sup> and it was observed that tyrosine does have a tendency to delay natural gas hydrate induction time. Kakati, et al. <sup>240</sup> further suggested that the addition of tyrosine to PVP enhances the kinetic inhibition effect of PVP by 37 % on natural gas hydrate.

The experimental results using infrared spectroscopy<sup>241</sup>, neutron scattering<sup>232</sup> and Raman spectroscopy <sup>226</sup> also reveal that the amino acids can cause perturbation of water molecules through the strengthening of hydrogen bond network between water molecules and amino acids <sup>232, 241</sup> The amino acids with shorter side chain tend to have lower hydrophobicity and higher inhibition potential.



Many other studies <sup>225, 242</sup>, also states that the effectiveness of amino acids to inhibit the hydrate growth strongly depends on their hydrophobicity. The amino acids with higher hydrophobicity tend to be less effective as kinetic hydrate inhibitor than the ones with lower hydrophobicity.

### ***Summary***

The above literature review shows that most studies using amino acids as hydrate inhibitors have been conducted using pure CO<sub>2</sub> gas. But, no comprehensive hydrate inhibition studies using amino acids as CH<sub>4</sub> gas hydrates have been conducted to date. Therefore in section 4.2, the thermodynamic and kinetic inhibition effect of amino acids L-Histidine, Glycine, Asparagine, Phenylalanine and L-alanine at different concentration (1-5 wt%) has been investigated using pure methane gas and different pressure conditions. This will allow to evaluate the feasibility of using amino acids as hydrate inhibitors on the large scale.

### 2.3 Enhancing Hydrate Inhibition using Synergents

In order to enhance the inhibition effectiveness of hydrate inhibitors, the effect of mixing synergents like polyvinylpyrrolidone (PVP), poly-vinyl caprolactam (PVCap), Sodium Chloride (NaCl), poly-ethylene oxide (PEO) and anti-freezing polymers with hydrate inhibitors have been considered in different kinds of previous work.<sup>229a, 243</sup>

Synergents are polymeric compounds normally do not show any hydrate inhibition itself but can significantly enhance the kinetic inhibition performance of hydrate inhibitors when added in small quantities.<sup>229a, 243</sup> They can help to reduce the required quantity of hydrate inhibitors. As per the general observation, the synergistic effect of polymeric compounds could be due to presence of alkoxy (R-O) group in synergents. The alkoxy groups in polymeric compounds disturb the hydrate cage formation, which reduces the number of water cages. The less number of water cages reduces the workload of KHI, which enhances their overall effectiveness.<sup>244</sup>

The polymer and hydrate surface interaction is not structured specific and the most likely mechanism by which large lactam ring size polymers provide hydrate inhibition is the perturbation of bulk water structure assenting with Abrahamsen and Kelland<sup>47</sup>. However, more research is required to understand the acting mechanism of these synergistic compounds. According to O'Reilly, et al.<sup>245</sup>, the polyvinylpyrrolidone (PVP) has a tendency to inhibit the hydrate crystal growth and many modelling studies

also suggest that it prevents the nucleation of the hydrate crystals by destabilizing the SI hydrate clusters from a distance without directly interacting with the hydrate surface.<sup>245</sup>

### **2.3.1 Sodium Chloride (NaCl)**

The synergistic effect of NaCl on the hydrate inhibition performance of PVP (poly-vinyl-pyrrolidone) in deep water drilling fluid was examined by Zhao, et al.<sup>246</sup>. The NaCl exhibited a strong synergistic effect on the performance of PVP and enhanced both the hydrate nucleation inhibition and hydrate growth inhibition strength of PVP.

It was observed that in deep water drilling fluid with 0.5 wt% of PVP, the addition of 10 wt% NaCl prolonged the hydrate induction time from 60 min to over 1000 min, at the same water depth conditions of 2 ° C and 100 bars and sub-cooling temperature of 14.2 ° C. According to Zhao, et al.<sup>246</sup>, at higher sub-cooling temperature of 16.4 ° C, the mixture of 10 wt% NaCl + 1.5 wt% PVP gave an induction time of 600 min. This prolonged induction time allows safer deepwater drilling.

The kinetic inhibition effect of addition L-tyrosine and NaCl as synergents with PVP on a gas mixture containing methane, ethane, and propane was investigated by Kakati, et al.<sup>240</sup>. Their experimental results show that the addition of L-tyrosine and NaCl enhances the inhibition effectiveness of PVP. According to Kakati, et al.<sup>240</sup>, the addition of 1wt% PVP as an inhibitor with gas mixture delayed the hydrate induction time from 27 to 45 min. But, the addition of mixture 0.5 wt% PVP + 0.25 wt% NaCl +

0.25wt% L-tyrosine with gas mixture delayed the hydrate induction time from 27 to 65 min.

### **2.3.2 Poly-vinyl caprolactam (PVCap)**

The kinetic and thermodynamic inhibition effect of nine ILs on CH<sub>4</sub> hydrate formation by mixing them with polymeric hydrate inhibitor PVCap was studied by the Lee, et al.<sup>247</sup>. These ILs included: [EMIM-BF<sub>4</sub>], [EMP-Cl], [BMP-BF<sub>4</sub>], [HEMP-Cl], [HEMP-BF<sub>4</sub>], [BMP-Br], [EMP-Br], [EMP-BF<sub>4</sub>] and [BMP-Cl]. According to Lee, et al.<sup>247</sup>, the selected ILs performed better as kinetic hydrate inhibitor and the hydrate induction time at 3wt% ILs (7 MPa) was found to be within the range of 4.5-139.4 min. This range was enhanced to 9.3-184.9 min when 0.5 wt % PVCap was added with ILs (0.5 wt% IL + 0.5 wt% PVCap).

The PVCap acts as a synergent and it can enhance the kinetic inhibition effectiveness of selected ILs even at low concentration (0.5 wt%) as stated by Lee, et al.<sup>247</sup>. Their experimental results indicated that the addition of PVCap helped to reduce the amount of IL required for hydrate inhibition from 3 wt% to 0.5 wt%. This has a significant effect on overall capital cost required for the purchase of ILs.

Later, the above study was extended by using a different gas mixture and varying concentration of PVCap (0.1wt%, 0.5 wt% and 1wt% PVCap) in IL + PVCap mixture by Lee, et al.<sup>248</sup>. It was found that by keeping the concentration of IL constant and increasing the concentration of PVCap alone, the induction time of hydrate formation is

enhanced significantly. The hydrate induction time for mixture A (0.5 wt% HEMP-BF<sub>4</sub> + 0.1 wt% PVCap) was 84 min, for mixture B (0.5 wt% HEMP-BF<sub>4</sub> + 0.5 wt% PVCap) was 500 min and for mixture C (0.5 wt% HEMP-BF<sub>4</sub> + 1 wt% PVCap) was 1350 min at 7.7 MPa. This shows that the concentration of PVCap has a significant impact on the effectiveness of IL + PVCap solution as KHI.

The synergistic effect of glycol ether compounds on the kinetic inhibition performance PVCap (poly-vinyl caprolactam) using the methane-rich gas mixture containing CO<sub>2</sub> and N<sub>2</sub> was investigated by Yang and Tohidi <sup>249</sup>. They found that glycol ether compounds significantly delayed the hydrate nucleation time and also delayed the catastrophic growth of hydrates significantly. They proposed that the presence of glycol ether molecules tend to increase the adsorption of PVCap molecules on the hydrate growth sites more than on hydrate nucleation sites. In addition to that, the synergistic effect of glycol ether compounds can also be attributed to the molecular size of these molecules.

The hydrate inhibition strength of mixture containing mono-ethylene glycol (MEG) and PVCap on a synthetic natural gas mixture containing 90 mol % methane and traces of ethane, propane, and butane was investigated by Kim, et al. <sup>250</sup>. According to Kim, et al. <sup>250</sup>, the mixture of 0.2 wt% PVCap + 20 wt% MEG delayed the hydrate induction time significantly and the hydrate fraction was less than 0.19. They found that the mixture of 0.2 wt% PVCap + 30 wt% MEG delayed the hydrate induction up to 24

hrs. This shows that the mixing of MEG with a small amount of PVCap results in the inducement of synergistic effect that helps to delay the hydrate induction time and also prevent the agglomeration and deposition of hydrate particles.

The 5 to 6 rings structures like cyclopentane, tetrahydrofuran or tetrahydropyran are the largest rings that can be lodged into the large SII ( $5_{12}6_4$ ) cages by the help of the gas such as methane.<sup>251</sup> The poly-vinyl caprolactam (PVCap) as a synergist (like glycol ether) may provide better kinetic hydrate inhibition performance due to the fact that most of the lactam ring sizes in polymers are too large to be accommodated into any of the  $5_{12}6_2$  or  $5_{12}6_4$  hydrate cavity.

### ***2.3.3 Poly-ethylene Oxide***

Polyethylene oxide (PEO) as a non-ionic homopolymer of ethylene oxide that exists as a white powder and can act as an antioxidant.<sup>252</sup> It is used in various papermaking applications and is usually obtained as dry granules. It is a linear polymer and is soluble in water. It shows an inverse solubility-temperature relationship and as the water temperature rises the PEO-water system gets separated into phases.<sup>253</sup> It is considered to be a weak thermodynamic inhibitor<sup>254</sup> and is unable to act as a kinetic inhibitor itself.<sup>50</sup>

The use of PEO as a hydrate inhibitor for the pure methane, ethane and propane gas was reported by Englezos and Ngan <sup>254a</sup>. They studied the hydrate inhibition strength of PEO at different concentrations (5- 25 wt%) within the temperature range of

273.55 – 285.3 K and pressure range of 0.187-9.961 MPa. Englezos and Ngan <sup>254a</sup>, reported PEO as a poor hydrate inhibitor compared to electrolytes and alcohols.

The synergistic effect of PEO on the kinetic inhibition performance of commercial kinetic inhibitors like Luvicap EG (INH 3), Luvitec K90 (INH 4), Luvitec VPC 55 (INH 5) and many others using pure methane gas and methane-ethane gas mixture was investigated by Lee and Englezos <sup>255</sup>.

The addition of 0.5 wt% INH 3 to pure methane sample delayed the hydrate induction time from 0.5 min to 86 min. However, the addition of mixture 0.5 wt% INH 3 + 0.025 wt% PEO delayed the hydrate induction time from 0.5 min to 148 min. Similarly, the addition of 0.025 wt% PEO with INH 4 helped to delay the hydrate induction time from 0.5 min to 15.6 min. In case of INH 5, the addition of 0.025wt% of PEO helped to delay the hydrate induction time from 0.5 min to 82 min respectively. The addition of PEO also helps to reduce the memory effect of the commercially used kinetic hydrate inhibitors.<sup>256</sup>

The synergistic effect of PEO and Polypropylene oxide (PPO) on kinetic inhibition strength of inhibitor PVP and L-tyrosine using pure methane, pure CO<sub>2</sub> and pure propane gases in a flow mini-loop apparatus was investigated by Talaghat <sup>252</sup>. He found that the hydrate induction time is prolonged significantly when the small dosage of PEO and PPO is added with the kinetic inhibitors PVP and L-tyrosine.

The PEO and PPO are high molecular weight polymers that are not kinetic inhibitor themselves, but their addition in solution with inhibitors decreases the accessibility of water molecules to guest CH<sub>4</sub> molecules and this helps to delay the hydrate formation or induction time.<sup>252</sup> The bulkier structure of these polymers is also likely to cause steric hindrance to water molecules and block the guest diffusion.

The addition of 200 ppm of PVP in a blank sample of pure methane gas helps to delay the hydrate induction time from 50 to 80 min at 8 MPa, reported by Talaghat<sup>252</sup>. However, the addition of mixture 200 ppm PVP + 100 ppm PEO in a blank pure methane sample helps to delay the hydrate induction time from 50 to 95 min. Similarly, the addition of PEO with L-tyrosine helped to delay the methane hydrate induction time from 320 to 420 min.

### ***Summary***

It is evident from the above literature review that most studies using PEO as a synergent has been conducted on commercial kinetic hydrate inhibitors like Luvitec, PVP, and Luvicap. But no work has been reported showing the synergistic effect of PEO on the hydrate inhibition performance of ionic liquids and amino acids. Hence, in Section 4.1 and Section 4.2, the synergistic effect of PEO on the kinetic inhibition performance of selected ionic liquids and amino acids has been experimentally investigated using the quaternary gas mixture (QM) and pure methane gas. The



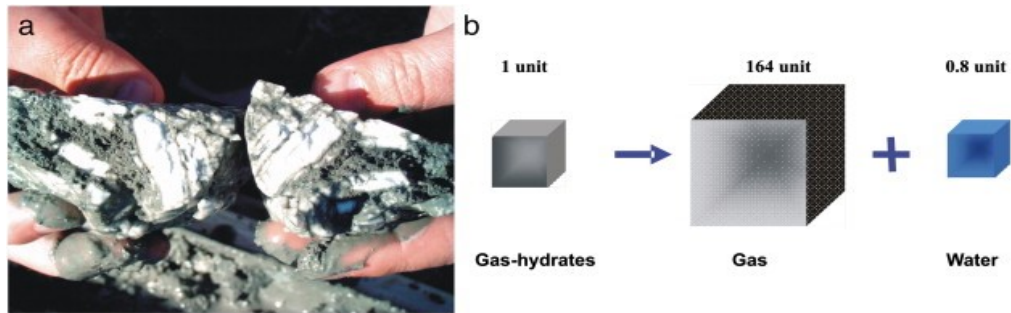
synergents can help to reduce the dosage of the required hydrate inhibitor and reduce the overall CAPEX.

## 2.4 Factors affecting the rate of hydrate formation

The formation of gas hydrates is a nuisance for the oil and gas sector, but the gas hydrates also have many positive uses which include transportation and storage of natural gas<sup>257</sup>, separation of gas<sup>258</sup>, CO<sub>2</sub> capture<sup>259</sup>, desalination<sup>260</sup>, refrigeration<sup>261</sup>, coal mine gas separation<sup>262</sup>, and separation of undesirable (toxic or incombustible) species from biogases.<sup>263</sup> The transportation of natural gas in the hydrate form hold strong future prospects due to the economic feasibility of converting gas to hydrates<sup>264</sup>.

The gas hydrates possess good storage properties and one volume of hydrate can hold up to 180 volumes of natural gas at STP<sup>265</sup>. Therefore, there is a strong industrial interest in the development of hydrate production plants and processes that can convert gas to hydrates and transport them over the long distances.

As shown in Figure 2-5, the gas molecules within hydrate clusters are highly compressed and one volume of gas hydrates has a tendency to hold 164 volumes of methane and 0.8 volume of water [Figure 2-5]<sup>266</sup> Therefore, they are considered to be the future energy resource and medium for natural gas storage and transportation.



*Figure 2-5:*The amount of pure methane gas and water present in the one volume of the gas at Standard Temperature and Pressure (STP).<sup>266</sup>

The hydrates formation rate is the major parameter, in design and operation of hydrate production units that can convert gas into hydrates <sup>267</sup>. It is widely accepted that high pressure and low-temperature conditions stimulate the rate of hydrate formation. Luo, et al. <sup>268</sup>, stated that the methane consumption rate increases as the temperature is reduced and the methane consumption rate increases as the pressures is raised across the bubble column. However, there are many other factors that can stimulate the rate of hydrate formation. The hydrate formation rate can be accelerated by the addition of zeolite in pure water <sup>269</sup>, the addition of surfactant in system <sup>270</sup>, and use of the fixed bed column filled with sand. <sup>271</sup>

The chemical aspects used to enhance the rate of hydrate formation includes the use of hydrate thermodynamic promoters like tetra hydro furan (THF)<sup>272</sup> and kinetic promoters like sodium dodecyl sulfate <sup>273</sup>.The mechanical aspects used to enhance the

rate of hydrate formation includes magnetic stirring or agitation<sup>274</sup>, use of baffles<sup>275</sup> and bubbling of gas using a nozzle.<sup>268</sup> These aspects are related to different types of reactors which include stirred tank and bubble tower reactors. Among all the mechanical aspects, the magnetic stirring is mainly used in the hydrate formation studies. As the stirred tank is easier to construct and maintain on the laboratory scale, most hydrate formation studies are conducted using the stirred tanks.<sup>276</sup> A brief review of work conducted on hydrate formation kinetics using magnetic stirring is provided below.

#### ***2.4.1 Mechanical agitation***

The mechanical agitation is widely used in the batch process reactor to speed up the rate of reaction. In the hydrate formation studies, the mechanical agitation is mainly provided by the help of a magnetic stirrer.<sup>276</sup> Previous studies suggest that the stirring aids in reducing hydrate formation time and enhances the hydrate formation rate and gas storage capacity of hydrate.<sup>275</sup>

The methane hydrate formation in a semi-continuous stirred tank reactor with and without the stirrer was observed by Hao, et al.<sup>275</sup>. It was found that the stirrer strongly affects the rate of hydrate formation and enhances the rate of mass transfer and heat transfer in the hydrate formation process.

The stirring helps to reduce the hydrate formation time according to Hao, et al.<sup>275</sup> and the optimum stirring velocity and stirring time for the selected stirred tank reactor was found to be 320 RPM (Rotations per minute) and 30 min. They also

suggested the use of baffle along with the stirrer to enhance the rate of hydrate formation inside the stirred tank reactor. However, the long stirring time can result in the decomposition of the hydrates formed in the reactor.

The hydrate first tends to appear at the gas/water interface and then nurture into a stiff hydrate film that impedes any further growth of the hydrate crystals under still conditions according to Xiao, et al.<sup>277</sup>. The stirring helps to renew the gas\water interfacial area and reduces the hydrate formation time and speeds up the rate of hydrate formation at early stages of the formation. The two main stages of hydrate formation inside the stirred reactor identified are the formation of hydrate slurry and the eventual block caused by the hydrate clusters.

A series of experiments where only the stirring rate was varied and the other factors were kept consistent was conducted by Englezos, et al.<sup>278</sup>. It was observed that the hydrate formation time is lower at the higher stirring rates. According to Englezos, et al.<sup>278</sup>, the average supersaturation needed for the hydrate nucleation is less at higher stirring rates. The experiments were performed at different stirring rates ranging from 300 to 450 RPM at the same pressure and temperature conditions. They observed that at the stirring rate of 400 RPM or greater, the kinetic parameter is no longer affected by the further increase in the stirring rate. In order to avoid extensive rippling on the gas-liquid interface, the 400 RPM was selected as the optimum stirring rate for the methane hydrate formation.

The growth of hydrate crystals was observed as a two-step process by Englezos, et al.<sup>278</sup>. In the first step, the dissolved gas tends to diffuse from the bulk of the solution to the hydrate crystal water interface. The in the second step, the gas molecules are incorporated into the water structure framework by an adsorption process.

The kinetics of methane hydrate decomposition in a semi-batch stirred tank reactor at different stirring rates was investigated by Kim, et al.<sup>279</sup>. They observed that the methane hydrate decomposition rate at a fixed stirring rate (RPM) is affected by the length of the stirring time. Also, the stirring time required to obtain methane hydrate decomposition also depends on the stirring rate (RPM). At the stirring rate of 640 and 700 RPM, the decomposition rates were found equal to the stirring times three minutes or higher. The longer stirring time aids in removing any excess gas from water to get a homogenous hydrate crystal during the initiation of the decomposition phase.

It was observed that the hydrate decomposition rate increases as the stirring speed is increased and the maximum hydrate decomposition rate was obtained at the stirring rate of around 640 RPM by Kim, et al.<sup>279</sup>. However, at the stirring speeds higher than 640 RPM, the decomposition rate was found to reach its upper limit. Kim, et al.<sup>279</sup>, proposed the upper limit is reached due to the fact that the mass-transfer resistances are abolished at stirring rate of 640 RPM and higher. It was also observed that the optimum stirring rate to obtain maximum hydrate decomposition is dependent on the

temperature and pressure conditions. Higher stirring rates are required at lower pressures and vice versa.

The effect of different stirring rates on the hydrate formation rate was also experimentally investigated by Ke and Svartaas<sup>280</sup>. They found that the higher stirring rates offer better hydrate formation rate in the isochoric system<sup>280</sup>. According to Ke and Svartaas<sup>280</sup>, the continuous stirring in the isochoric cell aids in reducing mass and heat transfer resistances and it also provides a homogenous environment for the hydrates formation<sup>31, 281</sup>. Moreover, the continuous stirring helps to improve the water gas interfacial area and also helps to improve hydrate formation rate<sup>265</sup>. Many modeling and simulation studies on hydrate kinetics are based on this concept.<sup>274b, 282</sup>

The faster stirring speed or higher stirring rates decreases the metastable crystal formation time according to Skovborg, et al.<sup>283</sup>, which in turn speeds up more hydrate formation within the system. Parent and Bishnoi<sup>284</sup>, also observed that the faster stirring speed enhances heat and mass transfer rates and facilitate accelerated hydrate formation by hindering temperature and composition gradients in bulk phase. Turner, et al.<sup>281</sup>, observed an acceleration in the hydrates formation rate when the hydrate cell impeller speed was accelerated from 400 rpm to 500 rpm during the experiments.

The low stirring rate is not adequate for hydrates formation, as at low stirring rate the hydrate crystals are likely to accumulate at the gas-liquid interface, which obstructs the heat and mass transfer and also reduces the hydrates formation rate according to Vysniauskas and Bishnoi<sup>274b</sup>. Interestingly, there also exists an upper threshold limit above which higher stirring rate or faster stirring speed has no effect on hydrates formation and above that threshold limit, negative effects can be detected within the system<sup>285</sup>.

It was suggested by Mork<sup>286</sup> that all hydrate kinetic experiments rely on the experimental system mechanics and specifications. Therefore, the model used for a single experimental system may not be appropriate for other experimental systems<sup>286</sup>. Though, the improvement in any factor that affects the gas-liquid interfacial area like stirring rate, may assist to accelerate the hydrate formation significantly<sup>286</sup>.

### ***Summary***

Based on the literature review, it was found that most of the hydrate formation rate studies have been conducted at the stirring rates of 200-700 RPM. Ke and Svartaas<sup>287</sup>, reported the effect of stirring rate on methane hydrate crystal formation within the range of 220 to 650 RPM in an isochoric cell. Furthermore, no experimental work was found to be reported on the higher stirring rates of 1000 RPM and above. Also no experimental work was found to be reported at lower stirring rates of 200 RPM and below. This indicates that there is a knowledge gap and in order to understand the



effect of stirring on the rate of hydrate formation it's essential to conduct experiments at low stirring rates of 200 RPM and below and also conduct experiments at higher stirring rates of 1000 RPM and above.

In the Section 4.1.1, the number of experiments were conducted at the stirring rates varying from 100 to 1400 RPM using the quaternary gas mixture (QM) was used in the High-pressure autoclave cell (HPC). The optimum stirring rate at which maximum hydrate formation occurs has been determined along with the interval of CHG.

## CHAPTER 3: EXPERIMENTAL METHODOLOGY

The chapter 3, provides experimental details about the methods and procedure used for testing the ionic liquids and amino acids as hydrate inhibitors. The experimental work has been conducted using pure methane gas and quaternary gas mixture (QM) which imitates natural gas mixture. The list of ionic liquids and amino acids tested in this work along with their purity index and relevant solubility in aqueous solution has also been provided.

A brief description of the experimental equipment used in this thesis experimental has been provided in section 3.2. Two different types of apparatus such as Rocking Cell Assembly (RC-5) and High-Pressure Cell (HPC) has been used in this work. The RC-5 has been used to test the ionic liquid and amino acid inhibitors. The HPC has been used to investigate the effect of stirring on the hydrate formation. The equipment calibration and experimental result validations are also shown in the section 3.23.

### **3.1 Materials**

The list of ionic liquids (ILs), synergents and amino acids used in this work is shown in Table 3-1 and Table 3-3. These ILs were purchased from Iolitec ionic liquid technologies GmbH, Germany (purity  $\geq 98\%$ ) and synergents were purchased from Sigma Aldrich Korea (purity  $\geq 98\%$ ). The amino acids used in this work were purchased from the Sigma Aldrich USA. All the sample solutions were prepared using distilled

water at the room temperature using the Mettler Toledo electronic mass balance with a precision of  $\pm 0.0001$  g.

The Table 3-1, shows the ionic liquids and synergents tested as the hydrate inhibitors in this work. These ionic liquids were tested at different concentrations (1-10 wt%) and pressure conditions (40-120 bars) on the pure methane gas and the specially designed quaternary gas mixture (QM). The ILs [EA][Of], [DMA][Of], [DMEA][Of] and [TBA][Of] were tested on the pure methane gas (purity  $\geq 99$  %) purchased from the Buzwair gas factories (Qatar). The ILs [PMPy-Cl] and [PMPy-Triflate] were tested as hydrate inhibitor on a specially designed quaternary gas mixture (QM) also purchased from the Buzwair gas factories.

Table 3-1: *List of Ionic Liquids (ILs) and synergents studied in this dissertation*


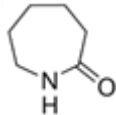
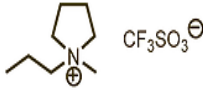
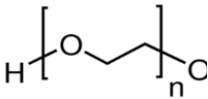
Ionic Liquids (ILs)	Structure	Synergents	Structure
1-Methyl-1-Propylpyrrolidinium Chloride [PMPy-Cl]		Polyethylene Oxide (PEO)	
1-Methyl-1-Propylpyrrolidinium Triflate [PMPy-Triflate]		Caprolactam (VCAP)	

Table 3-2: List of Ionic Liquids (ILs) studied in this dissertation

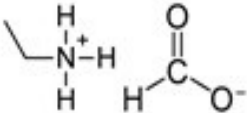
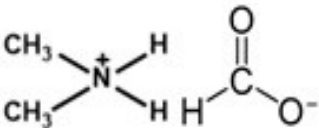
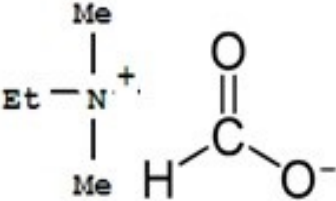
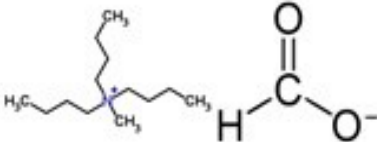
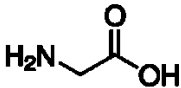
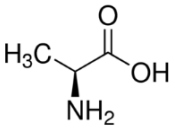
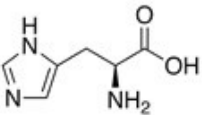
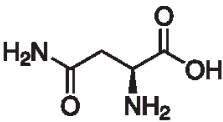
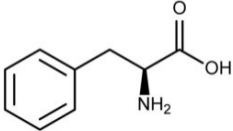
Ionic Liquids	Structure
Ethyl-ammonium Formate [EA][Of]	
Di-methyl-ammonium Formate [DMA][Of]	
Di-methyl-ethyl-ammonium Formate [DMEA][Of]	
Tri-butyl-methyl-ammonium Formate [TBA][Of]	

Table 3-3, shows the amino acids tested as the hydrate inhibitors in this work.

Table 3-3: List of amino acids used in this work

Amino Acid	Structure	M.W (g/mol)	Solubility in water at 25 ° C (per 100 ml) <sup>288</sup>	Traits <sup>289</sup>	Hydrophobicity <sup>290</sup>
Glycine		75.06	24.99 g	Non-polar, Exists as zwitterion can fit into both hydrophilic and hydrophobic environments	-0.4
Alanine		89.09	16.72 g	Non-polar, Hydrophobic	1.8
Histidine		155.15	4.19 g	Polar, Hydrophilic	-3.2
Asparagine		132.12	2.94 g	Polar, Hydrophilic	-3.5
Phenylalanine		165.19	2.96 g	Non-polar, hydrophobic	2.8

These amino acids were tested at different concentrations (1-5 wt%) and pressure conditions (40-100 bars) on the pure methane gas using the rocking cell assembly (RC-5).

### 3.1.1 Gas mixture

The ILs [PMPy-Cl] and [PMPy-Triflate] were tested as hydrate inhibitor on a specially designed quaternary gas mixture (QM) purchased from the Buzwair gas factories (Qatar). The components of the QM mixture are shown in Table 3-4. The purchased gas mixture composition was confirmed using the GC-analysis.

Table 3-4: Mol Composition of the QM mixture as per GC analysis

Components	Composition (Mol %)
<b>Methane C<sub>1</sub></b>	84.20
<b>Ethane C<sub>2</sub></b>	9.90
<b>n-hexane C<sub>6+</sub></b>	0.015
<b>Carbon Dioxide CO<sub>2</sub></b>	2.46
<b>Nitrogen N<sub>2</sub></b>	2.19

### 3.1.2 GC-Analysis for Quaternary Gas Mixture (QM)

The GC-Analysis for the quaternary gas mixture (QM) was conducted by the Gas Processing Center (GPC) located at the Qatar University using the PerkinElmer Calrus 580 Gas Chromatograph. The detail GC analysis numeric report is shown in Table 3-5.

As shown in Table 3-5, GC-analysis show that the quaternary gas mixture (QM) mainly consists of four components which include methane (85.24 %), ethane (10.03 %), carbon dioxide (2.49 %) and nitrogen (2.22 %).

Table 3-5: GC Analysis Report for the QM gas mixture

Peak #	Component Name	Time [min]	Area [uV*sec]	Area [%]	Cal. Range	Adjusted Amount	Amount [Norm. %]
1		0.011	2619.16	0.02		-----	0.00
2	C <sub>6+</sub>	3.142	6840.90	0.04		0.0153	0.02
3		11.564	4485.14	0.03		0.0045	0.00
4		11.705	4629.99	0.03		0.0046	0.00
5	CO <sub>2</sub>	11.934	589298.52	3.54	+	2.4625	2.49
6	C <sub>2</sub>	12.411	2434644.88	14.63	+	9.9036	10.03
7		13.556	956.27	0.01		0.0010	0.00
8		13.674	253.77	0.00		0.0003	0.00
9	N <sub>2</sub>	13.954	537574.20	3.23		2.1890	2.22
10	C <sub>1</sub>	14.467	13057499.01	78.48	+	84.1988	85.24
			<b>1.66 * 10<sup>7</sup></b>			<b>98.7795</b>	<b>100</b>

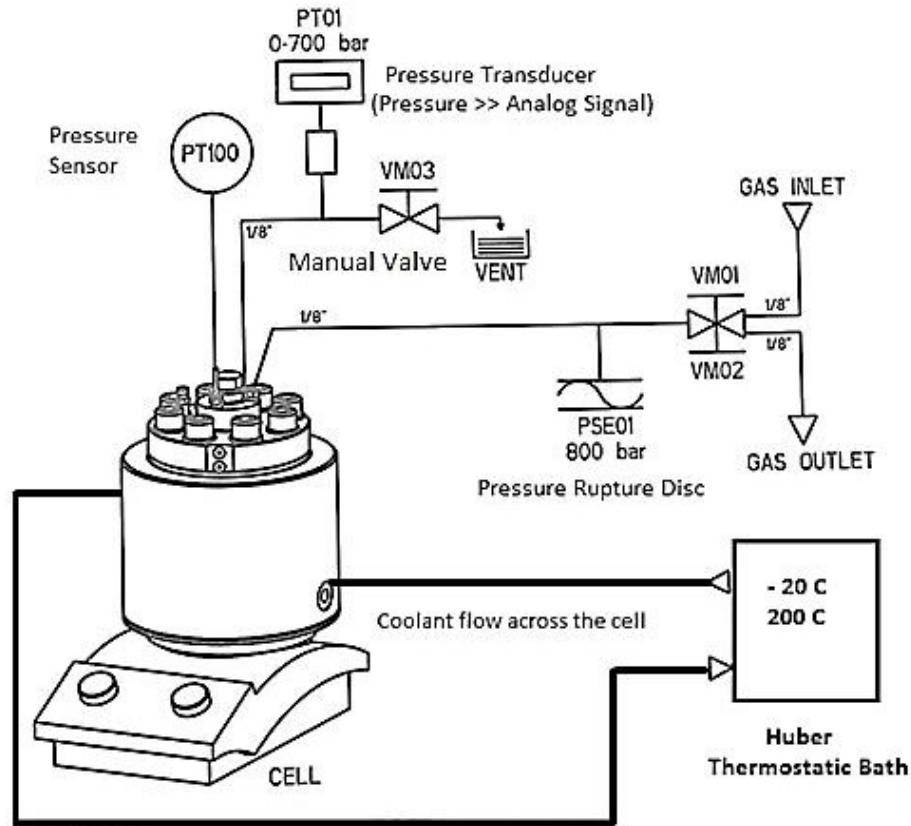
## **3.2 Equipment**

The experiments were carried out using the high-pressure cell (HPC) manufactured by Top Industrie France and the Rocking cell assembly (RC-5) manufactured by PSL systemtechnik GmbH Germany. The brief description of both equipment is provided below:

### ***3.2.1 High-Pressure Cell (HPC)***

The effect of stirring on QM mixture hydrate formation was analyzed in the high-pressure autoclave cell (HPC) purchased from the Top Industrie (France). As shown in Figure 3-1, the HPC cell is made up of Hastelloy (material: C276 + PTFE) and has the volume of 0.159 L and can be pressurized up to 700 bars and operated within the temperature range of -20°C to 200°C.



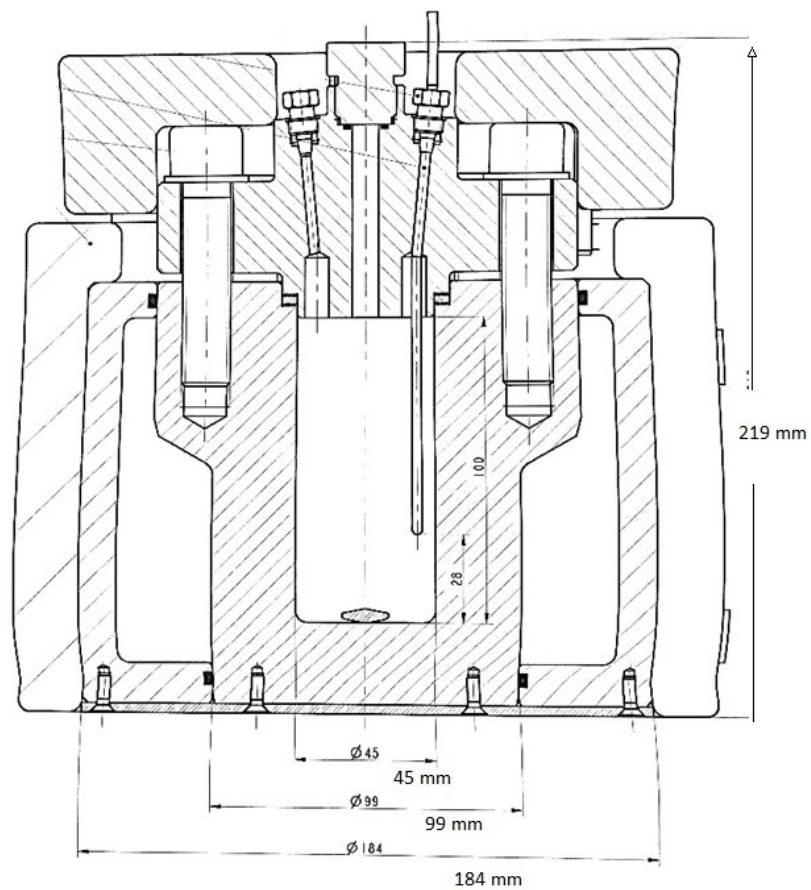


*Figure 3-1:* A schematic diagram of the High-pressure cell (HPC) used for studying the effect of stirring on the QM mixture hydrate formation.

The HPC has a data log system that takes reading after every 5 seconds. The Huber is connected to the HPC and it is used for cooling and heating the mixture solution inside the HPC.

As shown in Figure 3-1, the HPC consists of three manual high pressure (HP) 1/8" valves. The valves VM01 and VM02 are used for the gas inlet and gas out, while the valve VM03 is used for venting the gas into the atmosphere. The equipment also

consists of pressure safety rupture disc PSE01 (limit 800 bars) and pressure sensor PT100. The equipment is controlled by the help of software using the protocol specially written for the hydrate kinetic experiments. The CAD drawing showing the system dimensions is shown in Figure 3-2.



*Figure 3-2:* The CAD drawing showing the dimensions of the High-Pressure Cell (HPC)

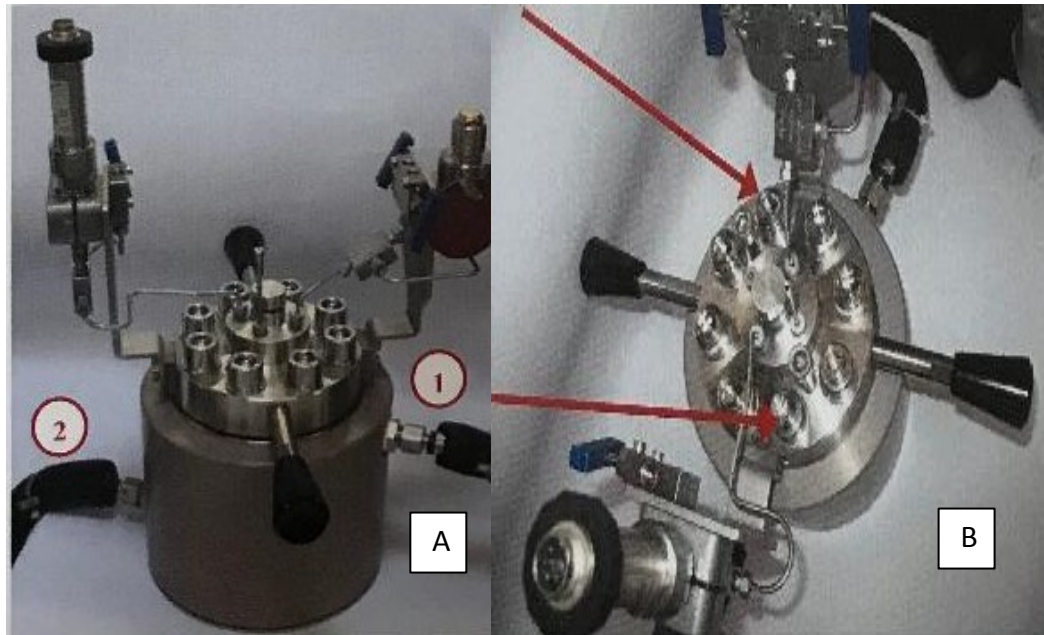
Figure 3-2, illustrates the dimensions of the HPC. The liquid sample cylinder is located at the centre of the cell and has the diameter of 45 mm. This length of the cell is 219 mm and diameter of the cell is 184 mm. Table 3-6, shows the HPC specifications provided by the manufacturer.

Table 3-6: *High-Pressure Cell (HPC) specifications by the manufacturer*

Factors	Specification
<b>Operating Pressure</b>	700 bar
<b>Maximum Pressure</b>	880 bar
<b>Operating Temperature</b>	-20 to 200 °C
<b>Material</b>	2.4819 (Hastelloy C276)
<b>Volume</b>	0.159 liter
<b>Internal diameter</b>	45 mm
<b>Valve</b>	1/8 "
<b>Mass of autoclave</b>	27 kg

Figure 3-3, demonstrates the top of the HPC (flange) consisting of eight stainless steel nuts (red arrows). After the liquid sample is filled inside the cylinder [Figure 3-4], these nuts are tightened by the help of the wrench. The Hastelloy body of the high-pressure cell below is then covered with the jacket to prevent heat losses during the

experiments.



*Figure 3-3:* A) A high-pressure cell assembly with the valves and pressure transducer, B) The top view of the high pressure cell

Figure 3-4, highlights the liquid sample cylinder where the magnetic stirrer is located. The internal diameter of this cylinder is 45 mm and it can hold the liquid volume of up to 150 ml.



*Figure 3-4:* The liquid sample cylinder where the magnetic stirrer is located

Figure 3-5, indicates a magnetic stirrer which rotates via Lab Mixer manufactured by Fisher brand inside the liquid sample cylinder. The lab mixer provides the necessary stirring needed for the experiments and its rotational speed (RPM) can be varied between 0 to 1400 revolutions per minute (RPM).



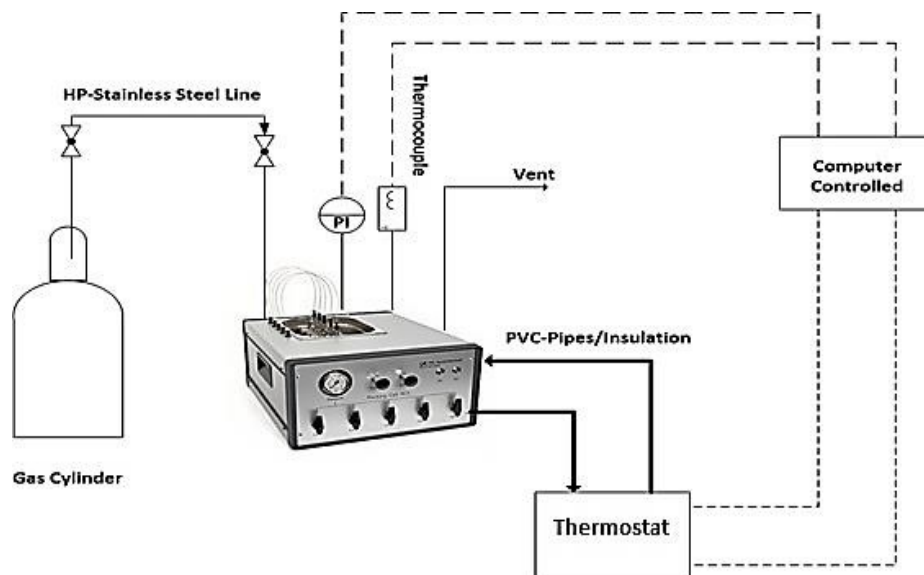
*Figure 3-5:* Magnetic stirrer inside the high-pressure cell that is agitated using the lab mixture placed below the high-pressure cell.

During the experiments, the liquid sample volume of 50 ml is added into this cylinder and then this cylinder is carefully tightened by the help of the stainless steel nuts located at the top. The cylinder also consists of the seal that needs to be replaced after the period of 6 months. This seal is used to prevent any gas leakages.

### **3.2.2 *Rocking Cell Assembly (RC-5)***

All experiments using ionic liquids (Table 3-1) and amino acids (Table 3-3) were conducted using a hydrate rocking cell assembly (RC-5) purchased from PSL Systemtechnik GmbH [Figure 3-6]. The rocking cell apparatus consists of 5 stainless steel cells that operate in parallel to each other and are connected to the same skid that rocks the cells.

The RC-5 consists of the 5-stainless steel cells that are submerged in the bath. The heating and cooling of the cells is carried out via the water bath (Huber) attached to the RC-5 bath [Figure 3-6].



*Figure 3-6:* A schematic diagram of Rocking Cell assembly (RC-5) used for the inhibitors test.

These cells can be operated up to 200 bars (2900 psi) and have temperature range within  $-10^{\circ}\text{C}$  to  $60^{\circ}\text{C}$ . Each cell has a capacity of  $40.13\text{ cm}^3$  and entails a stainless steel ball with the diameter of 1.7 cm that spins back and forth inside the cell to provide the necessary agitation and turbulence within the cell.<sup>40</sup> The detail system specification for the RC-5 is shown in



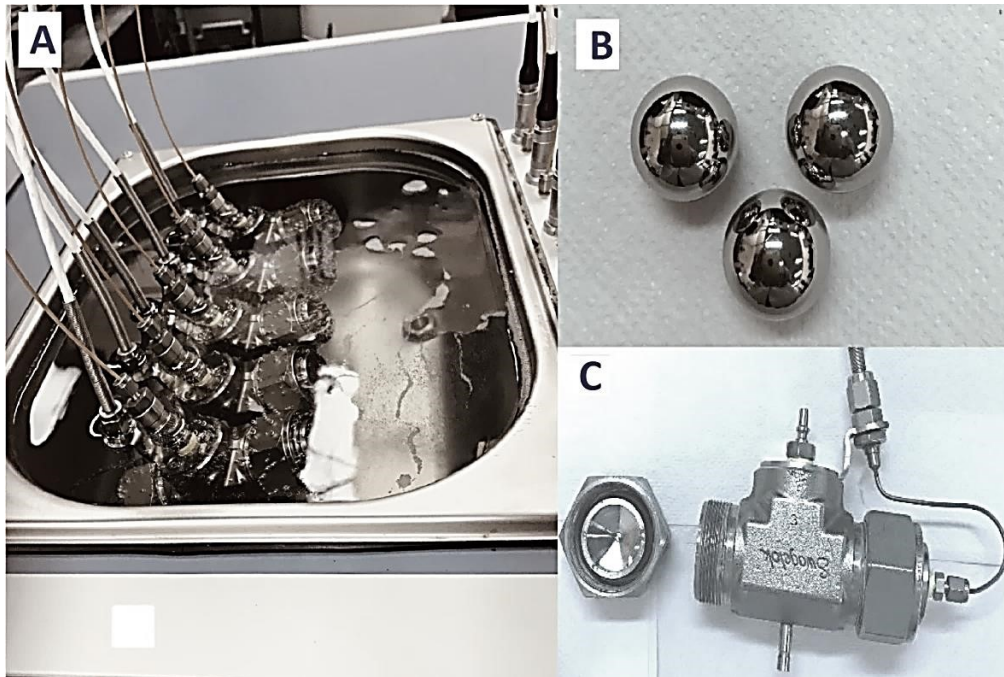
Table 3-7: *System specification for the Rocking Cell Assembly (RC-5) provided by the manufacturer*

Factor	Specification
<b>Number of test cells</b>	5
<b>Rocking Rate:</b>	1 to 20 rocks per minute
<b>Rocking Angle:</b>	1 to 45 °
<b>Pressure range:</b>	up to 200 bar (2,900 psi)
<b>Temperature range:</b>	-10 °C ... +60 °C (+14 °F ... +140 °F)
<b>The volume of test chamber:</b>	40.13 cm <sup>3</sup>
<b>The material of test chamber:</b>	stainless steel (AISI 316L)
<b>Data recording:</b>	After every 1 to 30 sec.
<b>Bath Volume:</b>	9.5 Liters
<b>Cooling liquid:</b>	Mixture of water-glycol
<b>Power consumption:</b>	90 W (RC5), max. 2,900 W (thermostat)
<b>Voltage input:</b>	230 V~ (115 V~ on request)
<b>Experimental duration</b>	Upt o 30 days
<b>Dimensions (WxDxH):</b>	51 x 60 x 29 cm (20 x 24 x 11 in) - without thermostat
<b>Weight:</b>	21 kg (46 lb) - without thermostat
<b>The diameter of the stainless steel balls</b>	17 mm

A diluted solution of inhibitors with the volume of 15 cm<sup>3</sup> measured in the cylinder is added to each cell and the cells are carefully tighten up via wrench to prevent any leakages. These cells are then placed on a rocking skid, which is submerged in a

cooling bath. The agitation is carried out inside the cells by rocking the cells back and forth with the hold angle of  $30^{\circ}$  and at rocking frequency of 10 rocks/min [Figure 3-7].

Figure 3-7, exhibits the key components of the rocking cell assembly which includes the cooling bath (a), stainless steel balls (b) and stainless steel cell with cap (c).



*Figure 3-7:* a) Shows cells submerged in cooling bath, b) Shows the stainless steel balls that provide agitation inside the cells, c) Shows the stainless steel rocking cell with a temperature sensor and the cap (lab pictures).

Once the cells are submerged in the cooling bath, each cell is pressurized alone with the gas until the desired pressure. Normally, cells are pressurized in a sequence ranging from 40-120 bars to obtain a wide range of the hydrate vapor liquid equilibrium data. The temperature and pressure readings of the cells are monitored by the help of the built-in data log system throughout the experiment.

The cooling bath, in which the cells are submerged, is connected to an external cooling circulator Huber Ministat 125 w that has a capacity to operate within the range of -25 °C to 60 °C. The temperature sensors have an accuracy of  $\pm 0.25$  °C and pressure sensors have the accuracy of 0.1 % .

### ***3.2.3 Equipment Calibration & Un-certainty***

Initially, the calibrations tests were conducted on the new RC-5 assembly to confirm the reliability of the data obtained. The test results were compared with the literature data and the simulation package.

Before using the RC-5, the 3 tests were conducted without inhibitors using the pure methane gas at different pressure conditions (40-120 bars) in the RC-5 and the tests results were compared with the already published results in the literature.<sup>291</sup> The experimental result matched well with the methane hydrate liquid vapor equilibrium (HLVE) data points provided in the literature [Figure 3-8]. This confirmed that the RC-5 is

well calibrated and reliable enough to be used for the hydrate inhibition studies.

The calibration results have been already reported as the supporting information in the published works. The comparison results clearly show that the experimental HLVE data points match well with the literature results, indicating that the RC-5 is well calibrated.

The combined standard un-certainty of the experiments (including the uncertainties from temperature, pressure measurements and the composition uncertainty of the gas mixture) for the RC-5 working with QM mixture was found to be 5.66 % and working with pure methane was found to be less than 2 %.

The pressure sensor uncertainty was found to be  $\pm 0.2$  bar and temperature sensors un-certainty was found to be  $\pm 0.2$  °C. The un-certainty for the experiments was determine using the procedure provided by Stephanie Bell <sup>292</sup> and the excel spreadsheet model provided by company Mahrenholtz + Partner (m+p) International (UK). The uncertainty in the reported hydrate induction or formation times was found to be  $\pm 0.5$  h.

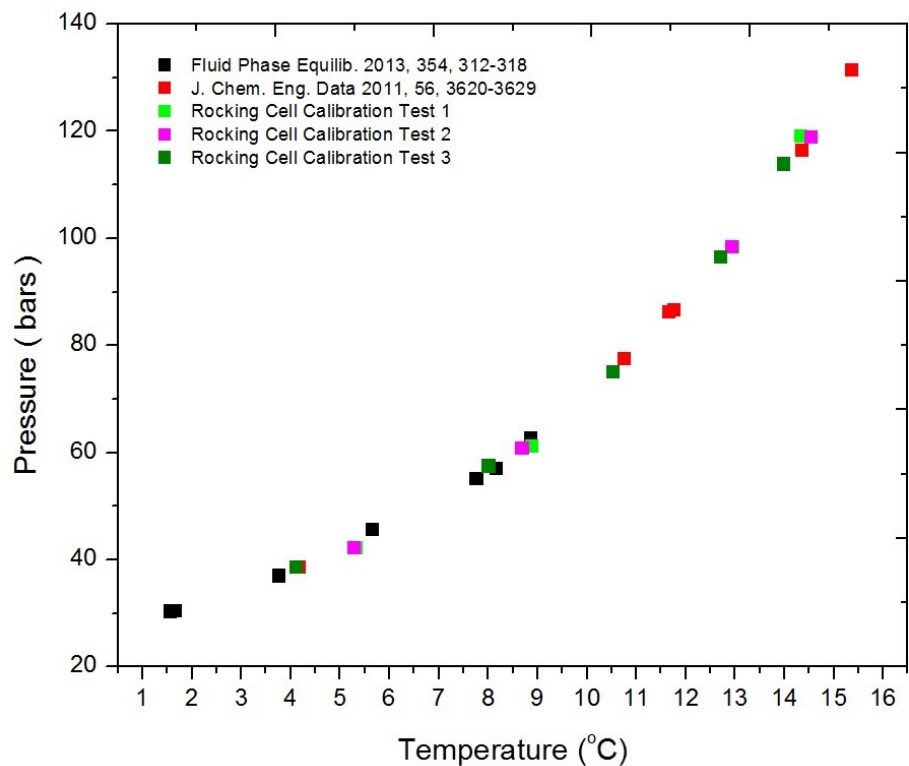
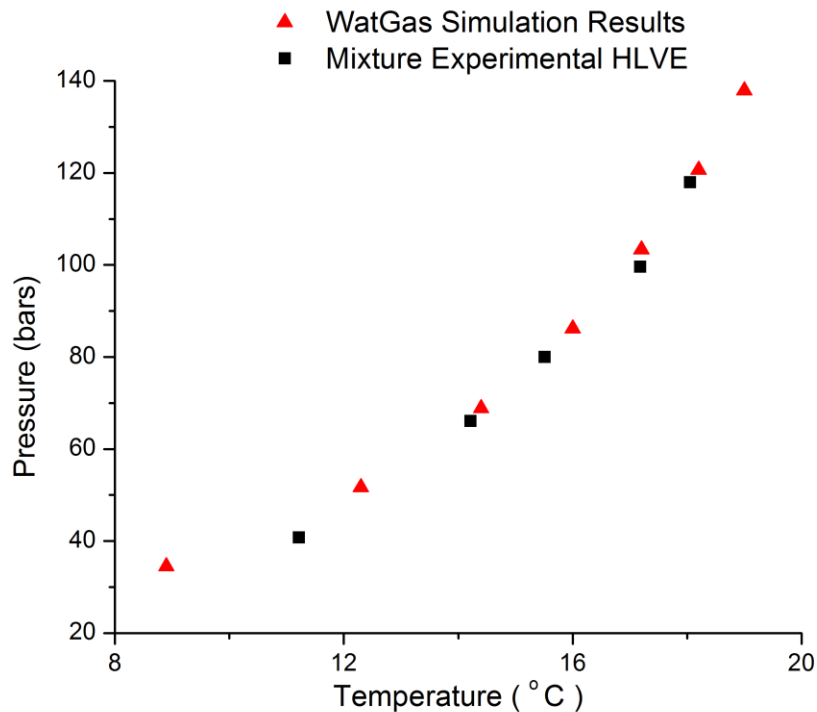


Figure 3-8: The comparison between the methane Hydrate liquid vapour equilibrium (HLVE) data points obtained experimentally from RC-5 and the methane HLVE data points reported in the literature previously.<sup>291</sup>

### ***Comparison with Simulation Package***

The QM mixture used in this study is a novel mixture and no hydrate liquid vapor equilibrium HLVE equilibrium data for it has been published in the literature. Therefore, the results obtained for the QM mixture were compared with the results of simulation software Wat-Gas v2011 [Figure 3-9]. The software is programmed by Nor Craft Software Company (Canada) and it is capable of performing hydrate formation

calculations and can also predict inhibitor quantities required to avoid hydrate problems. The program uses specific gravity method <sup>293</sup> to calculate the hydrate formation conditions using the Berge correlation.<sup>294</sup> The experimental results obtained for the QM mixture matches well with the simulation results of the Wat-Gas v2011 [Figure 3-9]. The matching of WatGas V2011 results with the RC-5 results indicates the reliability of the system.



*Figure 3-9:* Comparison of the Quaternary Gas Mixture (QM) HLVE data points obtained experimentally using RC-5 and the QM HLVE data points obtained using commercial simulation software WatGas V2011.

### **3.3 Experimental Procedures**

There were two different experimental procedures used in this work and each of the experimental procedure is discussed in detail in this section.

#### ***3.3.1 High-Pressure Cell (HPC)***

The following experimental method was used for studying the “Effect of Magnetic Stirring on QM hydrate formation” in the section 4.1.1. The 50 ml of de-ionized water was added to the liquid sample cylinder in the HPC and the cell is carefully closed by the help of the eight nuts located at the top of the cell. Then the HPC was pressurized up to desired pressure (98 bars) using QM mixture and using the lab mixer the stirring rate was adjusted to a specific value (Example 550 RPM) for each experiment accordingly.

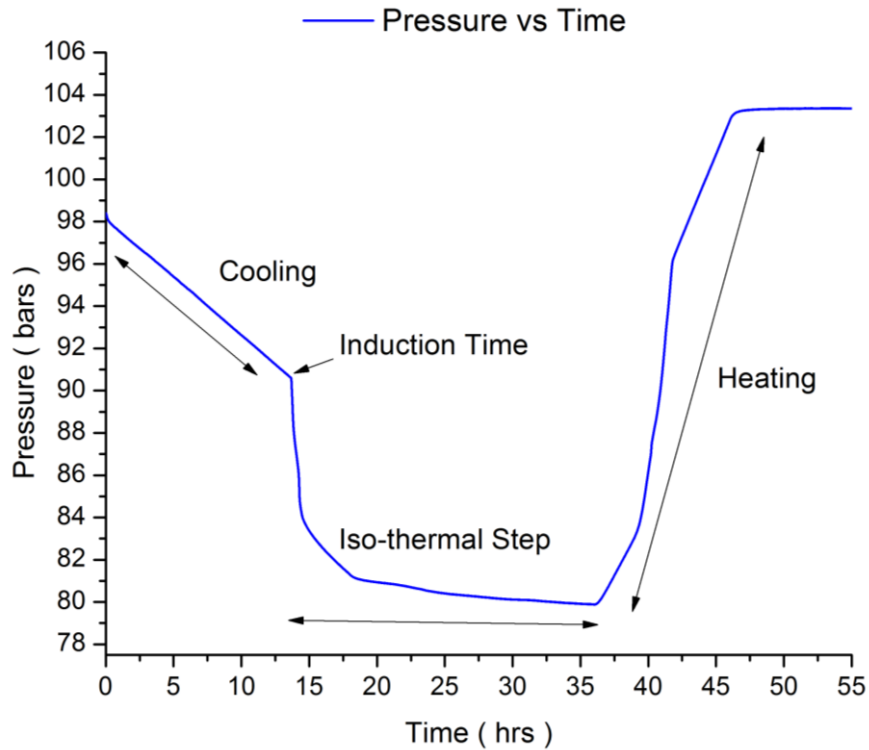


Figure 3-10: Experimental kinetic loop showing cooling, heating and isothermal steps in the stirring effect study on QM mixture inside the High-Pressure Cell (HPC).

As shown in Figure 3-10, before starting of the experiment, the system was stabilized at the temperature of 20 °C for one hour. Once the system was stabilized at 20 °C, keeping the stirring rate constant, the system was cooled from 20 °C to 2 °C in 18 hours (1 °C / hr ). The cooling step was followed by the isothermal step (constant cooling at 2 °C ) for 18 hours. The isothermal step facilitates the growth of the hydrate crystals within the HPC [Figure 3-10].



The formation of hydrates was indicated by the sharp pressure drop within the HPC [Figure 3-10]. In the end, the system was slowly heated from 2 °C to 30 °C in 14 hours (0.5 °C / hr) to dissociate away all the existing hydrate crystals within the HPC. Finally, the HPC was left stable for 30 °C for next 10 hours to ensure complete crystal dissociation. Each experiment was repeated at least three times and average hydrate formation time and average pressure drop at each stirring rate were determined.

### ***3.3.2 Rocking Cell Assembly (RC-5)***

The following experimental procedure was used for the testing of amino acids and ionic liquids as the gas hydrate inhibitors on the QM gas mixture and the pure methane gas in the sections 4.1, 4.2 and 4.3. Before initiating the experiment, the RC-5 is stabilized at the temperature of 20 °C for one hour. The mass transfer<sup>295</sup> and heat transfer aspects are crucial in hydrate formation process.<sup>296</sup> Therefore, once the RC-5 is stabilized at 20 °C the experiment is proceeded using isochoric pressure search method.<sup>44, 297</sup> This method was reported by Ohmura et al.<sup>298</sup> and it consists of cooling and heating cycles at a constant volume.<sup>299</sup>

Initially, the submerged cells are cooled from 20 °C to 2 °C in the time-frame of 9 hours with the cooling rate of 1.8 °C /hr, followed by an isothermal step of 24 hours at a fixed temperature of 2 °C. Finally, the cells are heated slowly at the rate of 0.1 °C per hour till the temperature reaches back to 20 °C [Figure 3-11]. The entire experimental process consists of three main step which includes cooling step, isothermal step and

heating step.

It was reported by Semenov, et al.<sup>300</sup>, that a constant heating rate of up to 0.5 °C/ hr does not affect the equilibrium point measurements. In this work, this rate is much slower (0.1 °C / hr). Furthermore, the extraction of hydrate dissociation point has been carried out using the procedure used by Tohidi, et al.<sup>301</sup>

The hydrate formation takes place during sub-cooling and the crystal growth is observed from the steep pressure drop that occurs during isothermal step when the temperature is kept constant at same volume [Figure 4].<sup>299</sup> The same protocol is used for all the experiments.

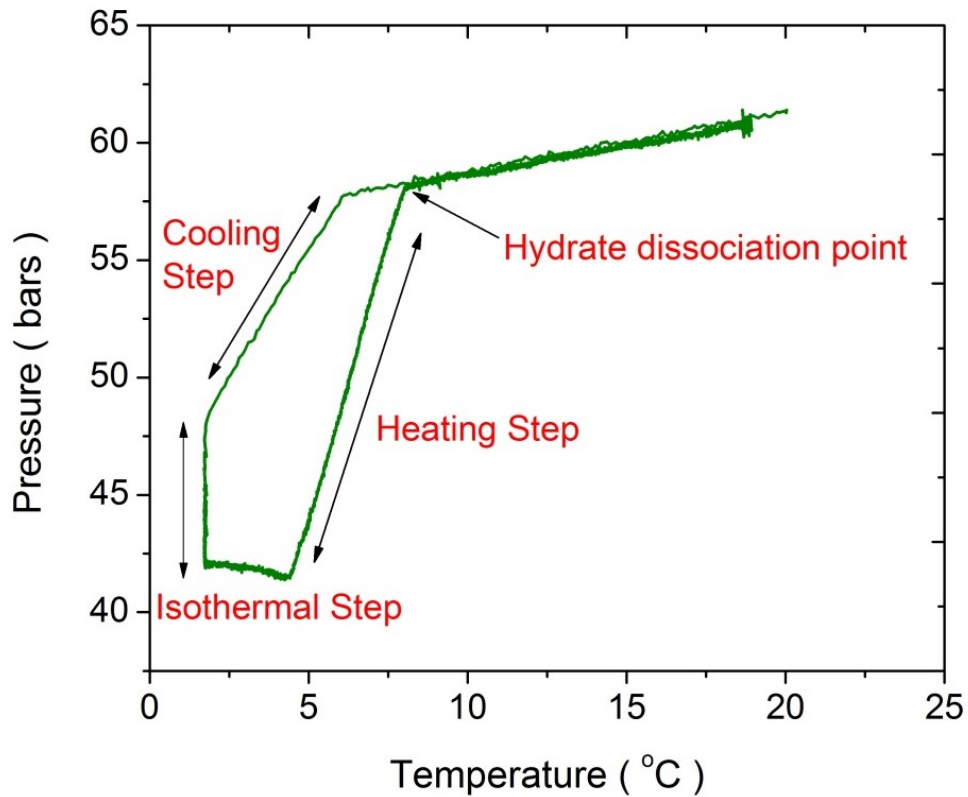
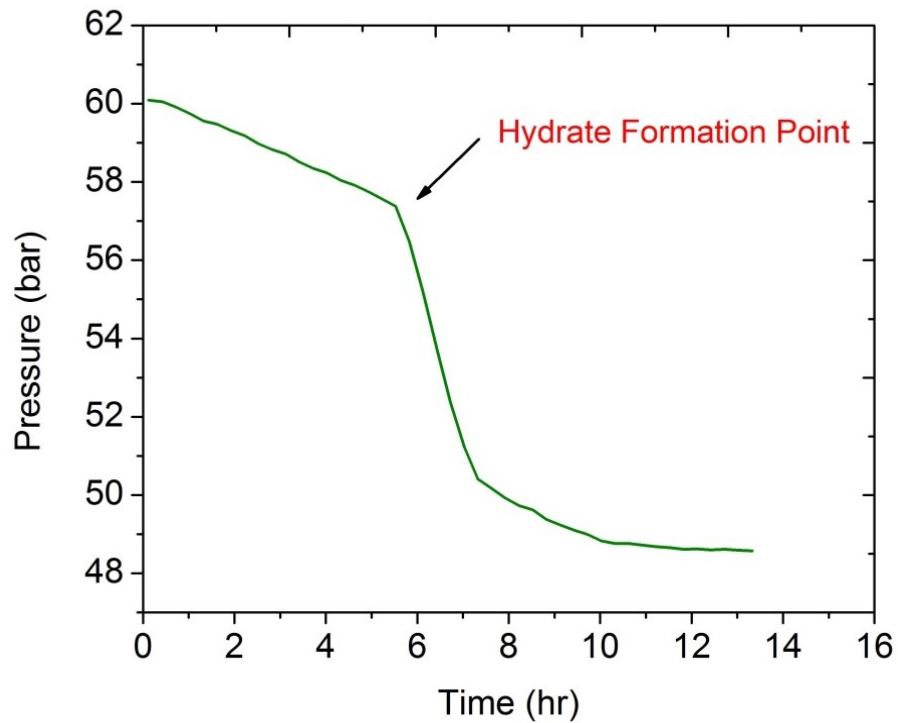


Figure 3-11: The experimental loop showing the hydrate formation and dissociation in the Rocking Cell Assembly (RC-5).

### 3.3.3 Extracting hydrate dissociation and formation point

The hydrate dissociation starts when the H-V (hydrate-vapour) and the H-L<sub>w</sub>-V (hydrate-liquid-vapour) equilibrium lines interconnect with each other,<sup>302</sup> and then the hydrate phase completely vanishes as the temperature is increased further.<sup>302</sup> This point on the H-L<sub>w</sub>-V equilibrium line is considered as a hydrate dissociation point [Figure 3-11]. The induction time is the time-frame where the first hydrate crystal formation is observed through an sudden decrease in pressure from the initial values.<sup>303</sup> The induction times with and without inhibitors were estimated from the pressure-time (P-t)

curves obtained for a specific sample solution [Figure 3-12]. The same intersection methodology used for hydrate dissociation point was used for determining hydrate induction point. The similar methodology was also used by Daraboina, et al.<sup>40</sup>



*Figure 3-12:* Shows the hydrate formation/ induction point that is considered to occur right before the steep pressure drop within the system.

## CHAPTER 4: EXPERIMENTAL RESULTS & DISCUSSION

The Chapter 4, provides the experimental results obtained for the tests conducted using ionic liquids, amino acids, and synergents. The results obtained for effect of stirring on hydrate formation is also discussed in detail. Moreover, the results obtained for the amino acids and ionic liquids as methane inhibitors have been compared with the 21 imidazolium ionic liquids, 5 choline ionic liquids and 2 industrial hydrate inhibitors methanol and mono-ethylene glycol reported in section 4.3 .

### **4.1 Hydrate Formation and Inhibition in the Quaternary gas mixture (QM)**

The natural gas extracted from the offshore is not purely methane and contain other components like ethane, propane and heavy hydrocarbon molecules. In addition to that, it also contains nitrogen, carbon dioxide, and hydrogen sulfide.<sup>304</sup> Therefore, in the first part of the work a synthetic quaternary gas mixture (QM) was designed. The QM consisted of four components of the natural gas (methane, ethane, nitrogen and carbon dioxide). The mole composition of these components was confirmed through the in-house GC-analysis. There were only four components selected to keep the uncertainty error below 10 % and the hydrogen sulfide was not included due to safety reasons.

#### ***4.1.1 Effect of Magnetic Stirring on QM hydrate formation***

In order to observe the effect of stirring on the rate of hydrate formation, a range of experiments was conducted at different stirring rates in the high-pressure cell (HPC) using the QM mixture. The experiments were conducted within the range of 100-1400 RPM (rotations per minute) using the lab mixer. Figure 4-1, illustrates the hydrate formation observed at different RPM inside the HPC. The pressure values are provided on the Y-axis and the respective time values are indicated on the X-axis.

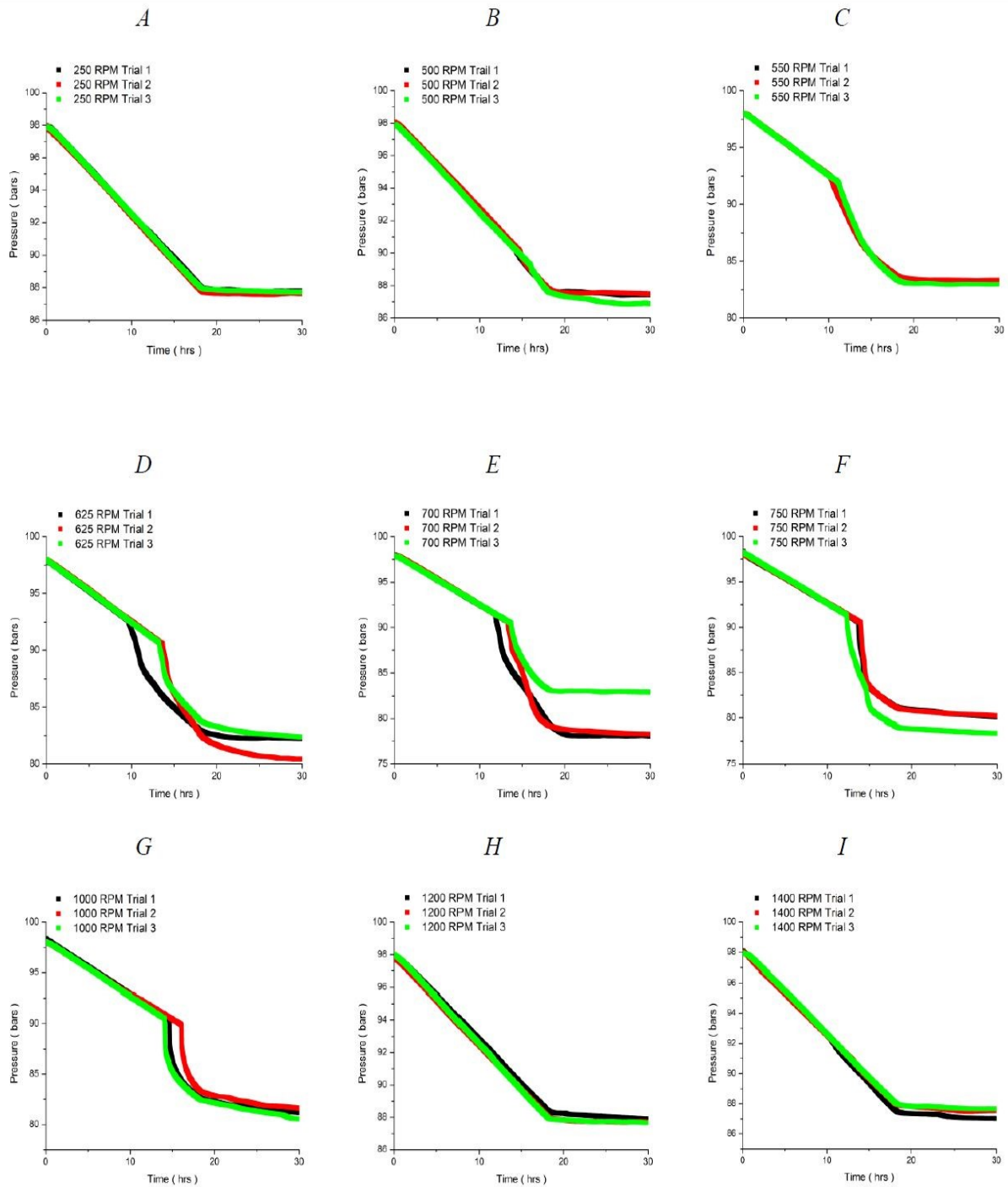


Figure 4-1: Pressure drops observed at different stirring rates (RPM) inside the high-pressure cell (HPC) using a Quaternary gas mixture (QM) at the constant pressure of 98 bars.

The initial pressure drop is likely to occur as the results of cooling when the gas dissolves within the aqueous solution, while the second pressure drop indicates the formation of hydrate crystals. Each experiment was repeated minimum three times and the average pressure drop at each stirring speed was evaluated. No hydrate formation was deduced at the low (250-500 RPM) and high stirring rates (1200-1400).

The stirring helps in reducing the hydrate formation time and Hao, et al. <sup>275</sup>, suggested that the use of baffle along with the stirrer to enhance the rate of hydrate formation inside the stirred tank reactor. However, the long stirring time can result in the decomposition of the hydrates formed in the reactor.

The kinetic experiments like these are not replicable, so each experiment was repeated at least three times and the average pressure drop at each RPM was evaluated to get an approximation of the amount of hydrate formed inside the HPC. The hydrate crystal formation was observed through the sharp pressure drop detected within the HPC during the cooling process. The pressure drop variable was taken as an indicator of the number of hydrate crystals formed inside the HPC.

As demonstrated in Figure 4-1, initially the experiments were carried out at low stirring rates of 250 to 500 RPM. At low stirring rates of 250 to 500 RPM, no significant hydrate crystal formation was detected within the HPC (Part A & B, Figure 11). According to Vysniauskas and Bishnoi <sup>274b</sup>, at low stirring rates, the hydrates nucleation is restricted due to the accumulation of hydrate crystals at the gas-liquid interface. This



accumulation of hydrate crystals at gas-liquid interface restricts the rate of mass and heat transfer and hinders the overall growth of hydrate crystals within the cell. This could be the major reason behind no significant hydrate crystal formation observed within the HPC at low stirring rates. When the stirring rate was accelerated from 550 to 1000 RPM (Part C, D, E, F & G of Figure 4-1), two sharp pressure drop curves were observed in the experiments.

The initial steep pressure drop occurs as the result of the absorption of a gas molecule in the liquid phase according to Chu, et al.<sup>159</sup> and the plateau detected shows that the liquid phase gets saturated with the gas molecule. Then as the hydrates formation initiates, another pressure drop is observed which indicates that hydrates crystals are growing within the HPC. Finally, there comes a saturation point where no further pressure drop is identified within the HPC.

The growth of hydrate crystals as a two-step process was proposed by Englezos, et al.<sup>278</sup>. In the first step, the dissolved gas tends to diffuse from the bulk of the solution to the hydrate crystal water interface. Then in the second step, the gas molecules are amalgamated into the water structure framework by an adsorption process.

There exists an upper threshold limit above which higher stirring rate has no effect on hydrates crystal formation according to Englezos, et al.<sup>285</sup> and above that upper threshold limit, opposing effects are observed within the system. A similar

scenario was observed at a higher stirring rate of 1200 -1400 RPM (Part H & I of Figure 4-1) where no significant hydrate crystal formation was detected within the HPC. Thus, it was deduced that the optimum-stirring zone at which maximum hydrate formation can be obtained for QM mixture lies within the range of 550 to 1000 RPM (Figure 4-1).

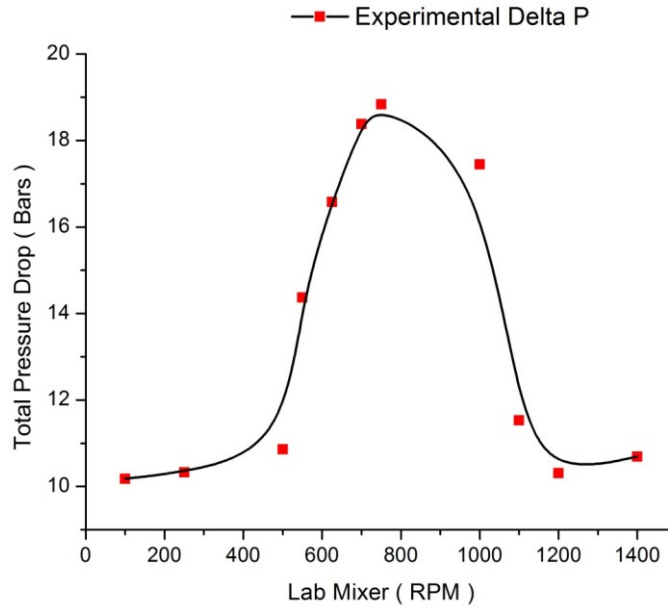
#### *4.1.1.1 Finding the optimum stirring rate*

In order to detect the optimum stirring speed (RPM) at which maximum hydrate formation occurs with the HPC, the overall average pressure drop calculated for the three trials at each RPM were evaluated and plotted against their respective RPM [Figure 4-2]. The hydrate formation rate was also observed by measuring the overall pressure drop within the HPC at the particular stirring rate.

The overall pressure drop was evaluated by finding the minimum pressure value obtained in the experimental trial during the cooling process and then subtracting this minimum value from the initial pressure value of 98 bars during the starting of the experimental trial [Figure 4-2].

Figure 4-2, provides a visual scheme of the rate of hydrates formation (indicated by the total pressure drop in HPC) with respect to different stirring rates within the HPC. The pressure drop values are indicated on the Y-axis and the respective stirring speed (RPM) is indicated on the X-axis. The results indicated that there exist a U-shape pattern

and threshold limit for the stirring speed.



*Figure 4-2:* The total average pressure drops observed within the HPC at different stirring speed evaluated by conducting a minimum of three experimental trials.

The experimental results indicate that within the chosen HPC system the hydrates formation rate with respect to different RPM generates a U-shape pattern. At low RPM (100-500 RPM), only single pressure drop due to the cooling process was observed within HPC. This average pressure drop was found to be within the range of 10 to 11 bars. No further pressure drop was detected within the HPC, even when during the isothermal step when the HPC was left stable at 2 °C for next 18 hrs. Therefore, it's

likely that no hydrate crystal formation took place at low RPM.

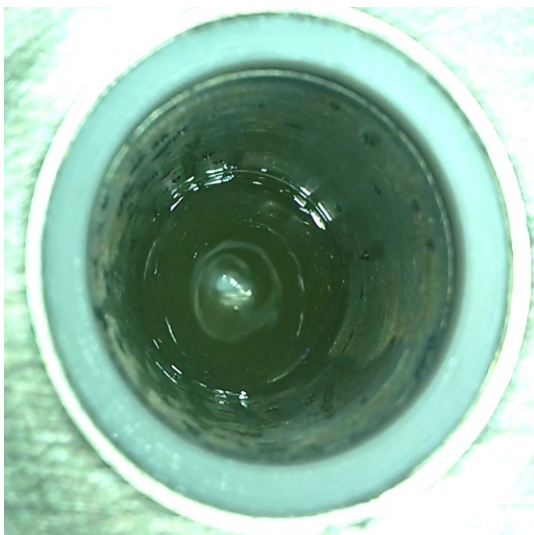
At moderate RPM (550-750 RPM), two pressure drops were detected within the HPC. The overall pressure drop within the HPC was found to be within the range of 14 to 19 bars. These pressure drops were found to be higher compared to the pressure drops observed at the lower RPM (100-500 RPM). This shows that good amount of hydrate formation occurs at moderate RPM (550-750 RPM).

The maximum pressure drop of  $18.8 \pm 0.2$  bars within HPC was found at 750 RPM, which indicates that maximum hydrate formation occurs at 750 RPM. Therefore, the 750 RPM was deduced as an optimum stirring speed at which the experimental trials must be carried out within the HPC to obtain maximum hydrate crystal formation [Figure 4-2].

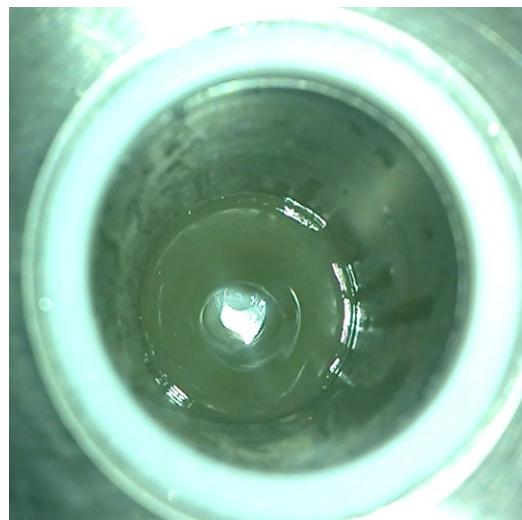
At higher RPM (1000-1400 RPM), the hydrates crystal formation within the HPC started to impede. The pressure drops across within the HPC was found to be 10 bars compared to 19 bars at 750 RPM, which shows an opposing effect of high stirring rates on the hydrates crystal formation within the HPC [Figure 4-2]

4.1.1.2 *Checking functioning of a magnetic stirrer at a higher stirring rate*

*A: Mixing at 750 RPM*



*B: Mixing at 1200 RPM*



*C: Mixing at 1400 RPM*



*Figure 4-3:* Shows the visual scenes of mixing taking place within the High-pressure cell (HPC) at different stirring rates.

The gas in HPC was vented and the cell was re-opened to check if the magnetic stirrer was operating rightly at high RPM (1000-1400 RPM) to provide the required agitation for the hydrate formation within the HPC [Figure 4-3].

On opening the cell and running dry sample trials at stirring speeds of 750 RPM, 1200 RPM and 1400 RPM it was found that the magnetic stirrer functions well and no mechanical problem was observed at these stirring rates [Figure 4-3]. The visual observation shows that the magnetic stirrer functions well even at high stirring rates and provide adequate mixing within the cell.

The stirrer rotates evenly at higher stirring rates (1000-1400 RPM) but still, no hydrate formation is observed within the HPC [Figure 4-3]. Thus, it was deduced that at the high stirring rates the hydrate crystal might be colliding heavily against the walls of the cell and breaking leaving no time for the hydrate nucleation to take place within the HPC.

It was detected by Kim, et al. <sup>279</sup> that the hydrate decomposition rate increases as the stirring speed is increased and at the certain stirring rate an upper limit is obtained. This upper limit is reached due to the fact that the mass-transfer resistances are eradicated at that certain stirring rate.

The optimum stirring rate to obtain maximum hydrate decomposition is dependent on the temperature and pressure conditions according to Kim, et al. <sup>279</sup>. Higher stirring rates are required at lower pressures and vice versa. Vysniauskas and Bishnoi <sup>274b</sup>, proposed that low stirring rate are not suitable for hydrates formation, as at low stirring rate the hydrate crystals are likely to gather at the gas-liquid interface, which blocks the heat and mass transfer and also decreases the hydrates formation rate.

There exists an upper threshold limit above which higher stirring has no effect on hydrates formation according to Englezos, et al. <sup>285</sup> and above that threshold limit, negative effects can be detected within the system <sup>285</sup>. The similar case was observed in the stirring rate experiments performed on the HPC using the QM gas mixture.

At low stirring rates (< 250 RPM) no hydrate formation was observed and at the high stirring rates (> 850 RPM) no hydrate formation was observed may be due to the high shear force that might be resulting in the dissociation of the hydrate crystals or not giving enough time for the hydrate nucleation. This indicates the counter effect of very high stirring rate on the hydrate crystal formation in the stirred vessels.

All hydrate kinetic experiments rely on the experimental system mechanics and specifications according to Mork <sup>286</sup>. Therefore, the model used for a single experimental system may not be appropriate for other experimental systems <sup>286</sup>.

However, the improvement in any factor that affects the gas-liquid interfacial area like stirring rate, may assist to accelerate the hydrate formation significantly <sup>286</sup>.

#### ***4.1.1.3 Identifying the interval of Catastrophic Hydrate Growth (CHG)***

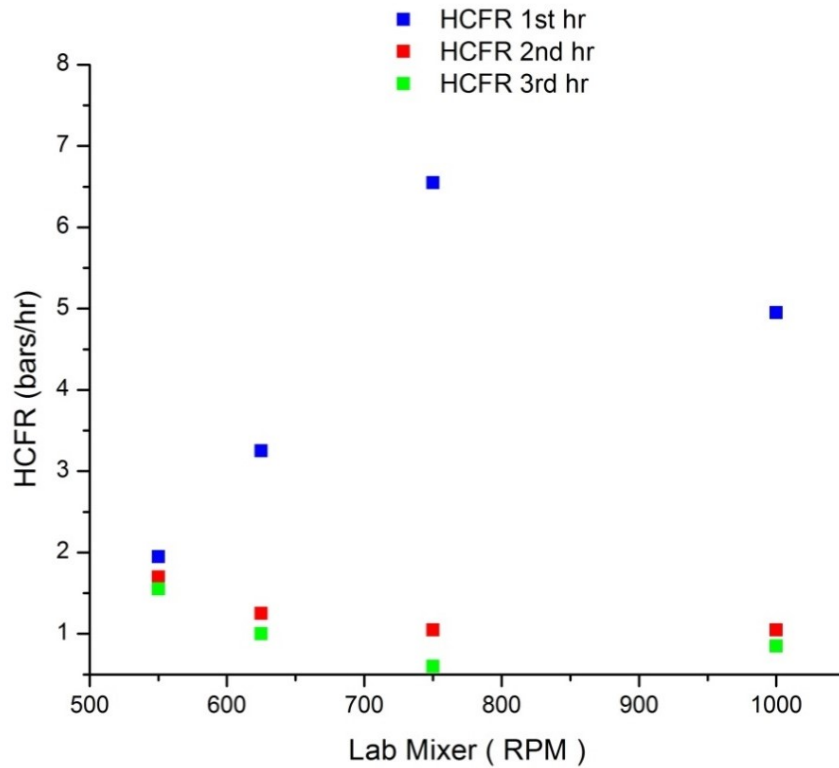
The phenomena of catastrophic hydrate growth (CHG) has been described in different kinds of literature <sup>249, 256, 305</sup> and basically, it's a time zone where spontaneous hydrate formation occurs within the system, mainly after initial hydrate formation or induction time<sup>249</sup>. The catastrophic hydrate formation is considered to be the major cause of plugging in oil and gas pipelines <sup>256</sup>.

The CHG is an interval when spontaneous hydrate formation occurs within the experimental system as stated by Zhao, et al. <sup>31</sup>. As CHG starts, a sharp drop in the pressure can be detected within the system and this eventually leads to the formation of hydrate plugs.<sup>31, 306</sup> Therefore, by operating the experimental system within optimum stirring range and by finding out the CHG interval, the best-operating conditions for the hydrates production plants can be deduced. The experimental trials carried out at moderate RPM (550-1000 RPM) were studied further to identify the interval of catastrophic hydrate growth (CHG) at these stirring rates.

The interval of CHG occurs after the initial hydrates nucleation or induction time as proposed by Zhao, et al. <sup>31</sup> and it's the interval where the rate of hydrate crystal growth is maximum, normally detected by the sharp pressure drop within the system. Therefore, the CHG interval was identified by measuring the sharp pressure drop that



occurs after the hydrates induction time within the HPC. This period was suggested as an interval of CHG within the HPC [Figure 4-4].



*Figure 4-4:* Hydrate crystal formation rate (HCFR) during the 1st, 2nd and 3rd hour after the hydrate induction time within the High-pressure cell (HPC).

According to Figure 4-4, the hydrate growth was found maximum first hour after the hydrates induction time. After the first hour of the hydrate induction time, the hydrate crystal formation rate tends to decrease till the HPC reaches its saturation point. Once the saturation point is reached, no further pressure drop is observed within

the HPC. As per the Figure 4-4, it can deduce that the first hour (1<sup>st</sup> hr) after the hydrates induction time can be categorized as the interval of CHG. In order to save electrical energy, the experimental trials can be halted the first hour after the hydrates induction time. This will help to save energy cost and time required for hydrate production on the laboratory scale and prospective industrial scale in future.

The following are the key findings deduced from the above experimental results that also agree with the previous literature findings:

1. There exists a threshold limit for the stirring rate, above and below which no hydrate formation occurs in the selected system. In the selected HPC system, the optimum stirring rate was observed to be within the range of 550-750 RPM.
2. The catastrophic hydrate formation occurs one hour after the hydrate induction time for the selected system. It's an interval where the rate of hydrate formation is maximum and after this interval, the rate of hydrate formation is likely to drop.
3. At higher stirring rates (1200-1400 RPM) no significant hydrate crystal formation is observed within the system. This may be due to the heavy collision of hydrate crystals with the wall of the HPC, causing the breakage of hydrate crystals when agitation is high.

#### ***4.1.2 Effect of Pyrrolidinium Ionic Liquids on QM hydrate inhibition***

No work has been previously reported on hydrate inhibition studies using a quaternary gas mixture (QM). Hence, two pyrrolidinium-based ionic liquids (ILs) 1-Methyl-1-Propyl-pyrrolidinium Chloride [PMPy][Cl] and 1-Methyl-1-Propyl-pyrrolidinium Triflate [PMPy][Triflate] were selected to test their inhibition effect on the quaternary gas mixture (QM) hydrate formation and dissociation.

##### ***4.1.2.1 Thermodynamic inhibition (TI) effect of pyrrolidinium ILs***

Firstly, a blank sample test with QM and deionized water in the RC-5 was carried out to get the QM gas mixture HLVE data points or hydrate dissociation points [Table 4-1]. It was essential to obtain QM gas mixture HLVE data points to test the thermodynamic inhibition effectiveness of the IL [PMPy][Cl] and [PMPy][Triflate]. Previously, no literature has reported the HLVE data points for the QM gas mixture used in this work.

Table 4-1: *Hydrates dissociation points for the QM gas mixture*

Pressure (Bar)	Temperature ( °C )
<b>40.79</b>	11.21
<b>66.10</b>	14.21
<b>80.02</b>	15.51
<b>99.63</b>	17.18
<b>117.95</b>	18.05

At starting, the experimental trials were carried out using the 1 wt% solution of the of the ILs [PMPy][Cl] and [PMPy][Triflate] [Figure 4-5]. The QM gas mixture HLVE data points obtained in Table 5, were compared with the HLVE data points obtained in the presence of 1wt% pyrrolidinium ILs. The HLVE data points were obtained at different pressure conditions (38-120 bars) and the pyrrolidinium ILs were observed to be more effective at lower pressures compared to higher pressures.

Figure 4-5, illustrates the thermodynamic shift in the Quaternary Mixture (QM) HLVE curve in the presence of 1wt% of pyrrolidinium-based ionic liquids. The QM blank sample HLVE data points are indicated in the black and the QM HLVE data points in the presence of 1wt% ionic liquids [PMPy][Cl] and [PMPy][Triflate] are indicated in the red and green.

According to the experimental results, no significant thermodynamic inhibition effect or shift in QM gas mixture HLVE takes place in the presence of 1wt% pyrrolidinium ILs. Only a slight shift of 0.5 °C was observed at the pressure close to 40 bars provided by the IL [PMPy][Cl] [Figure 4-5]. Tariq, et al.<sup>307</sup>, observed that IL as hydrate inhibitors are effective at the concentration of 5wt% and show only a slight thermodynamic effect at the concentration of 1wt%. Tariq, et al.<sup>307</sup>, also observed that the IL show a better thermodynamic effect at a lower pressure compared to higher pressures [Figure 4-5].

The thermodynamic effect of 1wt% choline based ILs on the Qatar Natural Gas (QNG) and observed that no significant thermodynamic hydrate inhibition occurs at the concentration of 1wt% was investigated by Mohamed, et al.<sup>58</sup>. An observable shift QNG gas mixture HLVE was only observed at the concentration of  $\geq 5$ wt%. The similar results are obtained using the pyrrolidinium ionic liquid as hydrate inhibitors for the QM gas mixture in this case study [Figure 4-5].

The structure of pyrrolidinium-based ionic liquids under high-pressure conditions using molecular dynamics simulation was examined by Sharma, et al.<sup>308</sup> and it was found that the strength of charge ordering and polarity ordering decreases as the applied pressure increases. They also observed that by increasing pressure, a significant decrease in the nearest neighbour pair correlations for both polar-polar and an apolar-apolar group of ionic liquids is observed.

The alky tails of ionic liquids cations go through an increased amount of gauche defects at high pressure compared to lower pressures according to Sharma, et al.<sup>308</sup>. This leads to increased bending or curling of the cation tails at high pressure. This could be the reason that the selected pyrrolidinium ionic liquids function better at a lower pressure compared to higher pressure.

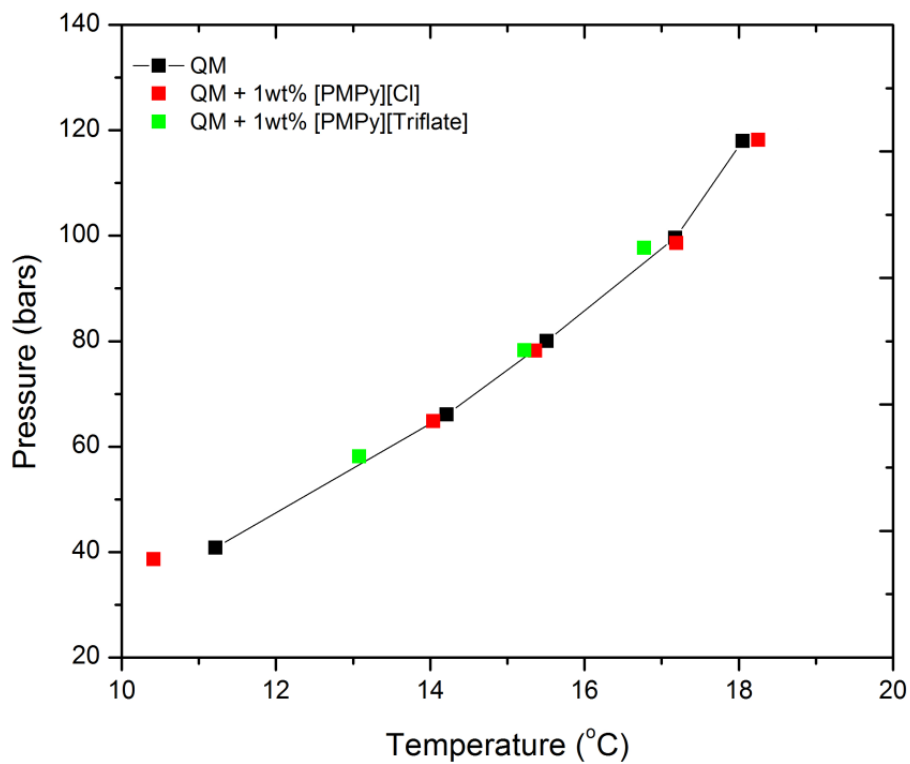
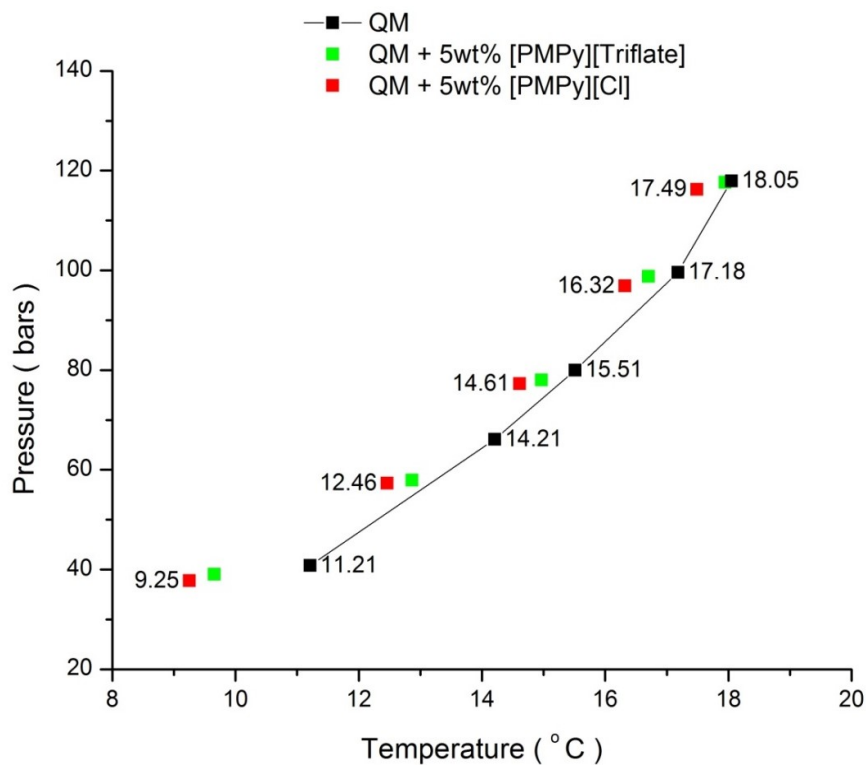


Figure 4-5: The shift in the HLVE curve of the quaternary gas mixture (QM) in the presence of 1wt% of pyrrolidinium-based ionic liquids. The above data has the uncertainty of  $\pm 0.2$  °C.

During the process of hydrate formation, the water molecules are likely to form loosely ordered clusters around the guest molecules like methane and ethane. Koh et al<sup>309</sup>, stated that These clusters then grow larger in size and become more structured at low temperatures.

The ionic liquids normally tend to function by disturbing hydrogen bonding between the water molecules within these clusters as stated by Shin et al<sup>310</sup>. The ILs tend to use their pair of anions to disturb the hydrogen bonding network of a water molecule.<sup>310-311</sup>. Therefore, it's likely that at 1wt% the number of anions (like chloride) in IL was not sufficient enough to disturb the hydrogen bonding within the QM hydrate clusters. This could be the reason that no significant thermodynamic inhibition effect was shown by selected pyrrolidinium ILs at 1wt% [Figure 4-5].



*Figure 4-6:* The shift in the HLVE curve of the quaternary gas mixture (QM) in the presence of 5wt% of pyrrolidinium-based ionic liquids. The above data has the uncertainty of  $\pm 0.2$  °C.

The next set of the experimental trials were conducted using higher concentration (5wt%) of pyrrolidinium ILs. Figure 4-6, illustrates the thermodynamic shift in the Quaternary Mixture (QM) HLVE curve in the presence of 5wt% of pyrrolidinium-based ionic liquids. At 5wt%, the number of ions present in the experimental samples increased. As the quantity of ions increases, the disturbance of



hydrogen bonding within the hydrate clusters takes place. This likely causes the shift in the QM gas mixture HLVE at different pressure conditions [Figure 4-6].

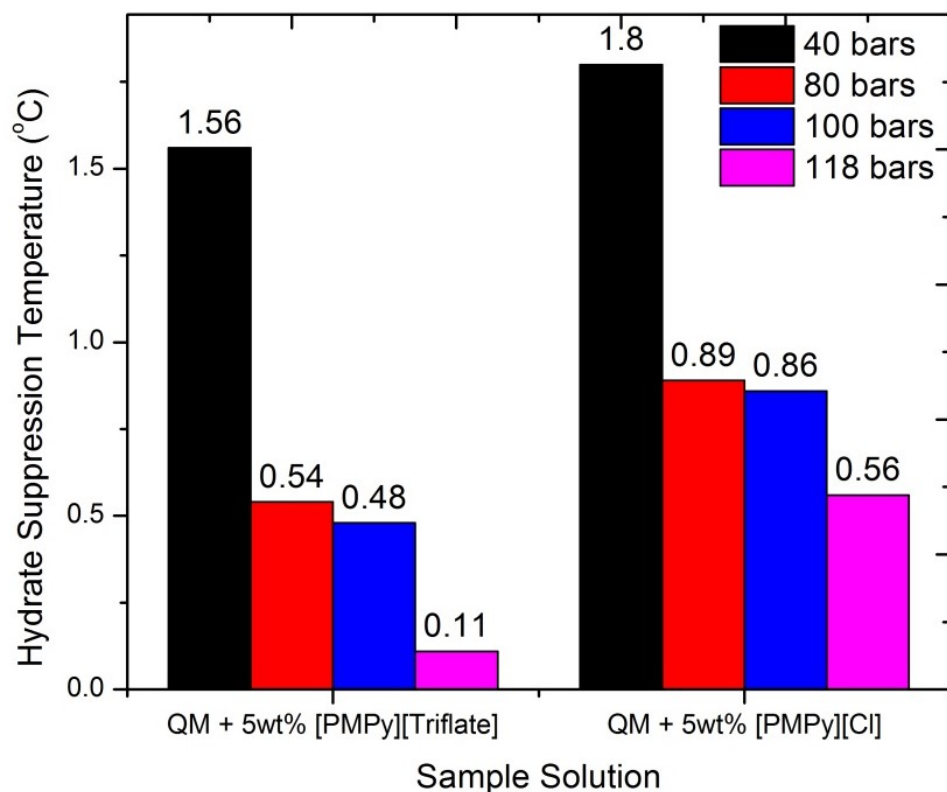
Figure 4-7, illustrates the temperature shift or hydrate suppression temperature obtained at different pressure conditions in the presence of 5wt% [PMPy][Triflate] and 5wt% [PMPy][Cl]. As presented in Figure 4-7, at 5wt% the IL [PMPy][Triflate] provided the temperature shift or hydrate suppression temperature of 1.56 °C, 0.54 °C, 0.48 °C and 0.11 °C at 40 bar, 80 bar, 100 bar and 118 bar respectively. Similarly, at 5wt% the IL [PMPy][Chloride] provided the HLVE temperature shift of 1.8 °C, 0.89 °C, 0.86 °C and 0.56 °C at 40 bar, 80 bar, 100 bar and 118 bar. This indicates that IL [PMPy][Cl] is slightly more effective than the IL [PMPy][Triflate] and in terms of effectiveness the ILs can be listed as:

**[PMPy][Cl] > [PMPy][Triflate]**

The effect of pyrrolidinium ILs on methane hydrate formation using ILs [HEMP][BF<sub>4</sub>] and [BMP][BF<sub>4</sub>] was tested by Kim, et al. <sup>171</sup>. As a thermodynamic hydrate inhibitor at 10wt%, the selected ILs provided the temperature shift of 1.3-1.6 °C. In comparison, the ILs [PMPy][Cl] and [PMPy][Triflate] in this work provided the temperature shift of (1.6-1.8 °C) at a lower concentration of 5wt% using QM. However,

the QM gas mixture used in this work consists of Nitrogen component which itself can act as the hydrate inhibitor.<sup>312</sup>

The nitrogen N<sub>2</sub> gas acts as a hydrate inhibitor for natural gas when it is added in the pipelines. According to Obanijesu, et al.<sup>313</sup>, the N<sub>2</sub> is a hydrate former itself but the pressure and temperature conditions required for the N<sub>2</sub> hydrate formation are relatively high. (-1 to 13.2 °C at 144 to 554 bar)<sup>314</sup> compared with methane gas. This is an interesting idea to explore further in future as the use of nitrogen for hydrate inhibition is more economical and requires less sophisticated infrastructure compared to the industrial inhibitor methanol.<sup>307</sup>



*Figure 4-7:* The hydrate suppression temperature obtained at different pressure conditions in the presence of 5wt% [PMPy][Triflate] and 5wt% [PMPy][Cl]. The data has an uncertainty of  $\pm 0.2$  °C.

The pyrrolidinium cation possesses shorter alkyl chains which facilitate ILs to form hydrogen bonding with water molecules effortlessly and they have strong electrostatic charges that enable strong interaction between an ion and a dipole.<sup>17</sup>

The overall inhibition performance of ionic liquids depends on both cations and anions and the thermodynamic inhibition effectiveness of ionic liquids enhances with the increase in pressure and concentration according to Long, et al.<sup>161</sup>.

It was reported by Russina, et al.<sup>315</sup>, that upon increasing the hydrostatic pressure on the imidazolium ionic liquid, the polar moieties with strong electrostatic interactions are unaffected by pressures, but the conformation of the alkyl tails are affected by pressure. Salminen, et al.<sup>316</sup>, stated that the pyrrolidinium cation based ionic liquids show more influence of tail modification on their microscopic properties than other classes of ionic liquids.

Cytotoxic studies of ionic liquids reveal that the pyrrolidinium cation based ionic liquids are less toxic than the piperidinium and imidazolium-based ionic liquids according to Salminen, et al.<sup>316</sup>. This makes the pyrrolidinium-based ionic liquids environmentally more benign. The pyrrolidinium based ionic liquids similarly show higher conductivities than piperidinium based ionic liquids. Table 4-2, shows the hydrate dissociation points in the presence of pyrrolidinium ILs.<sup>320</sup>

The thermodynamic inhibition effect of mixing ILs together in equal proportions was observed in the next stage. A sample solution was prepared to add ILs [PMPy][Cl] and [PMPy][Triflate] in equal proportions to observe their thermo effect on the QM and then results obtained were compared with the 10wt% methanol HLVE data [Figure 4-8].

methanol is a commercial thermodynamic inhibitor that is widely used in the oil and gas industry.<sup>317</sup>

Figure 4-8, illustrates the comparison between the QM HLVE data points obtained in the presence of 10 wt % methanol and the mixture 5wt% [PMPy][Triflate] + 5wt% [PMPy][Cl]. Based on the experimental trial results [Figure 4-8], it was found that the sample solution with mixture 5wt% [PMPy][Cl] + 5wt% [PMPy][Triflate] provided a thermodynamic inhibition effect close to 10 wt% methanol. This is one of the most significant findings of this research work and no similar effect has been reported in the literature elsewhere.

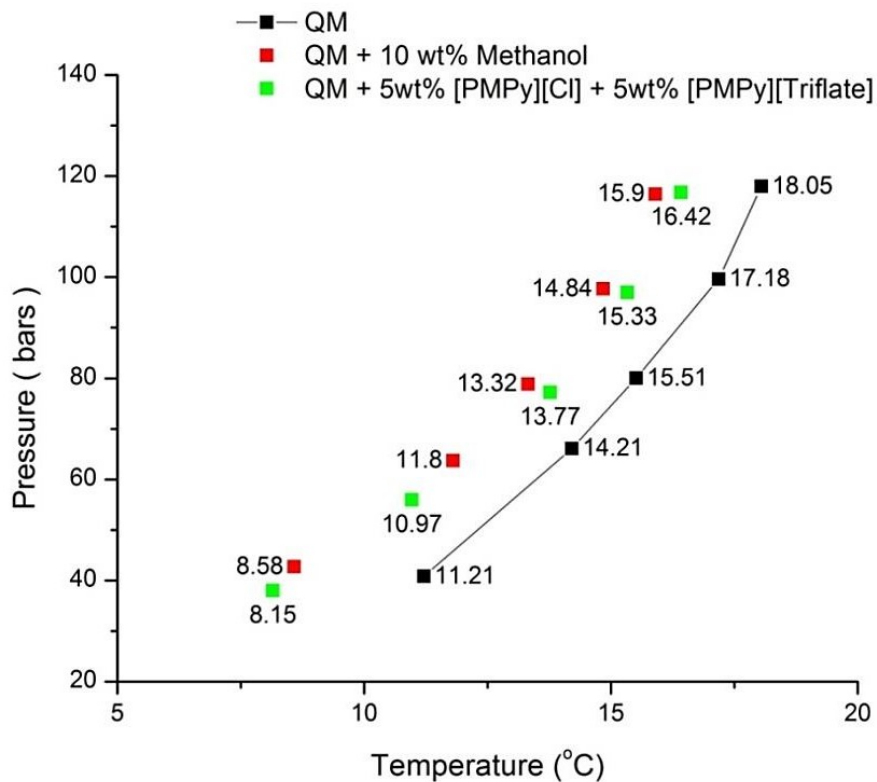


Figure 4-8: The shift in the HLVE curve of the quaternary gas mixture (QM) in the presence of 10 wt % methanol and the mixture 5wt% [PMPy][Triflate] + 5wt% [PMPy][Cl]. The data has an uncertainty of  $\pm 0.2$  °C.

It's important to consider the fact that the pyrrolidinium ILs used in this work have longer alkyl chains in comparison to methanol. Keshavarz, et al.<sup>291a</sup> stated that the thermodynamic inhibition effect of ILs decreases with the increase in the length of the alkyl chain.<sup>291a</sup> This may help methanol to provide better thermodynamic inhibition effect than the pyrrolidinium ILs [Figure 4-8].

The key factor that helps methanol to provide better thermodynamic inhibition effect is the presence of –OH group.<sup>318</sup> The strong interaction of –OH group with the hydrogen bonds in hydrate clusters and further interaction of –CH<sub>3</sub> group with the C-C or hydrogen bonds within hydrates clusters tend to cause disturbance of hydrate crystals.<sup>318</sup>

The presence of the –OH group is as well essential to make hydrogen bonds with “free water” and shift the thermodynamic equilibrium via hydrogen bonding. The Table 4-2, shows the hydrate dissociation points obtained for QM in the presence of 1 wt% and 5wt% pyrrolidinium ILs and in the presence of 10wt% methanol.

Table 4-2: *QM gas mixture hydrate dissociation points obtained in the presence of the ionic liquids (ILs)*

Mixture	P (bars)	T (°C)	Mixture	P (bars)	T (°C)
<b>QM + 1wt% [PMPy][Cl]</b>	38.65	10.41	QM + 1wt% [PMPy][Triflate]	58.16	13.08
	64.83	14.04		78.30	15.22
	78.22	15.36		97.72	16.77
	98.60	17.19		118.87	18.67
<b>QM + 5wt% [PMPy][Cl]</b>	37.77	9.25	QM + 5wt% [PMPy][Triflate]	39.07	9.66
	57.30	12.46		57.96	12.86
	77.28	14.62		77.99	14.97
	96.88	16.32		98.80	16.70
	116.27	17.49		117.67	17.94
<b>QM + 5wt% [PMPy][Triflate] + 5wt% [PMPy][Cl]</b>	37.99	8.15	QM + 10wt% Methanol	42.69	8.58
	55.94	10.97		63.72	11.80
	77.20	13.77		78.85	13.32
	96.97	15.33		97.70	14.84
	116.80	16.43		116.45	15.90



#### 4.1.2.2 *Kinetic inhibition effect of Pyrrolidinium Ionic liquids*

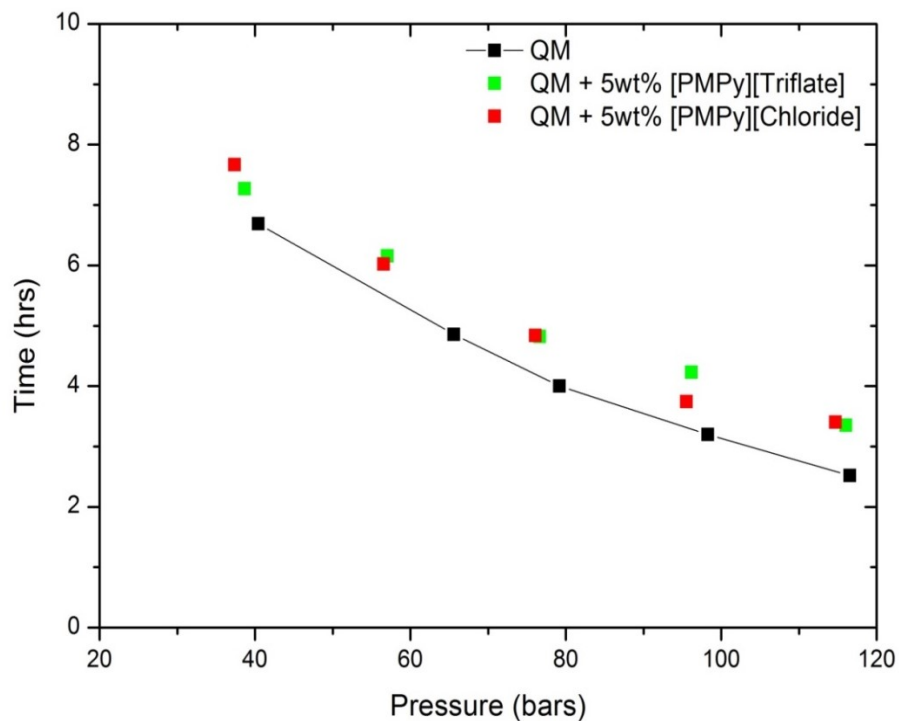
The hydrate nucleation depends on different factors, which includes subcooling temperature, water history, impurities, the composition of the gas, amount of agitation or turbulence and geometry of the system.<sup>7</sup> This is one of the reasons that hydrate kinetic experiments are not replicable and the results obtained from one system may not match the results of the other system.

The induction time is a good indicator of the efficiency of kinetic hydrate inhibitors in delaying hydrate nucleation and hydrate formation according to Ripmeester and Alavi<sup>319</sup>. The induction time may vary from seconds to days due to complex nature of hydrate nucleation.<sup>319</sup> Therefore, in this work the pyrrolidinium based ILs [PMPy][Triflate] and [PMPy][Cl] were tested for their ability to exhibit kinetic inhibition by using induction time as an indicator.

Figure 4-9, displays the time delay in the QM hydrate formation in the presence of 5wt% ILs [PMPy]Triflate] and IL [PMPy][Chloride]. The both ILs showed an almost similar kinetic effect at all pressure conditions. The hydrate formation in QM blank sample is shown in the black and the hydrate formation in the presence of 5wt% ionic liquid inhibitors [PMPy]Triflate] and IL [PMPy][Chloride] is shown in the green and red. The data has the uncertainty of  $\pm 0.5$  hr.

As indicated in Figure 4-9, both pyrrolidinium ILs exhibited the kinetic inhibition effect confirming their dual functional behaviour. This shows that the IL [PMPy][Triflate] and the IL [PMPy][Chloride] can act as the thermodynamic and kinetic hydrate inhibitor both at the same time.

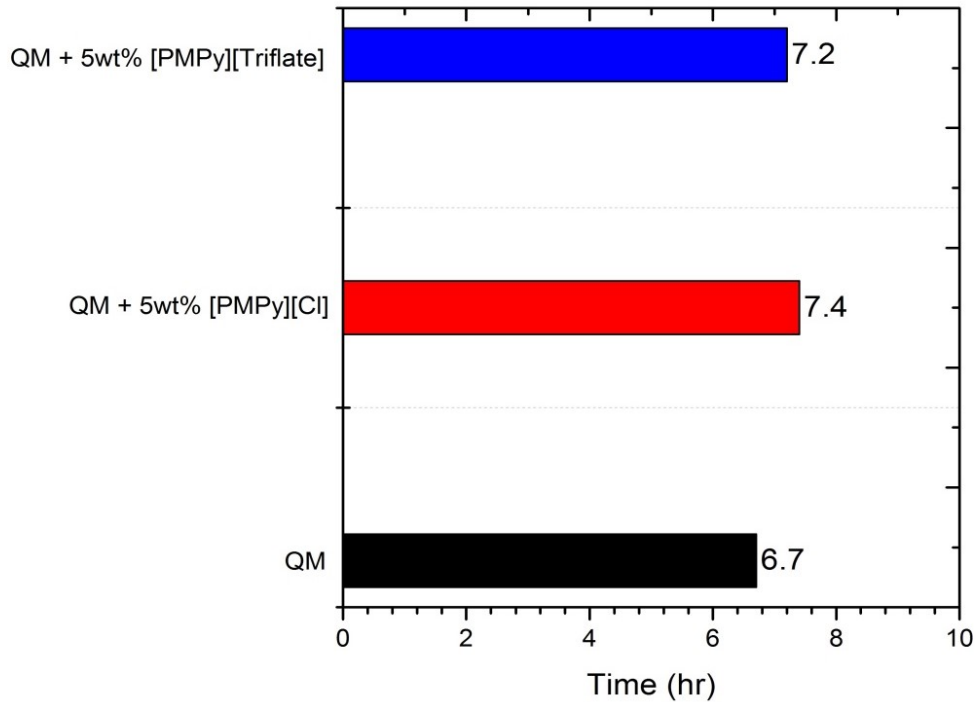
The two ILs tested showed the similar kinetic effect and the average time delay provided by the ILs was around 0.5-0.6 hrs at wide process conditions [Figure 4-9]. This time delay is not very significant from the scale-up perspective, therefore, it was essential to find a way to improve the kinetic inhibition effectiveness of the selected pyrrolidinium ILs.



*Figure 4-9:* The time delay in the quaternary gas mixture (QM) hydrate formation in the presence of 5wt% ILs [PMPy][Triflate] and IL [PMPy][Chloride]. The above data has the uncertainty of  $\pm 0.5$  hr.

Figure 4-10, illustrates the kinetic hydrate inhibition effect of adding 5wt% [PMPy][Cl] and 5wt% [PMPy][Triflate] with QM mixture at 40 bars. The IL [PMPy][Cl] seems to be slightly more effective than IL [PMPy][Triflate] in delaying hydrate formation time at 40 bars. The uncertainty of  $\pm 0.5$  hr exists in the data. The hydrate formation time in QM blank sample is shown in the black bar.

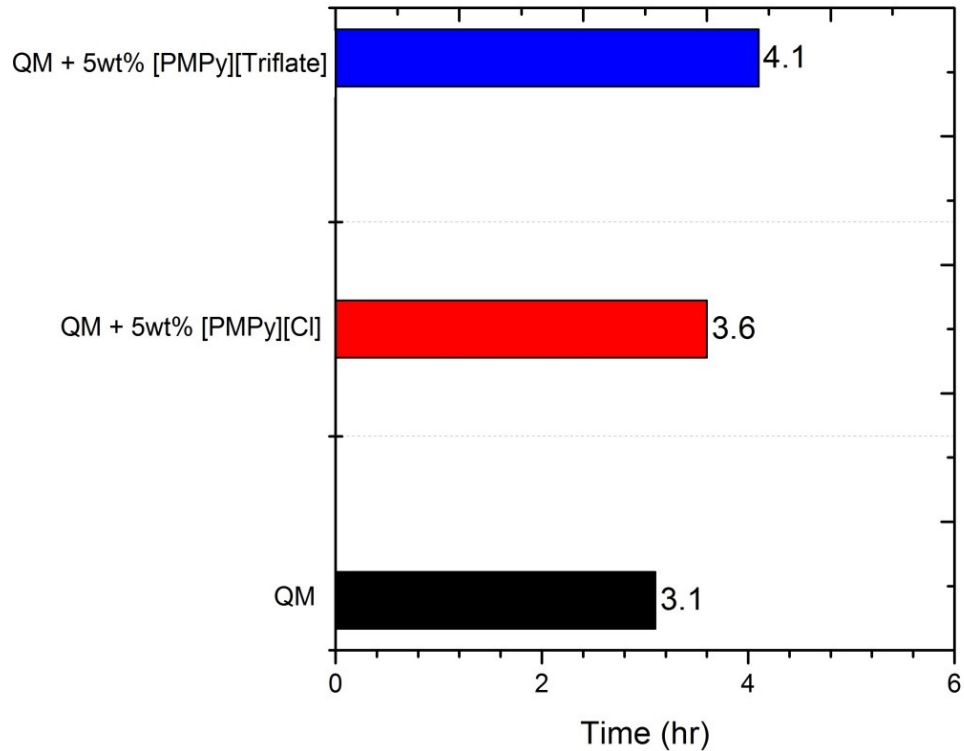
As shown in Figure 4-10, at low pressures (40 bars) the addition of IL 5wt% [PMPy][Cl] and 5wt% [PMPy][Triflate] with QM mixture delayed the average hydrate induction time from  $6.7 \pm 0.5$  hr to  $7.4 \pm 0.5$  hr and  $7.2 \pm 0.5$  hr respectively. The results cannot be compared with the literature as unlike thermodynamic results, the kinetic results are not replicable and no hydrate kinetic inhibition study has been conducted using QM gas mixture before.



*Figure 4-10:* The time delay in the quaternary gas mixture (QM) hydrate formation in the presence of 5wt% IL [PMPy][Cl] and 5wt% IL [PMPy][Triflate] at 40 bars. The uncertainty of  $\pm 0.5$  hr exists in the above data.

Figure 4-11, demonstrates the kinetic effect of adding 5wt% [PMPy][Cl] and 5wt% [PMPy][Triflate] with QM mixture at 100 bars. The IL [PMPy][Triflate] seems to be slightly more effective than IL [PMPy][Cl] in delaying hydrate formation time at 100 bars. At higher pressure (100 bars) the addition of IL 5wt% [PMPy][Cl] and 5wt% [PMPy][Triflate] with QM mixture delayed the average hydrate induction time from 3.1 hr  $\pm$  0.5 hr to 3.6  $\pm$  0.5 hr and 3.1  $\pm$  0.5 hr to 4.1  $\pm$  0.5 hr respectively [Figure 4-11].

Subsequently, in comparison to IL [PMPy][Cl], at higher pressures (100 bars) the IL [PMPy][Triflate] tends to provide the slightly longer time delay in hydrate formation and slightly stronger kinetic effect. The hydrate formation time in QM blank sample is shown in the black bar. The general observation of the hydrate formation trend indicates that the hydrate formation occurs faster at higher pressures compared to lower pressures.



*Figure 4-11:* The time delay in the quaternary gas mixture (QM) hydrate formation in the presence of 5wt% IL [PMPy][Cl] and 5wt% IL [PMPy][Triflate] at 100 bars. The uncertainty of  $\pm 0.5$  hr exists in the above data.

Figure 4-12, illustrates the kinetic inhibition effect of mix ionic liquids on the QM hydrate formation time. The kinetic inhibition effect of mix ionic liquids (ILs) is observed to be more effective than the kinetic inhibition effect provided by the single IL. The ionic liquids mixture delay the hydrate formation time within the range of 1.5 to 2 hrs. This slightly indicates that the kinetic inhibition strength of the selected pyrrolidinium ILs tends to increase with their respective concentration.

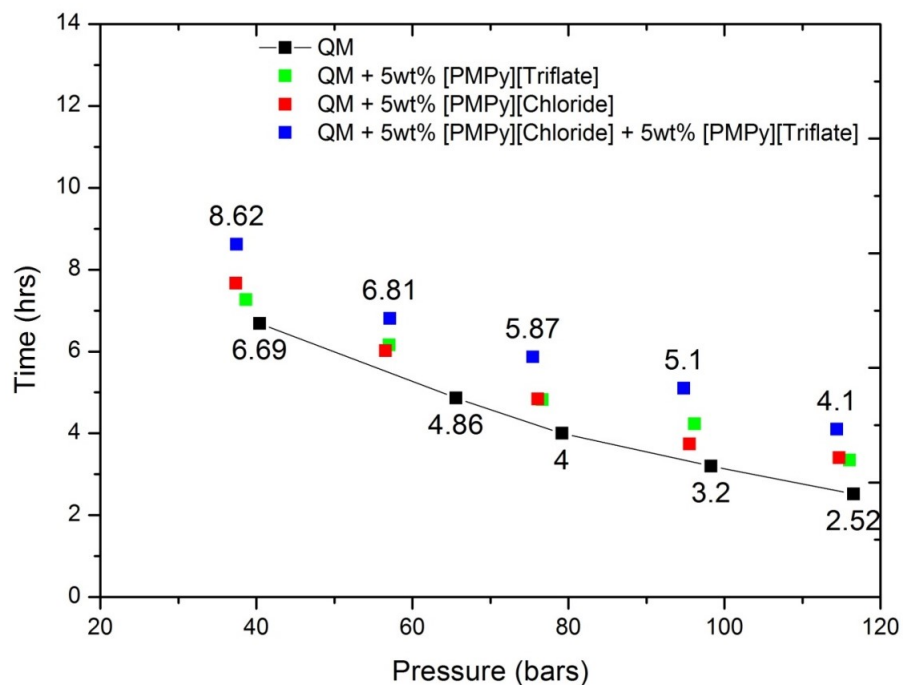


Figure 4-12: The time delay in the quaternary gas mixture (QM) hydrate formation in the presence of a mixture of 5wt% IL [PMPy][Cl] and 5wt% IL [PMPy][Triflate] at different pressure conditions. The uncertainty of  $\pm 0.5$  hr exists in the above data.

As shown in Figure 4-12, the delay provided by the ILs mixture in the hydrate induction time is higher compared to 5wt% IL. This indicates that at higher concentration the kinetic and thermodynamic inhibition effect of the IL is likely to increase simultaneously. The delay in the hydrate induction time is higher at lower pressures and a maximum delay of up to  $2 \pm 0.5$  hr is observed at pressures close to 40 bar.

The following are the key findings that can be deduced from the above experimental results that agree well with the literature:

1. The formation of hydrates take faster at higher pressures (100 bars) compared to lower pressures (40 bars)
2. The experimental results show that the selected ILs [PMPy][Cl] and [PMPy][Triflate] both have a tendency to act as dual function inhibitors.
3. At 1wt% no significant thermo or kinetic inhibition effect is displayed by the selected ILs. However, the higher concentration of ILs helps to enhance their kinetic and thermodynamic inhibition performance both at the same time.
4. The IL [PMPy][Cl] as a thermodynamic inhibitor provided hydrate suppression temperature within the range of 0.8-1.8 °C ( $\pm 0.2$  °C) and as a kinetic inhibitor delayed hydrate formation by 0.8-1.3 hrs ( $\pm 0.5$ ). [PMPy][Cl] is found to be more effective than the IL [PMPy][Triflate] as a thermodynamic inhibitor. However, IL [PMPy][Triflate] acts better as a kinetic hydrate inhibitor at higher pressures (100 bars).
5. The experimental results show that the equal ratio mixture of ILs [PMPy][Cl] + [PMPy][Triflate] provided a thermodynamic effect similar to 10wt% methanol.
6. The equal ratio mixture of ILs [PMPy][Cl] + [PMPy][Triflate] provided the kinetic inhibition effect better than the equal ratio mixtures of [PMPy][Cl] + VCAP and PMPy][Triflate] + VCAP respectively.



### ***4.1.3 Co-effect of Pyrrolidinium Ionic Liquids and synergents on QM hydrate inhibition***

In order to improve the thermodynamic and kinetic inhibition effectiveness of the pyrrolidinium, ILs the synergents compounds poly-ethylene oxide (PEO) and Caprolactum (VCAP) were added in equal proportions with the pyrrolidinium ILs. The PEO is a water-soluble polymer, while VCAP is the monomer. The hydrate dissociation points experimentally obtained for the QM gas mixture using the RC-5 for the IL-synergent mixtures are shown in Table 4-3.

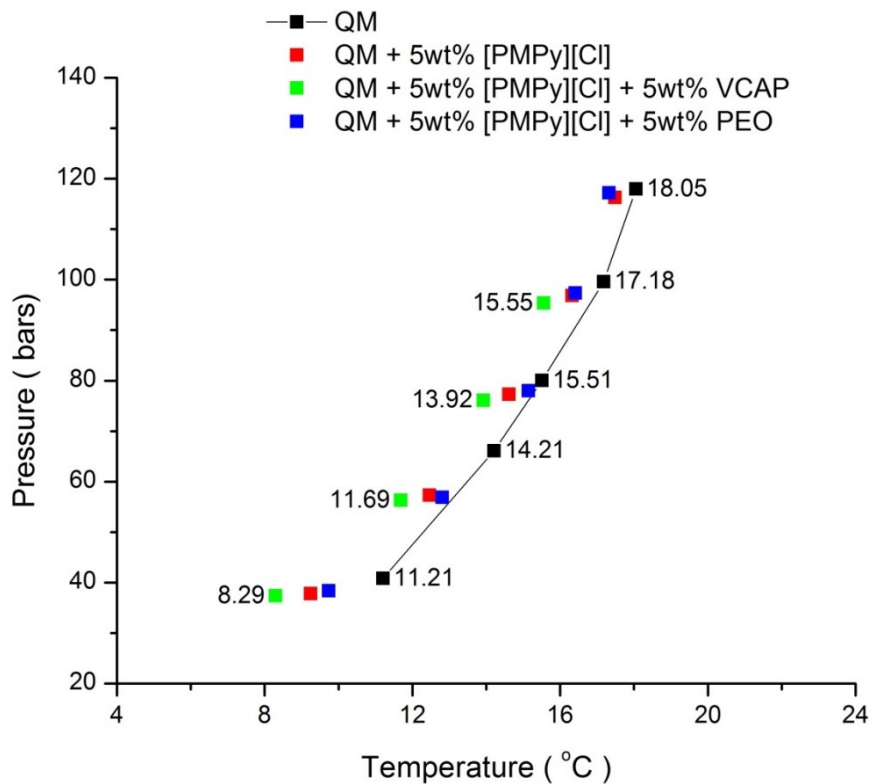
#### ***4.1.3.1 Thermodynamic Inhibition effect of pyrrolidinium IL + Synergents***

Figure 4-13, illustrates the effect of adding VCAP and PEO in equal proportions with the IL [PMPy][Cl] at different operating conditions. The IL-synergent mixture [PMPy][Cl] + PEO showed no significant thermodynamic effect, which indicates that PEO is a poor thermodynamic hydrate inhibitor. Engelo et. al.<sup>254</sup>, reported PEO as a weak thermodynamic inhibitor.

As shown in Figure 4-13, in comparison to mixture [PMPy][Cl] + PEO, the mixture [PMPy][Cl] + VCAP showed an observable shift temperature shift of  $2.2 \pm 0.2$  °C at 40 bars. This temperature shift is better than the temperature shift of  $1.8$  °C  $\pm$   $0.2$  °C, provided by the IL [PMPY][Cl] by itself at low pressure (40 bars) [Figure 4-13].

At higher pressures (100 bars), the IL-synergent mixture [PMPy][Cl] + VCAP provided the temperature shift of  $1.3\text{ }^{\circ}\text{C} \pm 0.2\text{ }^{\circ}\text{C}$ , which is a better than the temperature shift of  $0.86\text{ }^{\circ}\text{C} \pm 0.2\text{ }^{\circ}\text{C}$  provided by the IL [PMPy][Cl] itself at the higher pressure (100 bars). Accordingly, in terms of effectiveness, these inhibitor solutions can be listed as:

[PMPy][Cl] + VCAP > [PMPy][Cl] > [PMPy][Cl] + PEO



*Figure 4-13:* The shift in the HLVE curve of the quaternary gas mixture (QM) in the presence of equal ratio IL-synergent mixtures [PMPy][Cl] + PEO and [PMPy][Cl] + VCAP at wide process conditions. The above data has the uncertainty of  $\pm 0.2$  °C .

Similarly, the synergents PEO and VCAP were added in equal ratio with the IL [PMPy][Triflate]. A similar thermo effect was observed and IL-synergent mixture [PMPy][Triflate] + VCAP provided a temperature shift of  $2.0$  °C  $\pm 0.2$  °C lower pressures (40 bars), which is higher than the temperature shift of  $1.56$  °C  $\pm 0.2$  °C provided by the IL [PMPy][Triflate] by itself [Figure 4-14].

Figure 4-14, exhibits the thermodynamic inhibition (TI) effect of equal ratio IL-synergent mixtures [PMPy][Triflate] + PEO and [PMPy][Triflate] + VCAP at wide process conditions on QM gas mixture. The IL-synergent mixture [PMPy][Triflate] + VCAP seems to be thermodynamically more effective and it shifted the QM HLVE by 2.0 °C at lower pressures (40 bars) and by 0.7 °C at higher pressures (100 bars). The above data has the uncertainty of  $\pm 0.2$  °C.

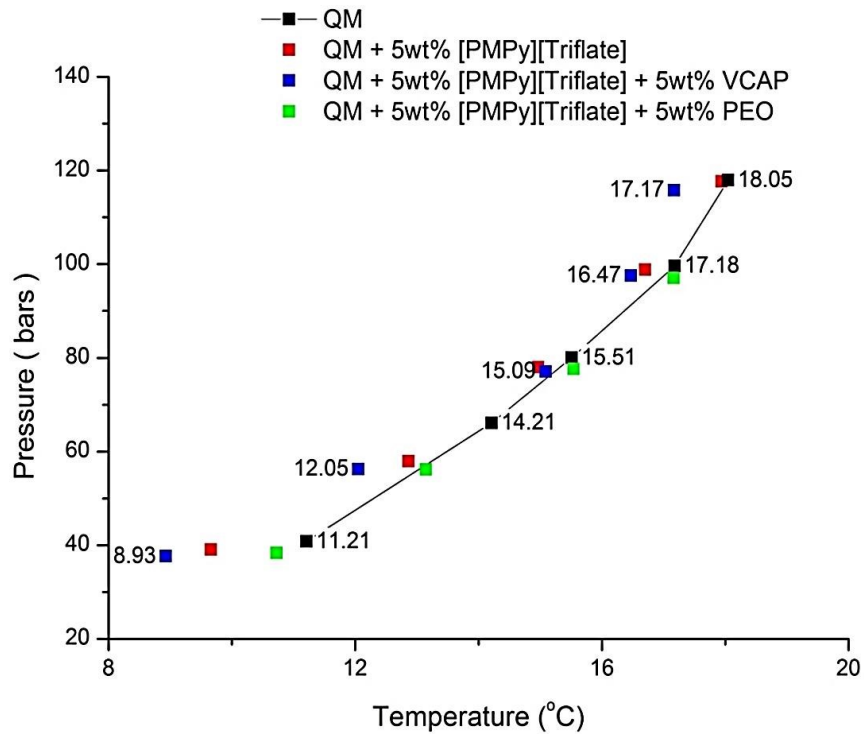


Figure 4-14. The shift in the HLVE curve of the quaternary gas mixture (QM) in the presence of equal ratio IL-synergent mixtures [PMPy][Triflate] + PEO and [PMPy][Triflate] + VCAP. The above data has the uncertainty of  $\pm 0.2$  °C.

At higher pressures (100 bars), the IL-synergent mixture [PMPy][Triflate] + VCAP provided the temperature shift of  $0.7\text{ }^{\circ}\text{C} \pm 0.2\text{ }^{\circ}\text{C}$ , which is again higher than the temperature shift of  $0.48\text{ }^{\circ}\text{C} \pm 0.2\text{ }^{\circ}\text{C}$  provided by the IL [PMPy][Triflate] itself. On contrary, the IL-synergent mixture [PMPy][Triflate] + PEO showed no thermodynamic inhibition at both low and high pressures. This helps us to deduce that PEO is not a suitable synergent for the thermodynamic hydrate inhibition [Figure 4-14]. Therefore, in terms of effectiveness, these inhibitor solutions can be listed as:

[PMPy][Triflate] + VCAP > [PMPy][Triflate] > [PMPy][Triflate] + PEO

Table 4-3: *The hydrate dissociation points experimentally obtained for the IL-synergent mixtures.*

Mixture	P (bars)	T (°C)	Mixture	P (bars)	T (°C)
	38.37	9.74		38.34	10.73
<b>QM + 5wt% [PMPy][Cl] + 5wt% PEO</b>	56.88	12.81	QM + 5wt% [PMPy][Triflate] + 5wt% PEO	56.18	13.14
	78.03	15.14		77.61	15.54
	97.34	16.41		97.05	17.16
	117.21	17.32			
	37.36	8.29		37.65	8.93
<b>QM + 5wt% [PMPy][Cl] + 5wt% VCAP</b>	56.3	11.69	QM + 5wt% [PMPy][Triflate] + 5wt% VCAP	56.25	12.06
	76.1	13.92		77.10	15.09
	95.35	15.55		97.60	16.47
				115.83	17.17

#### 4.1.3.2 Kinetic Inhibition effect of Pyrrolidinium ILs + Synergents

The PEO was found to be a poor thermodynamic inhibitor, but as a synergent, it significantly enhanced the kinetic inhibition effectiveness of IL [PMPy][Cl] and [PMPy][Triflate] and delayed the hydrate induction time by 6-20 hrs at different pressures. In comparison, the VCAP was found to be a weak kinetic inhibitor and it did not provide any significant delay in the hydrate induction time.

The PEO is a low toxic water-soluble polymer<sup>320</sup> that holds an oxygen atom at its center, that helps it to form strong hydrogen bonds within the water bulk system<sup>321</sup>. The hydrophilic part of the polymeric alkyl chain of PEO helps it to be completely miscible in water, whereas hydrophobic part helps it to reach closer to a guest molecule (CH<sub>4</sub>) and pushes the water molecules away from it<sup>322</sup>.

As far as hydrate inhibition is concerned, the PEO has been reported as a poor hydrate inhibitor and is incapable to show as hydrate inhibition itself.<sup>252, 254a, 323</sup> However, it acts well as a synergent and addition of low dosage of water-soluble polymers PEO with hydrate inhibitors can significantly enhance kinetic inhibition strength of inhibitors by binding with free water molecules. Previously, PEO has been used as a synergistic material to enhance the kinetic inhibition strength of inhibitors in various gas hydrate inhibition studies.<sup>40, 252, 255, 323a, 324</sup>

Figure 4-15, shows the kinetic inhibition (KI) effect or delay in the QM gas mixture hydrate formation in the presence of equal ratio IL-synergent mixtures [PMPy][Cl] + PEO and [PMPy][Cl] + VCAP. The IL-synergent mixture [PMPy][Cl] + PEO seems to be kinetically more effective and it delays the hydrate formation by 16 hrs at low pressures (40 bars) and by 6 hrs at high pressures (120 bars).

As shown in Figure 4-15, at lower pressures (~37 bars), the IL [PMPy][Cl] delayed the hydrate formation time from  $6.7 \pm 0.5$  hr to  $7.6 \pm 0.5$  hr. In comparison, the IL-synergent mixture [PMPy][Cl] + VCAP delayed it to  $8.3 \pm 0.5$  hr, while the the IL-synergent mixture [PMPy][Cl] + PEO delayed it to  $22.7 \pm 0.5$  hr.

Similarly, at higher pressures (~100 bars), the IL [PMPy][Cl] delayed the hydrate formation time from  $3.1 \pm 0.5$  hr to  $3.6 \pm 0.5$  hr. In comparison, the IL-synergent mixture [PMPy][Cl] + VCAP delayed it to  $4.1 \pm 0.5$  hr, while the IL-synergent mixture [PMPy][Cl] + PEO delayed it to  $9.1 \pm 0.5$  hr. This indicates that PEO is a strong kinetic synergent and addition of PEO with the inhibitors can help to increase their kinetic effect significantly [Figure 4-15].

Accordingly, in terms of effectiveness as kinetic hydrate inhibitors selected inhibitor and their mixtures can be listed as:





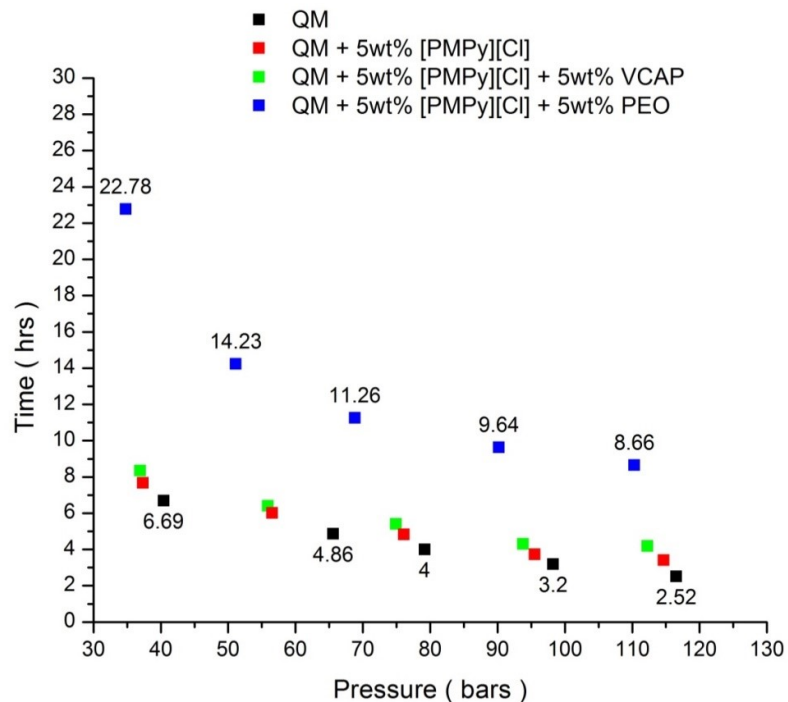
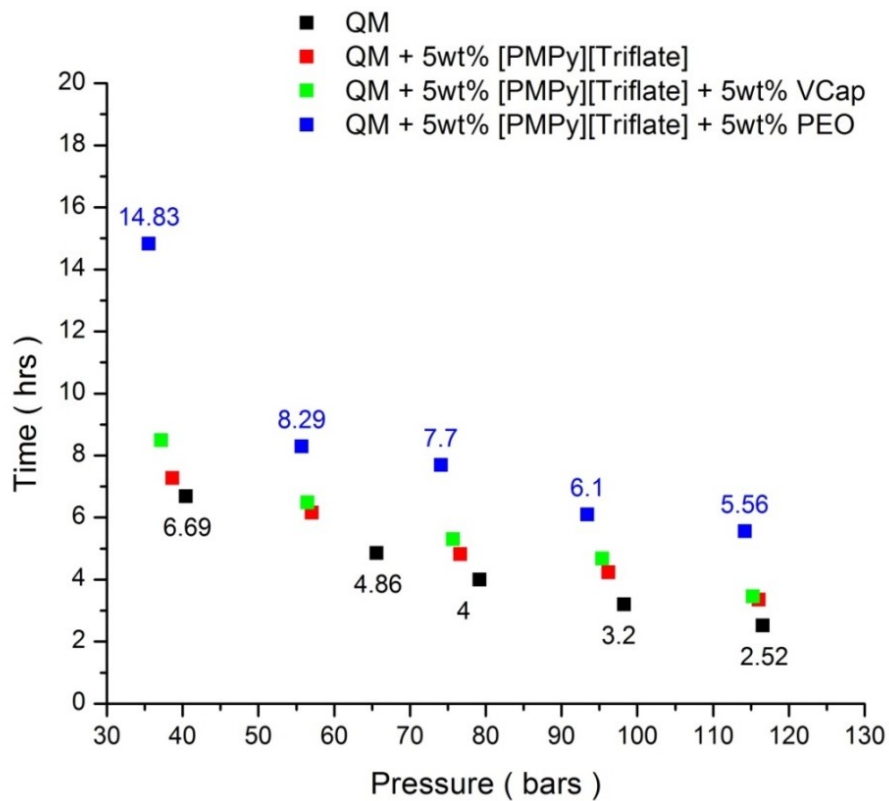


Figure 4-15: The delay in the QM gas mixture hydrate formation time in the presence of equal ratio IL-synergent mixtures [PMPy][Cl] + PEO and [PMPy][Cl] + VCAP. The above data has the uncertainty of  $\pm 0.5$  hr.

Figure 4-16, shows the kinetic inhibition (KI) effect or delay in the QM gas mixture hydrate formation in the presence of equal ratio IL-synergent mixtures [PMPy][Triflate] + PEO and [PMPy][Triflate] + VCAP at wide process conditions. The IL-synergent mixture [PMPy][Triflate] + PEO seems to be kinetically more effective and it delays the hydrate formation by 8 hrs at low pressures (40 bars) and by 3 hrs at high pressures (120 bars). The above data has the uncertainty of  $\pm 0.5$  hr.

As indicated in Figure 4-16, at lower pressures ( $\sim 37$  bars), the IL [PMPy][Triflate] delayed the hydrate formation time from  $6.7 \pm 0.5$  hr to  $7.3 \pm 0.5$  hr. In comparison, the IL-synergent mixture [PMPy][Triflate] + VCAP delayed it to  $8.5 \pm 0.5$  hr, while the the IL-synergent mixture [PMPy][Triflate] + PEO delayed it to  $14 \pm 0.5$  hr.



*Figure 4-16:* The delay in the QM gas mixture hydrate formation time in the presence of equal ratio IL-synergent mixtures [PMPy][Triflate] + PEO and [PMPy][Triflate] +VCAP. The above data has the uncertainty of  $\pm 0.5$  hr.

Similarly, at higher pressures (~100 bars), the IL [PMPy][Triflate] delayed the hydrate formation time from  $3.1 \pm 0.5$  hr to  $4.1 \pm 0.5$  hr. In comparison, the IL-synergent mixture [PMPy][Triflate] + VCAP delayed the hydrate formation time to  $4.2 \pm 0.5$  hr, while the the IL-synergent mixture [PMPy][Triflate] + PEO delayed it to  $6.1 \pm 0.5$  hr [Figure 4-16]. Therefore, in terms of effectiveness as kinetic hydrate inhibitors selected inhibitor and their mixtures can be listed as:

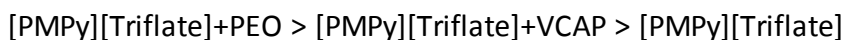


Figure 4-15 and Figure 4-16, clearly indicate that PEO is an effective kinetic synergent and it can substantially enhance the kinetic inhibition ability of the IL inhibitors. It can help to reduce the amount of inhibitor required for the hydrate inhibition and also possess good solubility in aqueous solution avoiding the chances of precipitation within the system.

The following are the key findings that can be deduced from the above experiments:

1. The monomer caprolactam (VCap) is more suited to act as a thermodynamic synergents. It can help to shift the QM HLVE curve by  $0.3\text{-}0.5$  °C. On contrary, the polymer PEO (Polyethylene Oxide) is a poor thermodynamic synergent and

addition of it with ILs does not help to improve their thermodynamic inhibition performance.

2. The Polymer PEO is more suited to act as the kinetic synergent and its addition with the ILs can help to delay the hydrate formation time by 6-20 hrs. On contrary, VCAP does not perform well as the kinetic synergent

## 4.2 Hydrate Formation and Inhibition in pure methane (CH<sub>4</sub>) gas

The synthetic quaternary gas mixture (QM) used for hydrate formation and inhibition study in the first part of this work was a novel gas mixture and its results cannot be compared with the literature results. Therefore, the next part of the experiments was conducted using pure methane gas and the results obtained were compared with the literature results to figure out how effective the chosen ionic liquids and amino acids inhibitors are against the already reported ionic liquids and amino acids inhibitors. This comparative study is essential for industrial scale up and computational modelling and simulation work in the future.

In the second part of work, four ionic liquids (Ethyl-ammonium formate [EA][Of], Dimethyl-ammonium formate [DMA][Of], Dimethyl-ethyl-ammonium formate [DMEA][Of]. and Tri-butyl methyl ammonium formate [TBMA][Of] ) and 5 amino acids (L-Alanine, L-Pheny-alanine, Asparagine, Histidine, Glycine) were tested as the inhibitors for the pure methane gas on the rocking cell assembly (RC-5) at different concentrations and operating conditions in the presence and absence of synergent PEO.

### 4.2.1 *Effect of Ammonium Ionic liquids on CH<sub>4</sub> hydrate inhibition*

The cost of ionic liquids is a major concern for their usage on the large industrial scale. George, et al. <sup>325</sup>, synthesized number of ionic liquids with the objective of reducing the ionic liquids cost by using inexpensive feedstock like sulfuric acid and simple amines combined into a range of protic ionic liquids containing hydrogen sulfate [HSO<sub>4</sub>]<sup>-</sup> anion.

The most effective way of reducing the cost for the large-scale ionic liquid production is through the use of protic ionic liquids (ILs with protonated amine for a cation) according to George, et al.<sup>325</sup>, and the concept is already being implemented in BASF BASIL process.<sup>76a</sup>

The protic ionic liquids do not require purification and number of synthesis steps can be reduced from 30 steps to 7 steps, making them less expensive than the traditional imidazolium liquids. It is estimated, that the bulk production of the tri-ethyl ammonium hydrogen sulfate [HNEt<sub>3</sub>][HSO<sub>4</sub>] can be as low as *\$1.24 per Kg*.<sup>326</sup> Therefore, in this study for the first time ammonium based protic ionic liquids containing formate anions were tested as the hydrate inhibitors.

These ILs are likely to be cheaper than the protic ILs liquids containing sulfate anions. The use of such ionic liquids as hydrate inhibitors is likely to have a lower environmental impact due to a reduction in the waste by-products, solvent losses, energy requirement and CO<sub>2</sub> generation.<sup>302</sup>

The four ammonium based ionic liquids tested include: Ethyl-ammonium formate [EA][Of], Dimethyl-ammonium formate [DMA][Of], Dimethyl-ethyl-ammonium formate [DMEA][Of] and Tri-butyl methyl ammonium formate [TBMA][Of]. These ammonium ILs are increasingly used as an electrolyte in different fuel cells and battery applications<sup>327</sup>

and for CO<sub>2</sub> capture<sup>328</sup>. However, they have not been tested as the hydrate inhibitors. Therefore, it was of great research interest to test these ammonium ILs as the CH<sub>4</sub> hydrate inhibitors. In section 4.3, a comparison will be drawn between the effectiveness of pyrrolidinium and ammonium-based ionic liquids.

#### ***4.2.1.1 Thermodynamic inhibition effect of Ammonium based ILs***

In the first part (4.1.2 & 4.1.3), the 1wt% pyrrolidinium IL showed no thermodynamic effect. Therefore, in the second part, the experimental trial were carried out using 5wt% of ammonium ILs to study thermodynamic inhibition effect of ILs [EA] [Of], [DMA] [Of], [DMEA] [Of] and [TBMA] [Of] [Figure 4-17].

The Figure 4-17, shows the shift in HLVE curve of methane (CH<sub>4</sub>) hydrate in the presence of 5wt% ammonium based ionic liquids at wide process conditions. The ammonium based ILs showed the slight average temperature shift of around 0.5 °C, except for the IL [TBA][Of] which showed no temperature shift.

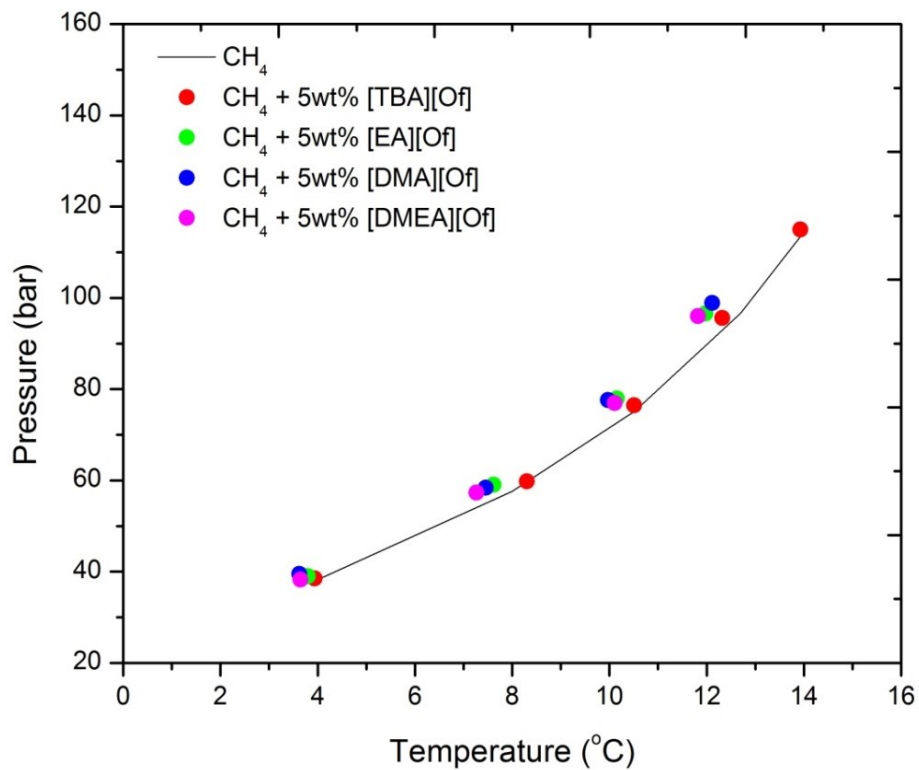


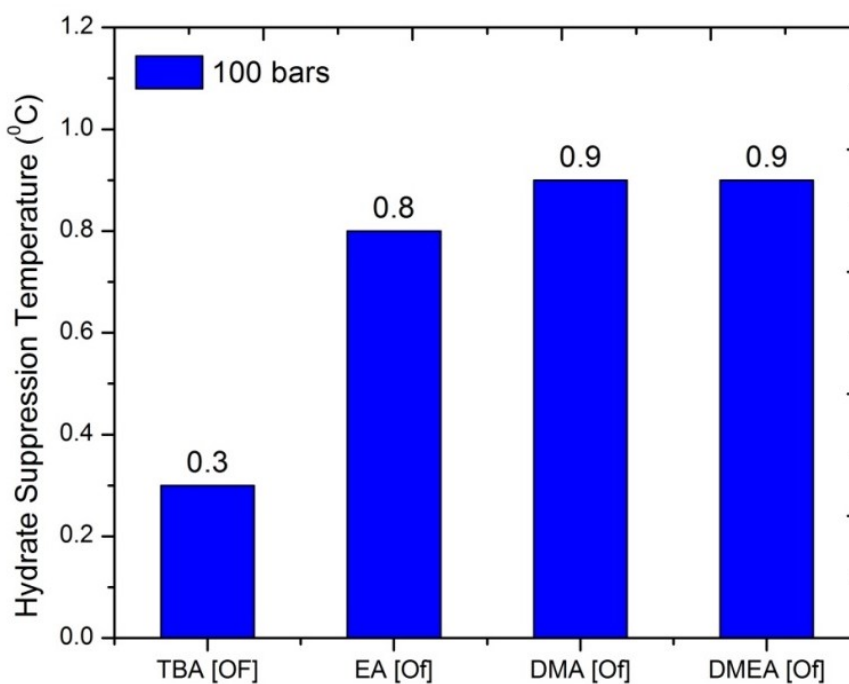
Figure 4-17: The shift in HLVE curve of methane (CH<sub>4</sub>) hydrate in the presence of 5wt% ammonium based ionic liquids. The data has an uncertainty of  $\pm 0.2$  °C.

As exhibited in Figure 4-17, the selected ammonium based ILs showed slight thermodynamic inhibition effect at all operational pressures (40-100 bars). At lower pressure (~40 bars), the 5wt% DMA [Of] was found to be the most effective thermodynamic hydrate inhibitor and it provided an average temperature shift of  $0.7 \pm 0.2$  °C. The 5wt% TBA [Of] was found to be the least effective thermodynamic hydrate inhibitor at lower pressures.



In comparison, at higher pressures (~100 bars), the selected ammonium ILs showed better thermodynamic inhibition effect. As shown in Figure 4-18, at 5wt% the ammonium ILs DMA [Of], DMEA [Of] and EA [Of] showed a similar thermodynamic inhibition effect and provided the average temperature shift of around  $0.9 \pm 0.2$  °C. [Figure 4-18].

Figure 4-18, illustrates the CH<sub>4</sub> hydrate suppression temperatures at 100 bars observed using 5wt% ammonium-based ILs. The average hydrate suppression temperature provided by IL EA [Of], DMA [OF], DMEA [OF] was around 0.8 °C. The TBA [Of] was found to be the least effective and it provided the hydrate suppression temperature of around 0.3 °C.



*Figure 4-18:* The CH<sub>4</sub> hydrate suppression temperatures at 100 bars observed using 5wt% ammonium-based ILs. The data has an uncertainty of  $\pm 0.2$  °C.

The next set of experimental trials was conducted at the concentration of 10 wt%. In comparison to 5wt%, at the concentration of 10wt%, the selected ammonium ILs showed a better thermodynamic effect at all pressures [Figure 4-19].

Figure 4-19, indicates the shift in CH<sub>4</sub> HLVE curve in the presence of 10 wt% ammonium based ionic liquids at wide process conditions. The 10 wt% ammonium based ILs showed the average temperature shift of around 2.0 °C, except for the IL [TBA][Of] which only showed a slight temperature shift of around 0.8°C.

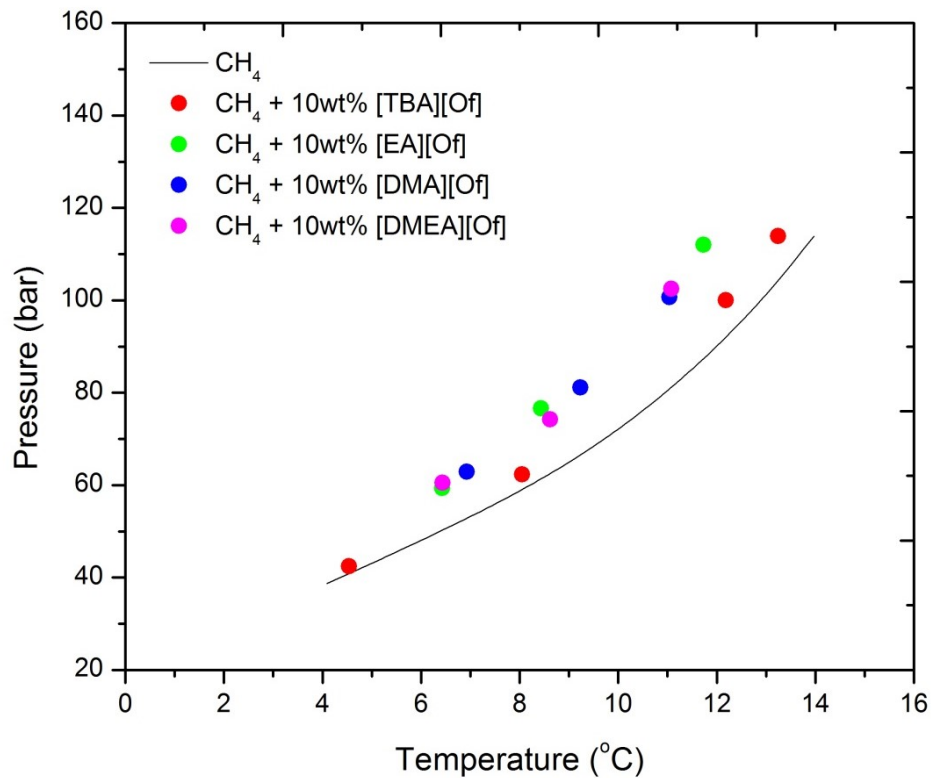
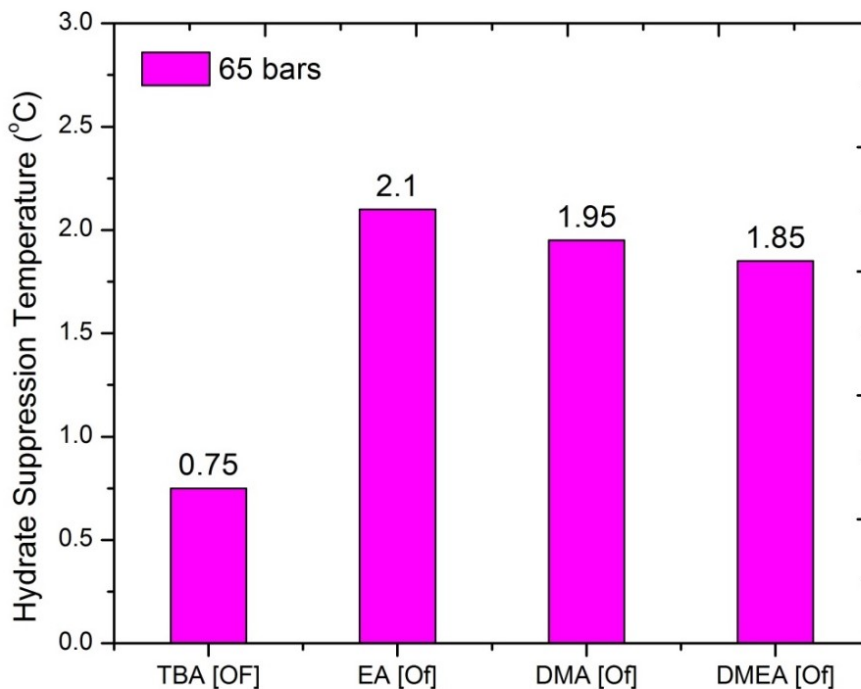


Figure 4-19: The shift in HLVE curve of methane (CH<sub>4</sub>) hydrate in the presence of 10 wt% ammonium based ionic liquids at wide process conditions. The data reported has an uncertainty of  $\pm 0.2$  °C.

As presented in Figure 4-20, at moderate pressures (~65 bars) the ILs EA [Of], DMA [Of] and DMEA [Of] provided an average temperature shift of around  $2.0 \pm 0.2$  °C. The IL EA [Of] was found to be the most effective thermodynamic inhibitor and it provided the temperature shift of  $2.1 \pm 0.2$  °C. The IL TBA [Of] was found to be the least

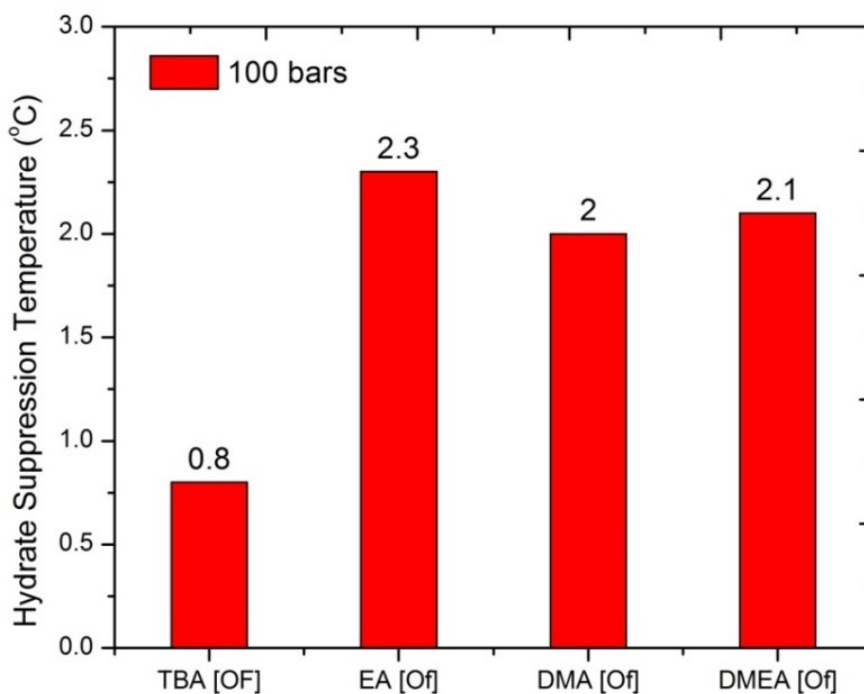
effective thermodynamic inhibitor and it provided the temperature shift of  $0.75 \pm 0.2$  °C [Figure 4-20].



*Figure 4-20:* The CH<sub>4</sub> hydrate suppression temperatures at 65 bars observed using 10 wt% ammonium-based ILs. The reported data has an uncertainty of  $\pm 0.2$  °C.

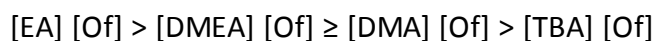
Similarly, at higher pressures (~100 bars), the ILs EA [Of], DMA [Of] and DMEA [Of] again provided an average temperature shift of around  $2.1 \pm 0.2$  °C. The average hydrate suppression temperature provided by IL EA [Of], DMA [Of], DMEA [Of] was

around 2.0 °C. The TBA [Of] was found to be the least effective and it provided the hydrate suppression temperature of around 0.8 °C [Figure 4-21]. The Table 4-4, shows the hydrate dissociation points for the ammonium based ILs used in this work at different pressure conditions.



*Figure 4-21:* The CH<sub>4</sub> hydrate suppression temperatures at 100 bars observed using 10 wt% ammonium-based ILs. The reported data has an uncertainty of  $\pm 0.2$  °C.

As shown in Figure 4-21, the IL EA [Of] was found to be the most effective thermodynamic hydrate inhibitor and it provided the temperature shift of  $2.3 \pm 0.2$  °C. The IL TBA [Of] was found to be the least effective thermodynamic inhibitor may be due to its non-protic nature and it provided the temperature shift of about  $0.8 \pm 0.2$  °C [Figure 4-21]. Hence, in terms of effectiveness as a thermodynamic inhibitor at 10 wt% (~100 bars) the selected ammonium ILs can be listed as:



In case of the similar anion, the IL with shorter alkyl chain tend to be more effective according to <sup>156</sup>. They proposed that the thermodynamic inhibition using ILs occurs as a result of the presence of strong electrostatic charges in ILs and the ability of ILs anions and cations of ILs to form hydrogen bonding with the water molecules.

The thermodynamic inhibition effect of the ILs is small at low pressure and gets better as the pressure increases according to Partoon, et al. <sup>157</sup>. In our case, the thermodynamic inhibition effect of ILs was high at low pressure and it decreases as the pressure increases.

The thermodynamic inhibition effect of ILs enhances with the increase in the concentration of the selected ILs, as stated by Partoon, et al. <sup>157</sup>. It was observed by Sabil, et al. <sup>329</sup>, that the thermodynamic inhibition effectiveness of ILs increases with the increase in their respective concentration. The similar case was also observed in this

work and the thermodynamic inhibition effectiveness of both pyrrolidinium ILs and ammonium ILs enhanced with the increase in their respective concentration.

The shorter alkyl chain ILs tend to be more effective thermodynamic hydrate inhibitor than the longer ones according to the Chu, et al.<sup>160</sup>. It was proposed by Long, et al.<sup>330</sup> that ILs with shorter alkyl chain in the cation tend to offer better thermodynamic inhibition effect compare to ILs with longer alkyl chain.

The longer alkyl chain might lead to increase in the hydrophobicity factor of ILs, which in turn affects the hydrogen bonding ability of IL with the water molecules.<sup>331</sup> Long, et al.<sup>330</sup> also observed that the thermodynamic inhibition tendency of the IL strongly relies on the anion size.

The smaller size anions offer higher charge density, which causes stronger electrostatic interaction between IL and water molecules resulting in an effective hydrate formation suppression.<sup>329</sup> The similar case was also observed with selected ammonium based ILs and in terms of effectiveness as cation can be listed as [EA] > [DMA] > [DMEA] > [TBA]. The IL [EA][Of] possess shorter alkyl chain in the cation which may help it to offer better thermodynamic inhibition effect.

Table 4-4: *CH<sub>4</sub> Hydrate dissociation points in the presence of 5wt% and 10 wt% ammonium based ionic liquids.*

Ionic Liquids	P (bars)	T (°C)	Ionic Liquids	P (bars)	T (°C)
CH <sub>4</sub> + 5wt% [EA][Of]	39.01	3.8	CH <sub>4</sub> + 10 wt% [EA][Of]	59.38	6.43
	59	7.61		76.63	8.43
	77.91	10.15		112.01	11.73
	96.58	11.98			
CH <sub>4</sub> + 5wt% [DMA][Of]	39.51	3.62	CH <sub>4</sub> + 10 wt% [DMA][Of]	62.91	6.92
	58.37	7.46		81.1	9.23
	77.63	9.97		100.64	11.04
	98.86	12.12			
CH <sub>4</sub> + 5wt% [DMEA][Of]	59.24	7.16	CH <sub>4</sub> + 10 wt% [DMEA][Of]	60.55	6.44
	71.12	9.22		74.26	8.62
	84.9	10.72		102.5	11.08
	96.79	11.62			
	115.01	13.33			
CH <sub>4</sub> + 5wt% [TBA][Of]	38.46	3.94	CH <sub>4</sub> + 10 wt% [TBA][Of]	42.41	4.54
	59.8	8.3		62.32	8.049
	76.43	10.51		100	12.18
	95.62	12.32		113.94	13.25
	114.96	13.93			

COSMO-RS analysis conducted by Khan, et al. <sup>170</sup> depict that the thermodynamic inhibition effect of ILs is due to their hydrogen bonding affinity with water molecules and the ILs does not participate in the hydrate crystalline structure.



It's the factors like hydrophobic nature and solubility that play a key role in inhibition effectiveness of the some ILs according to Mohamed, et al. <sup>58</sup>. In the section (4.3), the thermodynamic results obtained for ammonium-based ILs will be compared with the pyrrolidinium-based ILs and choline-based ILs at 5wt%. The further comparison of ammonium-based ILs will be made at 10 wt% of the amino acids, imidazolium-based ILs and other hydrate inhibitors reported in the literature.

The following are the key points that can be deduced from the thermodynamic study of the ammonium based ILs that agree with the literature.

1. In the case of the similar anion, the IL with shorter alkyl chain like [EA][Of] tend to be more effective
2. The thermodynamic inhibition effectiveness of ILs increases with the increase in their respective concentration
3. The thermodynamic inhibition effect of ILs with respect to pressure increase was not clear.

#### 4.2.1.2 *Kinetic inhibition effect of Ammonium based ILs*

The selected ammonium based ILs were tested for their kinetic inhibition effect in order to confirm their dual functional behavior at the concentrations of 5wt% and 10wt%. Figure 4-22, shows the time delay in the CH<sub>4</sub> hydrate formation in the presence of 5wt% ammonium based ILs [TBA][Of], [EA][Of], [DMA][Of] and [DMEA][Of]. All ILs showed almost similar kinetic inhibition effect. The IL [TBA][Of] was observed to be the

most effective kinetic hydrate inhibitor at 5 wt% and it delayed the hydrate formation by around 2.5 hr at 40 bars.

As indicated in Figure 4-22, the 5wt% ammonium based ILs were found to be most effective at lower pressures (40 bars), the IL [TBA] [Of] delayed the hydrate formation time from  $9.0 \pm 0.5$  hr to  $11.5 \pm 0.5$  hr, the IL [DMA] [Of] delayed it to  $9.8 \pm 0.5$  hr and the IL [DMEA] [Of] delayed it to  $9.5 \pm 0.5$  hr. At higher pressures (100 bars) all the ammonium IL showed a similar kinetic effect and the delay in the hydrate formation time was within the range of 0.5 to 1 hr [Figure 4-22].

At higher concentration of 10 wt%, no hydrate formation was observed at low pressure ( $\sim 40$  bars). The experiments were repeated three times, but no hydrate formation was detected at low pressure ( $\sim 40$  bars). As presented in Figure 4-23, the hydrate formation was only observed at pressures close to 60 bars.

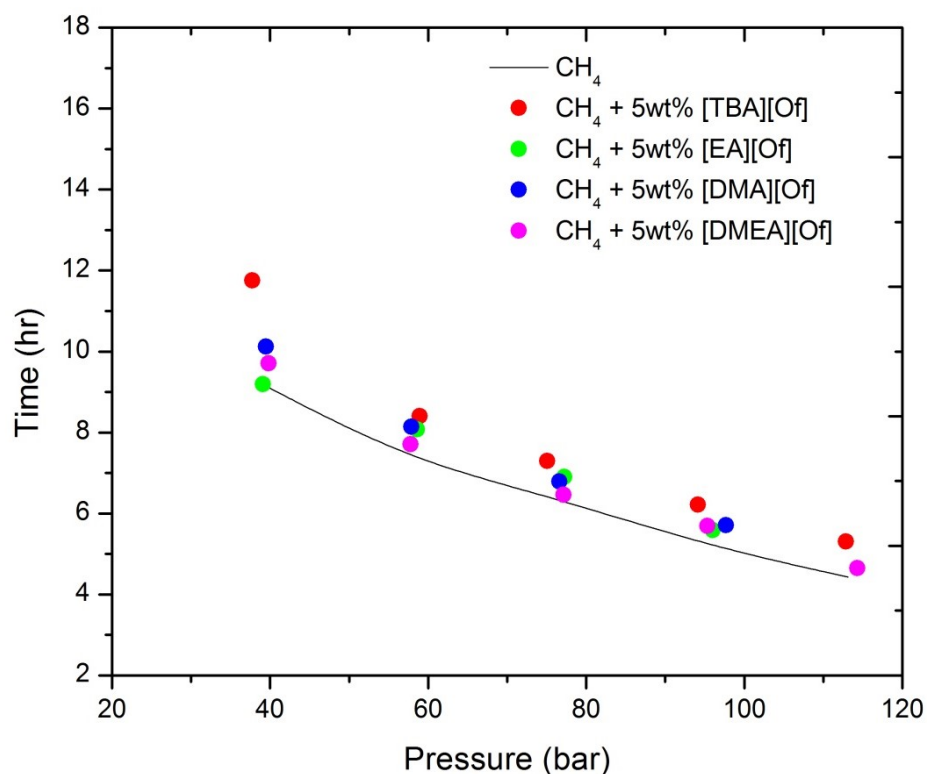


Figure 4-22: The time delay in the CH<sub>4</sub> hydrate formation in the presence of 5wt% ammonium based ILs [TBA][Of], [EA][Of], [DMA][Of] and [DMEA][Of]. The data has the uncertainty of  $\pm 0.5$  hr.

As presented in Figure 4-23, at 10 wt% and pressures close to 60 bars, all the ammonium-based ILs showed the similar kinetic effect and delayed the hydrate formation time from 0.5-1.5 hr. At the pressure close to 100 bars, the IL [EA] [Of] delayed the hydrate formation time from  $5.0 \pm 0.5$  hr to  $7.36 \pm 0.5$  hr, and it was found to be the most effective kinetic hydrate inhibitor compared to other ammonium ILs.

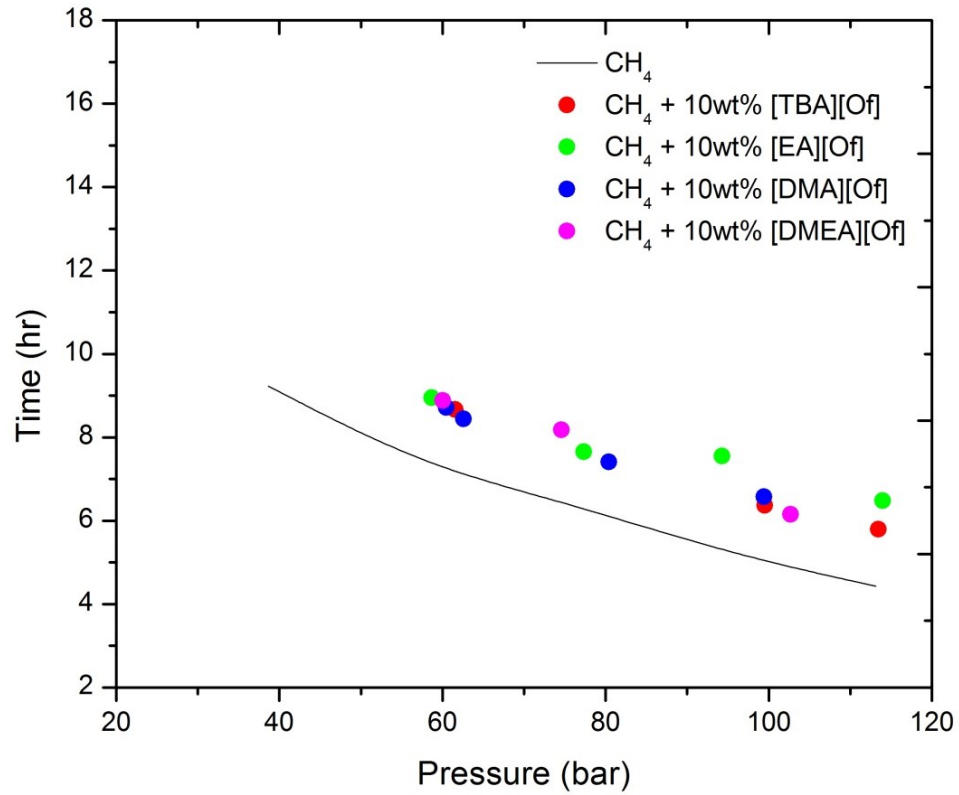


Figure 4-23: The time delay in the CH<sub>4</sub> hydrate formation in the presence of 10 wt% ammonium based ILs [TBA][Of], [EA][Of], [DMA][Of] and [DMEA][Of]. The data has the uncertainty of 0.5 hr.

Thus, in terms of effectiveness at 10 wt% and pressures close to 100 bars, the ILs can be listed as:

$$[\text{EA}][\text{Of}] > [\text{DMA}][\text{Of}] \geq [\text{TBA}][\text{Of}] \geq [\text{DMEA}][\text{Of}]$$

The ILs that have shorter alkyl chain and stronger electrostatic forces tend to be more effective kinetic hydrate inhibitor according to Rasoolzadeh, et al.<sup>164</sup>. It was also observed that the effect of cations is much more significant than the effect of anions in the selected ILs.

The hydrate induction time for ILs increases with their concentration, as observed by Lee, et al.<sup>169</sup>. The X-ray diffraction pattern of some ILs shows that no amalgamation of IL in the hydrate crystal structure occurs.

Generally, it is known that the kinetic hydrate inhibitors like ionic liquids inhibit the hydrate formation by adsorbing on the hydrate surface and slowing the diffusion of guest molecules to the hydrate water surface.<sup>331</sup> The actual mechanism of hydrate inhibition by kinetic hydrate inhibitor is still not clear. However, three key mechanisms have been reported in the literature previously.

The first mechanism proposes that inhibitors adsorb on the surfaces of growing hydrate crystal (sub-critical or super-critical size), thus inhibiting further growth.<sup>50</sup> The second mechanism proposes that inhibitors adsorb on the surface of the “foreign” particles that would otherwise act as a site for heterogeneous hydrate nucleation.<sup>51</sup> The third mechanism, based on the simulation observation, proposes that perturbation of

liquid water structure by inhibitors prevent the growth of hydrate crystals to the critical cluster size or destabilizes the partially formed hydrate clusters completely.<sup>52</sup>

The following finding can be deduced from the above experimental results:

1. The higher concentration favours both the thermodynamic and kinetic hydrate inhibition in the selected ammonium ILs.
2. The selected ammoniums ILs have the tendency to act as the dual functional inhibitors showing both the kinetic and thermodynamic hydrate inhibition at the same time.
3. The selected ammoniums ILs have the same anion but different cations. The shorted alkyl chain cations like [EA] are likely to be more suited for the thermodynamic and kinetic hydrate inhibition due to likely presence of extra pair of protons.

#### ***4.2.2 Co-effect of Ammonium-based Ionic liquids and Synergent on CH<sub>4</sub> hydrate formation***

Poly-ethylene oxide (PEO) worked as an exceptional kinetic synergent with pyrrolidinium ILs in the first part and it exponentially enhanced the kinetic inhibition effect of pyrrolidinium ILs. Therefore, PEO was also tested with ammonium-based to enhance their kinetic inhibition performance. However, this time lower dosage (1wt %) of PEO was used instead of a higher dosage of 5wt% used in the previous section.

The most effective 5wt% ammonium based IL with the addition of the 1wt% PEO was found to be [DMEA] [Of]. In the IL-synergent mixtures containing [5wt% [DMA] [Of] + 1wt% PEO] and [5wt% [TBA] [Of] + 1wt% PEO] no hydrate formation was observed at low pressures (> 60 bars). The hydrate formation was only observed at the pressures above 60 bars [Figure 4-24].

Figure 4-24, presents the kinetic inhibition (KI) effect or delay in the CH<sub>4</sub> hydrate formation time in the presence of 5wt% ammonium ILs + 1 wt% PEO mixtures at wide process conditions. The IL + synergent mixture 5wt% [DMEA][Of] + 1 wt% PEO was observed to be kinetically most effective and it delayed the hydrate formation by 20 hrs at 55 bars and by 10 hrs at 100 bars. The hydrate formation in the CH<sub>4</sub> blank sample is shown in the black.

As shown in Figure 4-24, at the pressure close to 55 bars, the IL-synergent mixture [5wt% [DMEA] [Of] + 1wt% PEO] delayed the hydrate formation time from  $7.7 \pm 0.5$  hr to  $29.6 \pm 0.5$  hr and the IL-synergent mixture [5wt% [EA] [Of] + 1wt% PEO] delayed it to  $20.3 \pm 0.5$  hr.

Similarly, at the higher pressure close to  $100 \pm 2$  bars the IL-synergent mixture [5wt% [DMEA] [Of] + 1wt% PEO] delayed the hydrate formation time from  $5.0 \pm 0.5$  hr to  $14.9 \pm 0.5$  hr and the IL-synergent mixture [5wt% [EA] [Of] + 1wt% PEO] delayed it to  $13.8 \pm 0.5$  hr [Figure 4-24].



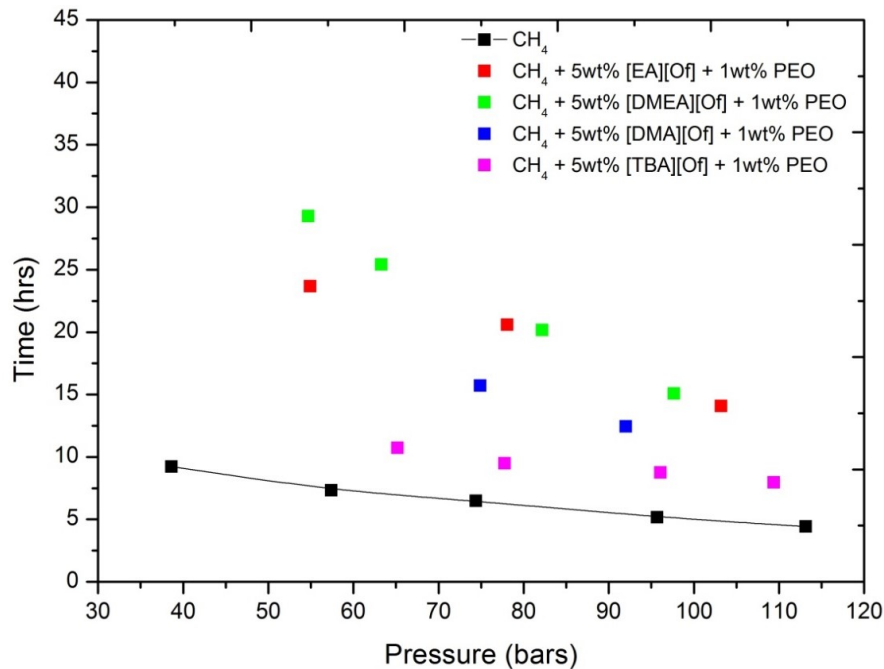
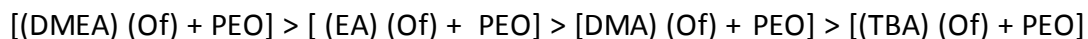


Figure 4-24: The kinetic delay in the CH<sub>4</sub> hydrate formation in the presence of 5wt% ammonium ILs + 1 wt% PEO mixtures at wide process conditions. The data has the uncertainty of  $\pm 0.5$  hr.

The IL-synergent mixture [5wt% [TBA] [Of] + 1wt% PEO] delayed the hydrate formation time from  $5.3 \pm 0.5$  hr to  $8.5 \pm 0.5$  hr and the IL-synergent mixture [5wt% [DMA] [Of] + 1wt% PEO] delayed it to  $12.46 \pm 0.5$  hr respectively at pressures close to 92 bars  $\pm 0.5$  bars [Figure 4-24]. Hence, in terms of effectiveness, the 5wt% ammonium based IL and their mixture with 1wt% PEO can be listed as:



As mentioned in the previous section, the PEO is a low toxic water-soluble polymer<sup>320</sup> that holds an oxygen atom at its centre, which allows it to form strong hydrogen bonds within the water bulk system<sup>321</sup>. The hydrophilic part of the polymeric alkyl chain of PEO helps it to be completely miscible in water, whereas hydrophobic part helps it to reach closer to a guest molecule (CH<sub>4</sub>) and pushes the water molecules away from it<sup>322</sup>.

However, PEO is a poor hydrate inhibitor and is incapable to show as hydrate inhibition itself.<sup>252, 254a, 323</sup>. But, it acts well as a synergent and addition of low dosage of PEO with ILs can significantly enhance their kinetic inhibition strength of KHI, by providing disruption of water cages and also repeling water molecules away.

### ***4.2.3 Effect of Amino Acids on CH<sub>4</sub> hydrate inhibition***

In recent years, the research interest has diverted towards the use of biological compounds that have high biodegradation rate in sea water. Previously, the natural antifreeze proteins found in fish, insects, plants, and bacteria have been used for hydrate inhibition studies.<sup>332</sup> According to Perfeltdt, et al.<sup>333</sup>, these proteins and peptides are expected to biodegrade easily.<sup>333</sup> Therefore, in this work the biological molecules like amino acids have been tested as the hydrate inhibitors.

The amino acids are the biological compounds that naturally exist in nature.<sup>186</sup> Amino acids are manufactured on large scale and available readily. Till date, no comprehensive kinetic and thermodynamic hydrate inhibition study has been conducted using amino acids on pure methane gas (> 99 %) . This makes them attractive compounds to be tested as the hydrate inhibitors. Amino acids as inhibitors are considered to be non-toxic, biodegradable and easier to produce in higher purity.<sup>186</sup> They can be obtained at low cost in large quantities and this makes them an attractive option to be used as a gas hydrate inhibitor<sup>187</sup>. Previously many studies have reported the use of amino acids as corrosion inhibitors<sup>57a, 188</sup>

The amino acids are non-volatile in nature which offers them an advantage over other inhibitors<sup>191</sup>. Due to better stability and compatibility, the amino acids can also be easily recovered from the pipelines. The structure and chemical properties of amino acids are also well understood which makes it easier to understand their inhibition

mechanism.<sup>176</sup>

#### ***4.2.3.1 Thermodynamic Inhibition effect of Amino Acids***

Initially, the experiments were conducted using 1wt% of amino acids. At 1 wt%, like ionic liquids, the pure amino acids samples did not show any thermodynamic inhibition effect on methane hydrates. This clearly shows that 1wt% quantity is not sufficient enough to disrupt or perturb methane hydrate crystal formation [Figure 4-25].

Figure 4-25, shows the HLVE curve of CH<sub>4</sub> in the presence of 1wt% amino acids. No shift in methane HLVE was observed, which indicates that no thermodynamic hydrate inhibition takes place within the system in the presence of 1wt% amino acids. The CH<sub>4</sub> HLVE in the blank sample is shown in the black. The data has the uncertainty of  $\pm 0.2$  °C.

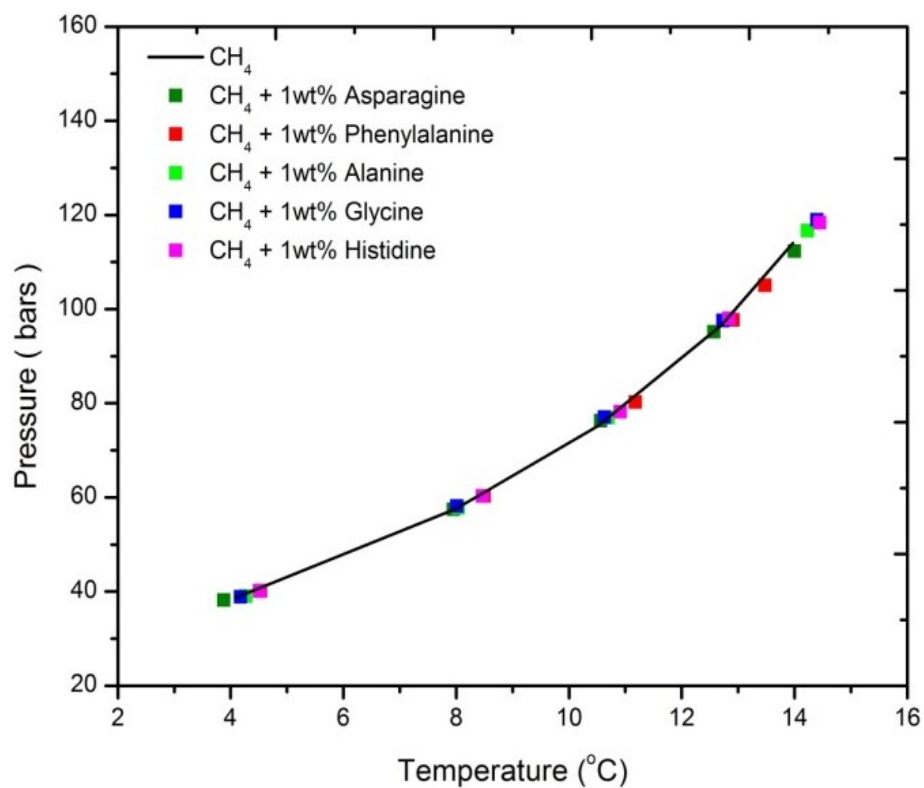


Figure 4-25: The HLVE curve of CH<sub>4</sub> in the presence of 1wt% Amino Acids. The data has the uncertainty of  $\pm 0.2$  °C.

Amino acids like asparagine and L-phenyl alanine have low solubility (< 3 wt %) in water due to which their inhibition effect cannot be studied at higher concentration. Therefore, the amino acids with higher solubility in water ( $\geq 4$ wt %) were selected to study their inhibition effectiveness at higher concentrations [Figure 4-26].

Figure 4-26, illustrates the thermodynamic inhibition (TI) effect or shift in CH<sub>4</sub> HLVE in the presence of 4-5 wt% amino acids. The amino acids L-alanine and glycine were found to be most effective and they shifted the CH<sub>4</sub> HLVE by 0.9 °C. The amino acid Histidine showed no significant thermodynamic inhibition effect at higher concentration.

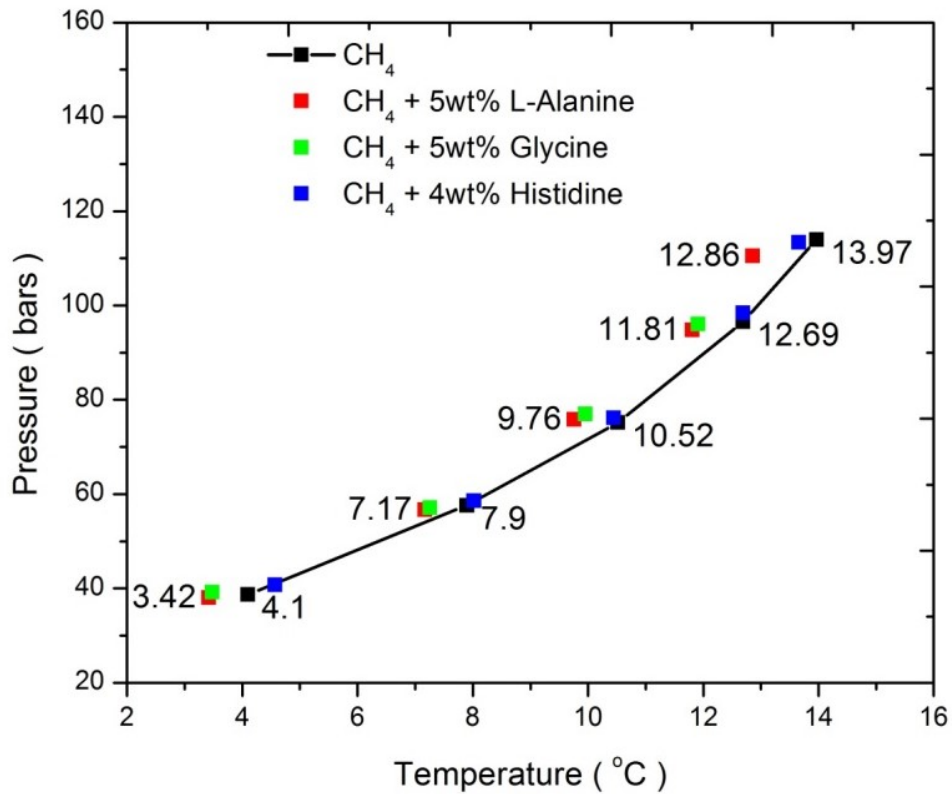


Figure 4-26: The shift in HLVE curve of CH<sub>4</sub> in the presence of 4-5 wt% amino acids (AA). The data has the uncertainty of  $\pm 0.2$  °C.

As presented in Figure 4-26, at higher concentration (5 wt%), both L-alanine and glycine showed the similar thermodynamic effect and provided the temperature shift of  $0.9 \pm 0.1$  °C at higher pressures (~100 bars ) and the temperature shift of  $0.7 \pm 0.1$ °C at lower pressures (~60 bars). However, histidine showed no thermodynamic inhibition effect at higher concentration [Figure 4-26].

Therefore, in terms of effectiveness as a thermodynamic hydrate inhibitor, the amino acids can be listed as:

**L-Alanine  $\geq$  glycine > histidine**

Figure 4-27 and Figure 4-28, illustrate the thermodynamic inhibition effect of 10 wt% glycine and 10 wt% alanine on the methane hydrate formation studied by Bavoh, et al. <sup>334</sup>. It was observed by Bavoh, et al. <sup>334</sup>, that 10 wt% glycine and 10 wt% alanine provides a temperature shift of around 1.5 °C and 1.7 °C at  $98 \pm 2$  bars.

As shown in Figure 4-27, as the concentration of amino acid L-alanine increases its thermodynamic inhibition effect increases and vice versa. The CH<sub>4</sub> hydrate dissociation points for 10 wt% of L-Alanine was obtained from Bavoh, et al. <sup>334</sup> Similarly, as the concentration of amino acid Glycine increases its thermodynamic inhibition effect also increases. Bavoh, et al. <sup>334</sup>, conducted further experimental trials using 15 wt% and 20 wt% of glycine. They found that at  $98 \pm 2$  bar, the 15 wt% Glycine provided the

temperature shift of up to 2.27 °C and the 20 wt% Glycine provided the temperature shift of up to 2.9 °C [Figure 4-28].

The experimental results of this study and Bavoh, et al.<sup>334</sup> study clearly shows that the thermodynamic inhibition effect of amino acid glycine increases with the concentration. However, the major objective of this work was to use amino acids as low dosage hydrate inhibitors ( $\leq 5\text{wt}\%$ ), as the higher concentrations of amino acids ( $> 10\text{ wt}\%$ ) can cause storage issues on the large industrial scale.



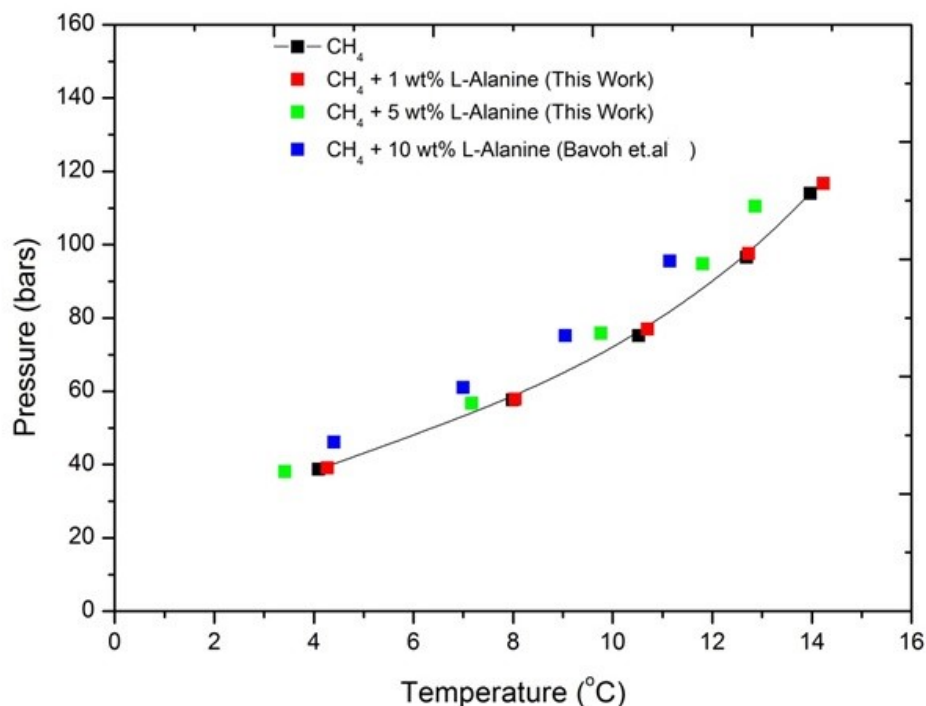


Figure 4-27: The shift in the HLVE curve of CH<sub>4</sub> at different concentrations of L-Alanine. The data has the uncertainty of  $\pm 0.2$  °C.

The thermodynamic hydrate inhibition effect occurs due to hydrogen bonding and electrostatic force of attraction via zwitterion interactions between amino acids and water molecules according to Sa, et al.<sup>335</sup>. The molecular structure of amino acids is made up of hydrophilic and hydrophobic head.<sup>236</sup> This may allow amino acids to act as zwitterions in an aqueous environment.<sup>232</sup> Its the ability of amino acids to act as zwitterions that is likely to cause a strong electrostatic force of interaction between electric charges of amino acids and water molecules, resulting in disruption of water cages in hydrate clathrates according to Sa, et al.<sup>335</sup>. The carboxylic and amine groups of

amino acids may also facilitate the formation of hydrogen bonds with water molecules.

Figure 4-28, illustrates the thermodynamic inhibition (TI) effect or shift in  $\text{CH}_4$  HLVE at different concentrations of glycine. As the concentration of amino acid glycine increases the thermodynamic inhibition effect of glycine increases and vice versa. The  $\text{CH}_4$  hydrate dissociation points for 10-20 wt% of Glycine was obtained from Bavoh, et al.<sup>334</sup>

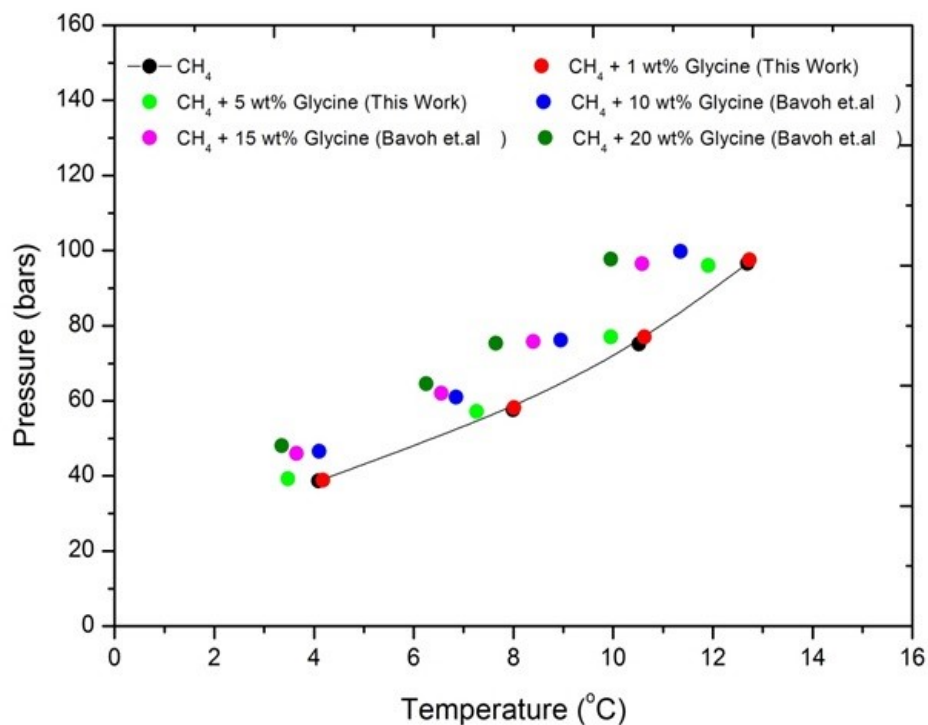


Figure 4-28: The shift in HLVE curve of CH<sub>4</sub> at different concentrations of Glycine. The data has the uncertainty of  $\pm 0.2$  °C.

The gas hydrate inhibition is carried out by thermodynamic hydrate inhibitors, through competing for water molecules and disruption of water activity in the hydrate cages via hydrogen bonding, as suggested by Laage, et al.<sup>336</sup>. This concept is closely related to the hydrophobic effect<sup>337</sup>. Most hydrophobic molecules tend to be non-polar and do not dissolve well in water according to Akhavan, et al.<sup>337</sup>. These molecules often form clusters know as micelles and they tend to repel away the water molecules.<sup>337</sup> Amino acids are proposed to act in a similar way and the presence of amino acids

disrupts the water activity in the hydrate cages through hydrogen bonding with water molecules.

As the length of the alkyl side chain of amino acids increases, the hydrophobicity enhances and kinetic inhibition performance of the particular amino acid decreases according to Sa, et al.<sup>191</sup>. This shows that longer alkyl chain adversely affects the kinetic inhibition performance of the amino acids. The longer alkyl side chains support the thermodynamic inhibition performance of the amino acids.<sup>191</sup>

The thermodynamic inhibition strength of amino acids tends to increase with the increase in the size and the side alkyl chain of amino acids according to Sa, et al.<sup>191</sup>. This is mainly due to enhanced hydrophobic effect as a result of longer alkyl side chains. Thus, the kinetic hydrate inhibition performance of amino acids depends on their hydrophobicity and the length of the alkyl side chain.<sup>191, 338</sup>.

On contrary, the Bavoh, et al.<sup>334</sup>, stated that the amino acids with shorter side alkyl chain like Glycine and L-Alanine show better thermodynamic inhibition effect than those with longer side alkyl chain like arginine.<sup>334</sup> This is due to the fact that as the alkyl chain of amino acids reduces in size the solvation with water molecules increases, which increases the thermodynamic inhibition impact of these amino acids.<sup>339</sup> The CH<sub>4</sub> hydrate dissociation points at different pressures and amino acid concentrations are provided in Table 4-5.

Table 4-5: *CH<sub>4</sub> Hydrates dissociation points (P-T) obtained in the presence of the amino acids at different concentrations*

Amino Acids	P (bars)	T (°C)	Amino Acids	P (bars)	T (°C)
	116.69	14.23		110.49	12.86
CH <sub>4</sub> + 1wt% L-Alanine	97.63	12.73	CH <sub>4</sub> + 5 wt% L-Alanine	94.80	11.81
	76.95	10.70		75.83	9.76
	57.78	8.04		56.71	7.17
	39.05	4.27		38.08	3.42
	118.96	14.40		96.06	11.91
CH <sub>4</sub> + 1wt% Glycine	97.55	12.73	CH <sub>4</sub> + 5 wt% Glycine	76.99	9.95
	77.04	10.63		57.09	7.26
	58.16	8.01		39.20	3.48
	38.89	4.18		-	-
	118.40	14.45		113.40	13.66
	97.99	12.84		98.45	12.69
CH <sub>4</sub> + 1wt% Histidine	78.21	10.91	CH <sub>4</sub> + 4 wt% Histidine	76.17	10.44
	60.28	8.47		58.56	8.02
	40.11	4.51		40.74	4.57
	112.33	14.00		105.09	13.48
	95.15	12.57		97.67	12.91
CH <sub>4</sub> + 1 wt% Asparagine	76.30	10.56	CH <sub>4</sub> + 1wt% Phenylalanine	80.29	11.18
	57.43	7.95		60.27	8.50
	38.22	3.88		40.14	4.53

In this work, it has also been observed that the solubility factor plays a key role and the amino acids with higher solubility in aqueous solutions are likely to act as better thermodynamic inhibitors. Akhavan, et al. <sup>337</sup>, likewise reported that the thermodynamic inhibition strength of amino acids relies on the solubility of amino acids. The higher the

solubility, the better is the inhibition effect of the amino acids. It's likely that as the solubility of amino acid increases their hydrogen bonding ability increases which increases disruption and water re-orientation in hydrate cages.

The following, are the key experimental findings that match well with the literature statements:

1. The higher concentration of amino acids is likely to provide better hydrate inhibition.
2. The shorter alkyl chain amino acids like glycine and alanine are more suited to act as the hydrate inhibitor due to the fact that as the alkyl chain of amino acids reduces in size the solvation with water molecules increases, which increases the thermodynamic inhibition impact of these amino acids.
3. The amino acids with lower solubility in aqueous solution leave behind undissolved particles, which can cause precipitation in the aqueous phase. Therefore, such amino acids do not take part in the inhibition process and no significant shift in hydrate HLVE is observed using these types of the amino acids.
4. Glycine and L-alanine, due to their high solubility in aqueous solution, are likely to be the potential hydrate inhibitor both thermodynamically and kinetically.
5. The thermodynamic hydrate inhibition effect of amino acids is likely to occur due to hydrogen bonding and electrostatic force of attraction via zwitterion interactions between amino acids and water molecules.

#### 4.2.3.2 *Kinetic inhibition effect of Amino Acids*

The selected amino acids did not show any thermodynamic inhibition effect at the concentration of 1 wt%. But, at 1wt% the amino acids exhibited the slight kinetic inhibition effect and delayed the hydrate formation by up to 1 hr [Figure 4-29]. At 1wt%, the amino acids were found to be most effective at low pressures and at a high pressure no kinetic inhibition effect was shown by the selected amino acids.

Figure 4-29, depicts the time delay in the CH<sub>4</sub> hydrate formation in the presence of 1 wt% amino acids. The amino acid asparagine was found to be the most effective kinetic hydrate inhibitor and it delays hydrate formation by 45 min at 55 bars. The hydrate formation in the CH<sub>4</sub> blank sample is shown in the black.

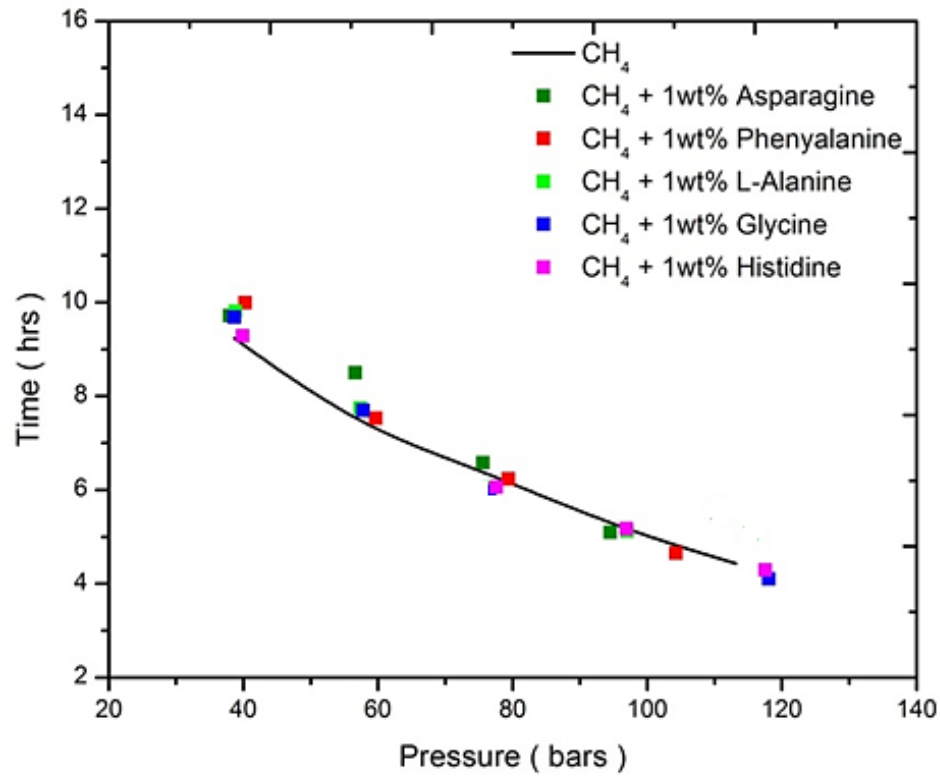


Figure 4-29: The time delay in the CH<sub>4</sub> hydrate formation in the presence of 1 wt% amino acids. The data has the uncertainty of  $\pm 0.5$  hr.

At 1wt% and pressure of around  $55 \pm 0.5$  bars, the Asparagine was found to be the most effective kinetic hydrate inhibitors with an average time delay of about 45 min [Figure 4-29] and the amino acids in terms of kinetic inhibition effectiveness can be listed as:

Asparagine > L-alanine > glycine > phenylalanine



The kinetic inhibition effect of L-alanine, aspartic Acid, asparagine, phenylalanine, and histidine on CO<sub>2</sub> hydrates at a low concentration ( < 0.1 wt%) was studied by Sa, et al. <sup>224</sup>. It was found that aspartic acid and asparagine exhibit higher kinetic inhibition than alanine.

The hydrophilic and electrically charged chain of amino acids (like asparagine) is likely to disrupt the water structure and the hydrophobic part of such amino acid side-chain is likely to strengthen the water structures.<sup>224</sup> Hence, the amino acids with stronger hydrophilic side chain like asparagine are likely to be more effective in delaying hydrate formation as they can cause more disruptions in water structure.

The amino acids with lower hydrophobicity tend to function better as a kinetic hydrate inhibitor according to Sa, et al. <sup>225</sup>. The more hydrophilic amino acids (like Asparagine) delay hydrate formation and growth by disrupting the water hydrogen bond network.

The extent of perturbation caused by a particular amino acid is likely to affect its kinetic hydrate inhibition effectiveness and the perturbation depends on the hydrophobicity factor of amino acids. <sup>226</sup> Therefore, the amino acids with lower hydrophobicity tend to be more effective as kinetic hydrate inhibitor than the ones with higher hydrophobicity.

The kinetic inhibition effect of glycine on tetra hydro furan (THF) hydrate formation at an atmospheric pressure was studied by Naeiji, et al. <sup>235</sup> and it was found that 1wt% of glycine delayed the THF hydrate induction time by 4 min. Consequently, in comparison to THF, the 1wt% Glycine shows much better kinetic results with methane and delays methane induction time by 27 min at lower pressures [ < 40 bars].

Similarly, the kinetic inhibition effect of glycine on ethane hydrate formation at 20 bars was studied by Rad, et al. <sup>236</sup> and they observed that 1wt% Glycine delayed ethane induction time by 58 min. However, Rad, et al. <sup>236</sup>, stated that by increasing the concentration of glycine from 1wt% to 3wt% the delay in ethane induction time got reduced to 45 min.

Phenylalanine and Asparagine both have limited solubility in water, as a result, it was difficult to test their effectiveness at higher concentration ( $\geq 4\text{wt}\%$ ). Therefore, L-Alanine, Glycine, and Histidine were tested at higher concentration ( $\geq 4\text{wt}\%$ ) to check for their effectiveness in delaying hydrate crystal formation. The further experiments were conducted at a higher concentration based on the solubility of the selected amino acids [Figure 4-30].

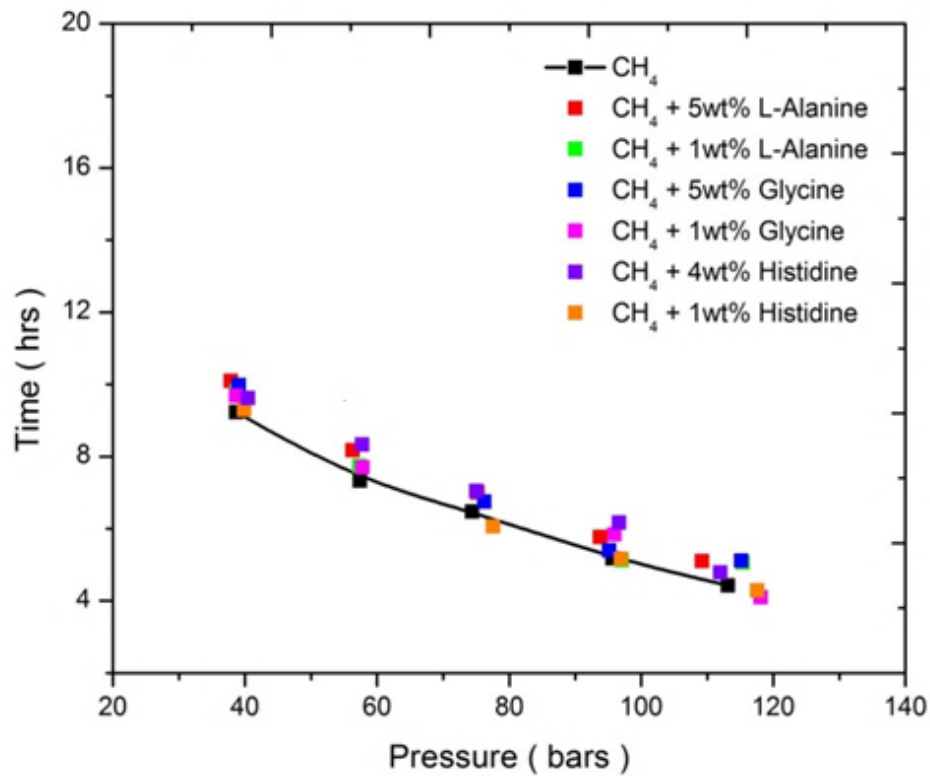


Figure 4-30: The time delay in the CH<sub>4</sub> hydrate formation in the presence of 5 wt% amino acids. The data has the uncertainty of  $\pm 0.5$  hr.

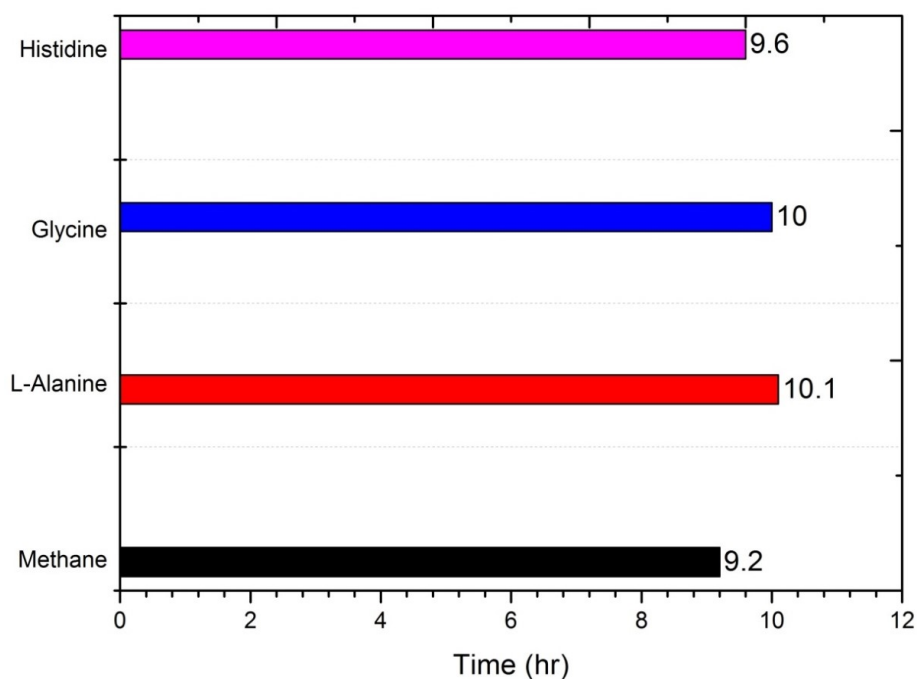
Figure 4-30, shows the time delay in the CH<sub>4</sub> hydrate formation in the presence of 5 wt% amino acids. The amino acid Asparagine and Glycine were found to be effective kinetic hydrate inhibitors and they delay hydrate formation by 52 min and 44 min at 40 bars. The hydrate formation in the CH<sub>4</sub> blank sample is shown in the black [Figure 4-30]. Thus, in terms of effectiveness at higher concentration (4-5wt%) and low pressures the amino acids can be listed as:

## L-Alanine > Glycine > Histidine

Figure 4-31, illustrates the delay in the CH<sub>4</sub> hydrate formation in the presence of amino acids L-Alanine, Glycine and Histidine at the low pressure of 40 bars. The L-Alanine and Glycine both provided the similar delay in the CH<sub>4</sub> hydrate formation and were found to be more effective than the Histidine

As presented in Figure 4-31, the Glycine and L-Alanine were found to be kinetically more effective than the Histidine, The Histidine has limited solubility in water (< 4,19 wt%) at 25 °C and as the temperatures are reduced from 20 °C to 2 °C the precipitation is likely to occur within the rocking cells. This is likely to affect the kinetic inhibition effectiveness of the histidine.

As shown in Figure 4-30, at high concentration ( 4-5wt%) the selected amino acids did not show any significant delay in the hydrate inhibition and it seems that the higher concentration does not affect the kinetic inhibition strength of the amino acids.



*Figure 4-31:* The time delay in the CH<sub>4</sub> hydrate formation in the presence of amino acids 5wt% L-Alanine, 5wt% Glycine and 4wt% Histidine at the low pressure of 40 bars. The data has the uncertainty of  $\pm 0.5$  hr.

The experimental and simulation result of various studies also indicate that glycine and L-alanine are likely to be the most suited kinetic hydrate inhibitors and the higher concentration of amino acids does not have a significant effect on the kinetic inhibition strength of amino acids.<sup>224, 224-225, 228, 235, 242</sup> Hence, our experimental results agree with the following literature statements:

1. The hydrophilic amino acids like asparagine are likely to act better as a kinetic hydrate inhibitor. However, the Asparagine has a limited solubility (< 2.94 wt.%) in aqueous solution. Hence, it may not be able to provide a significant delay in hydrate formation due to likely precipitation factor.
2. The glycine and L-alanine are strong candidates as kinetic hydrate inhibitors due to their higher solubility in aqueous solution.
3. The most likely mechanism that allows amino acids to show the kinetic effect is their ability to disrupt the water hydrogen bond network.
4. The higher concentration of amino acids did not show any significant effect on kinetic inhibition effectiveness of the amino acids. However, the higher concentration does have a significant effect on the thermodynamic inhibition effectiveness of the amino acids.
5. Amino acids have the ability to function as dual-functional inhibitors, providing the thermodynamic and kinetic inhibition both at the same time.

#### ***4.2.4 Co effect of Amino Acids and synergent on CH<sub>4</sub> hydrate inhibition***

Poly-ethylene oxide (PEO) worked well as a kinetic synergent with pyrrolidinium ILs and ammonium IL in previous sections [4.1.3 and 4.2.2]. Therefore, 1wt% of PEO was likewise tested with amino acids that have higher solubility like L-Alanine, Glycine, and Histidine to enhance their kinetic inhibition performance.

The PEO contains a hydrophilic oxygen atom at its centre and the polymerized hydrophobic ethylene chain is attached to this oxygen atom. Altamash, et al.<sup>340</sup>, proposed that at one end, it's likely that hydrophobic ethylene chain (attached with PEO oxygen atom) forces the water molecules away from CH<sub>4</sub> via Van der Waal hydrophobic interactions and acts as a shield for the CH<sub>4</sub> guest molecules. On the other end, it's likely that hydrophilic oxygen atoms of PEO form hydrogen bonds with water molecules via electrostatic force of attraction (CH<sub>2</sub>O---HOH---OCH<sub>2</sub>) which delays the hydrate formation time.<sup>340</sup>

Figure 4-32, demonstrates the kinetic inhibition (KI) effect or delay in the CH<sub>4</sub> hydrate formation time in the presence of amino Acids + 1 wt% PEO mixtures at wide process conditions. The amino acid + synergent mixture 5wt% L-alanine + 1 wt% PEO seems to be kinetically more effective and it delays the hydrate formation by 23 hrs at 60 bars and by 7.5 hrs at 90 bars. The hydrate formation in the CH<sub>4</sub> blank sample is shown in the black.

As indicated in Figure 4-32, at moderate pressure (60 bars), the amino acid-synergent mixture 5wt% L-alanine + 1wt% PEO delayed the hydrate formation time from  $7 \pm 0.5$  hr to  $30 \pm 0.5$  hr , the mixture 5wt% glycine + 1wt% PEO delayed it to  $24 \pm 0.5$  hr and the mixture 4wt% histidine + 1wt% PEO delayed it to  $22 \pm 0.5$  hr [Figure 4-32].

Therefore, in terms of effectiveness as the kinetic hydrate inhibitors, the mixtures at 60 bars can be listed as:

L-alanine + PEO > glycine + PEO > histidine + PEO

At higher pressure (90 bars), the amino acid-synergent mixture 5wt% L-alanine + 1wt% PEO delayed the hydrate formation time from  $5.5 \pm 0.5$  hr to  $13 \pm 0.5$  hr , the mixture 5wt% glycine + 1wt% PEO delayed it to  $12 \pm 0.5$  hr and the mixture 4wt% histidine + 1wt% PEO also delayed it to  $12 \pm 0.5$  hr [Figure 4-32].

Hence, in terms of effectiveness as the kinetic hydrate inhibitors, the mixtures at 90 bars can be listed as:

L-alanine + PEO > glycine + PEO  $\geq$  histidine + PEO



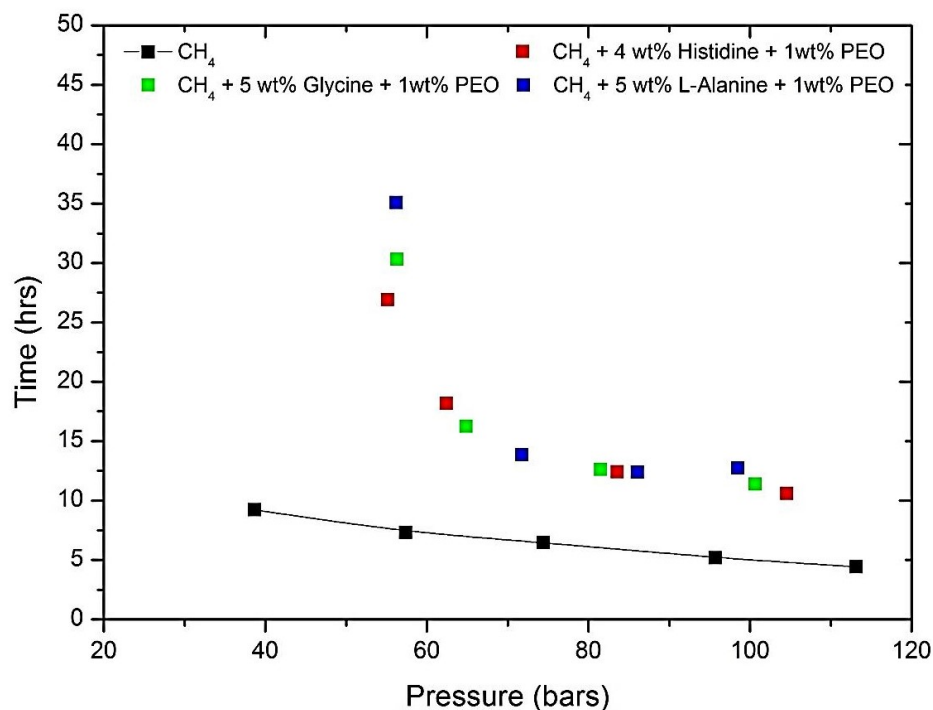


Figure 4-32: The time delay in the  $CH_4$  hydrate formation in the presence of amino acids 1 wt% PEO mixtures at wide process conditions. The data has the uncertainty of  $\pm 0.5$  hr.

In the presence of water, amino acids act as zwitterions and cause disruption of hydrogen bonding in water molecules. In the presence of PEO, the kinetic inhibition effectiveness of amino acids is significantly increased [Figure 4-32]. The Amino Acid-synergent mixture of L-Alanine + PEO was found more effective than the mixture of Glycine + PEO. According to Altamash, et al.<sup>340</sup>, this slightly indicates that the presence of extra methyl ( $-CH_3$ ) attached with L-alanine side chain enhances the hydrophobic interaction ( $H_3C-CH_2$ ) with PEO.<sup>340</sup>

The significant delay in the hydrate induction time in amino acids-PEO mixture also indicates that PEO in the water bulk acts as a shield and prevent the approach of gas molecules towards the water molecules. On the other end, the amino acid causes the disruption of hydrogen bonding within the water molecules. This provides an overall delay in the hydrate formation time.<sup>340</sup>

Histidine is more hydrophilic amino acid and hydrophilic amino acids are likely to show better kinetic effect. However, the major drawback of using Histidine is that it has the limited solubility in aqueous water ( $\leq 4\text{wt } \%$ ). On contrary, the amino acids Glycine and L-Alanine have higher solubility in water ( $> 15 \text{ wt } \%$ ). The higher solubility factor is likely to help Alanine and Glycine to act as a better kinetic and thermodynamic inhibitor for the  $\text{CH}_4$ . As the solubility of amino acid increases their hydrogen bonding ability strength increases which increases disruption and water re-orientation in hydrate cages.

340

In the above context, it has been deduced that the hydrophobicity and solubility are the two key factors that are likely to affect the kinetic and thermodynamic inhibition effectiveness of the amino acids. At the same concentration, the amino acids with lower hydrophobicity are likely to perform better as a kinetic hydrate inhibitor and then the amino acids with higher hydrophobicity are likely to perform better as thermodynamic hydrate inhibitor.

At different concentrations, the amino acids with higher solubility are likely to perform better as a kinetic and thermodynamic inhibitor at the same time. The following observations can be made from the above experimental results:

1. PEO helps to improve the kinetic inhibition effectiveness of the selected amino acids significantly, but it works better with the amino acids Glycine and L-Alanine.
2. The significant delay in the hydrate induction time in amino acids + PEO mixture indicates that PEO in the water bulk acts as a shield and prevent the approach of gas molecules towards the water molecule. On the other end, the amino acid causes the disruption of hydrogen bonding within the water molecules. This likely provides an overall delay in the hydrate formation time.

### 4.3 Inhibitors Effectiveness Comparison

In this section, a comparative study has been conducted and the thermodynamic results obtained for the ionic liquids and amino acids in section 4.1 and section 4.2 have been compared with the thermodynamic results of the ionic liquids and commercial hydrate inhibitors like methanol and mono-ethylene glycol reported in the literature. As kinetic results are not replicable, so the kinetic results obtained using only RC-5 in the presence of the synergent PEO for amino acids and ionic liquids were compared together in the section 4.3.4.

#### 4.3.1 Comparison with Choline based Ionic Liquids

Recently, Tariq, et al.<sup>304</sup>, used 5 wt% choline based ionic liquids as thermodynamic CH<sub>4</sub> hydrate inhibitor. The thermodynamic results obtained for the 5 wt% amino acids, 5wt% pyrrolidinium based IL and 5wt% ammonium based ILs in this work were compared with the 5wt% Choline based Ionic liquids such Choline butyrate (Ch-But), Choline iso-butyrate (Ch-iB), Choline Hexanoate (Ch-Hex) and Choline Octanoate (Ch-Oct).<sup>304</sup> [Figure 4-33].

Figure 4-33, displays the shift in the CH<sub>4</sub> HLVE curve in the presence of 5wt% Choline ILs (Ch-But, Ch-iB, Ch-Hex, Ch-Oct)<sup>304</sup>, 5wt% amino acids (L-Alanine, Glycine), 5wt% ammonium based ILs ([DMEA][Of],[TBA][Of],[EA][Of],[DMA][Of]) and 5wt% pyrrolidinium based ILs ([PMPy][Cl]). The CH<sub>4</sub> HLVE in the blank sample is shown in the black. The data reported has an uncertainty of  $\pm 0.2$  °C.

As illustrated in Figure 4-33, the amino acids L-alanine and glycine are observed to be more effective than other inhibitors. The 5wt% pyrrolidinium based IL [PMPy][Cl] did not show any significant thermodynamic inhibition effect on CH<sub>4</sub> hydrate formation. At 5wt%, the IL [PMPy][Cl] performed well with QM mixture and provided the temperature shift of about 1.8 °C at low pressures [Figure 4-7]. But, it did not provide any significant hydrate inhibition on pure methane at 5wt%. This may be due to the presence of small amount (2 mol %) of nitrogen (N<sub>2</sub>) component in the Quaternary gas mixture (QM) that may facilitate hydrate inhibition. <sup>312</sup>

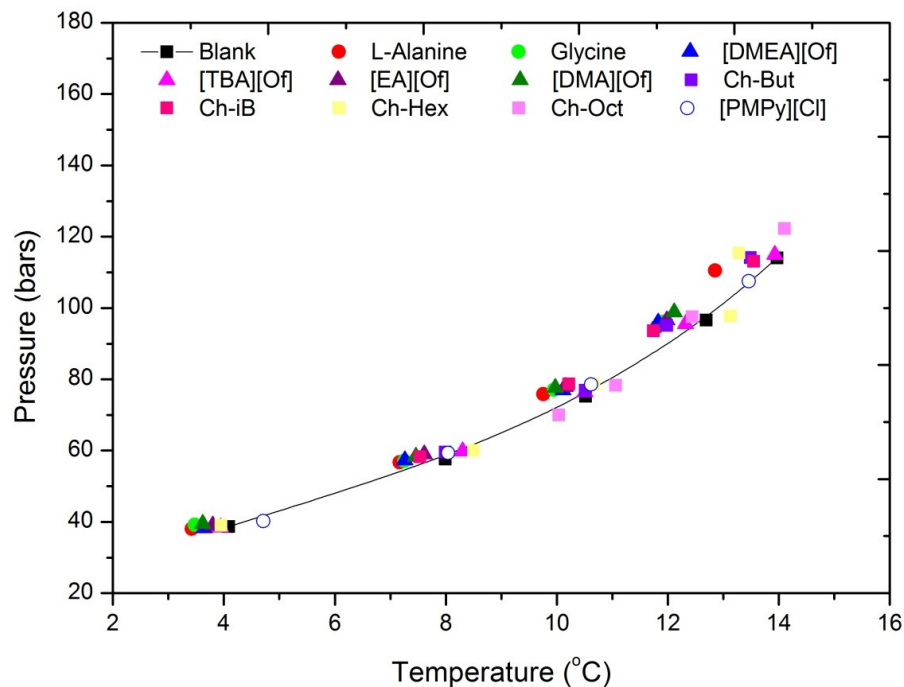


Figure 4-33: The shift in the CH<sub>4</sub> HLVE curve in the presence of 5wt% choline ILs<sup>304</sup>, 5wt% amino acids, 5wt% ammonium ILs and 5wt% pyrrolidinium ILs. The data has an uncertainty of  $\pm 0.2$  °C.

The use of nitrogen (N<sub>2</sub>) to dissociate hydrates has been investigated by Haneda, et al.<sup>341</sup> and Masuda, et al.<sup>342</sup>. Masuda, et al.<sup>342</sup>, purge the limestone cores embedded with hydrates with nitrogen gas and observed that the hydrates dissociated as the nitrogen passed through the hydrates. Panter, et al.<sup>312</sup>, stated that nitrogen can be viewed as a thermodynamic hydrate inhibitor and can be used to dissociate hydrate plugs.

As indicated in Figure 4-33, at 5wt% and pressure close to 40 bars, the L-alanine and glycine were found to be the most effective CH<sub>4</sub> thermodynamic hydrate inhibitors and in terms of the effectiveness the ionic liquids and amino acids inhibitors can be listed as:

L-alanine > glycine > [DMA][Of] > [DMEA][Of] > [EA][Of] > [TBA][Of] > Ch-Hex > [PMPy][Cl]

Similarly, at higher pressures close to 80 bars, the L-Alanine and Glycine were again found to be the most effective CH<sub>4</sub> hydrate inhibitors [Figure 4-33] and in terms of the effectiveness the ionic liquids and amino acids inhibitors can be listed as:

L-alanine > glycine > [DMA][Of] > [DMEA][Of] > [EA][Of] > Ch-iB > [TBA][Of] > Ch-But > [PMPy][Cl] > Ch-Hex > Ch-Oct

### 4.3.2 Comparison with Imidazolium-based Ionic Liquids

The thermodynamic inhibition effect of three ILs: [BMIM-BF<sub>4</sub>], [BMIM-N(CN)<sub>2</sub>] and [N<sub>2,2,2,2</sub>-Cl] on methane hydrate formation at a concentration of 10 wt % and the pressure range of 2.48-6.58 MPa was studied by Keshavarz, et al. <sup>291a</sup>. The average hydrate temperature shift using these ILs at 10 wt% was found to be within the range of 1.0-1.3 °C.

The thermodynamic inhibition effect of six imidazolium-based ionic liquids on methane hydrate formation at a concentration of 10 wt % within the pressure range of 3.6 to 11.2 MPa was investigated by Sabil, et al. <sup>329</sup>. The ILs investigated included: [BMIM][CH<sub>3</sub>SO<sub>4</sub>], [BMIM][CF<sub>3</sub>SO<sub>3</sub>], [BMIM][N(CN)<sub>2</sub>], [BMIM][Cl], [BMIM][Br], [BMIM][ClO<sub>4</sub>], [OH-EMIM][Cl] and [OH-EMIM][Br]. The IL [OH-EMIM][Cl] was found to be the most effective thermodynamic hydrate inhibitor with the average suppression temperature of 1.329 °C and the IL [BMIM][ClO<sub>4</sub>] was found to be the least effective thermodynamic hydrate inhibitor with the average suppression temperature of 0.37 K. Thus, the average hydrate temperature shift using these ILs at 10 wt% was found to be within the range of 0.37-1.3 °C.

A comprehensive study on the methane hydrate inhibition using seven imidazolium-based ILs at the fixed concentration of 10 wt% within the pressure range of 3.45 to 13.28 MPa was conducted by Long, et al. <sup>330</sup>. The seven ILs used for experiments



included: [Emim][ClO<sub>4</sub>], [Emim][SCN], [Emim][Ac], [Bmim]-[Ac], [OH-Emim][ClO<sub>4</sub>], [Emim][Cl] and [OH-Emmim][Cl].

The IL [Emim][Cl] was found to be the most effective thermodynamic hydrate inhibitor with hydrate suppression temperature of 1.7-1.9 °C and the IL [Emim][ClO<sub>4</sub>] was found to be the least effective thermodynamic hydrate inhibitor with the hydrate suppression temperature of 0.8 K. Thus, the average hydrate temperature shift using these ILs at 10 wt% was found to be within the range of 0.8-1.9 °C.

The thermodynamic inhibition effect of imidazolium-based ILs on methane hydrates at a concentration of 10 wt% and within the pressure range of 7 - 12 MPa using isochoric search method was studied by Zare, et al. <sup>165</sup>. The ILs used for experiments included: [BMIM][MeSO<sub>4</sub>], [EMIM][HSO<sub>4</sub>], [EMIM][EtSO<sub>4</sub>], [BMIM][BF<sub>4</sub>] and [OH-EMIM][BF<sub>4</sub>]. All the selected ILs showed the thermodynamic effect and the IL [OH-EMIM][BF<sub>4</sub>] were found to be the most effective IL. The hydrate suppression temperature for the selected ILs at 10 wt% was found to be within the range of 0.46 - 1.1 °C.

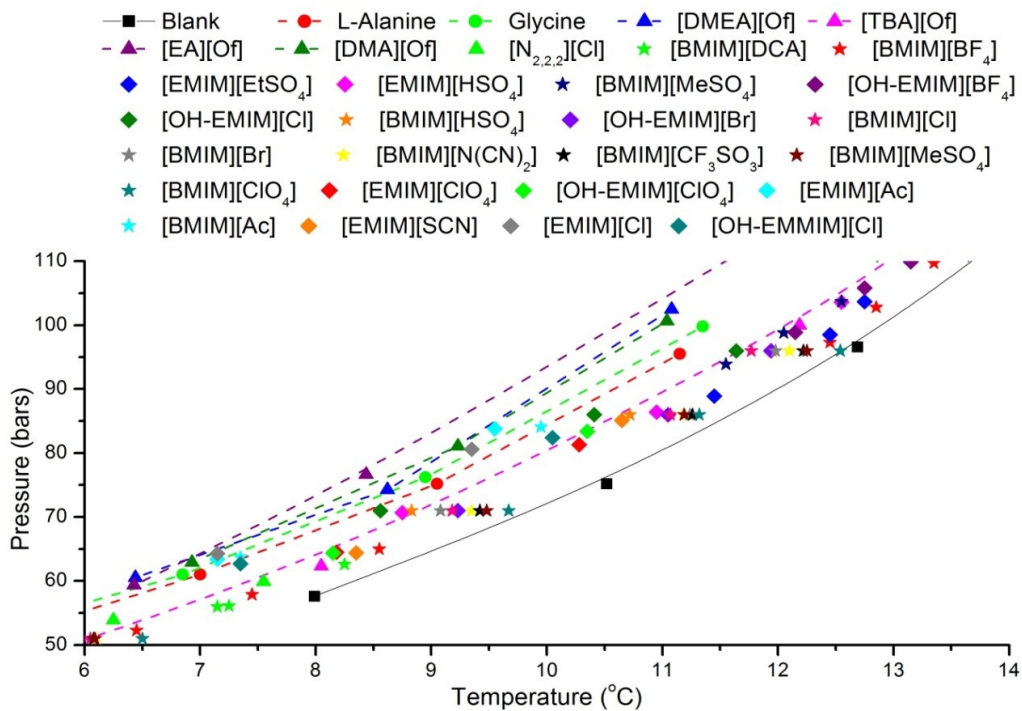


Figure 4-34: Comparison in the shift obtained for CH<sub>4</sub> HLVE curve in the presence of 10 wt% ammonium-based ILs [(DMEA)(Of), (DMA)(Of), (TBA)(Of) and (EA)(Of)] This work, 10 wt% amino acids [L-alanine, glycine]<sup>283</sup>, and 10 wt% imidazolium ILs [BMIM & EMIM]<sup>291a, 329-330, 343</sup>. The data reported has an uncertainty of  $\pm 0.2$  °C.

Figure 4-34, exhibit the comparison in the shift obtained for CH<sub>4</sub> HLVE in the presence of 10 wt% ammonium-based ILs [(DMEA)(Of), (DMA)(Of), (TBA)(Of) and (EA)(Of)]<sup>This work</sup>, 10 wt% amino acids [L-Alanine, Glycine]<sup>283</sup>, and 10 wt% imidazolium ILs [BMIM & EMIM]<sup>291a, 329-330, 343</sup>.

As shown in Figure 4-34, at 10 wt%, the ammonium-based ILs [(DMEA)(Of), (DMA)(Of) and (EA)(Of)] and the amino Acids [L-alanine, glycine] were found to be more effective than most imidazolium ILs reported in the literature. The CH<sub>4</sub> HLVE in the blank sample is shown in the black. In comparison to the ionic liquids inhibition results reported by Keshavarz, et al.<sup>291a</sup>, Long, et al.<sup>330</sup> and Zare, et al.<sup>165</sup> the ammonium based ILs ([EA][Of], [DMA][Of], [DMEA][Of]) and amino acids (L-alanine, glycine) in this work showed better thermodynamic effect by providing the temperature shift within the range of around 1.5-2.3 °C (75 bars), except for the IL [TBA][Of] which only provided the temperature shift of around 0.8-1.0 °C (75 bars).

The ammonium based ILs used in this work are protic in nature and consist of a free pair of the electron [H+] that may allow it to disrupt hydrogen bonding within the water molecules and provide the better thermodynamic effect than other ILs.<sup>344</sup> Although the L-alanine and glycine were not as effective as ammonium based ILs, but provided almost the similar temperature shift and were off by only 0.5 °C.

The amino acids with shorter side alkyl chain like glycine and L-alanine show better thermodynamic inhibition effect than most imidazolium ILs. This could be due to the fact that glycine and L-alanine have short alkyl chains and as the alkyl chain of amino acids reduces in size their solvation with water molecules increases, which increases the thermodynamic inhibition impact of these amino acids.<sup>339</sup>

Most ionic liquids reported in literature provides the CH<sub>4</sub> HLVE shift of about 0.7-1.5 °C at 10 wt%. In comparison, the ammonium-based ionic liquids used in this work provided the HLVE shift of about 0.8-2.3 °C and amino acids (glycine and L-alanine) provided the HLVE shift of about 1.5-1.7 °C.

### 4.3.3 Comparison with Methanol and Ethylene Glycol

Figure 4-35, shows comparison in the shift obtained for CH<sub>4</sub> HLVE in the presence of 10 wt% Ammonium-based ILs [(DMEA)(Of), (TBA)(Of) and (EA)(Of)]<sup>This work</sup>, 10 wt% amino acids [L-alanine, glycine]<sup>283</sup>, and 10 wt% ethylene glycol [EG].

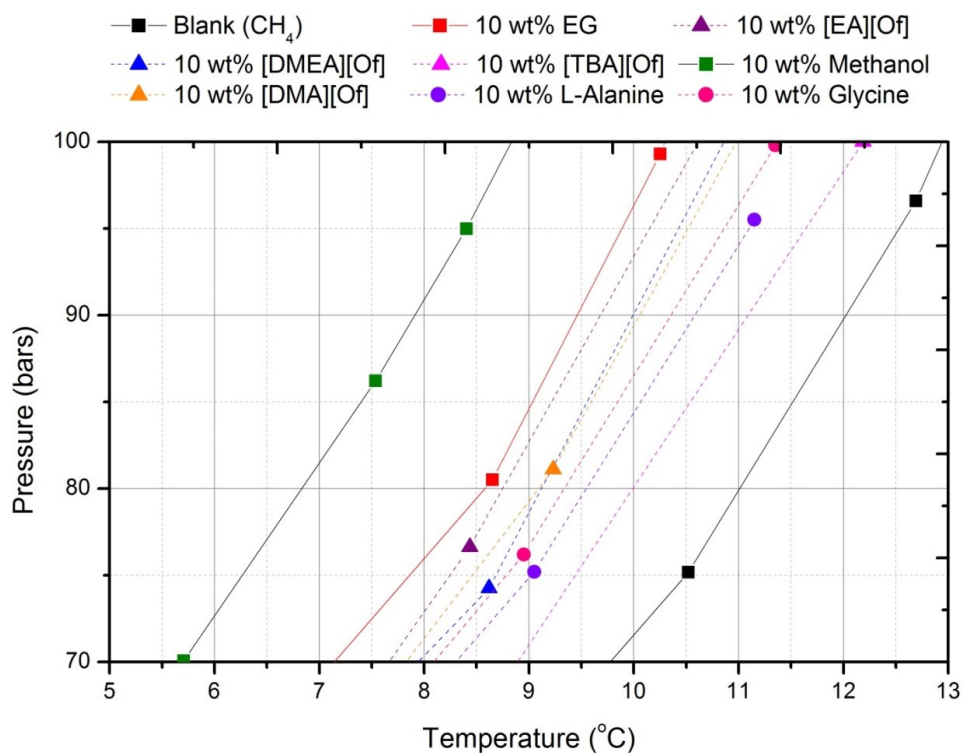


Figure 4-35: Comparison in the shift obtained for CH<sub>4</sub> HLVE curve in the presence of 10 wt% Ammonium-based ILs [(DMEA)(Of), (TBA)(Of) and (EA)(Of)], 10 wt% Amino Acids [L-alanine, glycine]<sup>283</sup>, and 10 wt% ethylene glycol [EG]. The data has an uncertainty of  $\pm 0.2$  °C.

As indicated in Figure 4-35, at 10 wt%, the ammonium-based IL [(EA)(Of)] was observed to provide the thermodynamic inhibition effect similar to EG and was off by  $0.5\text{ }^{\circ}\text{C}$  -  $0.2\text{ }^{\circ}\text{F}$  only. The  $\text{CH}_4$  HLVE in the blank sample is shown in the black. At the concentration (10wt%), the industrial inhibitors such as methanol provide the shift in HLVE of about  $3.5\text{-}4\text{ }^{\circ}\text{C}$ , followed by NaCl with HLVE shift of about  $2.5\text{-}4\text{ }^{\circ}\text{C}$  and Ethylene glycol (EG) with HLVE shift of about  $2\text{-}2.5\text{ }^{\circ}\text{F}$  [Figure 4-35].<sup>7</sup>

As illustrated in Figure 4-35, the ammonium-based IL [EA][Of] and the industrial hydrate inhibitor ethylene glycol [EG] provided similar thermodynamic inhibition effect within the respective pressure range at 10 wt%. At the pressure of 70 bars, the [EA][Of] shifted the  $\text{CH}_4$  HLVE curve by around  $2.2\text{ }^{\circ}\text{C}$ , while the EG shifted the  $\text{CH}_4$  HLVE curve by around  $2.6\text{ }^{\circ}\text{C}$ . The amino acids L-Alanine and Glycine shifted the  $\text{CH}_4$  HLVE curve by  $1.4\text{ }^{\circ}\text{C}$  and  $1.6\text{ }^{\circ}\text{C}$  respectively. While the IL [DMA][Of] and [DMEA][Of] provided a similar  $\text{CH}_4$  HLVE shift of around  $2.0\text{ }^{\circ}\text{C}$ . Hence, among all the tested inhibitors, the IL [EA][Of] was found to be the most effective one [Figure 4-35].

At the pressure above 80 bars, both EG and [EA][Of] provided almost similar temperature shift in the methane HLVE curve and both were off by  $0.25\text{ }^{\circ}\text{C}$ . At the pressure of 100 bars, the [EA][Of] provided the temperature shift of around  $2.4\text{ }^{\circ}\text{C}$  and the EG provided the temperature shift of around  $2.6\text{ }^{\circ}\text{C}$  [Figure 4-35].

This indicates that IL [EA][Of] has an ability to provide the thermodynamic inhibition effect similar to the EG. However, the ammonium-based ILs and amino acids used in this work were not found to be as effective hydrate inhibitors as the Methanol. The methanol provided thermodynamic temperature shift of around 4.0 °C and was found to be more effective than EG and the protic ionic liquids used in this work.

The major factor that may help methanol to provide better thermodynamic inhibition effect is the presence of –OH group. The strong interaction of –OH group with the hydrogen bonds in hydrate clusters and further interaction of –CH<sub>3</sub> group with the C-C bonds or hydrogen bonds within hydrates clusters is likely to cause strong disturbance or disorientation within hydrate crystal lattice. This may help to mitigate the hydrate formation and shift the methane HLVE to lower temperature.

The presence of the –OH group in methanol facilitates the forming of hydrogen bonds with “free water” and cause a shift in the CH<sub>4</sub> HLVE curve to lower temperatures via hydrogen bonding.<sup>319</sup> Therefore, in the future, it will be viable to synthesize ionic liquids with –OH group and that may help to beat methanol. Bavoh, et al.<sup>334</sup>, investigated the thermodynamic inhibition effect of glycine on methane hydrate formation at different concentrations (5-20 wt % ) and provided the respective hydrate dissociation points at different pressures. These results were compared with the 10 wt% of methanol [Figure 4-36].

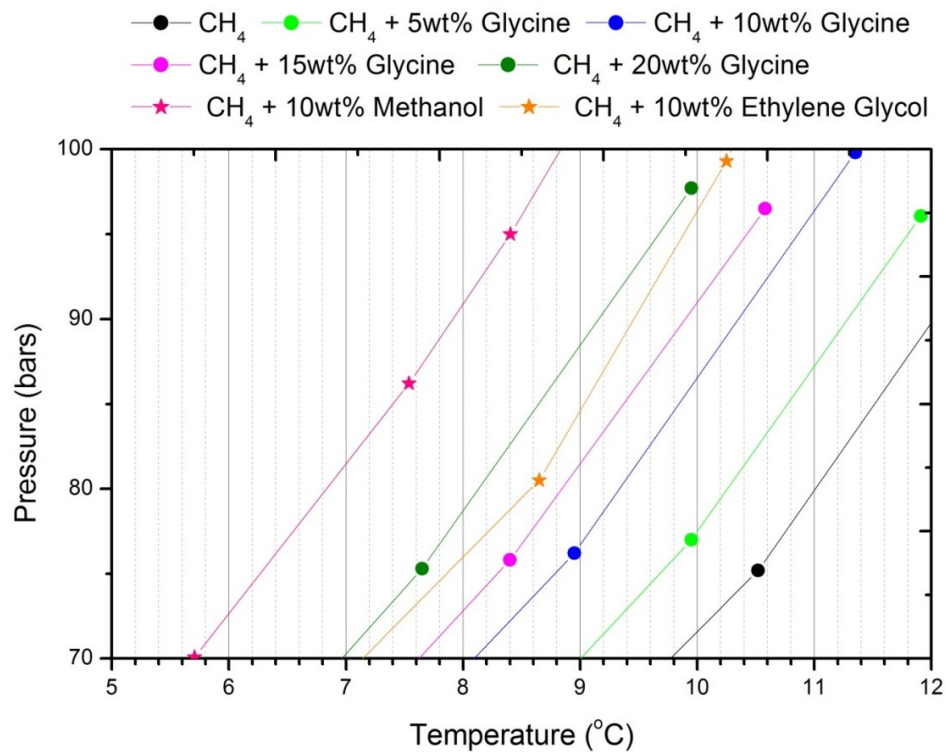


Figure 4-36: Comparison in the shift obtained in CH<sub>4</sub> HLVE curve in the presence of different concentrations of amino acid glycine<sup>334</sup> and 10 wt % methanol. The data reported has an uncertainty of  $\pm 0.2$  °C.

Figure 4-36, shows the comparison in the shift obtained in CH<sub>4</sub> HLVE curve in the presence of different concentrations of amino acid glycine and 10 wt % methanol. The higher concentration of Glycine (20 wt%) does not beat methanol (10 wt%) and was off by around 1.0 °C in terms of providing a shift in CH<sub>4</sub> HLVE curve. Interestingly, the higher concentration of glycine (20 wt%) beats ethylene glycol (10 wt%). The CH<sub>4</sub> HLVE in the



blank sample is shown in the black.

As illustrated in Figure 4-36, at 70 bars the 10 wt% methanol shifted the CH<sub>4</sub> HLVE curve from 9.8 °C to 5.8 °C, providing a temperature shift of around 4 °C. The Ethylene glycol shifted the CH<sub>4</sub> HLVE curve from 9.8 °C to 7.2 °C and provided the temperature shift of around 2.6 °C. In comparison, the 10 wt% and 20 wt% glycine provided the temperature shift of around 1.7 °C and 2.8 °C respectively.

At the concentration of 20 wt%, the glycine was able to provide better thermodynamic inhibition effect compared to ethylene glycol. This is the most significant finding of this work. However, the glycine was not able to beat methanol, but in terms of temperature shift the 20 wt% glycine was only off by 1.2 °C compared to 10 wt% methanol [Figure 4-36].

This shows that amino acid glycine due to its high solubility and solvation ability holds strong perspective to be used as a commercial thermodynamic hydrate inhibitor. However, compared to ethylene glycol and methanol, two times (2X) more concentration of glycine will be required to provide the similar thermodynamic effect. Also compared to ethylene glycol and methanol, the glycine has limited solubility (< 24.9 wt %) in the aqueous solution.

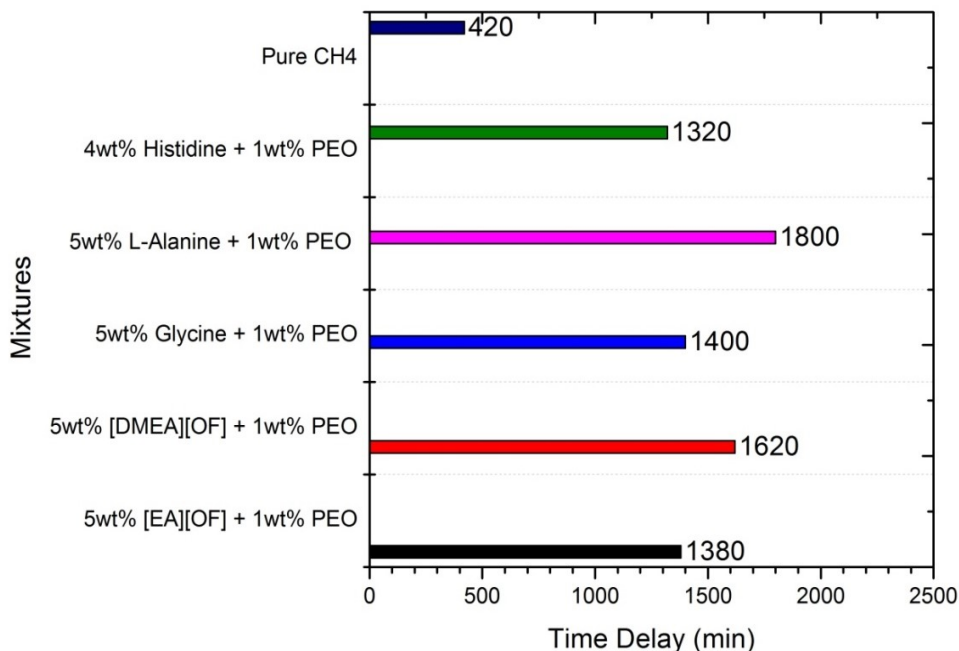
#### ***4.3.4 Comparison between Amino Acids & Ionic Liquids Synergent Mixtures***

As mentioned earlier, the hydrate nucleation relies on various factors, which includes subcooling temperature, water history, impurities, the composition of the gas, amount of agitation or turbulence and geometry of the system.<sup>7</sup> This is one of the reasons that hydrate kinetic experiments are not replicable and the results obtained from one equipment may not match the results of the other equipment. Mork<sup>286</sup>, also indicated that all hydrate formation and kinetic experiments rely on the experimental system mechanics and specifications. Therefore, the experimental kinetic results obtained using the RC-5 may not match the experimental kinetic results obtained using any other system.

In the above context, the kinetic results obtained using the same RC-5 system, under the similar subcooling conditions, were only compared together in this section. The average time delay in hydrate formation obtained using the pure amino acids and ionic liquids were found to be within the range of 0.5-1.5 hr. Therefore, the time delay obtained using the amino acid + PEO and ionic liquids + PEO mixtures were compared together in Figure 4-37 and Figure 4-38.

Figure 4-37, exhibits the comparison in the delay in CH<sub>4</sub> hydrate formation obtained for different amino acids + PEO and ionic liquids + PEO mixtures at 60 bars. The mixture 5wt% L-Alanine + 1wt% PEO seems to be kinetically most effective mixture and it delayed the CH<sub>4</sub> hydrate formation to 1800 min (30 hrs) at 60 bars. The hydrate

formation time in the CH<sub>4</sub> blank sample is indicated in the navy blue bar.



*Figure 4-37:* The comparison in the delay in CH<sub>4</sub> hydrate formation obtained for different amino acids + PEO and ionic liquids + PEO mixtures at 60 bars. The data has the uncertainty of  $\pm 0.5$  hr.

As indicated in Figure 4-37, it is observed that these mixtures are more effective at lower pressures compared to higher pressures. At the pressure close to 60 bars, the L-Alanine + PEO mixture was found to be most effective and it delays the hydrate formation time from 420 min to 1800 min. In comparison, at the same pressure, the [DMEA][Of] + PEO mixture delayed the hydrate formation time from 420 min to 1620

min.

Figure 4-38, illustrates the comparison in the delay in CH<sub>4</sub> hydrate formation obtained for different amino acids + PEO and ionic liquids + PEO mixtures at 78 bars. The mixture 5wt% [DMEA][OF] + 1wt% PEO seems to be kinetically most effective and it delayed the CH<sub>4</sub> hydrate formation time to 1284 min (21 hrs) at 78 bars. The hydrate formation time in the CH<sub>4</sub> blank sample is indicated in the navy blue bar.

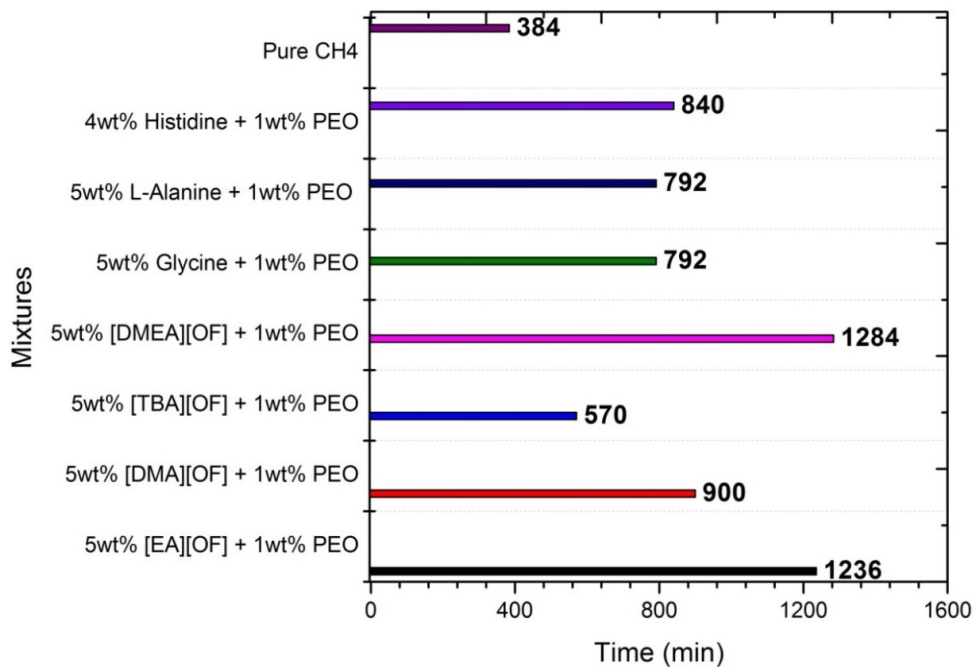


Figure 4-38: Shows the comparison in the delay in CH<sub>4</sub> hydrate formation obtained for different amino acids + PEO and ionic liquids + PEO mixtures at 78 bars. The above data has the uncertainty of  $\pm 0.5$  hr.

As shown in Figure 4-38, at a higher pressure of 78 bars, the [DMEA][Of] + PEO and [EA][Of] + PEO mixtures delayed the hydrate formation time from 384 min to 1284 and 1234 min respectively. The glycine and L-alanine mixture both provided a delay of around 792 min. Hence, in terms of effectiveness the mixtures at 78 bars can be listed as:

[DMEA][Of] + PEO > [EA][Of] + PEO > [DMA][Of] + PEO > histidine + PEO > L-alanine + PEO > glycine + PEO > [TBA][Of] + PEO.

As illustrated from the results in the Figure 4-37 and Figure 4-38, the extra methyl group attached to L-Alanine and [DMEA][Of] along with the polymerized hydrophobic ethylene chain of PEO may be working together to keep the water molecules away from CH<sub>4</sub> guest molecule for the longer period of time via Van der Waal hydrophobic interactions. The mixture may be acting as a strong shield for the CH<sub>4</sub> guest molecule against the water molecules. This might be making it difficult for the water molecules to approach CH<sub>4</sub> guest molecules and encapsulate it to form hydrate clusters.

#### **4.3.5 Economic Evaluation**

The complete economic evaluation of the usage of the proposed hydrate inhibitors and their mixtures is beyond the scope of this work. However, this section endeavours to provide a rough cost estimation based on the specs provided in the literature and current price values of chemicals available online. The economic evaluation can be subject large uncertainty and more research work is required to get an actual economic evaluation of the hydrate inhibitors and their mixtures used in this work.

According to Koh, et al. <sup>345</sup>, on average a small gas dominated field transfer gas from offshore to onshore facility at the flow rate of  $5.66 * 10^6 \text{ m}^3$  per day. The average water content present is  $3.155 * 10^4 \text{ kg}$  per day. The amount of methanol required to treat 1 Kg of water is around 0.65 Kg. This shows that amount of methanol required to treat water content is equivalent to  $2.05 * 10^4 \text{ kg}$  per day.

The current cost of methanol in bulk is around 1-3 \$/ kg (Courtesy: Hebei Yanxi Chemicals China). If the purchase cost of methanol is taken as 1 \$ / kg, the amount required for the purchase of methanol will be  $2.05 * 10^4 \text{ US \$}$  per day. Assuming that the field is operational 300 days a year, the methanol purchase will cost around 6.15 million US \$ per year.

On contrary, the amount of amino acid glycine and synergent PEO required to treat 1 Kg of water is around 0.05 Kg and 0.01 Kg respectively. This shows that amount of glycine and PEO required to treat water content is equivalent to 1557 Kg per day and 315.5 Kg per day. The current cost of glycine and PEO in bulk is around 2-3\$ / kg (Courtesy: Luojiang Chenming Biological China).

If the purchase cost of PEO and glycine is taken as 2 \$ / kg, the amount required for their purchase will be equivalent to 3786 US \$ per day. Assuming that the field is operational 300 days a year, the mixture of glycine + PEO will cost around 1.1 million US \$ per year.

This roughly estimated cost for the purposed hydrate mixture is calculated to be 6 times less than the cost of the methanol. However, the other factors like storage and regeneration costs should also be taken into account for the complete economic evaluation. This complete economic in collaboration with the industry in future.

## CHAPTER 5: CONCLUSIONS

The prospects of low environmental impact chemical compounds like amino acids and ionic liquids as hydrate inhibitors have been examined in this work at wide process conditions along with a separate study on the effect of stirring on the hydrate formation. The aim of this research work is to facilitate the on-going research in the fields of development of low environmental impact hydrate inhibitors and use of hydrates for natural gas storage and transportation.

Initially, in the stirring rate (RPM) study, the effect of stirring on the Quaternary Gas mixture (QM) was investigated using the high-pressure cell (HPC) at 98 bars. According to the experimental results, it was found that no significant hydrate formation occurs at low stirring rates (250-500 RPM). The hydrate formation was only observed within the stirring rate zone of 550-850 RPM and the optimum stirring rate for maximum hydrate formation was found to be 750 RPM. However, at a higher stirring rate (1000-1400 RPM) the rate of hydrate formation decreases and no hydrate formation is observed within the system at 1200 and 1400 RPMs.

It's likely that at low stirring rates there is not enough driving force available that can facilitate the hydrate formation and at the higher stirring rates heavy collision might be taking place within the hydrate crystals and the walls of the high-pressure cell, causing breakage of hydrate crystals and not allowing enough time for the hydrate



crystal to nucleate and grow larger in size.

In the first hydrate inhibition study, two pyrrolidinium-based ILs: 1-Methyl-1-Propyl-pyrrolidinium Chloride [PMPy][Cl] and 1-Methyl-1-Propyl-pyrrolidinium Triflate [PMPy][Triflate], were used to study the inhibition effect of these ILs on QM gas mixture at different concentrations (1-5 wt%) and pressure conditions (38-120 bars) using RC-5 assembly. The experimental results indicate that the selected pyrrolidinium ILs have a tendency to act as dual function inhibitors. The IL [PMPy][Cl] provided the temperature shift of about 0.8-1.8 °C ( $\pm 0.2$  °C) and delayed hydrate formation time by 0.8-1.3 hrs ( $\pm 0.5$  hr). In comparison, the IL [PMPy][Triflate] provided the temperature shift of about 0.11-1.56 °C ( $\pm 0.2$  °C) and delayed the hydrate formation time by 0.5-1 hrs ( $\pm 0.5$  hr). The IL [PMPy][Cl] was found to be more effective than IL [PMPy][Triflate].

In the same work, the co-effect of synergistic compounds caprolactam (VCap) and Poly-ethylene Oxide (PEO) with IL [PMPy][Cl] and IL [PMPy][Triflate] was studied in equal ratio. It was found that the addition of VCAP helps to improve the hydrate suppression temperature for IL [PMPy][Cl] from 1.8 °C to 2.2 °C and for IL [PMPy][Triflate] from 1.56 °C to 1.8 °C at low pressures (~38 bars). The water-soluble polymer PEO showed poor thermodynamic effect, but it helped to improve the kinetic effect of pyrrolidinium ILs and delayed the hydrate formation time from 6.7  $\pm$  0.5 hrs to 22.7  $\pm$  0.5 hrs for the IL [PMPy][Cl] and 6.7  $\pm$  0.5 hrs to 20  $\pm$  0.5 hrs for the IL

[PMPy][Triflate] at low pressures (~37 bars). In this work, it was observed that the use of synergents PEO can help to improve the kinetic inhibition effect of hydrate inhibitors significantly. This motivated us to look for new combinations of inhibitor + synergents mixtures that can help to mitigate the hydrate formation.

In the second hydrate inhibition study conducted using ammonium-based ionic liquids, the effect of ammonium-based ILs on the CH<sub>4</sub> hydrate inhibition was studied at different concentrations (5-10 wt%) and pressure conditions (40-120 bars) using the RC-5 assembly. The four ammonium based ionic liquids selected included: Ethyl-ammonium formate [EA][Of], Dimethyl-ammonium formate [DMA][Of], Dimethyl-ethyl ammonium formate [DMEA][Of] and Tri-butyl methyl ammonium formate [TBA][Of]. The ammonium based ILs, used in this work, were more economical than pyrrolidinium based ILs and were protic in nature except for [TBA][Of]. These ILs were synthesized of the materials that are economical and readily available like alkyl amines and formic acid. The selection of these ILs also allows to test the effect of mono, di and tri alkyl amines on the hydrate inhibition and no prominent hydrate inhibition study using similar ammonium based protic ILs was reported in literature till the date (Aug 2016).

The ionic liquids [EA][Of] was found to be the most effective hydrate inhibitor. It provided the average temperature shift of around 2.3 °C and the time delay of around 1.5 hr at 10 wt%. The ionic liquid [TBA][Of] was found to be the least effective

thermodynamic hydrate inhibitor with the average temperature shift of around  $0.8\text{ }^{\circ}\text{C}$  ( $\pm 0.2\text{ }^{\circ}\text{C}$ ) at 10 wt%. In terms of effectiveness as the thermodynamic hydrate inhibitors the ammonium-based ionic liquids can be listed as: [EA] [Of] > [DMEA] [Of]  $\geq$  [DMA] [Of] > [TBA] [Of]. The synergent PEO was added in low dosage (1wt %) with ammonium based ILs. The addition of PEO improved the kinetic inhibition effect of these ILs significantly and at pressures close to 55 bars, the IL-synergent mixture [5wt% [DMEA] [Of] + 1wt% PEO] delayed the hydrate formation time from  $7.7 \pm 0.5$  hr to  $29.6 \pm 0.5$  hr and the IL-synergent mixture [5wt% [EA] [Of] + 1wt% PEO] delayed it to  $20.3 \pm 0.5$  hr.

ILs can provide the kinetic and thermo effect both simultaneously as they have strong electrostatic charges and ability to form hydrogen bonding with water. The ionic liquids normally tend to function by disturbing hydrogen bonding between the water molecules within these clusters<sup>310</sup>. The ILs tend to use their pair of anions to disturb the hydrogen bonding network of a water molecule.<sup>310-311</sup> The selected ammonium based ionic liquids had similar anions but different cations. It was observed that the ionic liquids with shorter cationic alkyl chains are more effective than the ones with the longer cationic alkyl chains. This may be due to the presence of an extra pair of protons in shorter alkyl chains of selected ILs that may facilitate the disruption of hydrogen bonding between the water molecules, helping ammonium based ILs to provide better inhibition effect.

In the third hydrate inhibition study conducted using amino acids, the effect of biological molecules amino acids on the methane hydrate inhibition was tested at different concentrations and pressures conditions using the RC-5 assembly. Previously, most studies focused on the kinetic effect of amino acids on CO<sub>2</sub> hydrate inhibition and it was not clear if amino acids can function as dual functional inhibitors. Therefore, in this work, the thermodynamic inhibition strength of amino acids was examined closely along with their kinetic inhibition strength. The amino acids (AA) selected included: L-alanine, glycine, L-histidine, L-phenylalanine, and L-asparagine. Except for glycine and L-alanine, the other amino acids (L-histidine, L-phenylalanine, and L-asparagine) have low solubility in aqueous solution ( $\leq 4\text{wt}\%$ ).

The amino acids with lower solubility in aqueous solution leave behind undissolved particles, which can cause participation in the aqueous phase at high-pressure conditions. Therefore, such amino acids do not take part in the inhibition process and no significant shift in hydrate HLVE is observed using these types of the amino acids. The amino acids with higher solubility and shorter alkyl chain like glycine and L-alanine were found to be effective hydrate inhibitors. The amino acids are likely to provide hydrate inhibition due to their ability to act as zwitterions that is likely to cause a strong electrostatic force of interaction between electric charges of amino acids and water molecules, resulting in disruption of water cages in hydrate clathrates<sup>335</sup>. The carboxylic

and amine groups of amino acids may also facilitate the formation of hydrogen bonds with water molecules.

Based on the experimental results it was found that the thermodynamic inhibition effectiveness of both Glycine and L-Alanine enhances with the increase in their respective concentration. At the concentration of 5wt%, the glycine and L-alanine provided the average temperature shift of around 0.8 °C, but at low concentration (1wt%) no thermodynamic effect is exhibited by the selected amino acids. The PEO was added in low dosage (1wt%) with L-alanine, glycine and histidine. The amino acid-synergent mixture 5wt% L-alanine + 1wt% PEO delayed the hydrate formation time from  $7 \pm 0.5$  hr to  $30 \pm 0.5$  hr, the mixture 5wt% glycine + 1wt% PEO delayed it to  $24 \pm 0.5$  hr and the mixture 4wt% histidine + 1wt% PEO delayed it to  $22 \pm 0.5$  hr.

The PEO is a low toxic water-soluble polymer<sup>320</sup> that consists of an oxygen atom at its centre, which allows it to form strong hydrogen bonds within the water bulk system<sup>321</sup>. The hydrophilic part of the polymeric alkyl chain of PEO may help it to be completely miscible in water and cause disruption of hydrogen bonds in water molecules, whereas the hydrophobic part of it may help it to reach closer to a guest molecule (CH<sub>4</sub>) and push the water molecules away from it<sup>322</sup>

The thermodynamic results obtained for the amino acids and ionic liquids used in this work were compared with the 21 imidazolium ionic liquids and 5 choline ionic liquids reported in the literature. It was found that at low concentration (5wt%), the amino acids (L-alanine & glycine) show better hydrate inhibition effect (at certain pressures) than the ionic liquids used in this work and the choline based ionic liquids reported in the literature.

Furthermore, at higher concentration (10 wt%) both ammonium based ionic liquids and amino acids (glycine & L-alanine) were found to be more effective than most imidazolium ionic liquids and other types ionic liquids reported in the literature at the same concentration. The amino acids were found to be slightly less effective than the ammonium based ionic liquids and were off by only 0.5 °C. The IL EA[OF] was found to provide thermodynamic inhibition effect similar to commercially used hydrate inhibitor mono-ethylene glycol (MEG) and it was also observed that two times higher concentration (20 wt%) of glycine can provide better inhibition effect than 10 wt% MEG.

In this work, it has been deduced that both amino acids and ionic liquids are able to provide a temperature shift of about 0.8-2.0 °C and time delay of about 0.5-1.5 hr in hydrate formation. This time delay can be significantly extended to about 25-30 hr using low dosage (1wt%) of PEO and it equally works well with both ionic liquids and amino acids. The PEO can also help to reduce the required dosage of amino acids and ILs.

However, compared to ionic liquids the amino acids are more economical and environmentally suited compounds. Therefore, keeping the solubility factor into the account, the future research should be directed towards the use of amino acids and synergent mixtures as the hydrate inhibitors.

Following are the key points that can be deduced from the conclusion above:

1. There exists a threshold limit for the stirring rate above and below which no significant hydrate formation is likely to occur in the selected system. No hydrate formation occurs at low stirring rates (250-500 RPM). However, as the stirring rate is increased to 550 RPM (Rotations Per Minute) the hydrate formation is observed and it tends to increase significantly as the stirring rate is accelerated to 750 RPM. After 750 RPM, as the stirring rate is increased further, the rate of hydrate formation decreases within the selected system. At a higher stirring rate (1000-1400 RPM) no hydrate formation is observed within the system.
2. The pyrrolidinium-based ionic liquids tested as hydrate inhibitors on the QM mixture have the tendency to act as dual functional inhibitors and can provide the temperature shift of about 0.11-1.8 °C ( $\pm 0.2$  °C) and delay in hydrate formation time of about 0.5-1.3 hrs ( $\pm 0.5$  hr). The addition of PEO with the pyrrolidinium ILs in equal ratio can delay the hydrate formation time from  $6.7 \pm 0.5$  hrs up to  $22 \pm 0.5$  hrs ( $\sim 38$  bars). This indicates that PEO is an effective kinetic inhibition synergent.

3. The ammonium based ionic liquids tested as hydrate inhibitors on pure methane also tend to act as the dual functional inhibitors. The ionic liquids [EA][Of] was found to be the most effective hydrate inhibitor. It provided the average temperature shift of around  $2.3^{\circ}\text{C}$  and the time delay of around 1.5 hr at 10 wt%. The ionic liquid [TBA][Of] was found to be the least effective thermodynamic hydrate inhibitor with the average temperature shift of around  $0.8^{\circ}\text{C}$  at 10 wt%. The addition of PEO at the low dosage of 1wt% with the ammonium based ILs helped to delay the hydrate formation time from  $7.7 \pm 0.5$  hr up to  $29 \pm 0.5$  hr. This indicates that PEO has a tendency to exhibits kinetic synergistic effect even at a low dosage of 1 wt%.
4. The amino acids tested as the hydrate inhibitors on pure methane gas also exhibit dual functional behaviour. At 1w% the amino acids showed no significant hydrate inhibition. However, at 5wt% of the amino acids provided the temperatures shift of about  $0.8^{\circ}\text{C}$  and time delay of about 0.5-1 hr. The glycine and alanine were found to be effective hydrate inhibitors. The addition of 1wt% PEO with amino acids helped to delay the hydrate formation time from  $7 \pm 0.5$  hr to  $30 \pm 0.5$  hr. This indicates that the PEO has the tendency to shows a similar type of synergistic effect with both ionic liquids and amino acids.



5. The comparative study results indicate that the ammonium based ionic liquids [ EA(Of), DMA(Of) and DMEA(Of) ] and the amino acids [glycine and alanine] used in this work tend to show better thermodynamic inhibition effect (about 0.8-2.3 °C) compared to the imidazolium and other types of ILs reported in the literature at the same concentration (10 wt%) previously. The ammonium based ILs tend to show better thermodynamic inhibition effect than amino acids (about 0.5 °C ). The IL EA[Of] tends to show thermodynamic inhibition effect similar to mono-ethylene glycol (MEG) and the higher concentration of glycine (20 wt%) beats the inhibition effect of MEG (10 wt%).

## 5.1 Future Work

The work carried out in this dissertation has answered few major questions regarding the prospects of amino acids and ionic liquids as the future kinetic hydrate inhibitors and at the same time, many new questions also emerge out of this work.

The experimental results of this work show that both amino acids and ionic liquids can act as the thermodynamic and kinetic inhibitors at the same time. The ionic liquids with short cationic alkyl chain are more suited to act as the thermodynamic hydrate inhibitor, while the amino acids with higher solubility in the aqueous solution are more suited to act as the thermodynamic hydrate inhibitor.

It has also been observed that the polymeric compounds like polyethylene oxide have the potential to enhance the kinetic inhibition effectiveness of the amino acids and ionic liquids significantly when added in low dosage with them as a synergent. In addition to that, it has also been observed that mechanical factors like stirring rate also effects the rate of hydrate formation and a threshold limit exists above and below which the no hydrate formation occurs. All the above findings open many new arenas for research in the field of gas hydrates and offshore flow assurance. The following are some recommendations for future research that can be initiated using the results of the work performed in this dissertation:

**1) Effect of amino acids and ionic liquids on the hydrate inhibition in the oil-dominated systems**

In this work, the hydrate inhibition effect of amino acids and ionic liquids was studied on the gas dominated system. But, it will be interesting to check the hydrate inhibition effect of the same amino acids and ionic liquids on the oil-dominated system and compare the findings with this dissertation work results.

**2) Effect of amino acids mixtures on the hydrate inhibition in the gas dominated system**

In this work, it has been observed that the ionic liquid mixtures can provide a strong thermodynamic hydrate inhibition effect and can reach close to Methanol. In future, it will be interesting to check if the amino acid mixtures can provide the similar thermodynamic inhibition effect and if they can beat Methanol.

**3) Thermodynamic hydrate inhibition effect of amino acids with higher solubility in the aqueous solution**

In this work, the amino acids glycine and L-alanine, both with good solubility in aqueous solution has been identified as the potential thermodynamic and kinetic hydrate inhibitors. In future, it will be interesting to check if the amino acids with higher solubility than glycine (> 24 wt%) and L-alanine (> 15 wt%) can provide better hydrate inhibition.

#### **4) Hydrate formation in the shut-in conditions and during the start up**

In the future, it will be interesting to perform the same experiments on the rocking cell (RC-5) and high-pressure cell (HPC) without any rocking or stirring within the system. This can help to idealize a real-time offshore scenario when the pipeline is shut in and the presence of water and gas mixture at the lower surface of the pipeline leads to hydrate formation.

#### **5) Test the amino acids and ionic liquids as hydrate inhibitors on the field**

The laboratory scale results have shown that the selected amino acids and ionic liquids hold strong potential to inhibit hydrate inhibitors. However, it's essential that these inhibitors are added to the wellhead and tested on the offshore field. The performance of these inhibitors in the offshore field will determine the future market scope of these inhibitors.

#### **6) Test the effect of different water cuts on the hydrate formation**

In the current work, the water cut in the experimental samples was kept around 30 %. In future, it will be interesting to check the hydrate formation in the samples with a lower concentration of water contents ( < 30 wt% ). This will help to deduce the water content that is necessary for the formation of hydrates.

**7) Test the effect of different rocking rates on the hydrate formation**

In the current work, the rocking rate was kept constant and only pressure and temperature variables were varied in the RC-5. In future, a study can be conducted by varying the rocking rates and observing the effect of low and high rocking rates on the hydrate formation inside the cells in the RC-5 assembly.

**8) Built a pilot-scale plant to study the feasibility of using hydrates as a medium for natural gas storage and transportation**

It is well known that hydrate has good storage capacity and it will be viable to build a small hydrate production plant and test the feasibility of gas storage in hydrates.

Many new types of research works can be developed and constituted out of this dissertation. This dissertation is a step forward towards the goal of replacing conventional hydrate inhibitors with the environmentally benign hydrate inhibitors, reducing the inhibitor recovery unit cost and assuring offshore flow assurance

## ACKNOWLEDGMENT

This work was made possible by GSRA # 2-1-0603-14012 from the Qatar National Research Fund (a member of Qatar Foundation). The statements made herein are solely the responsibility of the author.

## LIST OF PUBLICATIONS

Three journal articles resulted and published from the work accomplished in this dissertation using (experimental studies conducted in section 4.1 and sections 4.23 and 4.24 in this manuscript). Following is the list of the publications:

1. Qureshi, M.F., Atilhan, M., Altamash, T., Tariq, M., Khraisheh, M., Aparicio, S. and Tohidi, B., 2016. Gas hydrate prevention and flow assurance by using mixtures of ionic liquids and synergent compounds: combined kinetics and thermodynamic approach. *Energy & Fuels*, 30(4), pp.3541-3548.
2. Qureshi, M.F., Atilhan, M., Altamash, T., Aparicio, S., Aminnaji, M. and Tohidi, B., 2017. High-pressure gas hydrate autoclave hydraulic experiments and scale-up modeling on the effect of stirring RPM effect. *Journal of Natural Gas Science and Engineering*, 38, pp.50-58
3. Altamash, T., Qureshi, M.F., Aparicio, S., Aminnaji, M., Tohidi, B. and Atilhan, M., 2017. Gas hydrates inhibition via combined biomolecules and synergistic materials at wide process conditions. *Journal of Natural Gas Science and Engineering*, 46, pp.873-883.

One publication work related to the work conducted on the ammonium-based protic ionic liquids in section 4.21 and 4.22 is under preparation for potential publication in Q1 Journal.

## REFERENCES

1. Sloan, E. D., Fundamental principles and applications of natural gas hydrates. *Nature* **2003**, *426* (6964), 353-363.
2. Bilgin, M., Geopolitics of European natural gas demand: Supplies from Russia, Caspian and the Middle East. *Energy Policy* **2009**, *37* (11), 4482-4492.
3. Barrette, P., Offshore pipeline protection against seabed gouging by ice: An overview. *Cold Regions Science and Technology* **2011**, *69* (1), 3-20.
4. Arnold, K. E., *Petroleum Engineering Handbook: Facilities and Construction Engineering*. Soc. of Petroleum Engineers: 2007.
5. Hill, T.; Johnson, T.; Hacala-Nicol, V. In *Steady-state, and interrupted, production through a deep water black oil system*, 7th North American Conference on Multiphase Technology, BHR Group: 2010.
6. Sloan, E. D., A changing hydrate paradigm—from apprehension to avoidance to risk management. *Fluid Phase Equilibria* **2005**, *228*, 67-74.
7. Sloan Jr, E. D.; Koh, C., *Clathrate hydrates of natural gases*. CRC press: 2007.



8. Sloan, D.; Creek, J.; Sum, A. K., Where and How Are Hydrate Plugs Formed? *Natural Gas Hydrates in Flow Assurance* **2010**, 13.
9. Kinnari, K.; Hundseid, J.; Li, X.; Askvik, K. M., Hydrate management in practice. *Journal of Chemical & Engineering Data* **2014**, 60 (2), 437-446.
10. Aminnaji, M.; Tohidi, B.; Burgass, R.; Atilhan, M., Effect of injected chemical density on hydrate blockage removal in vertical pipes: Use of MEG/MeOH mixture to remove hydrate blockage. *Journal of Natural Gas Science and Engineering* **2017**.
11. Kanu, A.; Al-Hajri, N.; Messaoud, Y.; Ono, N. In *Mitigating Hydrates in Subsea Oil Flowlines: Consider Production Flow Monitoring and Control*, IPTC 2014: International Petroleum Technology Conference, 2014.
12. Teixeira, A. M.; de Oliveira Arinelli, L.; De Medeiros, J. L.; Araújo, O. d. Q. F., *Monoethylene Glycol as Hydrate Inhibitor in Offshore Natural Gas Processing: From Fundamentals to Exergy Analysis*. Springer: 2017.
13. Hammerschmidt, E., Formation of gas hydrates in natural gas transmission lines. *Industrial & Engineering Chemistry* **1934**, 26 (8), 851-855.
14. Sloan, E. D., Gas Hydrates: Review of Physical/Chemical Properties. *Energy & Fuels* **1998**, 12 (2), 191-196.

15. Koh, C. A., Towards a fundamental understanding of natural gas hydrates. *Chemical Society Reviews* **2002**, *31* (3), 157-167.
16. Loveday, J. S.; Nelmes, R. J.; Guthrie, M.; Belmonte, S. A.; Allan, D. R.; Klug, D. D.; Tse, J. S.; Handa, Y. P., Stable methane hydrate above 2[thinsp]GPa and the source of Titan's atmospheric methane. *Nature* **2001**, *410* (6829), 661-663.
17. Kim, E.; Lee, S.; Lee, J. D.; Seo, Y., Influences of large molecular alcohols on gas hydrates and their potential role in gas storage and CO<sub>2</sub> sequestration. *Chemical Engineering Journal* **2015**, *267*, 117-123.
18. Sulaimon, A. A.; Tajuddin, M. Z. M., Application of COSMO-RS for pre-screening ionic liquids as thermodynamic gas hydrate inhibitor. *Fluid Phase Equilibria* **2017**, *450*, 194-199.
19. Aregbe, A. G., Gas Hydrate—Properties, Formation and Benefits. *Open Journal of Yangtze Gas and Oil* **2017**, (2), 27-44.
20. Gabitto, J. F.; Tsouris, C., Physical properties of gas hydrates: A review. *Journal of Thermodynamics* **2010**, *2010*.
21. Guo, B.; Song, S.; Ghalambor, A.; Lin, T. R., Chapter 15 - Flow Assurance. In *Offshore Pipelines (Second Edition)*, Gulf Professional Publishing: Boston, 2014; pp 179-231.

22. Makogon, Y. F., Natural gas hydrates – A promising source of energy. *Journal of Natural Gas Science and Engineering* **2010**, 2 (1), 49-59.
23. Gbaruko, B.; Igwe, J.; Gbaruko, P.; Nwokeoma, R., Gas hydrates and clathrates: Flow assurance, environmental and economic perspectives and the Nigerian liquified natural gas project. *Journal of Petroleum Science and Engineering* **2007**, 56 (1-3), 192-198.
24. Boschee, P., Gas Hydrate Control Using Monoethylene Glycol in the Gulf of Mexico. *Oil and Gas Facilities* **2012**, 1 (03), 14-18.
25. Bratland, O., Pipe flow 2: multi-phase flow assurance. *Ove Bratland Flow Assurance Consulting, Chonburi, Thailand* **2010**.
26. Lederhos, J.; Long, J.; Sum, A.; Christiansen, R.; Sloan Jr, E., Effective kinetic inhibitors for natural gas hydrates. *Chemical Engineering Science* **1996**, 51 (8), 1221-1229.
27. Sun, M.; Firoozabadi, A., Gas hydrate powder formation – Ultimate solution in natural gas flow assurance. *Fuel* **2015**, 146, 1-5.
28. Delavar, H.; Haghtalab, A., Thermodynamic modeling of gas hydrate formation conditions in the presence of organic inhibitors, salts and their mixtures using UNIQUAC model. *Fluid Phase Equilibria* **2015**, 394, 101-117.

29. Chen, J.; Yan, K.-L.; Chen, G.-J.; Sun, C.-Y.; Liu, B.; Ren, N.; Shen, D.-J.; Niu, M.; Lv, Y.-N.; Li, N.; Sum, A. K., Insights into the formation mechanism of hydrate plugging in pipelines. *Chemical Engineering Science* **2015**, *122*, 284-290.
30. Sami, N. A.; Das, K.; Sangwai, J. S.; Balasubramanian, N., Phase equilibria of methane and carbon dioxide clathrate hydrates in the presence of (methanol+MgCl<sub>2</sub>) and (ethylene glycol+MgCl<sub>2</sub>) aqueous solutions. *The Journal of Chemical Thermodynamics* **2013**, *65*, 198-203.
31. Zhao, X.; Qiu, Z.; Huang, W., Characterization of kinetics of hydrate formation in the presence of kinetic hydrate inhibitors during deepwater drilling. *Journal of Natural Gas Science and Engineering* **2015**, *22*, 270-278.
32. Jordan, M. M.; Weathers, T. M.; Jones, R. A.; Sutherland, L.; Giddings, D. M.; Abla, M., The Impact of Kinetics Hydrate Inhibitors Within Produced Water on Water Injection/Disposal Wells. In *SPE International Symposium and Exhibition on Formation Damage Control, 26-28 February.*, Society of Petroleum Engineers: Lafayette, Louisiana, USA 2014.

33. Li, X.; Gjertsen, L. H.; Austvik, T., Thermodynamic inhibitors for hydrate plug melting. *Annals of the New York Academy of Sciences* **2000**, *912* (1), 822-831.
34. Piemontese, M.; Rotondi, M.; Genesio, A.; Perciante, A.; Iolli, F. In *Successful Experience of Hydrate Plug Removal From Deepwater Gas Injection Flowline*, Offshore Mediterranean Conference and Exhibition, Offshore Mediterranean Conference: 2015.
35. Kashou, S.; Subramanian, S.; Matthews, P.; Thummel, L.; Fauchaux, E.; Subik, D.; Qualls, D.; Akey, R.; Carter, J. In *GOM Export Gas Pipeline, Hydrate Plug Detection and Removal*, Offshore Technology Conference, Offshore Technology Conference: 2004.
36. Sloan, E. D., *Natural gas hydrates in flow assurance*. Gulf Professional Publishing: 2010.
37. Davalath, J.; Barker, J., Hydrate inhibition design for deepwater completions. *SPE Drilling & Completion* **1995**, *10* (02), 115-121.
38. Nepomiluev, M.; Streletskaya, V. In *Subsea gas pipeline coiled tubing intervention for hydrate plug removal*, SPE Russian Oil and Gas Exploration & Production Technical Conference and Exhibition, Society of Petroleum Engineers: 2014.

39. Giavarini, C.; Hester, K., Hydrates Seen as a Problem for the Oil and Gas Industry. In *Gas Hydrates*, Springer: 2011; pp 97-116.
40. Daraboina, N.; Malmos, C.; von Solms, N., Synergistic kinetic inhibition of natural gas hydrate formation. *Fuel* **2013**, *108*, 749-757.
41. Xiao, C.; Adidharma, H., Dual function inhibitors for methane hydrate. *Chemical Engineering Science* **2009**, *64* (7), 1522-1527.
42. Jager, M. D.; Peters, C. J.; Sloan, E. D., Experimental determination of methane hydrate stability in methanol and electrolyte solutions. *Fluid Phase Equilibria* **2002**, *193* (1–2), 17-28.
43. Teixeira, A. M.; de Oliveira Arinelli, L.; de Medeiros, J. L.; Ofélia de Queiroz, F. A., Exergy analysis of monoethylene glycol recovery processes for hydrate inhibition in offshore natural gas fields. *Journal of Natural Gas Science and Engineering* **2016**, *35*, 798-813.
44. Tariq, M.; Rooney, D.; Othman, E.; Aparicio, S.; Atilhan, M.; Khraisheh, M., Gas hydrate inhibition: a review of the role of ionic liquids. *Industrial & Engineering Chemistry Research* **2014**, *53* (46), 17855-17868.
45. Swank, L.; Kapadia, K.; Webber, P.; Jones, R. In *Mitigation of Hydrates Using Continuous KHI Injection in Deepwater GoM*, Offshore Technology Conference, Offshore Technology Conference: 2017.

46. Mozaffar, H.; Anderson, R.; Tohidi, B., Effect of alcohols and diols on PVCap-induced hydrate crystal growth patterns in methane systems. *Fluid Phase Equilibria* **2016**, *425*, 1-8.
47. Abrahamsen, E.; Kelland, M. A., Comparison of Kinetic Hydrate Inhibitor Performance on Structure I and Structure II Hydrate-Forming Gases for a Range of Polymer Classes. *Energy & Fuels* **2017**.
48. (a) Cha, M.; Shin, K.; Kim, J.; Chang, D.; Seo, Y.; Lee, H.; Kang, S.-P., Thermodynamic and kinetic hydrate inhibition performance of aqueous ethylene glycol solutions for natural gas. *Chemical Engineering Science* **2013**, *99*, 184-190; (b) Balson, T.; Craddock, H.; Dunlop, J.; Frampton, H.; Payne, G.; Reid, P.; Fu, B., The development of advanced kinetic hydrate inhibitors. In *Chemistry in the Oil Industry VII*, 2002; pp 264-276.
49. Chua, P. C.; Kelland, M. A., Poly (N-vinyl azacyclooctanone): a more powerful structure ii kinetic hydrate inhibitor than poly (N-vinyl caprolactam). *Energy & Fuels* **2012**, *26* (7), 4481-4485.
50. King Jr, H.; Hutter, J. L.; Lin, M. Y.; Sun, T., Polymer conformations of gas-hydrate kinetic inhibitors: A small-angle neutron scattering study. *The Journal of Chemical Physics* **2000**, *112* (5), 2523-2532.

51. Storr, M. T.; Taylor, P. C.; Monfort, J.-P.; Rodger, P. M., Kinetic inhibitor of hydrate crystallization. *Journal of the American Chemical Society* **2004**, *126* (5), 1569-1576.
52. Long, F.; Fan, S.; Wang, Y.; Lang, X., Promoting effect of super absorbent polymer on hydrate formation. *Journal of Natural Gas Chemistry* **2010**, *19* (3), 251-254.
53. Kakati, H.; Mandal, A.; Laik, S., Synergistic effect of Polyvinylpyrrolidone (PVP) and L-tyrosine on kinetic inhibition of CH<sub>4</sub> + C<sub>2</sub>H<sub>4</sub> + C<sub>3</sub>H<sub>8</sub> hydrate formation. *Journal of Natural Gas Science and Engineering* **2016**, *34*, 1361-1368.
54. (a) Chong, F. K.; Eljack, F. T.; Atilhan, M.; Foo, D. C.; Chemmangattuvalappil, N. G., A systematic visual methodology to design ionic liquids and ionic liquid mixtures: Green solvent alternative for carbon capture. *Computers & Chemical Engineering* **2016**; (b) Chong, F. K.; Chemmangattuvalappil, N. G.; Eljack, F. T.; Atilhan, M.; Foo, D. C., Designing ionic liquid solvents for carbon capture using property-based visual approach. *Clean Technologies and Environmental Policy* **2016**, *18* (4), 1177-1188.



55. (a) Karadas, F.; Atilhan, M.; Aparicio, S., Review on the use of ionic liquids (ILs) as alternative fluids for CO<sub>2</sub> capture and natural gas sweetening. *Energy & Fuels* **2010**, *24* (11), 5817-5828; (b) Aparicio, S.; Atilhan, M.; Karadas, F., Thermophysical properties of pure ionic liquids: review of present situation. *Industrial & Engineering Chemistry Research* **2010**, *49* (20), 9580-9595; (c) Bandrés, I.; Alcalde, R.; Lafuente, C.; Atilhan, M.; Aparicio, S., On the viscosity of pyridinium based ionic liquids: an experimental and computational study. *The Journal of Physical Chemistry B* **2011**, *115* (43), 12499-12513; (d) Aparicio, S.; Atilhan, M.; Khraisheh, M.; Alcalde, R.; Fernández, J., Study on hydroxylammonium-based ionic liquids. II. Computational analysis of CO<sub>2</sub> absorption. *The Journal of Physical Chemistry B* **2011**, *115* (43), 12487-12498; (e) Atilhan, M.; Jacquemin, J.; Rooney, D.; Khraisheh, M.; Aparicio, S., Viscous behavior of imidazolium-based ionic liquids. *Industrial & Engineering Chemistry Research* **2013**, *52* (47), 16774-16785; (f) Sanz, V.; Alcalde, R.; Atilhan, M.; Aparicio, S., Insights from quantum chemistry into piperazine-based ionic liquids and their behavior with regard to CO<sub>2</sub>. *Journal of molecular modeling* **2014**, *20* (3), 1-14; (g) García, G.; Atilhan, M.; Aparicio, S.,

Theoretical Study on the Solvation of C60 Fullerene by Ionic Liquids. *The Journal of Physical Chemistry B* **2014**, *118* (38), 11330-11340.

56. Greaves, T. L.; Weerawardena, A.; Fong, C.; Krodziewska, I.; Drummond, C. J., Protic ionic liquids: solvents with tunable phase behavior and physicochemical properties. *The Journal of Physical Chemistry B* **2006**, *110* (45), 22479-22487.

57. (a) Ashassi-Sorkhabi, H.; Majidi, M.; Seyyedi, K., Investigation of inhibition effect of some amino acids against steel corrosion in HCl solution. *Applied surface science* **2004**, *225* (1), 176-185; (b) Gece, G.; Bilgiç, S., A theoretical study on the inhibition efficiencies of some amino acids as corrosion inhibitors of nickel. *Corrosion Science* **2010**, *52* (10), 3435-3443; (c) Morad, M. S. S.; Hermas, A. E. H. A.; Aal, M. S. A., Effect of amino acids containing sulfur on the corrosion of mild steel in phosphoric acid solutions polluted with Cl<sup>-</sup>, F<sup>-</sup> and Fe<sup>3+</sup> ions—behaviour near and at the corrosion potential. *Journal of Chemical Technology and Biotechnology* **2002**, *77* (4), 486-494.

58. Mohamed, N. A.; Tariq, M.; Atilhan, M.; Khraisheh, M.; Rooney, D.; Garcia, G.; Aparicio, S., Investigation of the performance of biocompatible

gas hydrate inhibitors via combined experimental and DFT methods. *The Journal of Chemical Thermodynamics* **2017**, *111*, 7-19.

59. Mohamed, N. A. Avoiding gas hydrate problems in qatar oil and gas industry: environmentally friendly solvents for gas hydrate inhibition. 2014.

60. Hussey, C. L., Room temperature haloaluminate ionic liquids. Novel solvents for transition metal solution chemistry. *Pure and applied Chemistry* **1988**, *60* (12), 1763-1772.

61. Wasserscheid, P.; Keim, W., Ionic liquids—new “solutions” for transition metal catalysis. *Angewandte Chemie International Edition* **2000**, *39* (21), 3772-3789.

62. Jiang, H.; Adidharma, H., Thermodynamic modeling of aqueous ionic liquid solutions and prediction of methane hydrate dissociation conditions in the presence of ionic liquid. *Chemical Engineering Science* **2013**, *102*, 24-31.

63. Welton, T., Room-temperature ionic liquids. Solvents for synthesis and catalysis. *Chemical reviews* **1999**, *99* (8), 2071-2084.

64. Fredlake, C. P.; Crosthwaite, J. M.; Hert, D. G.; Aki, S. N.; Brennecke, J. F., Thermophysical properties of imidazolium-based ionic liquids. *Journal of Chemical & Engineering Data* **2004**, *49* (4), 954-964.

65. Hasan, M.; Kozhevnikov, I. V.; Siddiqui, M. R. H.; Steiner, A.; Winterton, N., Gold Compounds as Ionic Liquids. Synthesis, Structures, and Thermal Properties of N, N'-Dialkylimidazolium Tetrachloroaurate Salts. *Inorganic Chemistry* **1999**, *38* (25), 5637-5641.
66. Freire, M. G.; Neves, C. M.; Shimizu, K.; Bernardes, C. E.; Marrucho, I. M.; Coutinho, J. A.; Lopes, J. N. C.; Rebelo, L. s. P. N., Mutual solubility of water and structural/positional isomers of N-alkylpyridinium-based ionic liquids. *The Journal of Physical Chemistry B* **2010**, *114* (48), 15925-15934.
67. Fumino, K.; Wulf, A.; Ludwig, R., Hydrogen bonding in protic ionic liquids: reminiscent of water. *Angewandte Chemie International Edition* **2009**, *48* (17), 3184-3186.
68. Tariq, M.; Forte, P.; Gomes, M. C.; Lopes, J. C.; Rebelo, L., Densities and refractive indices of imidazolium-and phosphonium-based ionic liquids: Effect of temperature, alkyl chain length, and anion. *The Journal of Chemical Thermodynamics* **2009**, *41* (6), 790-798.
69. Arzhantsev, S.; Ito, N.; Heitz, M.; Maroncelli, M., Solvation dynamics of coumarin 153 in several classes of ionic liquids: cation dependence of the ultrafast component. *Chemical physics letters* **2003**, *381* (3), 278-286.

70. Petkovic, M.; Seddon, K. R.; Rebelo, L. P. N.; Pereira, C. S., Ionic liquids: a pathway to environmental acceptability. *Chemical Society Reviews* **2011**, *40* (3), 1383-1403.
71. Peric, B.; Sierra, J.; Martí, E.; Cruañas, R.; Garau, M. A.; Arning, J.; Bottin-Weber, U.; Stolte, S., (Eco) toxicity and biodegradability of selected protic and aprotic ionic liquids. *Journal of hazardous materials* **2013**, *261*, 99-105.
72. Belieres, J.-P.; Angell, C. A., Protic ionic liquids: preparation, characterization, and proton free energy level representation. *The Journal of Physical Chemistry B* **2007**, *111* (18), 4926-4937.
73. Neto, J. d. R. M.; Torresi, R. M.; de Torresi, S. I. C., Electrochromic behavior of WO<sub>3</sub> nanoplate thin films in acid aqueous solution and a protic ionic liquid. *Journal of Electroanalytical Chemistry* **2016**, *765*, 111-117.
74. Hangarge, R. V.; Jarikote, D. V.; Shingare, M. S., Knoevenagel condensation reactions in an ionic liquid. *Green Chemistry* **2002**, *4* (3), 266-268.
75. Greaves, T. L.; Drummond, C. J., Protic ionic liquids: properties and applications. *Chemical reviews* **2008**, *108* (1), 206-237.

76. (a) Hallett, J. P.; Welton, T., Room-temperature ionic liquids: solvents for synthesis and catalysis. 2. *Chemical reviews* **2011**, *111* (5), 3508-3576; (b) Buzzeo, M. C.; Evans, R. G.; Compton, R. G., Non-haloaluminate room-temperature ionic liquids in electrochemistry—A review. *ChemPhysChem* **2004**, *5* (8), 1106-1120; (c) Pernak, J.; Goc, I.; Mirska, I., Anti-microbial activities of protic ionic liquids with lactate anion. *Green Chemistry* **2004**, *6* (7), 323-329.
77. Smiglak, M.; Reichert, W. M.; Holbrey, J. D.; Wilkes, J. S.; Sun, L.; Thrasher, J. S.; Kirichenko, K.; Singh, S.; Katritzky, A. R.; Rogers, R. D., Combustible ionic liquids by design: is laboratory safety another ionic liquid myth? *Chemical Communications* **2006**, (24), 2554-2556.
78. Meine, N.; Benedito, F.; Rinaldi, R., Thermal stability of ionic liquids assessed by potentiometric titration. *Green Chemistry* **2010**, *12* (10), 1711-1714.
79. Marsh, K. N.; Deev, A.; Wu, A. C.; Tran, E.; Klamt, A., Room temperature ionic liquids as replacements for conventional solvents—a review. *Korean Journal of Chemical Engineering* **2002**, *19* (3), 357-362.

80. Kim, K.-S.; Choi, S.; Demberehnyamba, D.; Lee, H.; Oh, J.; Lee, B.-B.; Mun, S.-J., Ionic liquids based on N-alkyl-N-methylmorpholinium salts as potential electrolytes. *Chemical Communications* **2004**, (7), 828-829.
81. Kim, K.-S.; Demberehnyamba, D.; Lee, H., Size-selective synthesis of gold and platinum nanoparticles using novel thiol-functionalized ionic liquids. *Langmuir* **2004**, 20 (3), 556-560.
82. Gordon, C. M.; Muldoon, M. J.; Wagner, M.; Hilgers, C.; Davis, J.; Wasserscheid, P., Synthesis and purification. WILEY-VCH: Weinheim: 2008; Vol. 1, pp 7-56.
83. (a) Hurley, F. H.; Wier, T. P., Electrodeposition of metals from fused quaternary ammonium salts. *Journal of The Electrochemical Society* **1951**, 98 (5), 203-206; (b) Robinson, J.; Osteryoung, R., An electrochemical and spectroscopic study of some aromatic hydrocarbons in the room temperature molten salt system aluminum chloride-n-butylpyridinium chloride. *Journal of the American Chemical Society* **1979**, 101 (2), 323-327.
84. Ratti, R., Ionic Liquids: Synthesis and Applications in Catalysis. *Advances in Chemistry* **2014**, 2014, 16.
85. Chauvin, Y.; Einloft, S.; Olivier, H., Catalytic dimerization of propene by nickel-phosphine complexes in 1-butyl-3-methylimidazolium

chloride/AlEt<sub>x</sub>Cl<sub>3-x</sub> (x= 0, 1) ionic liquids. *Industrial & engineering chemistry research* **1995**, 34 (4), 1149-1155.

86. Chauvin, Y.; Olivier-Bourbigou, H., Nonaqueous ionic liquids as reaction solvents. *Chemtech* **1995**, 25 (9), 26-30.

87. Williams, S. D.; Schoebrechts, J.; Selkirk, J.; Mamantov, G., A new room temperature molten salt solvent system: organic cation tetrachloroborates. *Journal of the American Chemical Society* **1987**, 109 (7), 2218-2219.

88. Suarez, P. A.; Dullius, J. E.; Einloft, S.; De Souza, R. F.; Dupont, J., The use of new ionic liquids in two-phase catalytic hydrogenation reaction by rhodium complexes. *Polyhedron* **1996**, 15 (7), 1217-1219.

89. Andreani, L.; Rocha, J. D., Use of ionic liquids in biodiesel production: a review. *Brazilian Journal of Chemical Engineering* **2012**, 29, 1-13.

90. (a) Blasucci, V.; Hart, R.; Mestre, V. L.; Hahne, D. J.; Burlager, M.; Huttenhower, H.; Thio, B. J. R.; Pollet, P.; Liotta, C. L.; Eckert, C. A., Single component, reversible ionic liquids for energy applications. *Fuel* **2010**, 89 (6), 1315-1319; (b) Deetlefs, M.; Seddon, K. R., Improved



preparations of ionic liquids using microwave irradiation. *Green Chemistry* **2003**, *5* (2), 181-186.

91. (a) Varma, R. S.; Namboodiri, V. V., An expeditious solvent-free route to ionic liquids using microwaves. *Chemical Communications* **2001**, (7), 643-644; (b) Vu, P. D.; Boydston, A. J.; Bielawski, C. W., Ionic liquids via efficient, solvent-free anion metathesis. *Green Chemistry* **2007**, *9* (11), 1158-1159.

92. Earle, M. J.; Seddon, K. R., Ionic liquids. Green solvents for the future. *Pure and applied chemistry* **2000**, *72* (7), 1391-1398.

93. Olivier, H., Recent developments in the use of non-aqueous ionic liquids for two-phase catalysis. *Journal of Molecular Catalysis A: Chemical* **1999**, *146* (1), 285-289.

94. Maase, M.; Massonne, K., Biphasic acid scavenging utilizing ionic liquids: The first commercial process with ionic liquids. ACS Publications: 2005.

95. Maase, M.; Massonne, K.; Halbritter, K.; Noe, R.; Bartsch, M.; Siegel, W.; Stegmann, V.; Flores, M.; Huttenloch, O.; Becker, M., Method for the separation of acids from chemical reaction mixtures by means of ionic fluids. Google Patents: 2008.

96. Plechkova, N. V.; Seddon, K. R., Applications of ionic liquids in the chemical industry. *Chemical Society Reviews* **2008**, *37* (1), 123-150.
97. Holbrey, J. D.; Rogers, R. D., Green chemistry and ionic liquids: synergies and ironies. ACS Publications: 2002.
98. Chauvin, Y., Olefin metathesis: The early days (Nobel lecture). *Angewandte Chemie International Edition* **2006**, *45* (23), 3740-3747.
99. Beste, Y.; Eggersmann, M.; Schoenmakers, H., Ionische Flüssigkeiten als Entrainer in der Extraktivdestillation. *Chemie Ingenieur Technik* **2004**, *76* (9), 1407-1407.
100. Arlt, W.; Seiler, M.; Jork, C.; Schneider, T., Ionic liquids as selective additives for separation of close-boiling or azeotropic mixtures. Google Patents: 2008.
101. Kazakov, A.; Magee, J.; Chirico, R.; Diky, V.; Muzny, C.; Kroenlein, K.; Frenkel, M., NIST Standard Reference Database 147: NIST Ionic Liquids Database-(ILThermo). Version.
102. (a) Tokuda, H.; Hayamizu, K.; Ishii, K.; Susan, M. A. B. H.; Watanabe, M., Physicochemical properties and structures of room temperature ionic liquids. 1. Variation of anionic species. *The Journal of Physical Chemistry B* **2004**, *108* (42), 16593-16600; (b) Ngo, H. L.;

LeCompte, K.; Hargens, L.; McEwen, A. B., Thermal properties of imidazolium ionic liquids. *Thermochimica Acta* **2000**, *357*, 97-102.

103. Rogers, R. D.; Seddon, K. R., Ionic liquids--solvents of the future? *Science* **2003**, *302* (5646), 792-793.

104. Moens, L.; Blake, D. M.; Rudnicki, D. L.; Hale, M. J., Advanced thermal storage fluids for solar parabolic trough systems. *TRANSACTIONS-AMERICAN SOCIETY OF MECHANICAL ENGINEERS JOURNAL OF SOLAR ENERGY ENGINEERING* **2003**, *125* (1), 112-116.

105. Holbrey, J. D.; Seddon, K. R., The phase behaviour of 1-alkyl-3-methylimidazolium tetrafluoroborates; ionic liquids and ionic liquid crystals. *Journal of the Chemical Society, Dalton Transactions* **1999**, (13), 2133-2140.

106. Bonhote, P.; Dias, A.-P.; Papageorgiou, N.; Kalyanasundaram, K.; Grätzel, M., Hydrophobic, highly conductive ambient-temperature molten salts. *Inorganic chemistry* **1996**, *35* (5), 1168-1178.

107. (a) Scurto, A. M.; Leitner, W., Expanding the useful range of ionic liquids: melting point depression of organic salts with carbon dioxide for biphasic catalytic reactions. *Chemical Communications* **2006**, (35), 3681-3683; (b) Scurto, A. M.; Newton, E.; Weikel, R. R.; Draucker, L.; Hallett, J.;

Liotta, C. L.; Leitner, W.; Eckert, C. A., Melting point depression of ionic liquids with CO<sub>2</sub>: Phase equilibria. *Industrial & Engineering Chemistry Research* **2008**, *47* (3), 493-501.

108. Domańska, U.; Morawski, P., Influence of high pressure on solubility of ionic liquids: experimental data and correlation. *Green Chemistry* **2007**, *9* (4), 361-368.

109. Balaban, A. T.; March, N. H.; Klein, D. J., Melting points and other properties of ionic liquids, with emphasis on the pressure dependence. *Physics and Chemistry of Liquids* **2008**, *46* (6), 682-686.

110. Trohalaki, S.; Pachter, R., Prediction of melting points for ionic liquids. *Molecular Informatics* **2005**, *24* (4), 485-490.

111. Carrera, G.; Aires-de-Sousa, J., Estimation of melting points of pyridinium bromide ionic liquids with decision trees and neural networks. *Green Chemistry* **2005**, *7* (1), 20-27.

112. Rebelo, L. P.; Canongia Lopes, J. N.; Esperança, J. M.; Filipe, E., On the critical temperature, normal boiling point, and vapor pressure of ionic liquids. *The Journal of Physical Chemistry B* **2005**, *109* (13), 6040-6043.

113. Paulechka, Y.; Zaitsau, D. H.; Kabo, G.; Strechan, A., Vapor pressure and thermal stability of ionic liquid 1-butyl-3-methylimidazolium Bis

(trifluoromethylsulfonyl) amide. *Thermochimica Acta* **2005**, *439* (1), 158-160.

114. MSS Esperança, J.; Canongia Lopes, J. N.; Tariq, M.; Santos, L. s. M.; Magee, J. W.; Rebelo, L. s. P. N., Volatility of Aprotic Ionic Liquids • A Review. *Journal of Chemical & Engineering Data* **2009**, *55* (1), 3-12.

115. Earle, M. J.; Esperança, J. M.; Gilea, M. A.; Lopes, J. N. C.; Rebelo, L. P.; Magee, J. W.; Seddon, K. R.; Widegren, J. A., The distillation and volatility of ionic liquids. *Nature* **2006**, *439* (7078), 831.

116. Tokuda, H.; Tsuzuki, S.; Susan, M. A. B. H.; Hayamizu, K.; Watanabe, M., How ionic are room-temperature ionic liquids? An indicator of the physicochemical properties. *The Journal of Physical Chemistry B* **2006**, *110* (39), 19593-19600.

117. Seeberger, A.; Andresen, A.-K.; Jess, A., Prediction of long-term stability of ionic liquids at elevated temperatures by means of non-isothermal thermogravimetric analysis. *Physical Chemistry Chemical Physics* **2009**, *11* (41), 9375-9381.

118. Kroon, M. C.; Buijs, W.; Peters, C. J.; Witkamp, G.-J., Quantum chemical aided prediction of the thermal decomposition mechanisms and temperatures of ionic liquids. *Thermochimica Acta* **2007**, *465* (1), 40-47.

119. Huddleston, J. G.; Visser, A. E.; Reichert, W. M.; Willauer, H. D.; Broker, G. A.; Rogers, R. D., Characterization and comparison of hydrophilic and hydrophobic room temperature ionic liquids incorporating the imidazolium cation. *Green chemistry* **2001**, *3* (4), 156-164.
120. Wasserscheid, P.; Welton, T., *Ionic liquids in synthesis*. John Wiley & Sons: 2008.
121. Badawy, W. A.; Ismail, K. M.; Fathi, A. M., Corrosion control of Cu–Ni alloys in neutral chloride solutions by amino acids. *Electrochimica Acta* **2006**, *51* (20), 4182-4189.
122. (a) Jacquemin, J.; Husson, P.; Mayer, V.; Cibulka, I., High-pressure volumetric properties of imidazolium-based ionic liquids: effect of the anion. *Journal of Chemical & Engineering Data* **2007**, *52* (6), 2204-2211;  
(b) Gardas, R. L.; Freire, M. G.; Carvalho, P. J.; Marrucho, I. M.; Fonseca, I. M.; Ferreira, A. G.; Coutinho, J. A., High-pressure densities and derived thermodynamic properties of imidazolium-based ionic liquids. *Journal of Chemical & Engineering Data* **2007**, *52* (1), 80-88.
123. Taguchi, R.; Machida, H.; Sato, Y.; Smith Jr, R. L., High-Pressure Densities of 1-Alkyl-3-methylimidazolium Hexafluorophosphates and 1-Alkyl-3-methylimidazolium Tetrafluoroborates at Temperatures from (313

to 473) K and at Pressures up to 200 MPa. *Journal of Chemical & Engineering Data* **2008**, 54 (1), 22-27.

124. Tomida, D.; Kumagai, A.; Kenmochi, S.; Qiao, K.; Yokoyama, C., Viscosity of 1-hexyl-3-methylimidazolium hexafluorophosphate and 1-octyl-3-methylimidazolium hexafluorophosphate at high pressure. *Journal of Chemical & Engineering Data* **2007**, 52 (2), 577-579.

125. Gu, Z.; Brennecke, J. F., Volume expansivities and isothermal compressibilities of imidazolium and pyridinium-based ionic liquids. *Journal of Chemical & Engineering Data* **2002**, 47 (2), 339-345.

126. (a) Madeira Lau, R.; Van Rantwijk, F.; Seddon, K.; Sheldon, R., Lipase-catalyzed reactions in ionic liquids. *Organic Letters* **2000**, 2 (26), 4189-4191; (b) Cull, S.; Holbrey, J.; Vargas-Mora, V.; Seddon, K.; Lye, G., Room-temperature ionic liquids as replacements for organic solvents in multiphase bioprocess operations. *Biotechnology and Bioengineering* **2000**, 69 (2), 227-233.

127. Mai, N. L.; Ahn, K.; Koo, Y.-M., Methods for recovery of ionic liquids—a review. *Process Biochemistry* **2014**, 49 (5), 872-881.

128. Palomar, J.; Lemus, J.; Gilarranz, M.; Rodriguez, J., Adsorption of ionic liquids from aqueous effluents by activated carbon. *Carbon* **2009**, *47* (7), 1846-1856.
129. (a) Freire, M. G.; Santos, L. M.; Fernandes, A. M.; Coutinho, J. A.; Marrucho, I. M., An overview of the mutual solubilities of water–imidazolium-based ionic liquids systems. *Fluid Phase Equilibria* **2007**, *261* (1), 449-454; (b) Freire, M. G.; Ventura, S. P.; Santos, L. M.; Marrucho, I. M.; Coutinho, J. A., Evaluation of COSMO-RS for the prediction of LLE and VLE of water and ionic liquids binary systems. *Fluid Phase Equilibria* **2008**, *268* (1), 74-84.
130. (a) Łuczak, J.; Hupka, J.; Thöming, J.; Jungnickel, C., Self-organization of imidazolium ionic liquids in aqueous solution. *Colloids and Surfaces A: Physicochemical and Engineering Aspects* **2008**, *329* (3), 125-133; (b) Łuczak, J.; Jungnickel, C.; Joskowska, M.; Thöming, J.; Hupka, J., Thermodynamics of micellization of imidazolium ionic liquids in aqueous solutions. *Journal of colloid and interface science* **2009**, *336* (1), 111-116.
131. Leng, Y.; Wang, J.; Zhu, D.; Ren, X.; Ge, H.; Shen, L., Heteropolyanion-Based Ionic Liquids: Reaction-Induced Self-Separation Catalysts for Esterification. *Angewandte Chemie* **2009**, *121* (1), 174-177.



132. Antonietti, M.; Kuang, D.; Smarsly, B.; Zhou, Y., Ionic liquids for the convenient synthesis of functional nanoparticles and other inorganic nanostructures. *Angewandte Chemie International Edition* **2004**, *43* (38), 4988-4992.
133. HUANG, K.; Rui, W.; Yan, C.; Huiquan, L.; Jinshu, W., Recycling and reuse of ionic liquid in homogeneous cellulose acetylation. *Chinese Journal of Chemical Engineering* **2013**, *21* (5), 577-584.
134. Massonne, K.; Siemer, M.; Mormann, W.; Leng, W., Distillation of ionic liquids. Google Patents: 2013.
135. Kreher, U. P.; Rosamilia, A. E.; Raston, C. L.; Scott, J. L.; Strauss, C. R., Self-associated, "distillable" ionic media. *Molecules* **2004**, *9* (6), 387-393.
136. Abu-Eishah, S. I., Ionic liquids recycling for reuse. In *Ionic Liquids-Classes and Properties*, InTech: 2011.
137. Zhao, H.; Xia, S.; Ma, P., Use of ionic liquids as 'green' solvents for extractions. *Journal of chemical technology and biotechnology* **2005**, *80* (10), 1089-1096.
138. Huddleston, J. G.; Willauer, H. D.; Swatloski, R. P.; Visser, A. E.; Rogers, R. D., Room temperature ionic liquids as novel media for

'clean' liquid–liquid extraction. *Chemical Communications* **1998**, (16), 1765-1766.

139. Earle, M. J.; McCormac, P. B.; Seddon, K. R., Diels–Alder reactions in ionic liquids. A safe recyclable alternative to lithium perchlorate–diethyl ether mixtures. *Green Chemistry* **1999**, *1* (1), 23-25.

140. Dibble, D. C.; Li, C.; Sun, L.; George, A.; Cheng, A.; Çetinkol, Ö. P.; Benke, P.; Holmes, B. M.; Singh, S.; Simmons, B. A., A facile method for the recovery of ionic liquid and lignin from biomass pretreatment. *Green Chemistry* **2011**, *13* (11), 3255-3264.

141. (a) Chun, S.; Dzyuba, S. V.; Bartsch, R. A., Influence of structural variation in room-temperature ionic liquids on the selectivity and efficiency of competitive alkali metal salt extraction by a crown ether. *Analytical Chemistry* **2001**, *73* (15), 3737-3741; (b) Visser, A. E.; Swatloski, R. P.; Reichert, W. M.; Griffin, S. T.; Rogers, R. D., Traditional extractants in nontraditional solvents: Groups 1 and 2 extraction by crown ethers in room-temperature ionic liquids. *Industrial & Engineering Chemistry Research* **2000**, *39* (10), 3596-3604.

142. Wei, G.-T.; Yang, Z.; Chen, C.-J., Room temperature ionic liquid as a novel medium for liquid/liquid extraction of metal ions. *Analytica Chimica Acta* **2003**, *488* (2), 183-192.
143. Blanchard, L. A.; Gu, Z.; Brennecke, J. F., High-pressure phase behavior of ionic liquid/CO<sub>2</sub> systems. *The Journal of Physical Chemistry B* **2001**, *105* (12), 2437-2444.
144. (a) Blanchard, L. A.; Brennecke, J. F., Recovery of organic products from ionic liquids using supercritical carbon dioxide. *Industrial & engineering chemistry research* **2001**, *40* (1), 287-292; (b) Scurto, A. M.; Aki, S. N.; Brennecke, J. F., CO<sub>2</sub> as a separation switch for ionic liquid/organic mixtures. *Journal of the American Chemical Society* **2002**, *124* (35), 10276-10277.
145. Blanchard, L. A.; Hancu, D.; Beckman, E. J.; Brennecke, J. F., Green processing using ionic liquids and CO<sub>2</sub>. *Nature* **1999**, *399* (6731), 28.
146. Virtanen, P.; Mikkola, J.-P.; Toukoniitty, E.; Karhu, H.; Kordas, K.; Eränen, K.; Wärnå, J.; Salmi, T., Supported ionic liquid catalysts—from batch to continuous operation in preparation of fine chemicals. *Catalysis Today* **2009**, *147*, S144-S148.

147. (a) Zhang, Z.; Wu, L.; Dong, J.; Li, B.-G.; Zhu, S., Preparation and SO<sub>2</sub> sorption/desorption behavior of an ionic liquid supported on porous silica particles. *Industrial & Engineering Chemistry Research* **2009**, *48* (4), 2142-2148; (b) Vangeli, O. C.; Romanos, G. E.; Beltsios, K. G.; Fokas, D.; Kouvelos, E. P.; Stefanopoulos, K. L.; Kanellopoulos, N. K., Grafting of Imidazolium Based Ionic Liquid on the Pore Surface of Nanoporous Materials • Study of Physicochemical and Thermodynamic Properties. *The Journal of Physical Chemistry B* **2010**, *114* (19), 6480-6491.
148. (a) Stepnowski, P., Preliminary assessment of the sorption of some alkyl imidazolium cations as used in ionic liquids to soils and sediments. *Australian Journal of Chemistry* **2005**, *58* (3), 170-173; (b) Letaief, S.; Elbokl, T. A.; Detellier, C., Reactivity of ionic liquids with kaolinite: melt intersalation of ethyl pyridinium chloride in an urea-kaolinite pre-intercalate. *Journal of Colloid and Interface Science* **2006**, *302* (1), 254-258.
149. Anthony, J. L.; Maginn, E. J.; Brennecke, J. F., Solution thermodynamics of imidazolium-based ionic liquids and water. *The Journal of Physical Chemistry B* **2001**, *105* (44), 10942-10949.
150. Lemus, J.; Palomar, J.; Heras, F.; Gilarranz, M. A.; Rodriguez, J. J., Developing criteria for the recovery of ionic liquids from aqueous phase by

adsorption with activated carbon. *Separation and purification technology* **2012**, *97*, 11-19.

151. Qi, X.; Li, L.; Tan, T.; Chen, W.; Smith Jr, R. L., Adsorption of 1-butyl-3-methylimidazolium chloride ionic liquid by functional carbon microspheres from hydrothermal carbonization of cellulose. *Environmental science & technology* **2013**, *47* (6), 2792-2798.

152. Gutowski, K. E.; Broker, G. A.; Willauer, H. D.; Huddleston, J. G.; Swatloski, R. P.; Holbrey, J. D.; Rogers, R. D., Controlling the aqueous miscibility of ionic liquids: aqueous biphasic systems of water-miscible ionic liquids and water-structuring salts for recycle, metathesis, and separations. *Journal of the American Chemical Society* **2003**, *125* (22), 6632-6633.

153. Deng, Y.; Long, T.; Zhang, D.; Chen, J.; Gan, S., Phase diagram of [Amim] Cl<sup>+</sup> salt aqueous biphasic systems and its application for [Amim] Cl recovery. *Journal of Chemical & Engineering Data* **2009**, *54* (9), 2470-2473.

154. Li, C.; Han, J.; Wang, Y.; Yan, Y.; Pan, J.; Xu, X.; Zhang, Z., Phase behavior for the aqueous two-phase systems containing the ionic liquid 1-

butyl-3-methylimidazolium tetrafluoroborate and kosmotropic salts. *Journal of Chemical & Engineering Data* **2009**, *55* (3), 1087-1092.

155. (a) Peng, X.; Hu, Y.; Liu, Y.; Jin, C.; Lin, H., Separation of ionic liquids from dilute aqueous solutions using the method based on CO<sub>2</sub> hydrates. *Journal of Natural Gas Chemistry* **2010**, *19* (1), 81-85; (b) Xiong, D.; Wang, H.; Li, Z.; Wang, J., Recovery of Ionic Liquids with Aqueous Two-Phase Systems Induced by Carbon Dioxide. *ChemSusChem* **2012**, *5* (11), 2255-2261.

156. Xiao, C.; Wibisono, N.; Adidharma, H., Dialkylimidazolium halide ionic liquids as dual function inhibitors for methane hydrate. *Chemical Engineering Science* **2010**, *65* (10), 3080-3087.

157. Partoon, B.; Wong, N. M.; Sabil, K. M.; Nasrifar, K.; Ahmad, M. R., A study on thermodynamics effect of [EMIM]-Cl and [OH-C 2 MIM]-Cl on methane hydrate equilibrium line. *Fluid Phase Equilibria* **2013**, *337*, 26-31.

158. Li, X.-S.; Liu, Y.-J.; Zeng, Z.-Y.; Chen, Z.-Y.; Li, G.; Wu, H.-J., Equilibrium hydrate formation conditions for the mixtures of methane+ ionic liquids+ water. *Journal of Chemical & Engineering Data* **2010**, *56* (1), 119-123.

159. Chu, C.-K.; Chen, P.-C.; Chen, Y.-P.; Lin, S.-T.; Chen, L.-J., Inhibition effect of 1-ethyl-3-methylimidazolium chloride on methane hydrate equilibrium. *The Journal of Chemical Thermodynamics* **2015**, *91*, 141-145.
160. Chu, C.-K.; Lin, S.-T.; Chen, Y.-P.; Chen, P.-C.; Chen, L.-J., Chain length effect of ionic liquid 1-alkyl-3-methylimidazolium chloride on the phase equilibrium of methane hydrate. *Fluid Phase Equilibria* **2016**, *413*, 57-64.
161. Long, Z.; He, Y.; Zhou, X.; Li, D.; Liang, D., Phase behavior of methane hydrate in the presence of imidazolium ionic liquids and their mixtures. *Fluid Phase Equilibria* **2017**, *439*, 1-8.
162. Richard, A. R.; Adidharma, H., The performance of ionic liquids and their mixtures in inhibiting methane hydrate formation. *Chemical engineering science* **2013**, *87*, 270-276.
163. Saikia, T.; Mahto, V., Evaluation of 1-Decyl-3-Methylimidazolium Tetrafluoroborate as clathrate hydrate crystal inhibitor in drilling fluid. *Journal of Natural Gas Science and Engineering* **2016**, *36*, 906-915.
164. Rasoolzadeh, A.; Javanmardi, J.; Eslamimanesh, A.; Mohammadi, A. H., Experimental study and modeling of methane hydrate formation

induction time in the presence of ionic liquids. *Journal of Molecular Liquids* **2016**, *221*, 149-155.

165. Zare, M.; Haghtalab, A.; Ahmadi, A. N.; Nazari, K.; Mehdizadeh, A., Effect of imidazolium based ionic liquids and ethylene glycol monoethyl ether solutions on the kinetic of methane hydrate formation. *Journal of Molecular Liquids* **2015**, *204*, 236-242.

166. Ficke, L. E.; Brennecke, J. F., Interactions of ionic liquids and water. *The Journal of Physical Chemistry B* **2010**, *114* (32), 10496-10501.

167. Del Villano, L.; Kelland, M. A., An investigation into the kinetic hydrate inhibitor properties of two imidazolium-based ionic liquids on Structure II gas hydrate. *Chemical Engineering Science* **2010**, *65* (19), 5366-5372.

168. Cha, J.-H.; Ha, C.; Han, S.; Hong, Y. K.; Kang, S.-P.; Kang, J. W.; Kim, K.-S., Experimental Measurement of Phase Equilibrium of Hydrate in Water+ Ionic Liquid+ CH<sub>4</sub> System. *Journal of Chemical & Engineering Data* **2015**, *61* (1), 543-548.

169. Lee, W.; Shin, J.-Y.; Kim, K.-S.; Kang, S.-P., Kinetic promotion and inhibition of methane hydrate formation by morpholinium ionic liquids with



chloride and tetrafluoroborate anions. *Energy & Fuels* **2016**, *30* (5), 3879-3885.

170. Khan, M. S.; Partoon, B.; Bavoh, C. B.; Lal, B.; Mellon, N. B., Influence of tetramethylammonium hydroxide on methane and carbon dioxide gas hydrate phase equilibrium conditions. *Fluid Phase Equilibria* **2017**, *440*, 1-8.

171. Kim, K.-S.; Kang, J. W.; Kang, S.-P., Tuning ionic liquids for hydrate inhibition. *Chemical Communications* **2011**, *47* (22), 6341-6343.

172. Bavoh, C. B.; Partoon, B.; Lal, B.; Keong, L. K., Methane hydrate-liquid-vapour-equilibrium phase condition measurements in the presence of natural amino acids. *Journal of Natural Gas Science and Engineering* **2016**.

173. (a) Madeira, P. P.; Bessa, A.; Álvares-Ribeiro, L.; Raquel Aires-Barros, M.; Rodrigues, A. E.; Uversky, V. N.; Zaslavsky, B. Y., Amino acid/water interactions study: a new amino acid scale. *Journal of Biomolecular Structure and Dynamics* **2014**, *32* (6), 959-968; (b) Vaitheeswaran, S.; Thirumalai, D., Interactions between amino acid side chains in cylindrical hydrophobic nanopores with applications to peptide stability. *Proceedings of the National Academy of Sciences* **2008**, *105* (46), 17636-17641; (c) van Oss, C. J., Long-range and short-range mechanisms of

hydrophobic attraction and hydrophilic repulsion in specific and aspecific interactions. *Journal of Molecular Recognition* **2003**, *16* (4), 177-190; (d) Vyas, N.; Ojha, A. K., Interaction of alanine with small water clusters; Ala-(H<sub>2</sub>O)<sub>n</sub> (n= 1, 2 and 3): A density functional study. *Journal of Molecular Structure: THEOCHEM* **2010**, *940* (1), 95-102.

174. Mueller, U.; Huebner, S., Economic aspects of amino acids production. In *Microbial Production of l-Amino Acids*, Springer: 2003; pp 137-170.

175. (a) Ikeda, M., Amino acid production processes. In *Microbial production of l-amino acids*, Springer: 2003; pp 1-35; (b) Park, J. H.; Lee, S. Y., Towards systems metabolic engineering of microorganisms for amino acid production. *Current opinion in biotechnology* **2008**, *19* (5), 454-460.

176. El Ibrahimy, B.; Jmiai, A.; Bazzi, L.; El Issami, S., Amino Acids and their Derivatives as Corrosion Inhibitors for Metals and Alloys. *Arabian Journal of Chemistry* **2017**.

177. (a) Kinoshita, S.; Udaka, S.; Shimono, M., Studies on the amino acid fermentation. Part 1. Production of L-glutamic acid by various microorganisms. *The Journal of general and applied microbiology* **2004**, *50* (6), 331-343; (b) Udaka, S., Screening method for microorganisms

accumulating metabolites and its use in the isolation of *Micrococcus glutamicus*. *Journal of bacteriology* **1960**, 79 (5), 754.

178. Shiiio, I.; ÔTSUKA, S.-I.; TAKAHASHI, M., Effect of biotin on the bacterial formation of glutamic acid: I. Glutamate formation and cellular permeability of amino acids. *The Journal of Biochemistry* **1962**, 51 (1), 56-62.

179. Takinami, K.; Yoshii, H.; Tsuru, H.; Okada, H., Biochemical Effects of Fatty Acid and its Derivatives on L-Glutamin Acid Fermentation. *Agricultural and Biological Chemistry* **1965**, 29 (4), 351-359.

180. Nara, T.; Samejima, H.; Kinoshita, S., Effect of penicillin on amino acid fermentation. *Agricultural and Biological Chemistry* **1964**, 28 (2), 120-124.

181. Hirasawa, T.; Shimizu, H., Recent advances in amino acid production by microbial cells. *Current opinion in biotechnology* **2016**, 42, 133-146.

182. Bohé, J.; Low, A.; Wolfe, R. R.; Rennie, M. J., Human muscle protein synthesis is modulated by extracellular, not intramuscular amino acid availability: a dose-response study. *The Journal of physiology* **2003**, 552 (1), 315-324.

183. Marchesini, G.; Bianchi, G.; Merli, M.; Amodio, P.; Panella, C.; Loguercio, C.; Fanelli, F. R.; Abbiati, R.; Group, I. B. S., Nutritional supplementation with branched-chain amino acids in advanced cirrhosis: a double-blind, randomized trial. *Gastroenterology* **2003**, *124* (7), 1792-1801.
184. Ha, E.; Zemel, M. B., Functional properties of whey, whey components, and essential amino acids: mechanisms underlying health benefits for active people. *The Journal of nutritional biochemistry* **2003**, *14* (5), 251-258.
185. Leuchtenberger, W.; Huthmacher, K.; Drauz, K., Biotechnological production of amino acids and derivatives: current status and prospects. *Applied microbiology and biotechnology* **2005**, *69* (1), 1-8.
186. (a) Kilberg, M. S.; Häussinger, D., *Mammalian Amino Acid Transport*. Springer Science & Business Media: 1992; (b) Zhang, D.-Q.; Xie, B.; Gao, L.-X.; Cai, Q.-R.; Joo, H. G.; Lee, K. Y., Intramolecular synergistic effect of glutamic acid, cysteine and glycine against copper corrosion in hydrochloric acid solution. *Thin Solid Films* **2011**, *520* (1), 356-361.

187. Gathergood, N.; Garcia, M. T.; Scammells, P. J., Biodegradable ionic liquids: Part I. Concept, preliminary targets and evaluation. *Green Chemistry* **2004**, *6* (3), 166-175.
188. (a) Ashassi-Sorkhabi, H.; Ghasemi, Z.; Seifzadeh, D., The inhibition effect of some amino acids towards the corrosion of aluminum in 1M HCl+ 1M H<sub>2</sub>SO<sub>4</sub> solution. *Applied Surface Science* **2005**, *249* (1), 408-418; (b) Amin, M. A.; Khaled, K.; Mohsen, Q.; Arida, H., A study of the inhibition of iron corrosion in HCl solutions by some amino acids. *Corrosion Science* **2010**, *52* (5), 1684-1695; (c) Barouni, K.; Bazzi, L.; Salghi, R.; Mihit, M.; Hammouti, B.; Albourine, A.; El Issami, S., Some amino acids as corrosion inhibitors for copper in nitric acid solution. *Materials Letters* **2008**, *62* (19), 3325-3327; (d) Quraishi, M.; Sharma, H. K., 4-Amino-3-butyl-5-mercapto-1, 2, 4-triazole: a new corrosion inhibitor for mild steel in sulphuric acid. *Materials Chemistry and Physics* **2003**, *78* (1), 18-21.
189. Zhang, D.-Q.; Cai, Q.-R.; He, X.-M.; Gao, L.-X.; Zhou, G.-D., Inhibition effect of some amino acids on copper corrosion in HCl solution. *Materials Chemistry and Physics* **2008**, *112* (2), 353-358.

190. Hanaor, D. A.; Ghadiri, M.; Chrzanowski, W.; Gan, Y., Scalable surface area characterization by electrokinetic analysis of complex anion adsorption. *Langmuir* **2014**, *30* (50), 15143-15152.
191. Sa, J.-H.; Lee, B. R.; Park, D.-H.; Han, K.; Chun, H. D.; Lee, K.-H., Amino acids as natural inhibitors for hydrate formation in CO<sub>2</sub> sequestration. *Environmental science & technology* **2011**, *45* (13), 5885-5891.
192. Zuend, S. J.; Coughlin, M. P.; Lalonde, M. P.; Jacobsen, E. N., Scaleable catalytic asymmetric Strecker syntheses of unnatural  $\alpha$ -amino acids. *Nature* **2009**, *461*, 968.
193. (a) Clarke, H.; Bean, H.,  $\alpha$ -Aminoisobutyric Acid. *Organic Syntheses* **1931**, 4-4; (b) Kendall, E.; McKenzie, B.; Tobie, W. C.; Ayres, G. B., dl-Alanine. *Organic Syntheses* **1929**, 4-4; (c) Shibasaki, M.; Kanai, M.; Mita, T., The catalytic asymmetric Strecker reaction. *Organic Reactions* **2008**.
194. Okafor, N., *Modern industrial microbiology and biotechnology*. CRC Press: 2016.
195. Ivanov, K.; Stoimenova, A.; Obreshkova, D.; Saso, L., Biotechnology in the production of pharmaceutical industry ingredients: amino acids. *Biotechnology & Biotechnological Equipment* **2013**, *27* (2), 3620-3626.

196. Ault, A., The monosodium glutamate story: the commercial production of MSG and other amino acids. *Journal of chemical education* **2004**, *81* (3), 347.
197. (a) Duthaler, R. O., Recent developments in the stereoselective synthesis of  $\alpha$ -aminoacids. *Tetrahedron* **1994**, *50* (6), 1539-1650; (b) Hermann, T., Industrial production of amino acids by coryneform bacteria. *Journal of biotechnology* **2003**, *104* (1-3), 155-172; (c) Kumagai, H., Microbial production of amino acids in Japan. In *History of Modern Biotechnology I*, Springer: 2000; pp 71-85.
198. Pearlstone, D. B.; Lee, J. I.; Alexander, R. H.; Chang, T. H.; Brennan, M. F.; Burt, M., Effect of enteral and parenteral nutrition on amino acid levels in cancer patients. *Journal of Parenteral and Enteral Nutrition* **1995**, *19* (3), 204-208.
199. (a) Newton, W. A.; Snell, E. E., Formation and interrelationships of tryptophanase and tryptophan synthetases in *Escherichia coli*. *Journal of bacteriology* **1965**, *89* (2), 355-364; (b) DEHGHAN, S. M.; FOULADI, J.; MOUSAVINEZHAD, S., L-tryptophan production by *Escherichia coli* in the presence of Iranian cane molasses. **2010**.

200. Araki, K.; Ozeki, T., Amino acids. *Kirk-Othmer Encyclopedia of Chemical Technology* **1992**.
201. Kusumoto, I., Industrial production of L-glutamine. *The Journal of nutrition* **2001**, *131* (9), 2552S-2555S.
202. KINOSHITA, S.; UDAKA, S.; SHIMONO, M., Studies on the amino acid fermentation. *The Journal of general and applied microbiology* **1957**, *3* (3), 193-205.
203. Kinoshita, S.; Tanaka, K.; Udaka, S.; Akita, S. In *Glutamic acid fermentation*, Proc Intern Symp Enzyme Chem, 1957; pp 464-468.
204. (a) Kinoshita, S., The production of amino acids by fermentation processes. In *Advances in applied microbiology*, Elsevier: 1959; Vol. 1, pp 201-214; (b) Chibata, I.; Tosa, T.; Sato, T., Continuous production of L-aspartic acid. *Applied biochemistry and biotechnology* **1986**, *13* (3), 231-240; (c) Kuethe, J. T.; Gauthier, D. R.; Beutner, G. L.; Yasuda, N., A Concise Synthesis of (S)-N-Ethoxycarbonyl- $\alpha$ -methylvaline. *The Journal of organic chemistry* **2007**, *72* (19), 7469-7472.
205. (a) Debabov, V. G., The threonine story. In *Microbial Production of L-Amino Acids*, Springer: 2003; pp 113-136; (b) Schneider, J.; Niermann, K.; Wendisch, V. F., Production of the amino acids L-glutamate, L-lysine,



L-ornithine and L-arginine from arabinose by recombinant *Corynebacterium glutamicum*. *Journal of biotechnology* **2011**, *154* (2-3), 191-198.

206. Cordwell, S. J., Microbial genomes and “missing” enzymes: redefining biochemical pathways. *Archives of microbiology* **1999**, *172* (5), 269-279.

207. Sato, T.; Mori, T.; Tosa, T.; Chibata, I.; Furui, M.; Yamashita, K.; Sumi, A., Engineering analysis of continuous production of L-aspartic acid by immobilized *Escherichia coli* cells in fixed beds. *Biotechnology and bioengineering* **1975**, *17* (12), 1797-1804.

208. Katchalski-Katzir, E.; Kasher, R.; Fridkin, M., Amino Acids: Physicochemical Properties. In *Encyclopedic Reference of Genomics and Proteomics in Molecular Medicine*, Springer Berlin Heidelberg: Berlin, Heidelberg, 2006; pp 55-68.

209. Nelson, D. L.; Lehninger, A. L.; Cox, M. M., *Lehninger principles of biochemistry*. Macmillan: 2008.

210. Katchalski-Katzir, E., Synthesis, physicochemical and biological properties of poly-alpha-amino acids--the simplest of protein models. *Acta Biochimica Polonica* **1996**, *43* (1), 217-226.

211. Chipot, C.; Maigret, B.; Rivail, J. L.; Scheraga, H. A., Modeling amino acid side chains. 1. Determination of net atomic charges from ab initio self-consistent-field molecular electrostatic properties. *The Journal of Physical Chemistry* **1992**, *96* (25), 10276-10284.
212. Blish, M. J.; Schlaeger, A. J., Recovery of amino acids. Google Patents: 1957.
213. Itoh, H.; Thien, M.; Hatton, T.; Wang, D., A liquid emulsion membrane process for the separation of amino acids. *Biotechnology and bioengineering* **1990**, *35* (9), 853-860.
214. Adachi, M.; Harada, M.; Shioi, A.; Sato, Y., Extraction of amino acids to microemulsion. *The Journal of Physical Chemistry* **1991**, *95* (20), 7925-7931.
215. Wang, J.; Pei, Y.; Zhao, Y.; Hu, Z., Recovery of amino acids by imidazolium based ionic liquids from aqueous media. *Green Chemistry* **2005**, *7* (4), 196-202.
216. Holbrey, J. D.; Visser, A. E.; Spear, S. K.; Reichert, W. M.; Swatloski, R. P.; Broker, G. A.; Rogers, R. D., Mercury (II) partitioning from aqueous solutions with a new, hydrophobic ethylene-glycol

functionalized bis-imidazolium ionic liquid. *Green chemistry* **2003**, 5 (2), 129-135.

217. (a) Branco, L. C.; Crespo, J. G.; Afonso, C. A., Studies on the selective transport of organic compounds by using ionic liquids as novel supported liquid membranes. *Chemistry-A European Journal* **2002**, 8 (17), 3865-3871; (b) Branco, L. C.; Crespo, J. G.; Afonso, C. A., Highly selective transport of organic compounds by using supported liquid membranes based on ionic liquids. *Angewandte Chemie* **2002**, 114 (15), 2895-2897.

218. Leodidis, E. B.; Hatton, T. A., Effects of average molecular charge on amino acid interfacial partitioning in reversed micelles. *Journal of colloid and interface science* **1991**, 147 (1), 163-177.

219. Molinari, R.; De Bartolo, L.; Drioli, E., Coupled transport of amino acids through a supported liquid membrane. I. Experimental optimization. *Journal of membrane science* **1992**, 73 (2-3), 203-215.

220. Noguchi, H.; Nakamura, H.; Nagamatsu, M.; Yoshio, M., The Solvent Extration of Amino Acids with Crown Ether. *Bulletin of the Chemical Society of Japan* **1982**, 55 (1), 156-158.

221. (a) Mutihac, L.; Patroescu, I., CROWN ETHERS IN SOLVENT-EXTRACTION PROCESSES. 1. THE EFFECTS OF VARIOUS

SOLVENTS ON THE AMINO-ACID EXTRACTION. *REVUE ROUMAINE DE CHIMIE* **1992**, 37 (4), 511-514; (b) Lipkowitz, K. B.; Raghothama, S.; Yang, J. A., Enantioselective binding of tryptophan by alpha.-cyclodextrin. *Journal of the American Chemical Society* **1992**, 114 (5), 1554-1562.

222. (a) Bryjak, M.; Wieczorek, P.; Kafarski, P.; Lejczak, B., Transport of amino acids and their phosphonic acid analogues through supported liquid membranes containing macrocyclic carriers. Experimental parameters. *Journal of membrane science* **1991**, 56 (2), 167-180; (b) Chen, H.; Ogo, S.; Fish, R. H., Bioorganometallic chemistry. 8. The molecular recognition of aromatic and aliphatic amino acids and substituted aromatic and aliphatic carboxylic acid guests with Supramolecular ( $\eta^5$ -Pentamethylcyclopentadienyl) rhodium– Nucleobase, nucleoside, and nucleotide cyclic Trimer hosts via non-covalent  $\pi$ –  $\pi$  and hydrophobic interactions in water: steric, electronic, and conformational parameters. *Journal of the American Chemical Society* **1996**, 118 (21), 4993-5001; (c) Kimura, E.; Fujioka, H.; Kodama, M., A new ditopic receptor molecule for ionic guest molecules. *Journal of the Chemical Society, Chemical Communications* **1986**, (15), 1158-1159.

223. Smirnova, S. V.; Torocheshnikova, I. I.; Formanovsky, A. A.; Pletnev, I. V., Solvent extraction of amino acids into a room temperature ionic liquid with dicyclohexano-18-crown-6. *Analytical and bioanalytical chemistry* **2004**, *378* (5), 1369-1375.
224. Sa, J.-H.; Kwak, G.-H.; Han, K.; Ahn, D.; Lee, K.-H., Gas hydrate inhibition by perturbation of liquid water structure. *Scientific reports* **2015**, *5*.
225. Sa, J.-H.; Kwak, G.-H.; Lee, B. R.; Park, D.-H.; Han, K.; Lee, K.-H., Hydrophobic amino acids as a new class of kinetic inhibitors for gas hydrate formation. *Scientific reports* **2013**, *3*, 2428.
226. Ide, M.; Maeda, Y.; Kitano, H., Effect of hydrophobicity of amino acids on the structure of water. *The Journal of Physical Chemistry B* **1997**, *101* (35), 7022-7026.
227. (a) Zeng, H.; Wilson, L. D.; Walker, V. K.; Ripmeester, J. A., Effect of antifreeze proteins on the nucleation, growth, and the memory effect during tetrahydrofuran clathrate hydrate formation. *Journal of the American Chemical Society* **2006**, *128* (9), 2844-2850; (b) Zeng, H.; Walker, V. K.; Ripmeester, J. A., Approaches to the design of better low-dosage gas hydrate inhibitors. *Angewandte Chemie* **2007**, *119* (28), 5498-5500.

228. Roosta, H.; Dashti, A.; Mazloumi, S. H.; Varaminian, F., Inhibition properties of new amino acids for prevention of hydrate formation in carbon dioxide–water system: Experimental and modeling investigations. *Journal of Molecular Liquids* **2016**, *215*, 656-663.
229. (a) Kelland, M. A., History of the Development of Low Dosage Hydrate Inhibitors. *Energy & Fuels* **2006**, *20* (3), 825-847; (b) Norland, A. K.; Kelland, M. A., Crystal growth inhibition of tetrahydrofuran hydrate with bis-and polyquaternary ammonium salts. *Chemical engineering science* **2012**, *69* (1), 483-491.
230. (a) Xu, P.; Lang, X.; Fan, S.; Wang, Y.; Chen, J., Molecular dynamics simulation of methane hydrate growth in the presence of the natural product pectin. *The Journal of Physical Chemistry C* **2016**, *120* (10), 5392-5397; (b) Xu, S.; Fan, S.; Fang, S.; Lang, X.; Wang, Y.; Chen, J., Pectin as an extraordinary natural kinetic hydrate inhibitor. *Scientific reports* **2016**, *6*.
231. Geiger, A.; Rahman, A.; Stillinger, F., Molecular dynamics study of the hydration of Lennard-Jones solutes. *The Journal of Chemical Physics* **1979**, *70* (1), 263-276.
232. Pertselmidis, A.; Saxena, A. M.; Soper, A. K.; Head-Gordon, T.; Glaeser, R. M., Direct evidence for modified solvent structure within the

hydration shell of a hydrophobic amino acid. *Proceedings of the National Academy of Sciences* **1996**, *93* (20), 10769-10774.

233. Carver, T. J.; Drew, M. G.; Rodger, P. M., Molecular dynamics calculations of N-methylpyrrolidone in liquid water. *Physical chemistry chemical physics* **1999**, *1* (8), 1807-1816.

234. Veluswamy, H. P.; Lee, P. Y.; Premasinghe, K.; Linga, P., Effect of bio-friendly amino acids on the kinetics of methane hydrate formation and dissociation. *Industrial & Engineering Chemistry Research* **2017**.

235. Naeiji, P.; Arjomandi, A.; Varaminian, F., Amino acids as kinetic inhibitors for tetrahydrofuran hydrate formation: experimental study and kinetic modeling. *Journal of Natural Gas Science and Engineering* **2014**, *21*, 64-70.

236. Rad, S. A.; Khodaverdilo, K. R.; Karamoddin, M.; Varaminian, F.; Peyvandi, K., Kinetic study of amino acids inhibition potential of glycine and l-leucine on the ethane hydrate formation. *Journal of Natural Gas Science and Engineering* **2015**, *26*, 819-826.

237. Liu, Y.; Chen, B.; Chen, Y.; Zhang, S.; Guo, W.; Cai, Y.; Tan, B.; Wang, W., Methane storage in a hydrated form as promoted by leucines for

possible application to natural gas transportation and storage. *Energy Technology* **2015**, *3* (8), 815-819.

238. Veluswamy, H. P.; Hong, Q. W.; Linga, P., Morphology study of methane hydrate formation and dissociation in the presence of amino acid. *Crystal Growth & Design* **2016**, *16* (10), 5932-5945.

239. Talaghat, M., Experimental investigation of induction time for double gas hydrate formation in the simultaneous presence of the PVP and L-Tyrosine as kinetic inhibitors in a mini flow loop apparatus. *Journal of Natural Gas Science and Engineering* **2014**, *19*, 215-220.

240. Kakati, H.; Mandal, A.; Laik, S., Synergistic effect of Polyvinylpyrrolidone (PVP) and L-tyrosine on kinetic inhibition of CH<sub>4</sub>+ C<sub>2</sub>H<sub>6</sub>+ C<sub>3</sub>H<sub>8</sub> hydrate formation. *Journal of Natural Gas Science and Engineering* **2016**, *34*, 1361-1368.

241. Hecht, D.; Tadesse, L.; Walters, L., Correlating hydration shell structure with amino acid hydrophobicity. *Journal of the American Chemical Society* **1993**, *115* (8), 3336-3337.

242. Sa, J.-H.; Kwak, G.-H.; Lee, B. R.; Ahn, D.; Lee, K.-H., Abnormal incorporation of amino acids into the gas hydrate crystal lattice. *Physical Chemistry Chemical Physics* **2014**, *16* (48), 26730-26734.



243. (a) Daraboina, N.; Linga, P.; Ripmeester, J.; Walker, V. K.; Englezos, P., Natural gas hydrate formation and decomposition in the presence of kinetic inhibitors. 2. Stirred reactor experiments. *Energy & Fuels* **2011**, *25* (10), 4384-4391; (b) Townson, I.; Walker, V. K.; Ripmeester, J. A.; Englezos, P., Bacterial inhibition of methane clathrate hydrates formed in a stirred autoclave. *Energy & Fuels* **2012**, *26* (12), 7170-7175; (c) Del Villano, L.; Kommedal, R.; Kelland, M. A., Class of kinetic hydrate inhibitors with good biodegradability. *Energy & Fuels* **2008**, *22* (5), 3143-3149.
244. Foo, C. W.; Ruan, L.; Lou, X., The inhibition performance in relation to the adsorption of a polymeric kinetic inhibitor towards THF hydrates in the presence of methanol, ethanol and monoethylene glycol. *Journal of Natural Gas Science and Engineering*.
245. O'Reilly, R.; Jeong, N. S.; Chua, P. C.; Kelland, M. A., Missing poly (N-vinyl lactam) kinetic hydrate inhibitor: high-pressure kinetic hydrate inhibition of structure II gas hydrates with poly (N-vinyl piperidone) and other poly (N-vinyl lactam) homopolymers. *Energy & Fuels* **2011**, *25* (10), 4595-4599.

246. Zhao, X.; Qiu, Z.; Zhou, G.; Huang, W., *Synergism of thermodynamic hydrate inhibitors on the performance of poly (vinyl pyrrolidone) in deepwater drilling fluid*. 2015; Vol. 23.
247. Lee, W.; Shin, J.-Y.; Cha, J.-H.; Kim, K.-S.; Kang, S.-P., Inhibition effect of ionic liquids and their mixtures with poly (N-vinylcaprolactam) on methane hydrate formation. *Journal of Industrial and Engineering Chemistry* **2016**, *38*, 211-216.
248. Lee, W.; Shin, J.-Y.; Kim, K.-S.; Kang, S.-P., Synergetic Effect of Ionic Liquids on the Kinetic Inhibition Performance of Poly (N-vinylcaprolactam) for Natural Gas Hydrate Formation. *Energy & Fuels* **2016**, *30* (11), 9162-9169.
249. Yang, J.; Tohidi, B., Characterization of inhibition mechanisms of kinetic hydrate inhibitors using ultrasonic test technique. *Chemical Engineering Science* **2011**, *66* (3), 278-283.
250. Kim, J.; Shin, K.; Seo, Y.; Cho, S. J.; Lee, J. D., Synergistic Hydrate Inhibition of Monoethylene Glycol with Poly(vinylcaprolactam) in Thermodynamically Underinhibited System. *The Journal of Physical Chemistry B* **2014**, *118* (30), 9065-9075.

251. (a) Michael, G.; MarkáRodger, P., Characterisation of the {111} growth planes of a type II gas hydrate and study of the mechanism of kinetic inhibition by poly (vinylpyrrolidone). *Journal of the Chemical Society, Faraday Transactions* **1996**, *92* (24), 5029-5033; (b) Manteghian, M.; Safavi, S. M. M.; Mohammadi, A., The equilibrium conditions, hydrate formation and dissociation rate and storage capacity of ethylene hydrate in presence of 1, 4-dioxane. *Chemical engineering journal* **2013**, *217*, 379-384.
252. Talaghat, M. R., Intensification of the performance of kinetic inhibitors in the presence of polyethylene oxide and polypropylene oxide for simple gas hydrate formation in a flow mini-loop apparatus. *Fluid Phase Equilibria* **2010**, *289* (2), 129-134.
253. Bailey, F.; Callard, R., Some properties of poly (ethylene oxide) 1 in aqueous solution. *Journal of applied polymer science* **1959**, *1* (1), 56-62.
254. (a) Englezos, P.; Ngan, Y. T., Effect of polyethylene oxide on gas hydrate phase equilibria. *Fluid Phase Equilibria* **1994**, *92*, 271-288; (b) Englezos, P.; Hall, S., Phase equilibrium data on carbon dioxide hydrate in the presence of electrolytes, water soluble polymers and montmorillonite. *The Canadian Journal of Chemical Engineering* **1994**, *72* (5), 887-893.

255. Lee, J. D.; Englezos, P., Enhancement of the performance of gas hydrate kinetic inhibitors with polyethylene oxide. *Chemical engineering science* **2005**, *60* (19), 5323-5330.
256. Lee, J. D.; Englezos, P., Unusual kinetic inhibitor effects on gas hydrate formation. *Chemical Engineering Science* **2006**, *61* (5), 1368-1376.
257. (a) Sun, Z.-g.; Wang, R.; Ma, R.; Guo, K.; Fan, S., Natural gas storage in hydrates with the presence of promoters. *Energy Conversion and Management* **2003**, *44* (17), 2733-2742; (b) Wang, W.; Bray, C. L.; Adams, D. J.; Cooper, A. I., Methane storage in dry water gas hydrates. *Journal of the American Chemical Society* **2008**, *130* (35), 11608-11609; (c) Hao, W.; Wang, J.; Fan, S.; Hao, W., Evaluation and analysis method for natural gas hydrate storage and transportation processes. *Energy conversion and management* **2008**, *49* (10), 2546-2553.
258. (a) Naeiji, P.; Mottahedin, M.; Varaminian, F., Separation of methane–ethane gas mixtures via gas hydrate formation. *Separation and Purification Technology* **2014**, *123*, 139-144; (b) Ricaurte, M.; Dicharry, C.; Renaud, X.; Torr , J.-P., Combination of surfactants and organic compounds for boosting CO<sub>2</sub> separation from natural gas by clathrate hydrate formation. *Fuel* **2014**, *122*, 206-217; (c) Liu, H.; Mu, L.; Wang, B.; Liu, B.;

- Wang, J.; Zhang, X.; Sun, C.; Chen, J.; Jia, M.; Chen, G., Separation of ethylene from refinery dry gas via forming hydrate in w/o dispersion system. *Separation and Purification Technology* **2013**, *116*, 342-350.
259. ZareNezhad, B.; Mottahedin, M., A rigorous mechanistic model for predicting gas hydrate formation kinetics: the case of CO<sub>2</sub> recovery and sequestration. *Energy Conversion and Management* **2012**, *53* (1), 332-336.
260. (a) Park, K.-n.; Hong, S. Y.; Lee, J. W.; Kang, K. C.; Lee, Y. C.; Ha, M.-G.; Lee, J. D., A new apparatus for seawater desalination by gas hydrate process and removal characteristics of dissolved minerals (Na<sup>+</sup>, Mg<sup>2+</sup>, Ca<sup>2+</sup>, K<sup>+</sup>, B<sup>3+</sup>). *Desalination* **2011**, *274* (1), 91-96; (b) Cha, J.-H.; Seol, Y., Increasing gas hydrate formation temperature for desalination of high salinity produced water with secondary guests. *ACS Sustainable Chemistry & Engineering* **2013**, *1* (10), 1218-1224.
261. Takeuchi, F.; Ohmura, R.; Yasuoka, K., Statistical-thermodynamics modeling of clathrate-hydrate-forming systems suitable as working media of a hydrate-based refrigeration system. *International Journal of Thermophysics* **2009**, *30* (6), 1838-1852.

262. Zhong, D.-L.; Daraboina, N.; Englezos, P., Recovery of CH<sub>4</sub> from coal mine model gas mixture (CH<sub>4</sub>/N<sub>2</sub>) by hydrate crystallization in the presence of cyclopentane. *Fuel* **2013**, *106*, 425-430.
263. Kondo, W.; Ohtsuka, K.; Ohmura, R.; Takeya, S.; Mori, Y. H., Clathrate-hydrate formation from a hydrocarbon gas mixture: Compositional evolution of formed hydrate during an isobaric semi-batch hydrate-forming operation. *Applied Energy* **2014**, *113*, 864-871.
264. (a) Javanmardi, J.; Nasrifar, K.; Najibi, S.; Moshfeghian, M., Economic evaluation of natural gas hydrate as an alternative for natural gas transportation. *Applied Thermal Engineering* **2005**, *25* (11), 1708-1723; (b) Kumar, R.; Linga, P.; Moudrakovski, I.; Ripmeester, J. A.; Englezos, P., Structure and kinetics of gas hydrates from methane/ethane/propane mixtures relevant to the design of natural gas hydrate storage and transport facilities. *AIChE journal* **2008**, *54* (8), 2132-2144.
265. Zhong, Y.; Rogers, R., Surfactant effects on gas hydrate formation. *Chemical Engineering Science* **2000**, *55* (19), 4175-4187.
266. Sain, K.; Gupta, H., Gas hydrates in India: Potential and development. *Gondwana Research* **2012**, *22* (2), 645-657.

267. Mork, M.; Gudmundsson, J. S. In *Hydrate formation rate in a continuous stirred tank reactor: experimental results and bubble-to-crystal model*, Proceedings of the Fourth International Conference on Gas Hydrates, Yokohama, 2002.
268. Luo, Y. T.; Zhu, J. H.; Fan, S. S.; Chen, G. J., Study on the kinetics of hydrate formation in a bubble column. *Chemical Engineering Science* **2007**, *62* (4), 1000-1009.
269. Kim, N. J.; Park, S. S.; Shin, S. W.; Hyun, J. H.; Chun, W., An experimental investigation into the effects of zeolites on the formation of methane hydrates. *International Journal of Energy Research* **2015**, *39* (1), 26-32.
270. Fan, S.; Yang, L.; Wang, Y.; Lang, X.; Wen, Y.; Lou, X., Rapid and high capacity methane storage in clathrate hydrates using surfactant dry solution. *Chemical Engineering Science* **2014**, *106*, 53-59.
271. Linga, P.; Daraboina, N.; Ripmeester, J. A.; Englezos, P., Enhanced rate of gas hydrate formation in a fixed bed column filled with sand compared to a stirred vessel. *Chemical Engineering Science* **2012**, *68* (1), 617-623.

272. (a) Ricaurte, M.; Dicharry, C.; Broseta, D.; Renaud, X.; Torr , J.-P., CO<sub>2</sub> removal from a CO<sub>2</sub>–CH<sub>4</sub> gas mixture by clathrate hydrate formation using THF and SDS as water-soluble hydrate promoters. *Industrial & Engineering Chemistry Research* **2012**, *52* (2), 899-910; (b) Torr , J.-P.; Ricaurte, M.; Dicharry, C.; Broseta, D., CO<sub>2</sub> enclathration in the presence of water-soluble hydrate promoters: Hydrate phase equilibria and kinetic studies in quiescent conditions. *Chemical engineering science* **2012**, *82*, 1-13.
273. (a) Lim, Y.-A.; Babu, P.; Kumar, R.; Linga, P., Morphology of carbon dioxide–hydrogen–cyclopentane hydrates with or without sodium dodecyl sulfate. *Crystal Growth & Design* **2013**, *13* (5), 2047-2059; (b) Kang, S.-P.; Lee, J.-W., Kinetic behaviors of CO<sub>2</sub> hydrates in porous media and effect of kinetic promoter on the formation kinetics. *Chemical Engineering Science* **2010**, *65* (5), 1840-1845.
274. (a) Englezos, P.; Kalogerakis, N.; Dholabhai, P.; Bishnoi, P., Kinetics of gas hydrate formation from mixtures of methane and ethane. *Chemical Engineering Science* **1987**, *42* (11), 2659-2666; (b) Vysniauskas, A.; Bishnoi, P., A kinetic study of methane hydrate formation. *Chemical Engineering Science* **1983**, *38* (7), 1061-1072; (c) Vysniauskas, A.; Bishnoi,



P., Kinetics of ethane hydrate formation. *Chemical Engineering Science* **1985**, *40* (2), 299-303.

275. Hao, W.; Wang, J.; Fan, S.; Hao, W., Study on methane hydration process in a semi-continuous stirred tank reactor. *Energy Conversion and Management* **2007**, *48* (3), 954-960.

276. He, Y.; Rudolph, E. S. J.; Zitha, P. L. J.; Golombok, M., Kinetics of CO<sub>2</sub> and methane hydrate formation: An experimental analysis in the bulk phase. *Fuel* **2011**, *90* (1), 272-279.

277. Xiao, P.; Yang, X.-M.; Sun, C.-Y.; Cui, J.-L.; Li, N.; Chen, G.-J., Enhancing methane hydrate formation in bulk water using vertical reciprocating impact. *Chemical Engineering Journal* **2018**, *336*, 649-658.

278. Englezos, P.; Kalogerakis, N.; Dholabhai, P. D.; Bishnoi, P. R., Kinetics of formation of methane and ethane gas hydrates. *Chemical Engineering Science* **1987**, *42* (11), 2647-2658.

279. Kim, H. C.; Bishnoi, P. R.; Heidemann, R. A.; Rizvi, S. S. H., Kinetics of methane hydrate decomposition. *Chemical Engineering Science* **1987**, *42* (7), 1645-1653.

280. Ke, W.; Svartaas, T. M. In *Effects of stirring and cooling on methane hydrate formation in a high-pressure isochoric cell*, Proceedings of the 7th

International Conference on Gas Hydrates, Edinburgh, Scotland, United Kingdom, 2011.

281. Turner, D. J.; Miller, K. T.; Sloan, E. D., Methane hydrate formation and an inward growing shell model in water-in-oil dispersions. *Chemical Engineering Science* **2009**, *64* (18), 3996-4004.

282. Ribeiro, C. P.; Lage, P. L., Modelling of hydrate formation kinetics: State-of-the-art and future directions. *Chemical Engineering Science* **2008**, *63* (8), 2007-2034.

283. Skovborg, P.; Ng, H.; Rasmussen, P.; Mohn, U., Measurement of induction times for the formation of methane and ethane gas hydrates. *Chemical Engineering Science* **1993**, *48* (3), 445-453.

284. Parent, J.; Bishnoi, P., Investigations into the nucleation behaviour of methane gas hydrates. *Chemical Engineering Communications* **1996**, *144* (1), 51-64.

285. Englezos, P.; Kalogerakis, N.; Dholabhai, P.; Bishnoi, P., Kinetics of formation of methane and ethane gas hydrates. *Chemical Engineering Science* **1987**, *42* (11), 2647-2658.

286. Mork, M., Formation rate of natural gas hydrate-reactor experiments and models. **2002**.

287. Ke, W.; Svartaas, T. M., Effects of stirring and cooling on methane hydrate formation in a high-pressure isochoric cell. *Journal of Materials Science and Engineering. B* **2013**, *3* (7B), 436.
288. Orella, C. J.; Kirwan, D., The solubility of amino acids in mixtures of water and aliphatic alcohols. *Biotechnology progress* **1989**, *5* (3), 89-91.
289. (a) Kidera, A.; Konishi, Y.; Oka, M.; Ooi, T.; Scheraga, H. A., Statistical analysis of the physical properties of the 20 naturally occurring amino acids. *Journal of Protein Chemistry* **1985**, *4* (1), 23-55; (b) Kawashima, S.; Kanehisa, M., AAindex: amino acid index database. *Nucleic acids research* **2000**, *28* (1), 374-374; (c) Olivier, M.; Hainaut, P., IARC TP53 Database. *Encyclopedia of Cancer* **2011**, 1799-1802.
290. Kyte, J.; Doolittle, R. F., A simple method for displaying the hydropathic character of a protein. *Journal of molecular biology* **1982**, *157* (1), 105-132.
291. (a) Keshavarz, L.; Javanmardi, J.; Eslamimanesh, A.; Mohammadi, A. H., Experimental measurement and thermodynamic modeling of methane hydrate dissociation conditions in the presence of aqueous solution of ionic liquid. *Fluid Phase Equilibria* **2013**, *354*, 312-318; (b) Tumba, K.; Reddy, P.; Naidoo, P.; Ramjugernath, D.; Eslamimanesh, A.; Mohammadi, A. H.;

Richon, D., Phase equilibria of methane and carbon dioxide clathrate hydrates in the presence of aqueous solutions of tributylmethylphosphonium methylsulfate ionic liquid. *Journal of Chemical & Engineering Data* **2011**, *56* (9), 3620-3629.

292. Bell, S., A beginner's guide to uncertainty of measurement. 2001.

293. Carroll, J., Chapter 3 - Hand Calculation Methods. In *Natural Gas Hydrates (Third Edition)*, Carroll, J., Ed. Gulf Professional Publishing: Boston, 2014; pp 59-110.

294. Zahedi, G.; Karami, Z.; Yaghoobi, H., Prediction of hydrate formation temperature by both statistical models and artificial neural network approaches. *Energy Conversion and Management* **2009**, *50* (8), 2052-2059.

295. Clarke, M. A.; Bishnoi, P. R., Determination of the intrinsic kinetics of CO gas hydrate formation using in situ particle size analysis. *Chemical Engineering Science* **2005**, *60* (3), 695-709.

296. ZareNezhad, B.; Varaminian, F., A generalized macroscopic kinetic model for description of gas hydrate formation processes in isothermal–isochoric systems. *Energy Conversion and Management* **2012**, *57*, 125-130.

297. Ilani-Kashkouli, P.; Mohammadi, A. H.; Naidoo, P.; Ramjugernath, D., Hydrate phase equilibria for CO<sub>2</sub>, CH<sub>4</sub>, or N<sub>2</sub>+

tetrabutylphosphonium bromide (TBPB) aqueous solution. *Fluid Phase Equilibria* **2016**, *411*, 88-92.

298. Ohmura, R.; Takeya, S.; Uchida, T.; Ebinuma, T., Clathrate Hydrate Formed with Methane and 2-Propanol: Confirmation of Structure II Hydrate Formation. *Industrial & Engineering Chemistry Research* **2004**, *43* (16), 4964-4966.

299. Mohammad-Taheri, M.; Zarringhalam Moghaddam, A.; Nazari, K.; Gholipour Zanjani, N., The role of thermal path on the accuracy of gas hydrate phase equilibrium data using isochoric method. *Fluid Phase Equilibria* **2013**, *338*, 257-264.

300. Semenov, A. P.; Medvedev, V. I.; Gushchin, P. A.; Yakushev, V. S., Effect of heating rate on the accuracy of measuring equilibrium conditions for methane and argon hydrates. *Chemical Engineering Science* **2015**, *137*, 161-169.

301. Tohidi, B.; Burgass, R.; Danesh, A.; Østergaard, K.; Todd, A., Improving the accuracy of gas hydrate dissociation point measurements. *Annals of the New York Academy of Sciences* **2000**, *912* (1), 924-931.

302. Kiyono, F.; Tajima, H.; Ogasawara, K.; Yamasaki, A., Method for predicting the dissociation condition of a simple hydrate phase on an H–Lw–

- V line in isochoric operation. *Fluid Phase Equilibria* **2005**, *235* (1), 112-121.
303. Kelland, M. A.; Moi, N.; Howarth, M., Breakthrough in Synergists for Kinetic Hydrate Inhibitor Polymers, Hexaalkylguanidinium Salts: Tetrahydrofuran Hydrate Crystal Growth Inhibition and Synergism with Polyvinylcaprolactam. *Energy & Fuels* **2013**, *27* (2), 711-716.
304. Tariq, M.; Connor, E.; Thompson, J.; Khraisheh, M.; Atilhan, M.; Rooney, D., Doubly dual nature of ammonium-based ionic liquids for methane hydrates probed by rocking-rig assembly. *RSC Advances* **2016**, *6* (28), 23827-23836.
305. Kim, S. M.; Lee, J. D.; Lee, H. J.; Lee, E. K.; Kim, Y., Gas hydrate formation method to capture the carbon dioxide for pre-combustion process in IGCC plant. *international journal of hydrogen energy* **2011**, *36* (1), 1115-1121.
306. Cha, M.; Shin, K.; Seo, Y.; Shin, J.-Y.; Kang, S.-P., Catastrophic Growth of Gas Hydrates in the Presence of Kinetic Hydrate Inhibitors. *The Journal of Physical Chemistry A* **2013**, *117* (51), 13988-13995.
307. Tariq, M.; Atilhan, M.; Khraisheh, M.; Othman, E.; Castier, M.; García, G.; Aparicio, S.; Tohidi, B., Experimental and DFT Approach on the

Determination of Natural Gas Hydrate Equilibrium with the Use of Excess N<sub>2</sub> and Choline Chloride Ionic Liquid as an Inhibitor. *Energy & Fuels* **2016**, *30* (4), 2821-2832.

308. Sharma, S.; Gupta, A.; Kashyap, H. K., How the structure of pyrrolidinium ionic liquids is susceptible to high pressure. *The Journal of Physical Chemistry B* **2016**, *120* (12), 3206-3214.

309. Koh, C. A.; Westacott, R. E.; Zhang, W.; Hirachand, K.; Creek, J. L.; Soper, A. K., Mechanisms of gas hydrate formation and inhibition. *Fluid Phase Equilibria* **2002**, *194–197* (0), 143-151.

310. Shin, B. S.; Kim, E. S.; Kwak, S. K.; Lim, J. S.; Kim, K.-S.; Kang, J. W., Thermodynamic inhibition effects of ionic liquids on the formation of condensed carbon dioxide hydrate. *Fluid Phase Equilibria* **2014**, *382*, 270-278.

311. Tariq, M.; Esperanca, J. M. S. S.; Soromenho, M. R. C.; Rebelo, L. P. N.; Lopes, J. N. C., Shifts in the temperature of maximum density (TMD) of ionic liquid aqueous solutions. *Physical Chemistry Chemical Physics* **2013**, *15* (26), 10960-10970.

312. Panter, J. L.; Ballard, A. L.; Sum, A. K.; Sloan, E. D.; Koh, C. A., Hydrate Plug Dissociation via Nitrogen Purge: Experiments and Modeling. *Energy & Fuels* **2011**, *25* (6), 2572-2578.
313. Obanijesu, E. O.; Barifcani, A.; Pareek, V. K.; Tade, M. O., Experimental study on feasibility of H<sub>2</sub> and N<sub>2</sub> as hydrate inhibitors in natural gas pipelines. *Journal of Chemical & Engineering Data* **2014**, *59* (11), 3756-3766.
314. Bahadori, A., Correlation accurately predicts hydrate forming pressure of pure components. *Journal of Canadian Petroleum Technology* **2008**, *47* (02).
315. Russina, O.; Celso, F. L.; Triolo, A., Pressure-responsive mesoscopic structures in room temperature ionic liquids. *Physical Chemistry Chemical Physics* **2015**, *17* (44), 29496-29500.
316. Salminen, J.; Papaiconomou, N.; Kumar, R. A.; Lee, J.-M.; Kerr, J.; Newman, J.; Prausnitz, J. M., Physicochemical properties and toxicities of hydrophobic piperidinium and pyrrolidinium ionic liquids. *Fluid Phase Equilibria* **2007**, *261* (1), 421-426.



317. Lederhos, J.; Long, J.; Sum, A.; Christiansen, R.; Sloan, E., Effective kinetic inhibitors for natural gas hydrates. *Chemical Engineering Science* **1996**, *51* (8), 1221-1229.
318. Vojta, D.; Vazdar, M., The study of hydrogen bonding and pi-dots, three dots, centered-pi interactions in phenol-dots, three dots, centered-ethynylbenzene complex by IR spectroscopy. *Spectrochimica Acta. Part A, Molecular and biomolecular spectroscopy* **2014**, *132*, 6-14.
319. Ripmeester, J. A.; Alavi, S., Molecular simulations of methane hydrate nucleation. *ChemPhysChem* **2010**, *11* (5), 978-980.
320. Indirect Food Additives and Polymers: Migration and Toxicology By Victor O. Sheftel (Ministry of Health, State of Israel, Jerusalem). Lewis Publishers: Boca Raton, FL. 2000. xvi + 1304 pp. \$129.95. ISBN 1-56670-499-5. *Journal of the American Chemical Society* **2000**, *122* (43), 10742-10742.
321. Davis, J. G.; Gierszal, K. P.; Wang, P.; Ben-Amotz, D., Water structural transformation at molecular hydrophobic interfaces. *Nature* **2012**, *491* (7425), 582-585.

322. Kang, S.-P.; Kim, E. S.; Shin, J.-Y.; Kim, H.-T.; Kang, J. W.; Cha, J.-H.; Kim, K.-S., Unusual synergy effect on methane hydrate inhibition when ionic liquid meets polymer. *RSC Advances* **2013**, *3* (43), 19920-19923.
323. (a) Daraboina, N.; Malmos, C.; von Solms, N., Investigation of Kinetic Hydrate Inhibition Using a High Pressure Micro Differential Scanning Calorimeter. *Energy & Fuels* **2013**, *27* (10), 5779-5786; (b) Jr., H. E. K.; Hutter, J. L.; Lin, M. Y.; Sun, T., Polymer conformations of gas-hydrate kinetic inhibitors: A small-angle neutron scattering study. *The Journal of Chemical Physics* **2000**, *112* (5), 2523-2532.
324. (a) Lou, X.; Ding, A.; Maeda, N.; Wang, S.; Kozielski, K.; Hartley, P. G., Synthesis of Effective Kinetic Inhibitors for Natural Gas Hydrates. *Energy & Fuels* **2012**, *26* (2), 1037-1043; (b) Xu, Y.; Yang, M.; Yang, X., Chitosan as green kinetic inhibitors for gas hydrate formation. *Journal of Natural Gas Chemistry* **2010**, *19* (4), 431-435; (c) Talaghat, M. R., Enhancement of the performance of modified starch as a kinetic hydrate inhibitor in the presence of polyoxides for simple gas hydrate formation in a flow mini-loop apparatus. *Journal of Natural Gas Science and Engineering* **2014**, *18*, 7-12.

325. George, A.; Brandt, A.; Tran, K.; Zahari, S. M. S. N. S.; Klein-Marcuschamer, D.; Sun, N.; Sathitsuksanoh, N.; Shi, J.; Stavila, V.; Parthasarathi, R.; Singh, S.; Holmes, B. M.; Welton, T.; Simmons, B. A.; Hallett, J. P., Design of low-cost ionic liquids for lignocellulosic biomass pretreatment. *Green Chemistry* **2015**, *17* (3), 1728-1734.
326. Chen, L.; Sharifzadeh, M.; Mac Dowell, N.; Welton, T.; Shah, N.; Hallett, J. P., Inexpensive ionic liquids:[HSO<sub>4</sub>]<sup>-</sup>-based solvent production at bulk scale. *Green Chemistry* **2014**, *16* (6), 3098-3106.
327. (a) Lee, S.-Y.; Ogawa, A.; Kanno, M.; Nakamoto, H.; Yasuda, T.; Watanabe, M., Nonhumidified intermediate temperature fuel cells using protic ionic liquids. *Journal of the American Chemical Society* **2010**, *132* (28), 9764-9773; (b) Nakamoto, H.; Watanabe, M., Brønsted acid–base ionic liquids for fuel cell electrolytes. *Chemical Communications* **2007**, (24), 2539-2541; (c) Yasuda, T.; Watanabe, M., Protic ionic liquids: Fuel cell applications. *MRS bulletin* **2013**, *38* (7), 560-566.
328. (a) Wang, C.; Luo, H.; Jiang, D. e.; Li, H.; Dai, S., Carbon Dioxide Capture by Superbase-Derived Protic Ionic Liquids. *Angewandte Chemie International Edition* **2010**, *49* (34), 5978-5981; (b) Zhang, Y.; Zhang, S.; Lu, X.; Zhou, Q.; Fan, W.; Zhang, X., Dual Amino-Functionalised

Phosphonium Ionic Liquids for CO<sub>2</sub> Capture. *Chemistry-A European Journal* **2009**, *15* (12), 3003-3011.

329. Sabil, K. M.; Nashed, O.; Lal, B.; Ismail, L.; Japper-Jaafar, A., Experimental investigation on the dissociation conditions of methane hydrate in the presence of imidazolium-based ionic liquids. *The Journal of Chemical Thermodynamics* **2015**, *84*, 7-13.

330. Long, Z.; Zhou, X.; Shen, X.; Li, D.; Liang, D., Phase Equilibria and Dissociation Enthalpies of Methane Hydrate in Imidazolium Ionic Liquid Aqueous Solutions. *Industrial & Engineering Chemistry Research* **2015**, *54* (46), 11701-11708.

331. (a) Larsen, R.; Knight, C. A.; Sloan, E. D., Clathrate hydrate growth and inhibition. *Fluid Phase Equilibria* **1998**, *150*, 353-360; (b) Hutter, J. L.; King, H.; Lin, M. Y., Polymeric hydrate-inhibitor adsorption measured by neutron scattering. *Macromolecules* **2000**, *33* (7), 2670-2679; (c) Kelland, M. A.; Svartaas, T. M.; Øvsthus, J.; Namba, T., A new class of kinetic hydrate inhibitor. *Annals of the New York Academy of Sciences* **2000**, *912* (1), 281-293.

332. (a) Kelland, M., A review of kinetic hydrate inhibitors: Tailor-made water-soluble polymers for oil and gas industry applications. Nova Science

Publishers, Inc.: New York: 2011; Vol. 8, pp 171-210; (b) Edwards, A. R., A molecular modeling study of the winter flounder antifreeze peptide as a potential kinetic hydrate inhibitor. *Annals of the New York Academy of Sciences* **1994**, 715 (1), 543-544.

333. Perfeldt, C. M.; Chua, P. C.; Daraboina, N.; Friis, D.; Kristiansen, E.; Ramløv, H.; Woodley, J. M.; Kelland, M. A.; von Solms, N., Inhibition of gas hydrate nucleation and growth: efficacy of an antifreeze protein from the longhorn beetle *Rhagium mordax*. *Energy & Fuels* **2014**, 28 (6), 3666-3672.

334. Bavoh, C. B.; Partoon, B.; Lal, B.; Keong, L. K., Methane hydrate-liquid-vapour-equilibrium phase condition measurements in the presence of natural amino acids. *Journal of Natural Gas Science and Engineering* **2017**, 37, 425-434.

335. Sa, J.-H.; Kwak, G.-H.; Han, K.; Ahn, D.; Cho, S. J.; Lee, J. D.; Lee, K.-H., Inhibition of methane and natural gas hydrate formation by altering the structure of water with amino acids. *Scientific Reports* **2016**, 6.

336. Laage, D.; Stirnemann, G.; Sterpone, F.; Rey, R.; Hynes, J. T., Reorientation and allied dynamics in water and aqueous solutions. *Annual review of physical chemistry* **2011**, 62, 395-416.

337. Akhavan, B.; Jarvis, K.; Majewski, P., Hydrophobic plasma polymer coated silica particles for petroleum hydrocarbon removal. *ACS applied materials & interfaces* **2013**, *5* (17), 8563-8571.
338. (a) Daraboina, N.; Ripmeester, J.; Walker, V. K.; Englezos, P., Natural gas hydrate formation and decomposition in the presence of kinetic inhibitors. 3. Structural and compositional changes. *Energy & Fuels* **2011**, *25* (10), 4398-4404; (b) Ohno, H.; Moudrakovski, I.; Gordienko, R.; Ripmeester, J.; Walker, V. K., Structures of hydrocarbon hydrates during formation with and without inhibitors. *The Journal of Physical Chemistry A* **2012**, *116* (5), 1337-1343.
339. Kim, K.-S.; Kang, S.-P. In *Investigation of pyrrolidinium- and morpholinium-based ionic liquids into kinetic hydrate inhibitors on structure I methane hydrate*, Proceedings of the 7th International Conference on Gas Hydrates (ICGH 2011), 2011; pp 17-21.
340. Altamash, T.; Qureshi, M. F.; Aparicio, S.; Aminnaji, M.; Tohidi, B.; Atilhan, M., Gas hydrates inhibition via combined biomolecules and synergistic materials at wide process conditions. *Journal of Natural Gas Science and Engineering* **2017**, *46*, 873-883.

341. Haneda, H.; Sakamoto, Y.; Kawamura, T.; Komai, T. In *Experimental study on dissociation behavior of methane hydrate by air*, Proceedings of the 5th International Conference on Gas Hydrates, 2005; pp 13-16.
342. Masuda, Y.; Konno, U.; Hasegawa, T.; Haneda, H.; Ouchi, H.; Kurihara, M. In *Prediction of methane hydrate dissociation behavior by nitrogen injection*, Proceedings of the 6th International Conference on Gas Hydrates, 2008; pp 6-20.
343. Zare, M.; Haghtalab, A.; Ahmadi, A. N.; Nazari, K., Experiment and thermodynamic modeling of methane hydrate equilibria in the presence of aqueous imidazolium-based ionic liquid solutions using electrolyte cubic square well equation of state. *Fluid Phase Equilibria* **2013**, *341*, 61-69.
344. Tsuzuki, S.; Shinoda, W.; Miran, M. S.; Kinoshita, H.; Yasuda, T.; Watanabe, M., Interactions in ion pairs of protic ionic liquids: Comparison with aprotic ionic liquids. *The Journal of chemical physics* **2013**, *139* (17), 174504.
345. Koh, C.; Westacott, R.; Zhang, W.; Hirachand, K.; Creek, J.; Soper, A., Mechanisms of gas hydrate formation and inhibition. *Fluid Phase Equilibria* **2002**, *194*, 143-151.